"THE DESIGN OF A MAXIMISED TRANSPARENT ROOF STRUCTURE, TO CREATE THE MOST OPTIMAL MICRO CLIMATE FOR THE KHALIFA INTERNATIONAL STADUM IN QATAR"

TUDelft

"THE DESIGN OF A MAXIMISED TRANSPARENT ROOF STRUCTURE, TO CREATE THE MOST OPTIMAL MICRO CLIMATE FOR THE KHALIFA INTERNATIONAL STADUM IN QATAR"

STUDENT

Andreja Andrejevic

STUDENT NUMBER

4097564

CONTACT INFORMATION

+31636176702
andrejaandrejevic@gmail.com

GRADUATION MENTORS

Prof. Dr. Ir. P.M. Bluyssen
Chair of Indoor Environment

Dr. Ir. P.C. Louter
Chair of Structural Design

EXTERNAL EXAMINER

Drs. Kees Dol
OTB

MSc

Building Technology

DATE

26/01/2016

ACKNOWLEDGEMENTS

This graduation represents my completion of a 6,5-year journey at Delft University of Technology. Where I first did my BSc studies in Architecture, Urbanism and Building sciences and finalising my MSc studies in Building Technology. I am very thankful for the incredible learning experience and the opportunity to study at one of the best Architecture and Built Environment faculties in the world. I would like to notify my gratefulness to the people who supported me intellectually, mentally and financially.

First, this graduation was not possible without my mentors Philomena Bluyssen and Christian Louter. Therefore, I would like to thank Philomena for her incredible guidance in climate design in terms of the stadium's indoor environmental quality. Christian for his outstanding guidance in structural design in terms of steel and glass structures.

Secondly, special thanks to Peter van den Engel to who gave me great consults on the design of stadium ventilation. Calcen Chan, who let me use his wind tunnel and helped me with the wind testing setup. And Paul de Ruiter who let me use the 3D-printers from the print lab.

Finally, I would like to thank my parents and family for their mental and financial support during all those years. And of course my dearest Eline, who has always supported me in good and bad times.

A journey to never forget.

CONTENT

ABSTRACT

This report discusses the design analysis process of designing a maximum transparent roof for a stadium in order to create the most optimal semi indoor stadium climate. To conduct such research, the following main question had to be asked: How can a maximised transparent roof for the Khalifa International Stadium (KIS) in Qatar, with efficient use of energy, create an optimal semi indoor climate in extreme summer weather conditions?

The research on creating a comfortable microclimate in stadia started in the early eighties, where at the time knowledge in this field was very little. During the nineties, more information came available on creating microclimates in large semi-indoor spaces. Thus academic experimenting began on the quality of air, lighting and acoustics in stadia. This resulted in new stadiums built with new techniques from these academic analyses. In the zeroes one discovered a lot of inconveniences in the findings of the nineties and started to improve the academic research on stadia. With the rise of computers, it was a lot easier to conduct more complex and feasible analyses. Which brings us till today, where climate adaptation with complex forms can be tested and actually be made with the use of new kinds of materials. Because of the help of computers, designs are becoming much easier to predict, which makes us challenge ourselves to design in the most extreme situations where efficient and sustainable engineering can be achieved. Designing a roof for a stadium or a whole stadium gives new insights in different use of materials, smart climate/ structural design and the quality of sustainable building.

Designing a roof for the Khalifa International Stadium (KIS) gives a clear insight in the complexity of the structural demands of a stadium and the relevance of climate adaptive building. From a climate till a structural perspective the design has to balance between both disciplines, without exceeding one another's preconditions. For such roof, a wide range of design and engineering analyses is required. By conducting wind, heat and lighting analyses certain design requirements are imposed. Resulting in an interesting primary structural roof design based on the wind and an interesting secondary structural roof design based on heat and lighting. A roof where climate design meets structural design and vice versa.

1. PRELIMINARY

"The design of a maximised transparent roof structure, to create the most optimal micro climate for the Khalifa International Stadium in Qatar"

1.1 PROBLEM STATEMENT

With the FIFA World Championship 2022 coming to Qatar, a lot of development is happening in the capital of Doha. The biggest occurring development is the construction of 12 stadiums, from which 9 are to be build new and 3 to be renovated and transformed. Initially, Qatar 2022 was going to be organised in summer, where the average temperature is around 36 ˚C, however the FIFA decided to move the event to the winter due to the extreme summer weather conditions. However, the stadia are not designed to be used just in winter, therefore the Qatar Football Association (QFA) stated that the stadia should be designed to conquer the summer heat. The following was stated: The target temperature in stadia may not occur higher than 26 ˚C, while the used cooling energy has to come from a self-sustaining source (QFA, 2010).
The new stadiums that are getting build can deal way easier with this challenge, since this climate principle can be integrated in the whole design. However, the to be renovated stadiums contend with the challenge that this climate requirement has to be added to the existing situation. This makes transforming an existing stadium that has to be energy efficient a huge defiance.

1.2 RESEARCH QUESTION

How can a maximised transparent roof for the Khalifa International Stadium (KIS) in Qatar, with efficient use of energy, create an optimal semi outdoor climate in extreme summer weather conditions?

1.3 RESEARCH GOAL

The main goal of this graduation project is creating a climate integrated structural transparent and/or translucent roof design for the Khalifa International Stadium (KIS) situated in Doha, Qatar. With designing an additional transparent roof to the KIS, the challenge of creating an ideal semi-outdoor climate should be tackled. In such way that the roof has to be climate adaptive. This means complying with the requirements of the Semi-Indoor Environmental Quality (S-IEQ) (Aerothermal Quality, Acoustical quality and Lighting quality) and the climate criteria of the QFA. These qualities combined will give the challenge to design a very complex structure for a transparent roof that in the end deals with all the climate challenges. Structural design supports climate design.

1.4 RESEARCH AND DESIGN METHODOLOGY

With the design of a stadium roof in such extreme weather conditions, the research and design approach has to come out of 2 disciplines; Climate Design and Structural Design. The research on Climate Design has to be the foundation for a proper Structural Design. The scheme, shown on the next page, explains how climate research and analysis evolves into a design of a roof structure (see fig. 1). From P1 till P2, the first period of the graduation project, the main focus will be on analysing and researching the stadium context, stadium case studies, stadium environmental qualities and setting up the climate analysis. With research on the stadium context, the main plans of Qatar 2022, the situation of the local climate and research the technical requirements regarding constructions of stadia will be investigated. After the context research, the focus will be on the literature of three case studies where three types of stadia will be discussed. Varying from stadia in extreme climates (Climate Design) to stadia with retractable large span roofs (Structural Design). The third part of the research will be the literature study on Semi-Indoor Environmental Quality in stadia. Where the focus will be on three key aspects of S-IEQ, namely Aerothermal Quality, Lighting Quality and Acoustical Quality. This research will reveal what the most important aspects are, that have be taken into account with the design of a stadium climate. Concluding these findings into climate design restrictions. After all the literature research, the last step in the period between P1 and P2 will be the set up of the climate analysis that will be conducted in the period between P2 and P3.

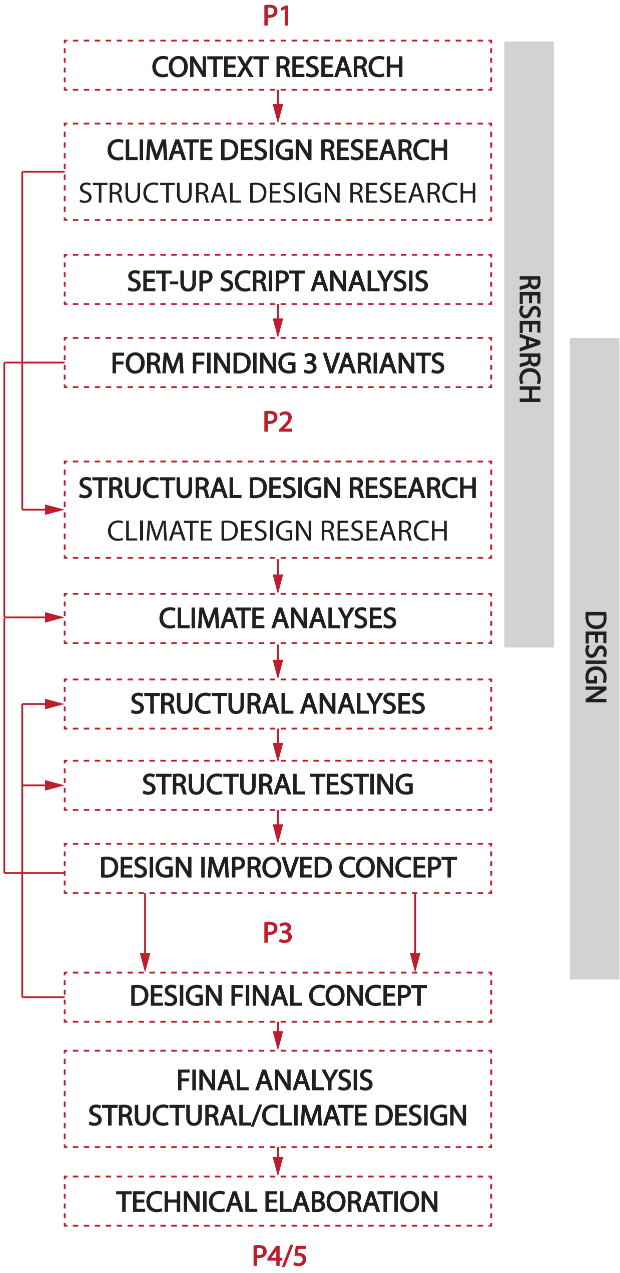

Fig. 1: Methodology (Andrejevic, 2016)

From P2 till P3, which is the second period, the main focus is researching different types of stadium roof structures, conducting the S-IEQ analysis and structural analysis and formulating the improved concept. With research on stadium roof structures, There will be dug into types of roof structures that are feasible to apply, such as conventional glass structures, lightweight large span glass structures and tensile/tensegrity glass structures. Next to the structural behaviour of glass, the climate behaviour of glass will also be investigated, given its mechanical properties. After the roof structure research, I start conducting the climate analysis on different variants where 1 best variant is going to be structurally analysed. After the analysis, the roof design gets improved and climatically analysed again. This way the roof design will be most optimally balanced on the two disciplines. From these analyses the improved concept gets formulated. The improved concept gets structurally tested with a Finite Element Method analysis (FEM).

From P3 till P4, the third period, the dedication is to design the final concept, conducting one final analysis and elaborate on all (technical) drawings. The final concept will meet the programme of demands and gets one final climate, structural and SWOT analysis, to prove the design's feasibility. After the final check, everything can be drawn out.

From P4 till P5, fourth and final period, it is al about finalising the report and final presentation.

2. RESEARCH FRAMEWORK

In the research framework, the situation of the World Cup of Qatar 2022 will be discussed. Firstly, there will be elaborated on the plans of Qatar 2022 and the stadium case (Khalifa International Stadium). Secondly, an extensive climate analysis on Doha, Qatar will be conducted and last but not least all the technical requirements are being discussed.

2.1 CONTEXT ANALYSIS QATAR 2022

2.1.1 FRAMEWORK PLANS QATAR 2022

To apply for a FIFA World Cup™ Qatar had to join a world wide bidding. This bidding is designed to get countries a plan of approach for the organisation of a world cup. At the end of the bidding a jury will decide which country has got the best plan and gets to organise the World Championship. In this case Qatar won the bidding for 2022. Qatar 2022 offers 7 host cities: Doha, Al-Daayen, Al-Rayyan, Al-Khor, Al-Wakrah, Al-Shamal and Umm Slal. These cities represent a total of 12 stadia. Of these stadia 9 are going to be build new and 3 are getting renovated (see fig. 2). The championship is planned in November and December, which means that the event will be in almost the coolest period (average 24 ˚C) of the year. However, the stadia have to be designed according to the most extreme climate situation, which is in summer. Because of these extreme weather conditions all of these facilities have strict climate requirements, such as a maximum semi-indoor temperature of 26 ˚C, high quality grass growth (exact sun lighting, ventilation and humidity conditions), right amount of shading, constant air flow, acoustics etc. Next to these climate issues, the biggest requirement and challenge is building zero carbon emission stadia. Coming from an initiative called ‘Green Qatar 2022’. (QFA, 2010)

Fig. 2: Planned stadiums Qatar 2022 (QFA, 2010)

2.1.2 KHALIFA INTERNATIONAL STADIUM, AL-RAYYAN, DOHA

The case study on which the focus of the design will be, is the Khalifa International Stadium (KIS) in Al-Rayyan. This stadium is 1 of the 3 stadia that is getting renovated and transformed. The KIS is the oldest stadium of Qatar that is still in use. It was opened in 1976 and renovated multiple times throughout the years for different kinds of events. The stadium holds a capacity of ca. 45000 seats and can be used for different types of sports (football, rugby, track & field etc.). (see fig. 3) (Legacy, 2016)

Fig. 3: Current situation Khalifa International Stadium (Legacy, 2016)

The western stand of the stadium is already partly roofed and provides that part of the stadium with some shading (see fig. 3). In the middle of the stadium there is a large arch placed to provide the field of lighting in the evening. With the last renovation the two arches were built with a structural view at the next transformation (see fig. 4a). The arches can be very suitable to create a suspended tensile roof structure. (see fig. 4b)

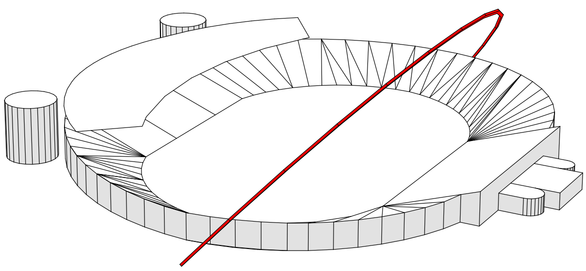

Fig. 4a: Model current situation (Andrejevic, 2016)

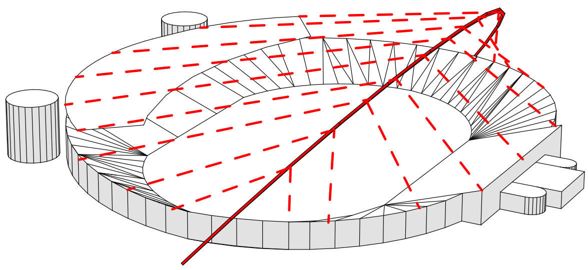

Fig. 4b: Tensile structure potential (Andrejevic, 2016)

To get a clear insight on the climate situation of Qatar, I used the weather analysis programme Climate Consult. With the help of this tool, a lot of information on the areas of sun, temperature, wind, humdity and shading is available. With the programme's analysis it is possible to get strategy results for the climate design. These strategy results might be useful in the early design stages of the roof.

2.2.1 SUN

The sun analysis gave information on the amount of illumination and radiation throughout the year. The illumination range shows the amount in Lux and the radiation range the amount in Wh/m^2. The recorded values of the measured illumination are direct normal and global horizontal to the earth surface. In June and July (months with most excessive heats) the global horizontal illumination and radiation are at their highest. The direct normal illumination and radiation are however a bit lower than average. Meaning the divided sunlight is at its best in June and July, in terms of diffuse light.

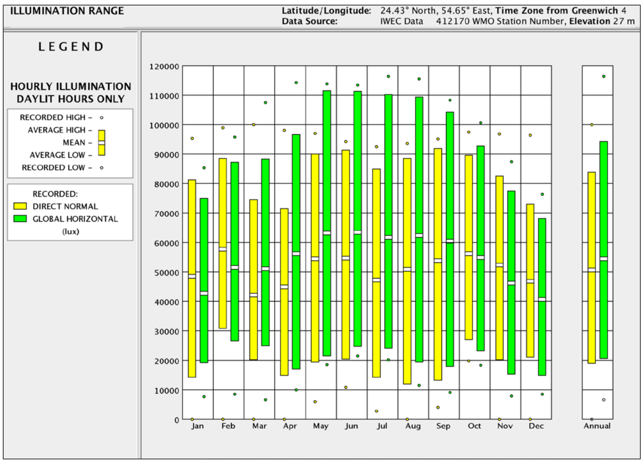

Illumination range

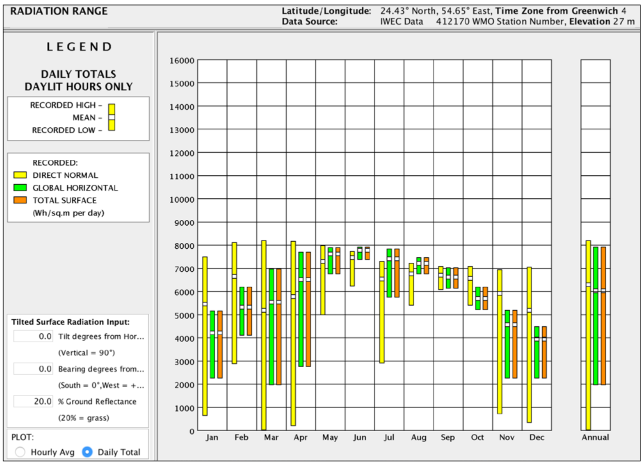

Radiation range

2.2.2 TEMPERATURE

The measured temperature throughout the year gives a clear insight in the excessive heat occurring in summer, especially in July. An average temperature of around 33 °C in June and almost 36 °C in July indicates the extreme heat stresses that can play out during the event. Next to the measured air temperature, an insight is given in the ground temperature. With a ground temperature between 25 °C and 30 °C at 0.5 metres depth in June and July, the grass has perfect ground conditions for growth. However, this will only be the case if the grass stays humidified and will not receive too much direct sunlight.

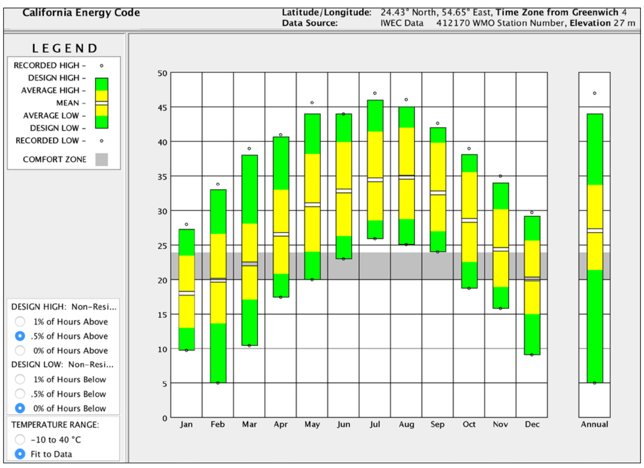

Temperature range

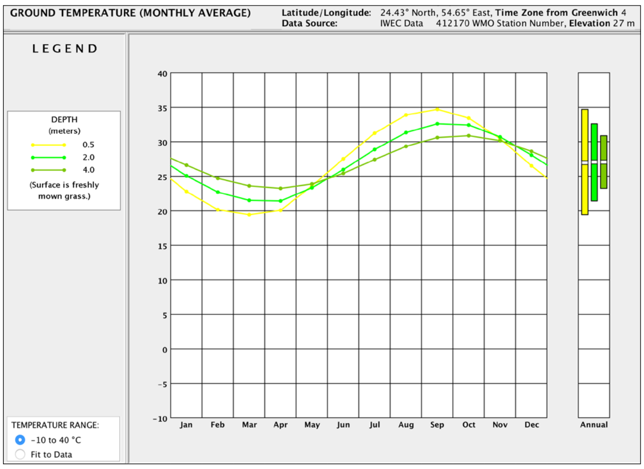

Ground temperature range

2.2.3 WIND

The climate consult analysis shows a constant wind speed average over the whole year. The yearly average is about 4 m/s with peaks in May and June. In June and July the mean wind speed is around 3.9 m/s with a standard deviation of approximately 4. The second graph shows the dominant wind direction with the temperature and the humidity of the wind. Showing that in June and July a warm, dry wind comes mostly from the West North West (WNW). A constant wind flow means good conditions for natural ventilation in summer.

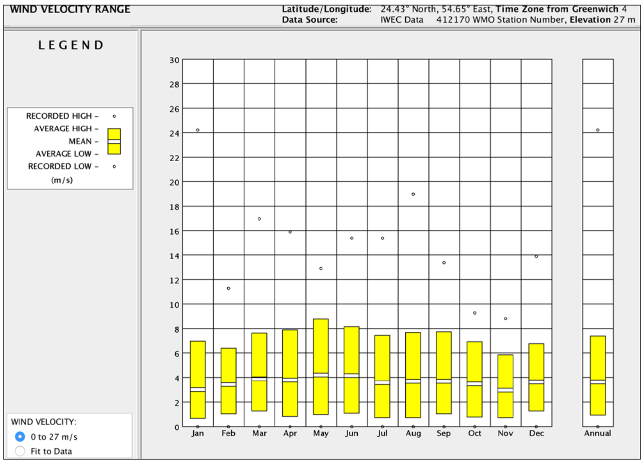

Wind velocity range

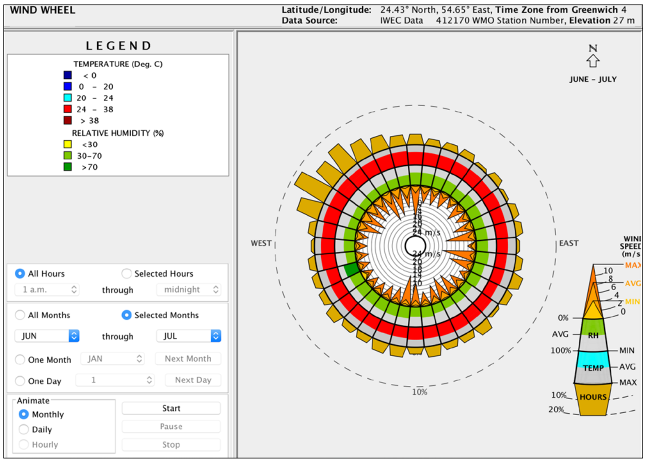

Wind wheel

2.2.4 HUMIDITY

The first graph shows the humidity versus the dry bulb during a period of a year. Showing, that the dry bulbs comparing to the humidity can be very excessive in June and July. The second graph shows the humidity range during the day, with very dry moments during the day and very humid moments during the night. This big difference in wet and dry during day and night can be a suitable outcome for the event. Dry hot temperatures during the day are easier to condition and the high humidity during the night can passively humidify the grass for the day.

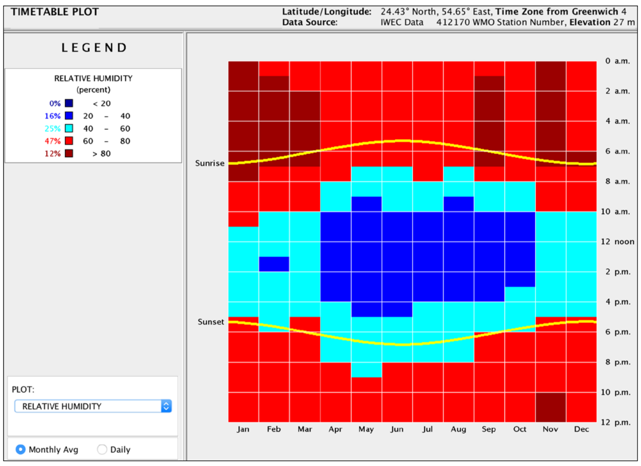

Humidity in relation to time

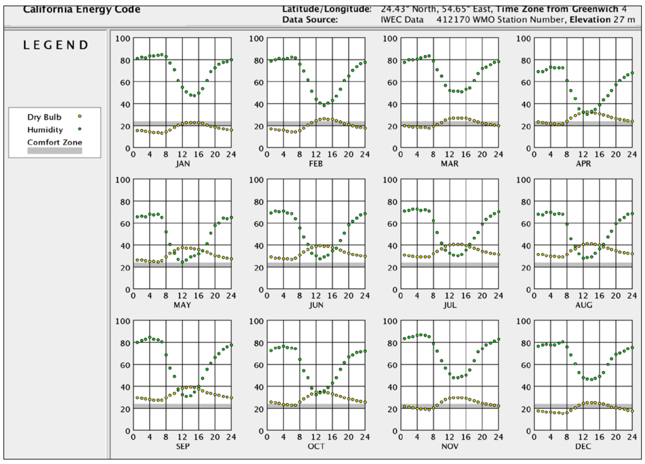

Dry bulb vs. Humidity

2.2.5 SHADING

The first graph shows the amount of heat coming from the sun in a period of a year. Giving an indication of comfort levels. During the day direct sunlight in summer it is not comfortable and a lot of shading is needed to get places cool and comfortable. The second graph gives an insight in how much shade is needed to reach a human comfort level, in terms of heat.

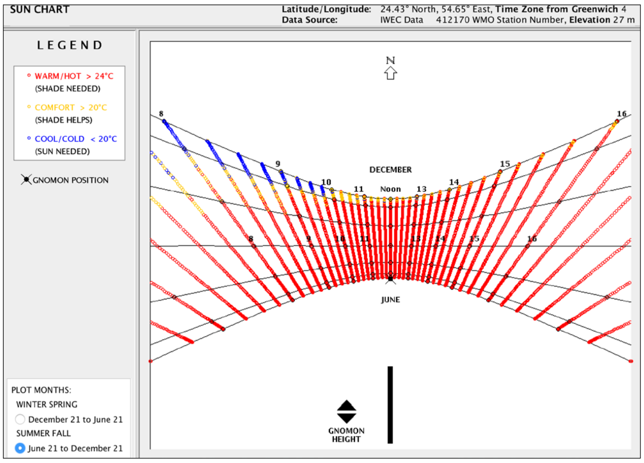

Sun chart

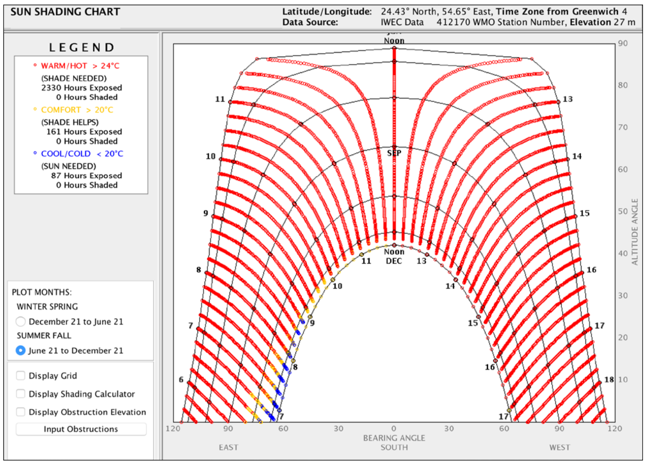

Shading chart

2.2.6 DESIGN STRATEGY RESULT

From the analysis of all different climate aspects, Climate Consult shows design strategies to tackle the excessive heat problems in Qatar for June and July. These design strategies are merely focused on large non residential buildings. A set of design strategies are shown below with in percentages the impact and feasibility of the design action. The most feasible actions are (from least to most):

- Fan-forced ventilation cooling (2.7%)
- Natural ventilation cooling (3.7%)
- Evaporative cooling (6.1%)
- Sun shading of surfaces (37.5%)
- Mechanical cooling and dehumidification (92.3%)

From the Climate Consult analysis can be concluded that the only good solution to fight the heat is to use the heat. In a smart and energy efficient way it can be feasible to convert heat into useful cold.

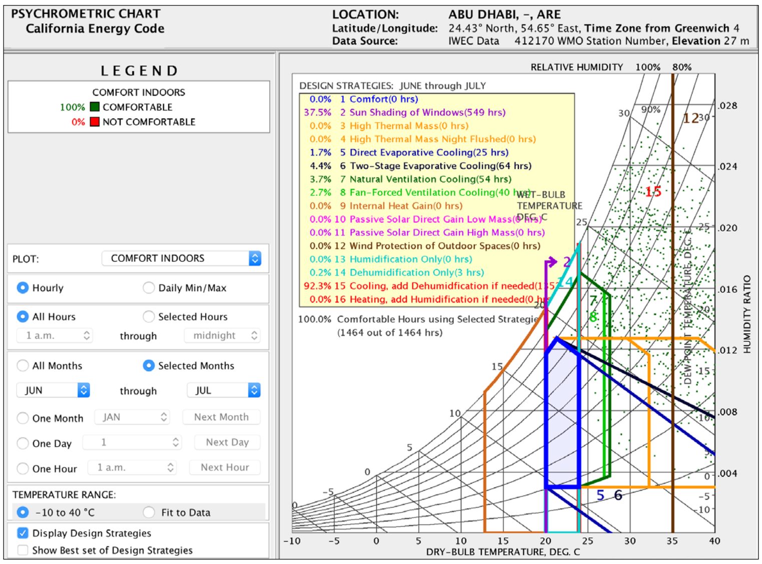

Design strategies plot

2.3.1 SEMI-INDOOR ENVIRONMENTAL QUALITY REQUIREMENTS

The Semi-Indoor Environmental Quality (S-IEQ) of the stadium must comply the technical requirements as described in the FIFA stadium guide. (FIFA, 2011) The stadium's micro climate prior is to provide comfort in all stages. This means creating a comfortable climate for the players as well as the spectators. Maintaining a climate for 2 groups with completely different demands, forced the FIFA to set a temperature range aim of 20-24 ˚C in all areas of a stadium, where preferably in the lower part a mean temperature of 20 ˚C and the higher part a mean temperature of 24 ˚C. The aerothermal comfort of a stadium can be based on a graph designed by Agota Szucs in 2004. (see fig. 5) (Szucs, 2004) This graph represents the requirements to create a comfortable micro climate. These comfort requirements are based on the following climate parameters: temperature, air flow velocity, solar radiation and humidity. When the given comfort requirements cannot be reached by the natural outdoor air flow, different ways of passive/active cooling are required. Possible ways of the required cooling are evaporative cooling, mist cooling, adiabatic cooling, solar cooling, PV cooling and solar sorption cooling (Sofotasiou, Hughes, & Calautit, 2014)

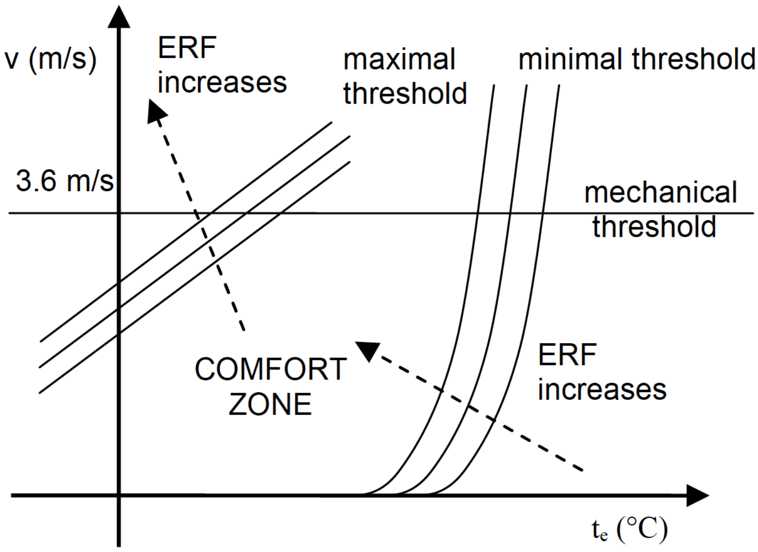

Fig. 5: Graph aerothermal comfort in relation to the human body (Sofotasiou et al., 2014)

2.3.2 ROOF REQUIREMENTS

A high number of the stadiums in Qatar are proposed with the design of an Oculus roof (a circular opening in a dome structure to provide space with light). Such roof design is tested in scale model wind tests and concluded to be much better applicable in cooler climates. In hotter climates, the air flow will stimulate the heating instead of the cooling of the stadium. In the case of Qatar is an Oculus design for a roof a huge climate challenge and in most cases not feasible. As written in the FIFA stadium guide, in hot climates stadia have to have preferably a closed roof provided the fact that the turf requirements are met. Requirements as exposure to direct sunlight, humidity and ventilation are needed to maintain a good turf. (FIFA, 2011) In short a closed roof needs to be, at some parts, as transparent as possible to fulfil the FIFA stadium requirements on creating an ideal micro climate. (Szucs, Moreau, & Allard, 2005) Since in the KIS the lighting arch is suitable for a tensile structure, the roof has to be a transparent lightweight large span structure.

2.3.3 ZERO CARBON EMISSION POLICY

Like mentioned before, the biggest technical challenge is going to get the event carbon neutral. With the 'Green Qatar 2022' initiative, Qatar pledges to do everything in its force to make the event 100% zero carbon emissive. To realise this initiative, solar collectors and photo voltaic panels are either to be integrated in the stadium roof or placed on a plant nearby a stadium. This way it is possible to make the stadium energy efficient but not zero carbon emissive. To achieve a zero carbon emission policy Sartori, Napolitano & Voss designed balance strategies to compensate the amount of delivered energy during the event in the future. (see fig. 6) (Sartori, Napolitano, & Voss, 2012)

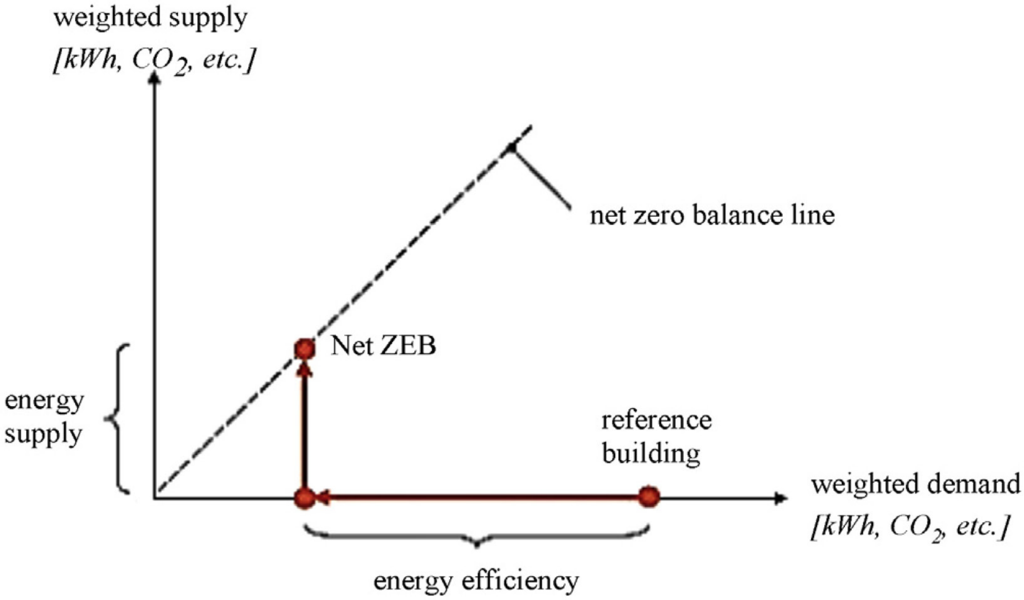

Fig. 6: Chart energy supply vs. energy efficiency for buildings (Sartori et al., 2012)

3. CASE STUDIES

Three case studies are being discussed: Paul Brown Stadium, Chase Field and Amsterdam ArenA. They all differ from problems that have occured during the design and engineering stages. Problems such as excessive hot climates, complex retractrable roof structures, natural turf growth etc.

3.1 CASE STUDY 1: PAUL BROWN STADIUM, CINCINNATI, OHIO, USA

The Paul Brown Stadium is the home of the Cincinnati Bengals (American Football) in Cincinnati. The stadium opened its doors in 2000 and was designed by NBBJ (architects) in cooperation with Arup Los Angeles (structural engineers) and Turf Diagnostics of Kansas City (turf consultants) (see fig. 7b). (Wikipedia, 2015b) The climate of Cincinatti characterises itself as a land climate, with cold winters and hot summers. In summer situation the sunlight reaches high levels of radiation, which can be in advantage of the natural turf, but a disadvantage to the user's comfort in the stadium (see fig. 7a).

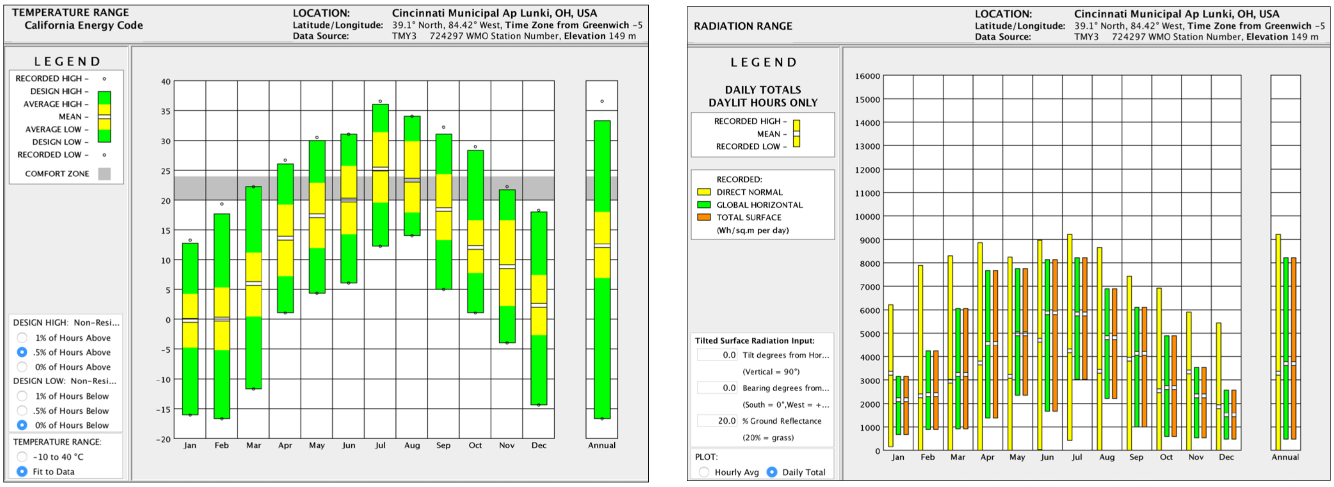

Fig. 7a: Weather measurements Cincinnati (Andrejevic, 2016)

Fig. 7b: Paul Brown Stadium (Wikipedia, 2015b)

During the design and the construction of the stadium the two biggest challenges were: the cladding loads on the large stand canopies and the sun and shadow patterns on the field during the day. The structural challenge of the cladding loads on the canopies was in the live load of the wind and the snow. To tackle this challenge, two designs were proposed; a lightweight metal canopy or a tensile fabric surface structure. To get the suitable design for the canopy, scale and computer models were tested. Through these tests live cladding loads were analysed and verified (see fig. 8). The most suitable solution was the tensile fabric structure, because of its light weight and louvers to reduce wind loads on the surface. (Soligo, Lankin, & Irwin, 1998)

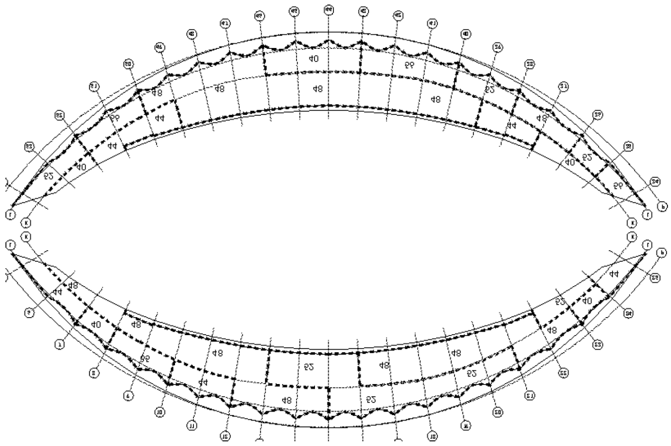

Fig. 8: Cladding loads roof overhang Paul Brown Stadium (Soligo et al., 1998)

Next to the structural behaviour, the stadium micro climate behaviour in relation to the turf was the other big challenge of the stadium. The experts of Turf Diagnostics of Kansas City focused on the behaviour of shading patterns on the field. To get clear insight in this behaviour, the shading patterns were analysed on the first day of every season for every hour. An example of an occurring shadow pattern on the first day of spring (21st of March, 8:00) is show in the figure below (see fig. 9). With these tests, the experts were able to get a more detailed insight of the amount of solar radiation occurring on the field (see fig. 9). By running multiple tests, the different companies could determine how large the canopies had to be and come with a feasible design. (Soligo et al., 1998)

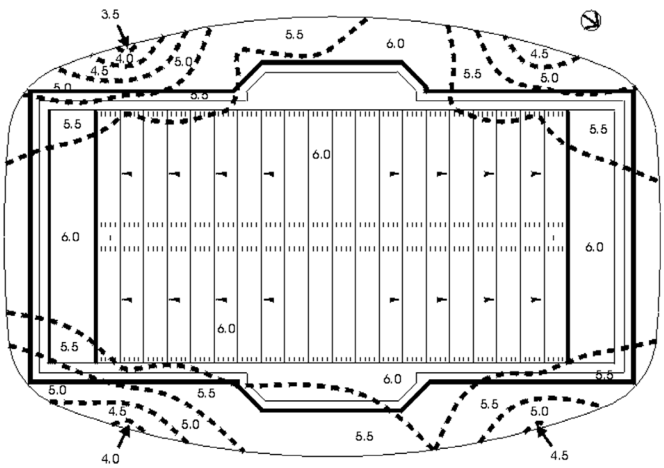

Fig. 9: Occurring radiation in kWh/m^2 Paul Brown Stadium (Soligo et al., 1998)

3.1.1 ENUMERATION DESIGN CHALLENGES

°Create right amount of shadowing on the spectators' stands
°Maintain right amount of lighting for natural turf
°Design feasible structure for canopy cantilever
°Design structure of the canopy aerodynamically

The Chase Field (former Bank One Ballpark) is the home of the Arizona Diamondbacks (Baseball) in Phoenix. This stadium opened in 1998 and was designed by Ellerbe Becket (architects) in cooperation with Martin & Martin (structural engineers) and M-E Engineers (mechanical designers/engineers) (see fig. 10b). (Wikipedia, 2015a)
The climate of Phoenix is very similar to Qatar's climate. With extreme temperatures and high radiation levels, it is hard to create an ideal microclimate during the whole day. Especially when every stadium design aspect is taken into consideration (see fig. 10a).

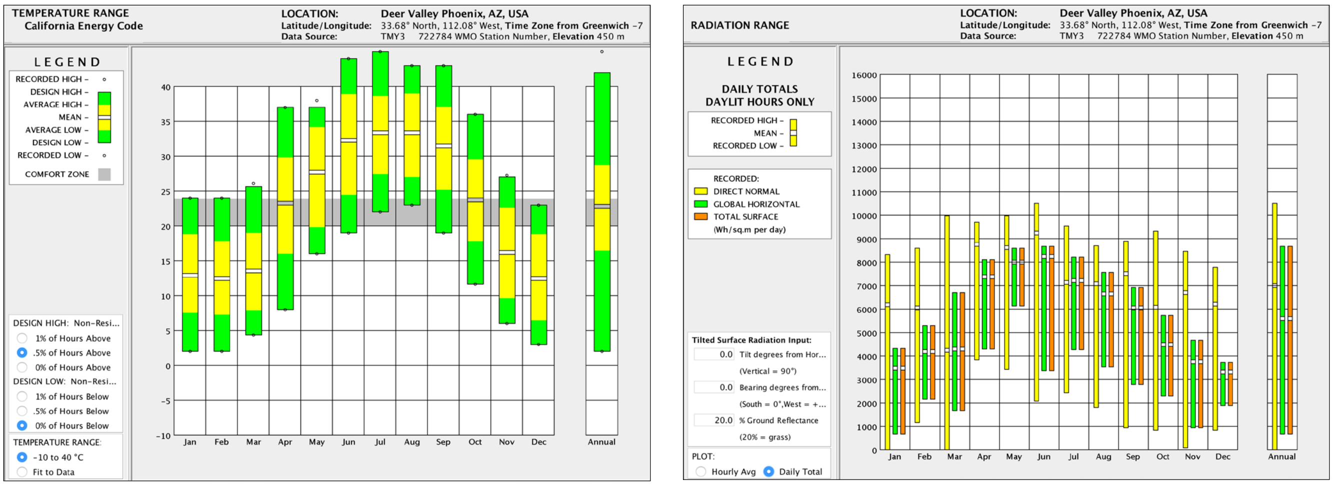

Fig. 10a: Weather measurements Phoenix (Andrejevic, 2016)

Fig. 10b: Chase Field (Wikipedia , 2015a)

The biggest challenge of the design of Chase Field was Phoenix's dry and hot climate. Excessive temperatures around 40 °C made the designers realise that it was more feasible to create a comfortable microclimate if the stadium could be closed. Therefore, a retractable roof was proposed (see fig. 11). With a retractable roof it was possible to close it for games during hot days and open it for cooler days. With an operable roof it was possible to make use of natural turf (natural turf is always preferred, since it is of more aesthetic value and safer for players to use).

Fig. 11: Chase Field retractable roof in closed position (Soligo et al., 1998)

To tackle the challenge in this design proposal some tests and analyses were conducted: climate analysis on air flows in relation to thermal lag, indoor air comfort analysis and wind live loads on the structure and cladding in different roof positions. The tests and analyses were conducted via wind tunnel models and computer models (see fig. 12). The most suitable structural solution, derived from the tests and analyses, was to make an aerodynamic stable lightweight roof made out of aluminium. In every position the roof had to ensure a positive aerodynamic damping. (Frazer, 2005)
The solution for a healthy semi indoor environment in relation to a healthy turf was to open the roof in the morning and afternoon until 4 hours before a game started in the evening. However, the microclimate became to hot after opening of the roof, so eventually they had to air condition the stadium. (Soligo et al., 1998)

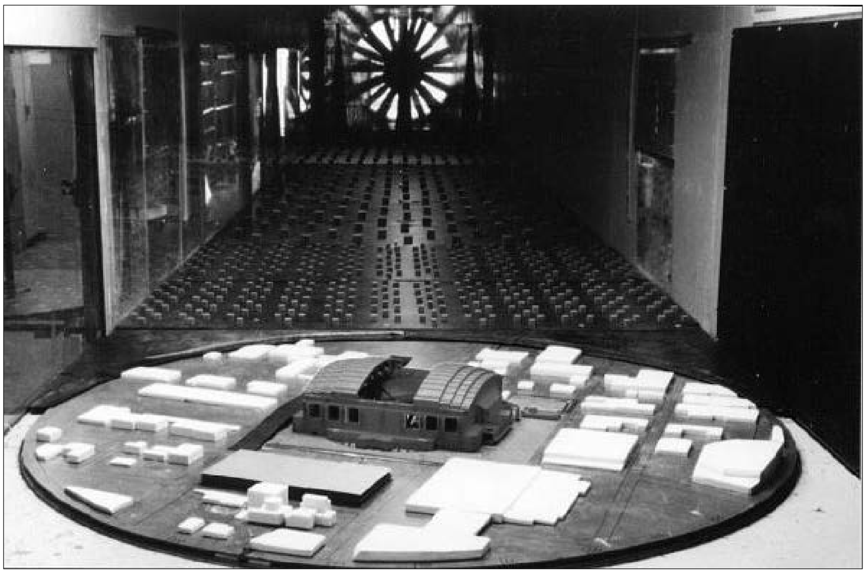

Fig. 12: Wind tunnel testing (Soligo et al., 1998)

3.2.1 ENUMERATION DESIGN CHALLENGES

˚Maintain right amount of lighting for natural turf
˚Create comfortable micro climate during Baseball games
˚Design roof that uses wind partly as ventilation source
˚Design roof that is capable to absorb occurring wind live loads

The Amsterdam ArenA is the home of Amsterdamsche Football Club Ajax (Football/Soccer) in Amsterdam. The stadium's opening was in 1996 and was design by Rob Schuurman & Sjoerd Soeters (architects), Arcadis (structural engineers) and E&M (mechanical engineers) (see fig. 13b). (Wikipedia, 2016) The weather of Amsterdam is in every season relatively mild, meaning average winter temperatures of around 4 ˚C and average summer temperatures of 18 ˚C. Further, what is interesting is the yearly constant wind velocity of around 5 m/s, which is similar to Qatar's wind velocity range. This constant wind can be an advantage of the ArenA's climate design (see fig 13a).

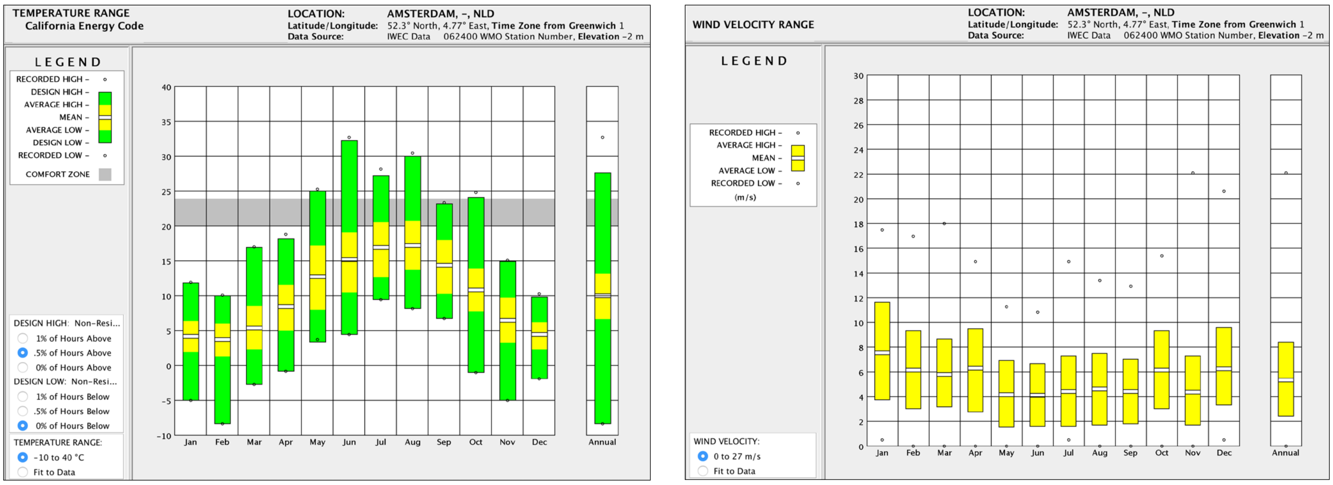

Fig. 13a: Weather measurements Amsterdam (Andrejevic, 2016)

Fig. 13b: Amsterdam ArenA (Wikipedia, 2016a)

Because of the ArenA's retractable roof, the design is semi-closed and caused particular problems and challenges concerning natural ventilation in a semi indoor microclimate. These problems were determined in 2007 and needed improvements. The challenges regarding natural ventilation were the ventilation rate and the air temperature distribution. The Amsterdam ArenA is located in a dense commercial area where the air of the wind gets forced in diverse directions, surrounding buildings create lee and possibly heat up the area (see fig. 14).

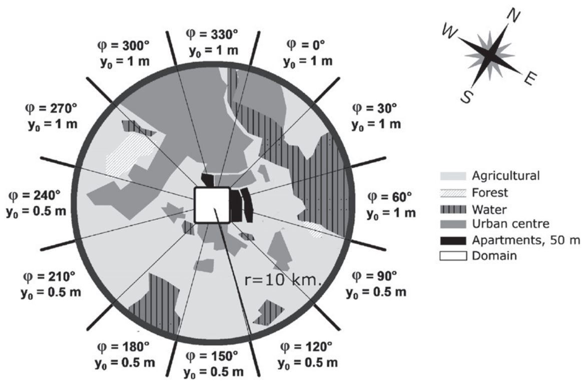

Fig. 14: Influence of Amsterdam ArenA on wind flow through urban area (Hoof & Blocken, 2009)

To deal with these challenges, the mechanical engineers improved the stadium's ventilation configurations by analysing the stadium and its urban area with computer models (see fig. 15a). As a result of an area wind analysis, stadium wind analysis and detailed ventilation analysis (see fig. 15b), the experts of E&M came with different ventilation configurations as improvements of ventilation rate and air temperature distribution, shown in the figure below (see fig. 16).

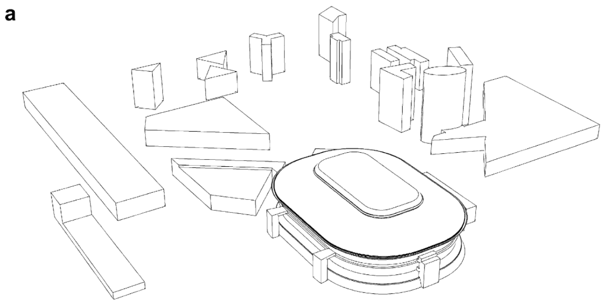

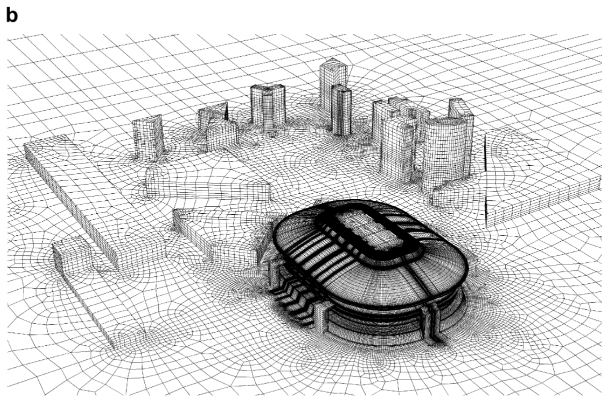

Fig. 15a: Computational model Amsterdam ArenA *Fig. 15b: Computational ventilation analysis on Amsterdam ArenA*
(Hoof & Blocken, 2009)

Figure 16a shows the existing ventilation situation at the edge of a ring. Figure 16b shows a solution where 8 operable windows connects the outdoor environment with the stadium microclimate. Figures 16c to 16e show ventilation solutions at the edge of the roof where steel cladding can be semi opened, opened or removed to improve the ventilation rate of the stadium. Combining these different ventilation solutions conclude an increase of the air exchange rate of 43%. Complex modelling can result in simple solutions to improve stadium design. (Hooff & Blocken, 2009)

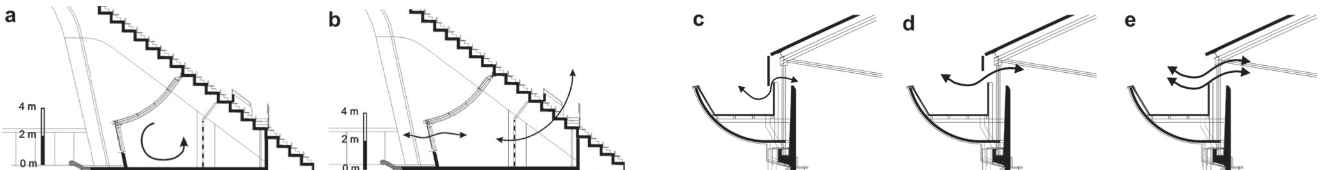

Fig. 16: Possible roof ventilation configurations (Hoof & Blocken, 2009)

3.3.1 ENUMERATION DESIGN CHALLENGES

˚Determine the amount of wind pressure occurring in densed area
˚Create constant air circulation in ArenA
˚Determine if mechanical, hybrid or natural ventilation system is needed
˚Design right ventilation configuration in roof

4. THEORY RESEARCH CLIMATE DESIGN

The research on Semi-Indoor Environmental Quality in stadia discusses three types of qualities, namely Aerothermal Quality, Lighting Quality and Acoustical Quality. Where the research on Aerothermal Quality elaborates on the comfort of the users (players and spectators) and the importance of roof geometry on climate design; the research on Lighting Quality elaborates on the amount of light needed for natural turf growth and lastly the research on Acoustical Quality digs into the importance of backward and forward reflection in stadium semi-indoor spaces. As a conclusion, climate design restrictions were set out of the researched literature.
By looking at what challenges on stadium climate were encountered, I can get a better insight on designing a suitable climate adaptive roof.

4.1 AEROTHERMAL QUALITY IN STADIA

4.1.1 USER'S COMFORT

In terms of thermal comfort in stadia the challenging climate factors can be divided in two parts: The climate factors which cannot be changed or improved by architecture, namely air temperature and air humidity (the human invariable factors). On the other hand, there are the climate factors that can be altered by architectural, façade, climate and structural design, namely solar air flow and solar radiation. To address these factors of thermal comfort it is necessary to base findings as air movement and the effect of solar radiation on applicable graphs and charts. (Bluyssen, 2009) From these charts aspects as physical conditions and body stresses can be measured. On the basis of existing thermal comfort charts, the following parameters can be evaluated: (Szucs, 2004)
°Olgyay's bioclimatic chart
°Wind Chill Index (WCI)
°Wind Chill Temperature (WCT)
The WCI and WCT give a summary of a complicated evaluation of the influence of temperature, humidity, air movement and solar radiation. Regarding thermal comfort on the area of air movement and solar radiation, it is consequent that the maintenance of thermal comfort that has passed the dry-bulb temperature has to be compensated with a certain air movement. (Arens, Gonzalez & Berglund, 1986) Shown in the Olgyay bioclimatic chart (see fig. 17):

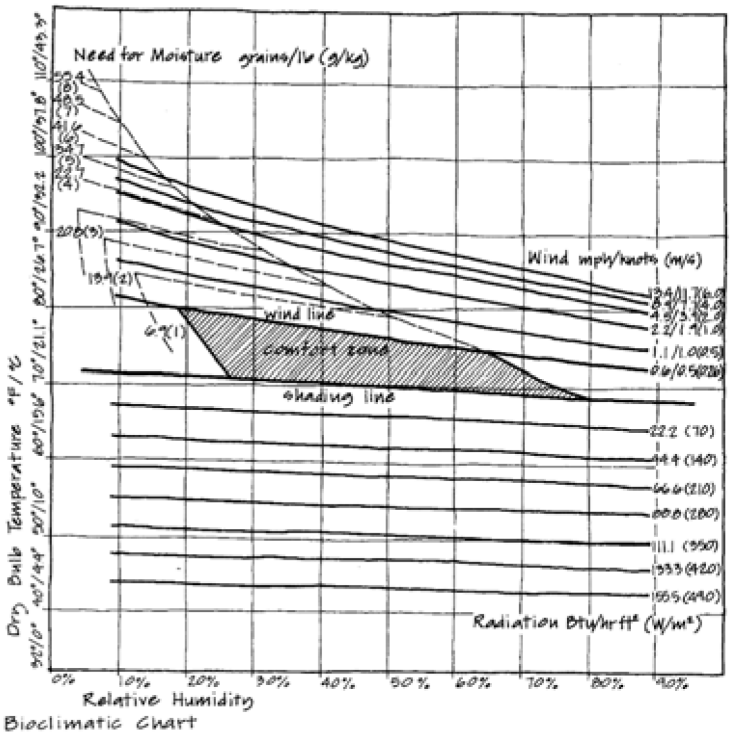

Fig. 17: Olgyay bioclimatic chart (Arens, Gonzalez & Berglund, 1986)

With an excessive external DBT, the velocity of the air movement will lift rapidly and this will cause in poor quality of thermal comfort.
Next to the amount of air movement, the chart gives an indication on solar radiation in relation to thermal comfort as well. By the use of the effective radiant field (ERF) value, the net radiant heat flux to and from the body can be determined. (Szucs, 2004) Which results in determining the thermal (dis)comfort of a human body from air temperature (see fig. 17).
The third aspect that can influence the thermal quality of a stadium, is the effect of external wind on cooling and heat perception. By use of the Wind Chill Index and the Wind Chill Temperature equations the relation of wind and temperature heat loss can be measured. See the following Siple and Passel equations (v=m/s) (value 12.15 is used for hot climates) (see fig. 18): (Auliciems & Szokolay, 1997)

$$WCI = (12.15 + 11.6\sqrt{v} - v)\times(33 - DBT)$$

$$WCT = 33 - 0.03738\times WCI$$

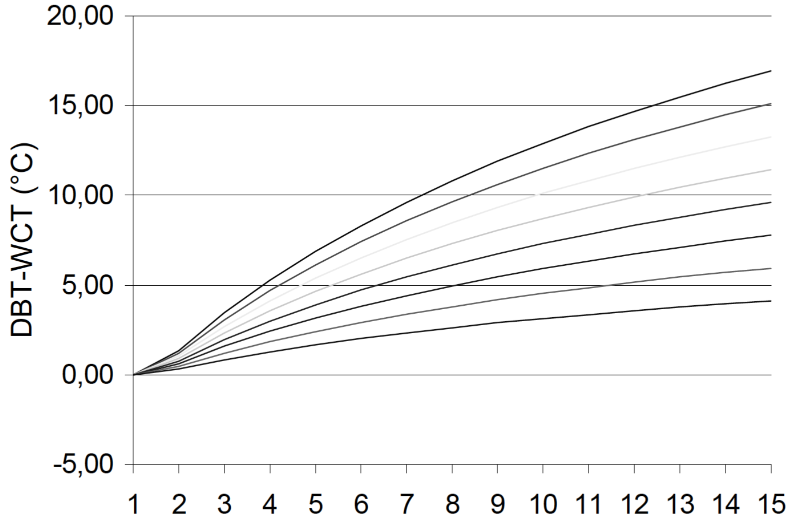

Fig. 18: Siple and Passel wind comfort equations with accessory chart (Auliciems & Szokolay, 1997)

With use of the wind chill index, it is eventual to determine the temperature decrease that is caused by the velocity of wind.
The fourth and last aspect is the amount of turbulance occurring from the wind circulation in the stadium. The influence of turbulance on the human body is the most significant by determining the user's comfort in a stadium. The following equation can determine the amount of turbulence. (Bluyssen, 2009)

$$T_u = \frac{\sigma_{v_a}}{v_a} \, [\%]$$

Where:

v_a = local air velocity in m/s
σ_{V_a} = standard deviation of local air velocity in m/s

With use of these charts and equations, it is possible to make a feasible indication whether a thermally comfortable climate is generated. A combination of all the complex climatic factors playing part in thermal comfort are enumerated in the following chart from Agota Szucs (earlier mentioned in the report) (see fig. 19). (Szucs, 2004)

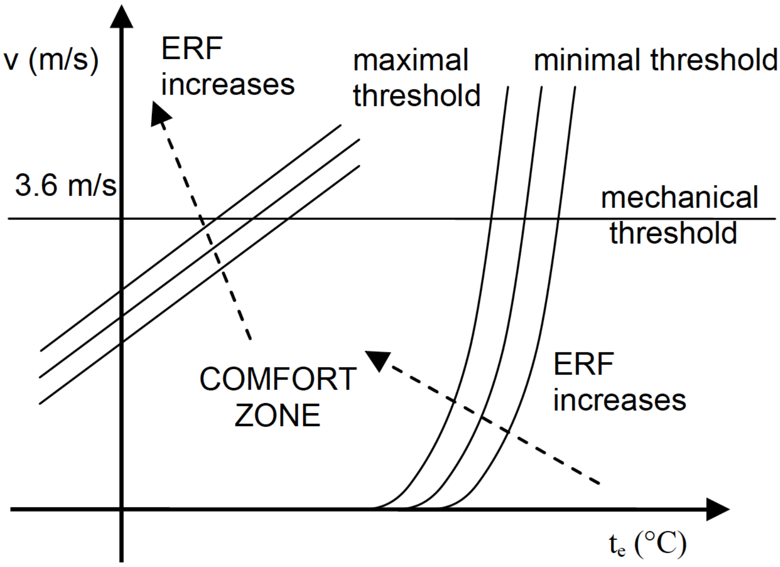

Fig. 19: Graph aerothermal comfort in relation to the human body (Szucs, 2004)

4.1.2 STADIUM ARCHITECTURE VS. AEROTHERMAL COMFORT IN HOT CLIMATES

Concluding from the user's comfort in a stadium, the architecture of a stadium can enhance and use the effect of air movement and solar radiation. This can lead to very exuberant designs, which are explained and illustrated in the chapter Case Studies. These designs derive from climate responsive thinking and bring interesting features on stadium roof design. Some of these popular features are; roof enhancing airflow, dividing stands in vertical/horizontal openings to increase air movement in the stadium's microclimate, solar radiative shading and reflecting canopies, etc. (see fig. 20a, 20b). (Szucs, Moreau, & Allard, 2008)

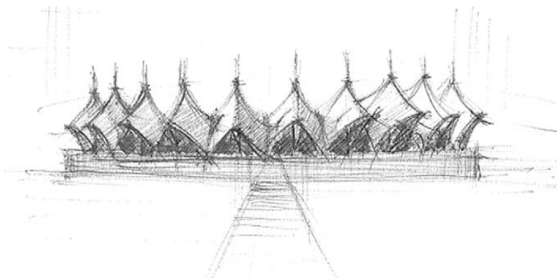

Fig. 20a: King Fahd Stadium concept drawing

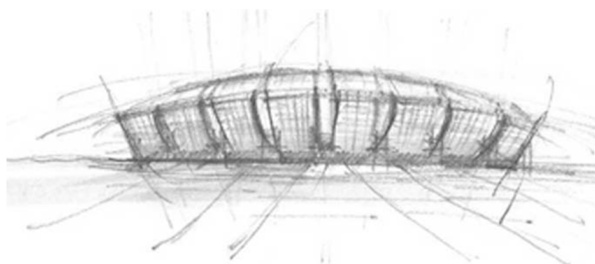

Fig. 20b: St. Nicolas Stadium concept drawing

(Szucs, Moreau, & Allard, 2008)

Shading, reflection and enhancing air movement can be of significant improvement in stadiums located in hot climates. Australian study in 2003 shows that stadia in hot climates with traditional transparent roofs intensify the semi-indoor solar radiation because of lighting demands. The increase of solar radiation results in hot heat stress for the users. They propose semi-transparency and use of fabrics in the roof and a shape that enhances the air movement in the upper rows of the stands. (Spagnolo, 2003) To generate air movement in the upper rows, that will result in a solid stadium air circulation, a wind adaptive roof geometry has to be designed. French study in 2007 shows, with the help of scale model wind tunnel tests, that different geometries improve the impact of air circulation on aerothermal comfort. (Bouyer, Vinet, Delpech, & Carré, 2007) The following geometries: large roof overhang (see fig. 21), roof inclination (see fig. 22) and roof porosity (see fig. 23). In the charts the Ψ_i stands for the turbulence and the average wind speed at a given i measurement point in relation to those measured at the reference point. In essence, Ψ_i characterises the wind speed in the stadium bowl compared to that measured without the stadium being there. The probability of occurance stands for the percentage of thermal stresses occurring at a human body. In short, the higher the Ψ_i, with a constant average wind speed of 5 m/s the better the aerothermal result. (Szucs et al., 2008)

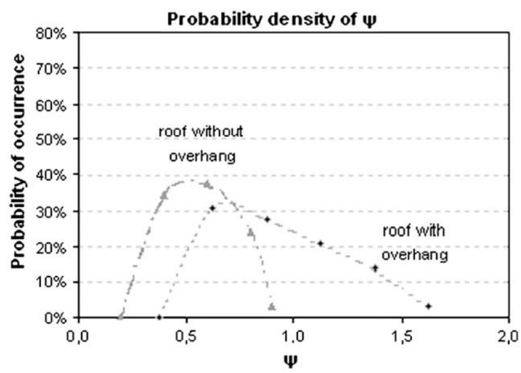

Fig. 21: Roof overhang vs. Aerothermal comfort

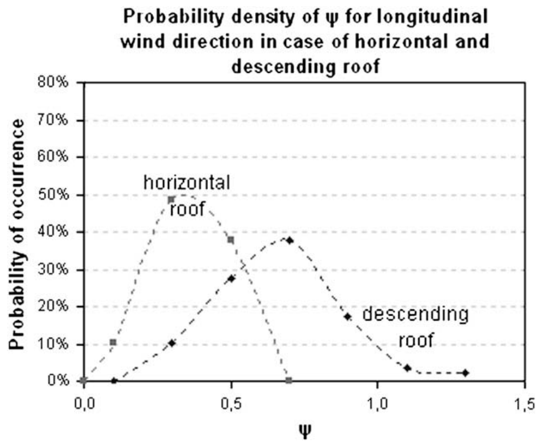

Fig. 22: Roof inclination vs. Aerothermal comfort

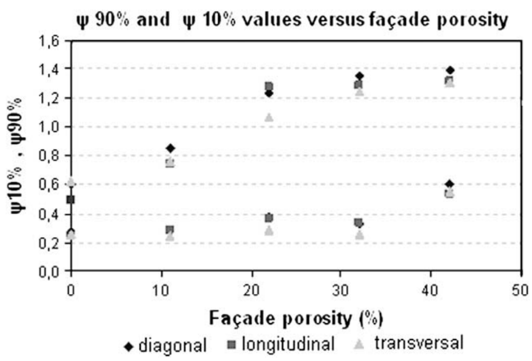

Fig. 23: Porosity vs. Aerothermal comfort (Bouyer, Vinet, Delpech & Carre, 2007)

4.1.3 CHALLENGES AEROTHERMAL QUALITY KIS

The complexity of the roof design for the KIS lies in the combination of an aerodynamic roof that provides aerothermal comfort, but does not bother the sports game. As mentioned and shown above, excessive external temperatures will make the reaching of a thermal comfort level, based on air movement and solar radiation, a complicated challenge. In the case of Qatar, especially with the use of external wind flow to ventilate the stadium will be challenging, since excessive DBT values are reached in summer. In this case, the challenge of the KIS has to be coming up with cooling strategies that make use of the air movement and external wind. Providing an air movement that decreases human thermal stresses with convective heat loss and accelerating evaporation. Based on the following equation (discussed in the chapter above): (Szucs et al., 2008)

$$\Psi_i = \frac{\overline{U}_i + \sigma_i}{\overline{U}_{ref} + \sigma_{ref}}$$

Where:

Ψ_i = the wind velocity in the stadium compared to the wind without the stadium
U_i = average wind velocity at point i
σ_i = standard deviation at point i
U_{ref} = average wind velocity at reference point
σ_{ref} = standard deviation at reference point

The determined influence of the wind on the human aerothermal comfort has to be combined with the turbulence intensity that occurs on the human body. As explained above the amount of turbulence can be calculated. However the amount of turbulence has to be measured on the human's body comfort. This measured comfort is expressed in Draught Rating (DR). To calculate the amount of DR the following equation can be used. (Bluyssen, 2009)

$$DR = (34 - t_a) \cdot (v_a - 0.05)^{0.62} \cdot (3.14 + 0.37 \cdot T_u \cdot v_a)\ [\%]$$

Where:

v_a = local air velocity in m/s
T_u = turbulence intensity (σ / v_a) in %
t_a = local air temperature in ˚C
when v_a < 0.05 m/s insert v_a = 0.05 m/s
when DR > 100% insert DR = 100%

The amount of DR following from the equation can be measured by the table shown on the next page. The table shows different building categories (see fig. 24). The concerning category in this situation is category C, which represents large spaces.

Category	**Thermal state of the body as a whole**			**Local discomfort Percentage of dissatisfied due to:**		
	Predicted percentage of dissatisfied (PPD) (%)	**Predicted mean vote (PMV)**	**Draught (DR) (%)**	**Vertical air temperature difference (%)**	**Warm or cool floor (%)**	**Radiant asymmetry (%)**
A	<6	–0.2<PMV<+0.2	<15	<3	<10	<5
B	<10	–0.5<PMV<+0.5	<20	<5	<10	<5
C	<15	–0.7<PMV<+0.7	<25	<10	<15	<10

Fig. 24: Table with categories of thermal comfort (Bluyssen, 2009)

Wind flow based roof design can make it possible to create a smart efficient cooling roof, that will be provide ultimate semi-indoor thermal comfort. The most feasible cooling strategies based on wind and air movement are the following; (Sofotasiou, Hughes & Calautit, 2014)

°evaporative mist-cooling (see fig. 25.1)

°down-draft evaporative cooling (see fig. 25.2)

Solar radiation can be used to drive solar powered cooling strategies as the following;

°solar sorption cooling (see fig. 25.3).

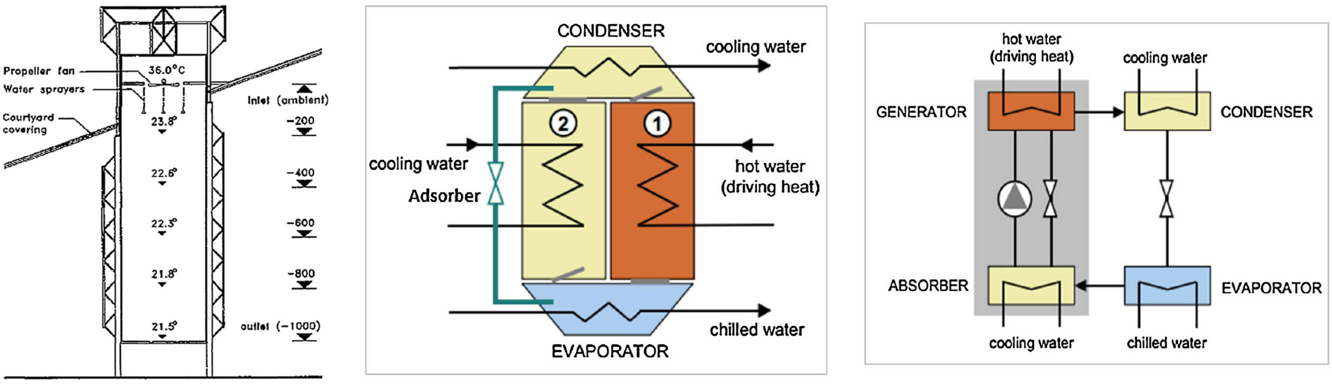

Fig. 25: Principle sketches (1) downdraft evaporative cooling, (2) evaporative mist-cooling and (3) solar sorption cooling (Sofotasiou, Hughes & Calautit, 2014)

4.2.1 LIGHTING IN RELATION TO NATURAL TURF

In modern day artificial turf becomes more common to use, however natural turf is still preferred, because of its game and player friendliness. Natural turf is easier to play on and players are less prone to injuries. (Tolloczko & Clarke, 1999) Since there is still a great demand for natural grass as turf, designers and turf engineers face major challenges on designing stadia with the right lighting quality to maintain health of the turf. Some stadium design advances are open stadia, half open stadia, retractable roof systems, transparent roofs, translucent roofs, etc.
For a workable natural turf, it is not only about the healthy appearance of the grass, but also its resistance to vibrations and response to fast healing. The two basic demands for high quality grass are photosynthesis (sunlight) and exchange of O_2 and CO_2 (ventilation). The most important demand is the amount of sunlight exposure. Therefore, the designers/engineers need to meet solar grass requirements.
As mentioned, photosynthesis is needed to grow grass, but in sunlight only a certain amount of the light spectrum can generate photosynthesis. About 45% of the total energy picked up by the sun is active for photosynthesis, also called PAR (Photosynthetically Active Radiation). PAR is comparable with the light a human being can receive visually (see fig. 27).

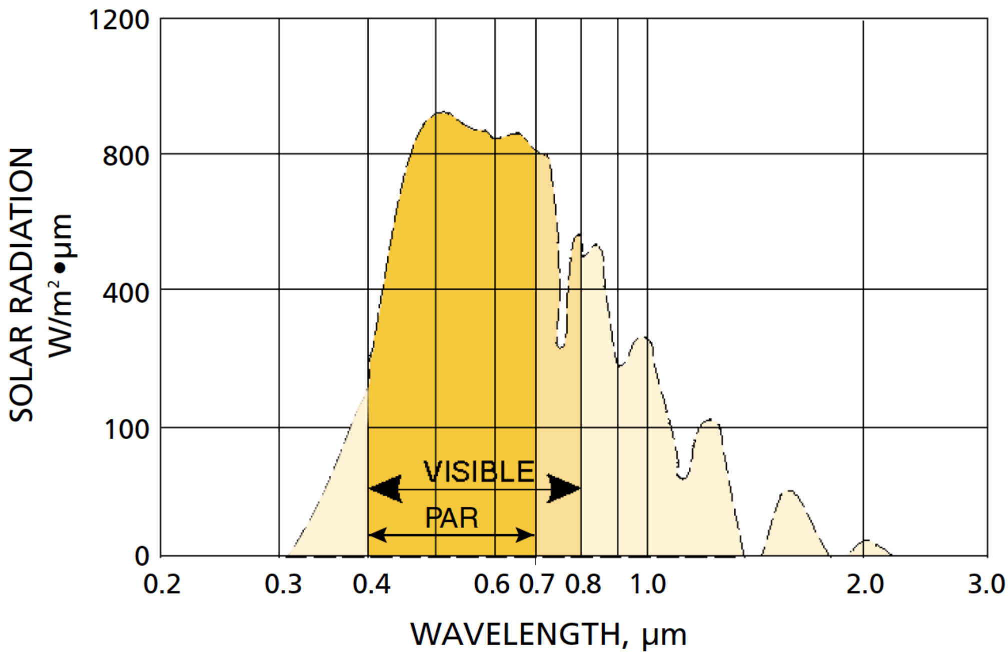

Fig. 26: PAR wavelength (Gamble, Soligo & Hunter, 2007)

From the grass perspective, PAR can be received through either direct sunlight on the pitch and/or diffuse sunlight which reflects from clouds or goes through translucent materials. Non-transparent and translucent materials that create shadow on the natural turf restrict the PAR and causes irregular grass growth. To prevent inconveniences, turf consultants generate 3D algorithmic computer tests, where they can determine the amount of PAR received by a pitch on a day (see fig. 27). (Danks, Good, & Philips, 2007) Where the standard requirement of daily PAR exposure is 3 MJ/m^2 (1. 4 Wh/m^2). With running these tests in an early design stage, poor grass growth can be prevented. (Gamble, Soligo, & Hunter, 2007)

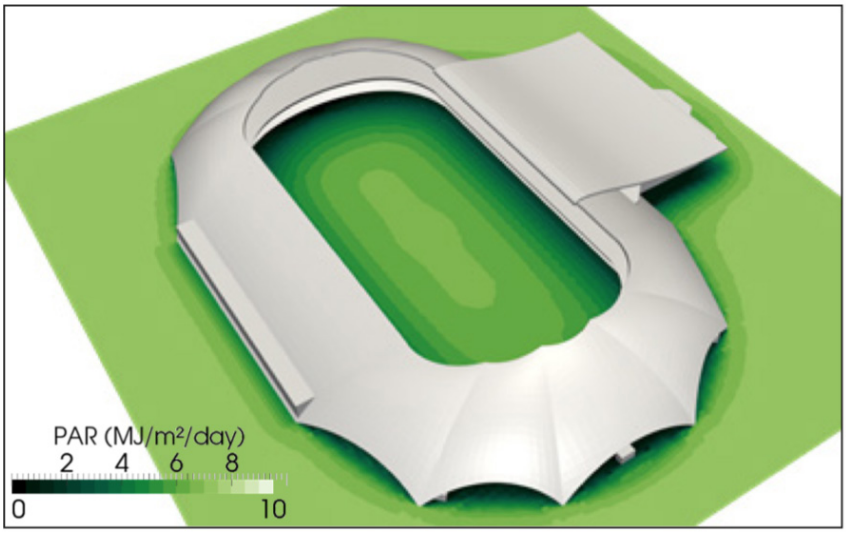

Fig. 27: Computational model shadow and PAR analysis (Danks, Good & Philips, 2010)

4.2.2 CHALLENGES LIGHTING QUALITY KIS

The challenges for the KIS in the field of lighting in relation to natural turf are to be very carefully combined with the demands of the aerothermal quality of the stadium. The turf needs to meet a certain amount of PAR, but too much solar radiation can lead to aerothermal discomfort. To prevent at both aspects unexpected inconveniences, the challenge is to run tests at a very early design stage where both issues merge into one solution. To determine the amount of PAR coming from the sun and/or the skies in general, the following equation can be used to make a good estimation.

$$PAR = 0.45 \cdot L_{e,\Omega} \left[\frac{Wh}{m^2}\right]$$

Where :
$L_{e,\Omega}$ = the radiant flux emitted, reflected, transmitted or received by a surface in Wh/m^2

However, the amount of PAR fluctuates throughout the year, meaning that the amount is dependant on different factors. These factors are the type of season and the presence of overcast. In the table below under the heading of Sun and Sky, the difference in the amount of PAR between overcast and the different seasons can be seen (see fig. 28). The overcast situation is in every season pretty much the same, while with clear wheather the amount of PAR in summer is 79. 47 mol PAR/day (17.4 Wh/m^2/day), which is ca. twice as high as in winter. (Navvab, 1999)

Table 4—Summary of average Photosynthetically Active Radiation (mol-PAR/day) from the sky and sun beam components using the daylight availability data of the location.

Sky	molPAR/Day	Sun	mol PAR/Day	Sun and Sky	mol PAR/Day
Overcast	11.30	Overcast	1.44	Overcast	12.74
Winter	17.65	Winter	18.43	Winter	36.08
Fall	12.78	Fall	39.42	Fall	52.21
Summer	26.06	Summer	53.41	Summer	79.47

Fig. 28: Table amount of PAR based on different aspects (Navvab, 1999)

4.3.1 ACOUSTICS IN STADIA

Since stadiums for the World Cup in Qatar are highly occupied, high noise issues have to be dealt with. Noise implies all aspects of acoustical quality, meaning from pleasant to unpleasant sound. Not only the stadium noise, but also the external noise influences have to be considered in acoustical design. Aspects of the acoustics of a stadium enclose the environmental noise, vibration, internal noise, reverberation time, sound absorption and the speech intelligibility (see fig. 29). (Bluyssen, 2009)

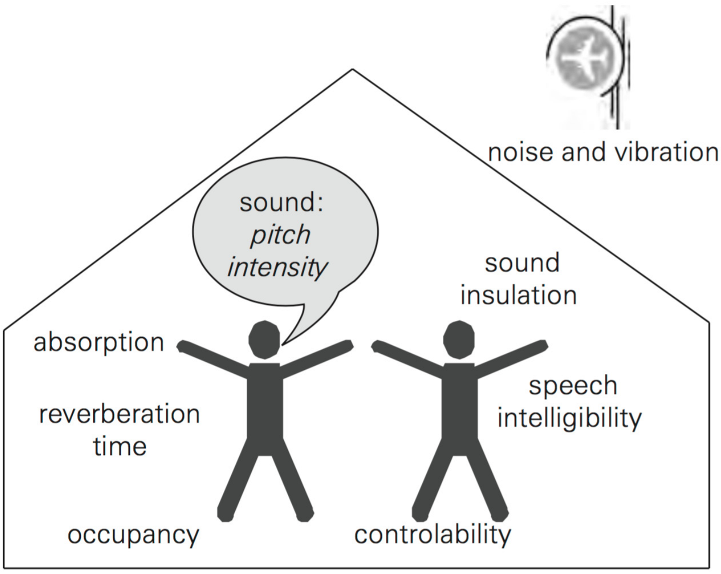

Fig. 29: Aspects of Acoustical quality (Bluyssen, 2009)

With accommodations as stadiums, with a plausible volume of ca. 1,000,000 m^3, the dimensions are so large, that the delay of sound reflections have to be considered in the acoustical calculations. The following chart shows the relation between space sizes and reverberation time (see fig. 30).

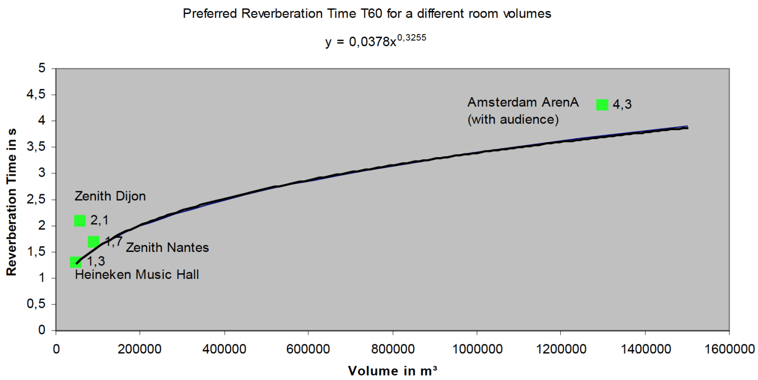

Fig. 30: Examples of reverberation times of large public spaces (Lautenbach, Heringa & Vercammen, 2007)

A relatively hard reflection, which reaches the ear just 50ms after the direct sound, is received as an echo. The delayed reflection can be disturbing for the room occupant, especially in large spaces where the reflection delays even more (more echo). The bigger the space, the longer relatively hard, high energetic reflections arrive at the occupant's ear. The reflection has to be -10 dB to not turn into an echo and disturb the occupants (see fig. 31). To get the reflection at a level of -10 dB, the intensity of the delayed sound has to be 10% of the incoming intensity and the absorption must be 90% or more. (Lautenbach, Heringa, & Vercammen, 2007)

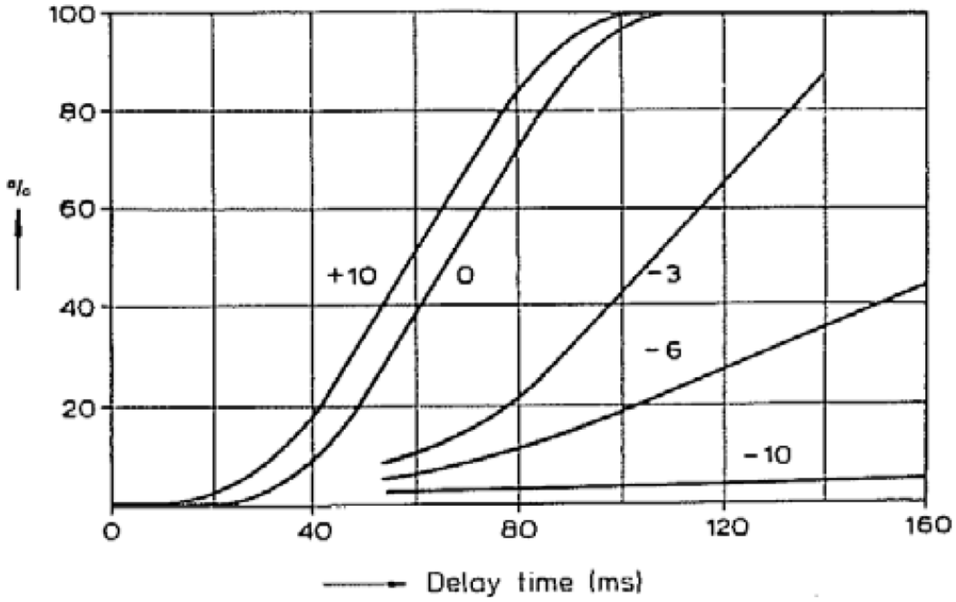

Fig. 31: Amount of reflection in relation to time delay (Lautenbach, Heringa & Vercammen, 2007)

4.3.2 CHALLENGES ACOUSTICAL QUALITY KIS

The design of a stadium has the challenge to repress large scale first order delayed sounds (reflections). Those challenges can be tackled by designing complex sound absorbing geometries or using loads of absorbing materials. For all considerations, the average absorbing coefficient has to be 0.9 in a frequency between 63-4000 Hz. Using the following equation the right amount of absorption in relation to a space's volume can be calculated. Ideal reverberation times are in between 1 and 3 seconds. (Lautenbach et al., 2007)

$$T = 0.166 \cdot \frac{V}{A} \text{ [s]}$$

With

V = Building volume in m^3
A = Absorption surface in m^2

Beyond the 1-3 second rule, the roof can be an enhancer of good forward sound reflection. Forward sound reflection is the type of reflection that does not get experienced as an echo. (Luxemburg, Hak, Heijnen, & Kivits, 2009) Forward sound reflection can improve the stadium atmosphere, which can effect the spectators' and players' experience in a positive way. The way to make a roof a forward reflective enhancer is to use absorbing materials at the rear areas of stadium stands. This way, the sound waves cannot reflect back at the end of the wave's journey. In the computational model below is shown how sound waves are analysed and what the impact of adding absorbing materials is (see fig. 31). (Culley & Pascoe, 2015)

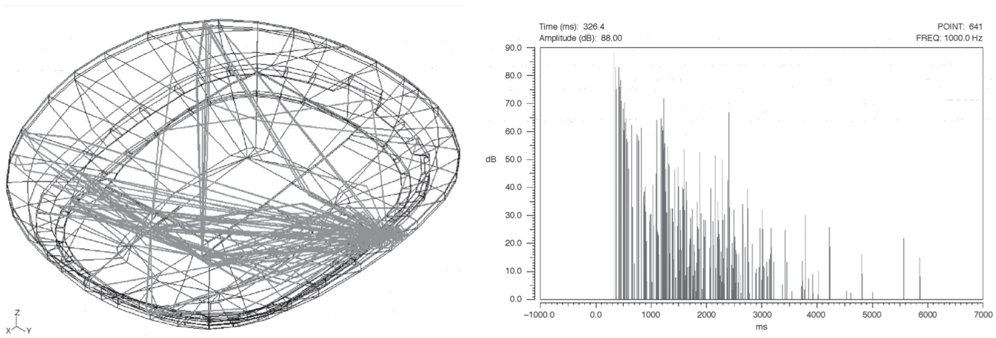

Fig. 32: Computational acoustical anlysis with accessory chart (Culley & Pascoe, 2015)

General:

°According to the QFA, the maximum microclimate temperature has to be **20-26 °C**

°According to FIFA, the transparency/translucency level has to be **>80%**

Aerothermal Quality:

°According to *Bouyer et. al, 2007*, the ψ_i has to between **1.0 and 1.5** in relation to the geometrical influence of the stadium roof. Therefore:

$$\psi_i = \frac{U_i + \sigma_i}{U_{ref} + \sigma_{ref}} \quad with \; 1.0 < \psi_i < 1.5$$

°According to *Bluyssen, 2009*, the draught rate in relation to the turbulence occurring on a human body has to be **less than 25%** for a category C building (large public buildings). Therefore:

$$DR = (34 - t_a) \cdot (v_a - 0.05)^{0.62} \cdot (3.14 + 0.37 \cdot T_u \cdot v_a) \quad with \; DR < 25\%$$

Lighting Quality:

°According to *Gamble et. al*, the average daily PAR has to be **1. 4 Wh/m² (3 MJ/m²) or higher.** Therefore:

$$PAR = 0.45 \cdot L_{e,\Omega} \quad with \; PAR > 1.4 \, \frac{Wh}{m^2}$$

Acoustical Quality:

°According to *Luxemburg et. al*, the sound reflection has to be **forward.**

°According to *Lautenbach et. al*, the optimal reverberation time for large arenas and stadiums is between **1 and 3 seconds.** Therefore:

$$T = 0.166 \cdot \frac{V}{A} \quad with \; 1.0s < T < 3.0s$$

These restrictions are the guideline to constantly test the design of the roof in relation to the Semi-Indoor Environmental Quality.

5. THEORY RESEARCH STRUCTURAL DESIGN

This chapter discusses the possibilities of large span structures applied to stadium roofs. Starting with the possibilities of applying steel as a primary structure followed by a comprehensive explanation on the use of glass roofs in the architectural practice. The third part of this chapter discusses different types of glass, glass production and glass treatments. At the end, the last chapter discusses two different types of smart hybrid glass structures that can be applied on the primary steel structure for the stadium. The purpose of this is chapter is researching the maximum possible span with glass as a secondary structure within the primary steel structure. This way the primary structure can be executed with a minimum amount of steel, while the secondary structure will supply maximum transparency/translucency and seek for its maximum span possible.

5.1 STEEL AS PRIMARY STRUCTURE

Use of structural steel in stadium engineering is often used as primary structure. The main reason of using steel is its high level of Yield (f_y) and Tensile strength (f_u) (see fig 33a). Meaning that steel offers the follow structural advantages: (Culley & Pascoe, 2015)
˚High weight/strength ration and can be used easily for large spans in an economical way.
˚Clear floor areas can be achieved.
˚Long term integrity when subjected to dynamic loading, because of high ductility.
˚Steel frameworks afford a light and strong material for fixings, which will tolerate a wide range of cladding materials.

Steel grade and subgrade	f_y: N/mm^2 Nominal thickness of element, t: mm $t \le 16$	$16 < t \le 40$	$40 < t \le 63$	$63 < t \le 80$	f_u: N/mm^2 Nominal thickness t: mm $3 \le t \le 100$
S275JR					
S275J0	275	265	255	245	410
S275J2					
S355JR	355	345	335	325	470
S355J0					
S355J2					
S355K2					
S355JOH	355	345	335	325	470
S355J2H					
S355K2H					

Fig. 33a: Strength values steel (Culley & Pascoe, 2015)

The strength of steel is determined by different structural shapes that can be used for different structural purposes. The following table gives an enumeration of different shapes with their different possibilities (see fig. 33b)

Mechanical properties:

Density: 7715 KG/m^3
Young's Modulus: 210 GPa
Shear Modulus: 79.3 GPa
Tensile Strength: 470-630 MPa
Yield Strength: 335 MPa
Compressive Strength: 170-310 MPa
Poisson's Ratio: 0.3
Thermal Conductivity: 13-17 W/mK (25˚C)
Expansion Coefficient: 15-18 x 10^{-7}/˚C

(Culley & Pascoe, 2015)

Shape		UK size range: mm	Use
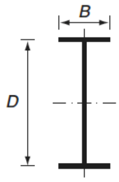	Universal beam (UB)	*B* × *D* × kg/m 127 × 76 × 13 to 1016 × 305 × 487	Beams
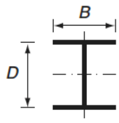	Universal column (UC) H-pile Bearing piles	152 × 152 × 23 to 356 × 406 × 634	Columns Shallow beams Heavy truss members
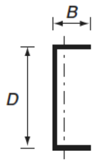	Parallel flange channel (PFC)	100 × 50 × 10 to 430 × 100 × 64	Bracings, ties Small beams
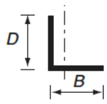	Equal angle (UKA)	*B* × *D* × *t* 90 × 90 × 7 to 200 × 200 × 24	Bracings Truss members Purlins Sheeting rails
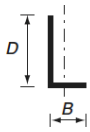	Unequal angle (A)	100 × 65 × 7 to 200 × 150 × 18	
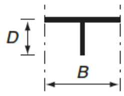	Structural tee (T)	*B* × *T* × kg/m (UB) 133 × 102 × 13 to 178 × 102 × 37 (UC) 152 × 76 × 12 to 305 × 152 × 79	Truss chords Plate stiffeners
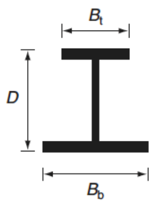	Asymmetric Slimflor beam (ASB)	280 ASB 74 to 300 ASB(FE) 249	Structural floors
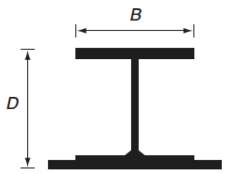	Slimflor beam (SFB)	152 × 152 × 64.4 to 354 × 406 × 707.4 kg/m	Structural floors
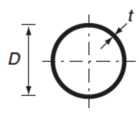	Circular hollow sections (CHS) and tubes	*D* × *t* 21.3 × 3.2 to 508 × 16 Tubes up to 2134 × 22:2	Columns Truss members Bracings, piles
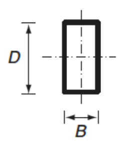	Rectangular hollow sections (RHS)	*D* × *B* × *t* 50 × 30 × 3.0 to 500 × 300 × 20	Columns Warren girders Vierendeel girders
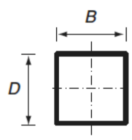	Square hollow sections (SHS)	40 × 40 × 3:0 to 800 × 800 × 60	As above
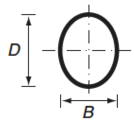	Oval sections	H × B × *t* 150 × 75 × 4.0 to 500 × 250 × 16	Architectural features

Fig. 33b: Structural shapes (Culley & Pascoe, 2015)

This chapter discusses the evolution of the glass roof in buildings. Discussing three types of *structural glass* and *structural glazing*: planar, single curved and double curved, the chapter will guide you through the typology of each structure and their climate qualities. Meaning that the typologies will discuss the most common ways of building such structures and the climate qualities will give insight in weather protection, solar shading, ventilation and acoustic comfort.

5.2.1 PLANAR ROOF STRUCTURES

The planar glazed roof defines itself functionally as a glass courtyard (see fig. 34a), used to give people an outside feeling with comfortable indoor climate qualities in small public buildings. The courtyard serves to enlighten the building and to connect spaces surrounding the courtyard. Making the glass courtyard a quiet transfer zone within buildings.

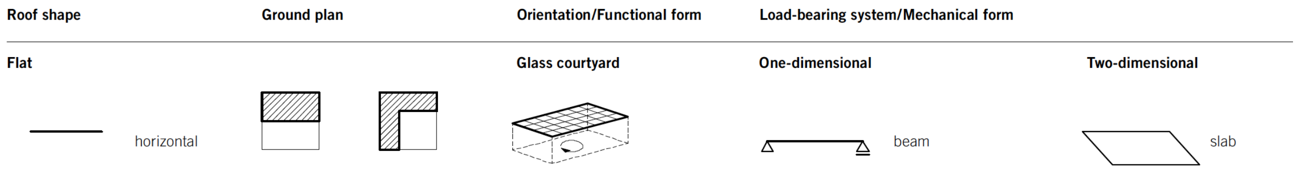

Fig. 34a: Characteristics planar glass roof (Wurm, 2007)

Structurally the planar roof is profiled as a one-dimensional system (see fig. 34b). Most conventional structural systems are carried out with beams made from steel with large glass cladding attached to it, also known as *structural glazing*. Meaning for load bearing steel structures that the possible span of glass panels is determinative for the distance between the primary beams or trusses, which results in deciding if secondary beams are needed in the load bearing structure. Reasonably lightweight primary steel structures can span up to 20 metres. However, recent developments show that beams can be made from glass with just the connections made out of steel, known as *structural glass*. For load bearing glass structures the maximum span possible is determinative for using glass beams for glass courtyards. The maximum span of glass depends on the amount of tension occurring in the beam. The larger the span, the larger the bending moment, the larger the occurring tension. Meaning glass beams with a reasonable weight limit to spans of ca. 10m. In short, the structural span decides whether the load bearing structure can be made out of glass or steel. (Wurm, 2007)

Fig. 34b: Structural glazed courtyard (left) & structural glass grid (right) (Wurm, 2007)

5.2.1.1 DESIGN CHALLENGES

Weather protection:

A planar glass roof can turn into a rainwater collector, which can result in unwanted live loads (see fig. 35). Therefor a slight slope in the roof should be taken into account. (Wurm, 2007)

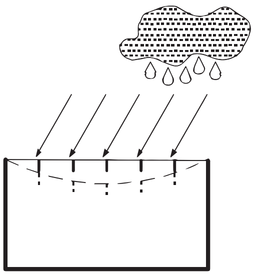

Fig. 35

Solar shading:

To protect a planar glass surface from sun, reflective metal blinds can be used on the inside or be considered in the design of the roof itself (see fig. 36). (Wurm, 2007)

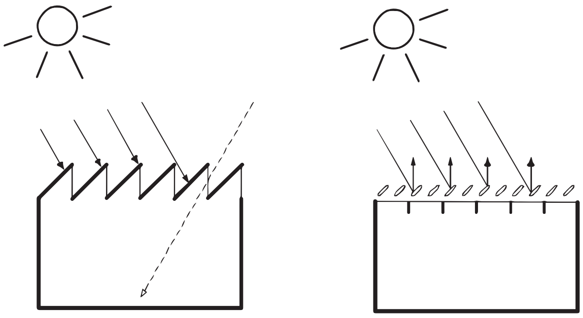

Fig. 36

Ventilation:

In combination with the integrated sun blinds, operable glass panels can be designed to naturally or hybrid ventilate (see fig. 37). (Wurm, 2007)

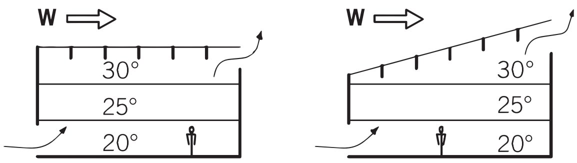

Fig. 37

Acoustic comfort:

As well as the ventilation and solar shading, operable glass panels can help reduce reverberation times that usually occur when reflected from hard flat surfaces (see fig. 38). (Wurm, 2007)

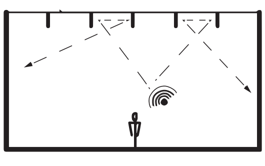

Fig. 38

5.2.2 SINGLE CURVED ROOF STRUCTURES

The single curved roof defines itself functionally as a glass band (see fig. 39a), used to protect large open public spaces from the weather. Unlike the glass courtyard, the glass band is used for places of traffic (walkers, bikers, cars & trains), like train stations, car terminals and arcades. Due to the single curvature it is possible to make much longer spans than the planar glass structures. Resulting the glass band to be mostly used as a transfer zone for large public traffic spaces (see fig. 39b).

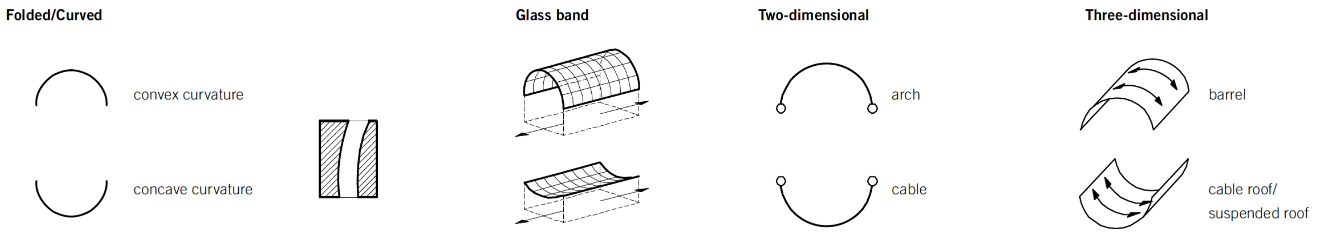

Fig. 39a: Characteristics single curved glass roof (Wurm, 2007)

Single curvatures in structures are defined as two-dimensional structure systems. The reason why larger spans are possible is because the arch form adapts to the natural flow of forces in the axis line of the cross section (see fig. 39a). Meaning that the effect of the single curvatures causing minimum bending stresses, resulting in use of less material. The form of the arch influences the ratio of tension and compression in the beam profile, meaning the larger the divergence between the axis line of the cross-section and the arch geometry, the larger the bending stress will get. (Froli & Lani, 2010) The arch geometry will be determinative on the use of glass (*structural glass*) or steel (*structural glazing*) as the load bearing structure. In resemblance with the planar glass roof, the spacing between the primary arches depend on the maximum span of the used glass cladding and if the use of secondary beams is needed. In short, for both materials, glass and steel, much larger spans can be made than with single curved structures. *Structural glazed* arches can span up to ca. 50 metres, while *structural glass* arches limit to ca. 15 metres. (Wurm, 2007)

Fig. 39b: Structural glazed barrel-vault (left) & Structural glass arch (right) (Wurm, 2007)

5.2.2.1 DESIGN CHALLENGES

Weather protection:

With a single curved glass surface, water can pour down the longitudinal sides of the roof. Preventing the water to pond on the roof. (see fig. 40). (Wurm, 2007)

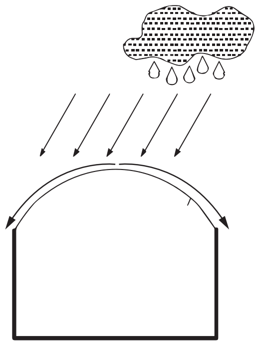

Fig. 40

Solar shading:

Because of the single curvature the sun blinds can be easily integrated in the roof structure. (see fig. 41). (Wurm, 2007)

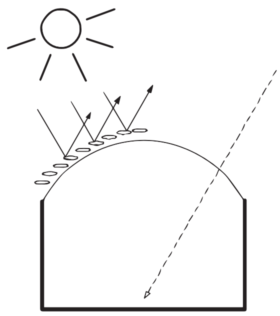

Fig. 41

Ventilation:

Single curved surfaces can improve the thermal flotation of natural/hybrid ventilation (see fig. 42). (Wurm, 2007)

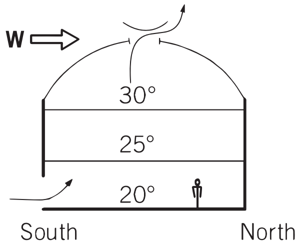

Fig. 42

Acoustic comfort:

Single curved surfaces extend the reverberation time and enhances the indoor loudness. Acoustic measures can be integrated in the structure, combined with the solar shading (see fig. 43). (Wurm, 2007)

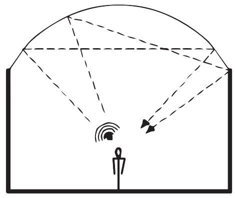

Fig. 43

5.2.3 DOUBLE CURVED ROOF STRUCTURES

The double curved roof defines itself functionally as a glass core (see fig. 44a). The double curved structure is often used to cover large open spaces where lighting is needed, like large concert halls, stadiums and arenas. Because of the double curvature, the glass core is possible to span even larger spaces than the glass band. This way large spaces, which are normally outside, can be protected from the weather, but still foresee the space of enough natural light (see fig. 44b).

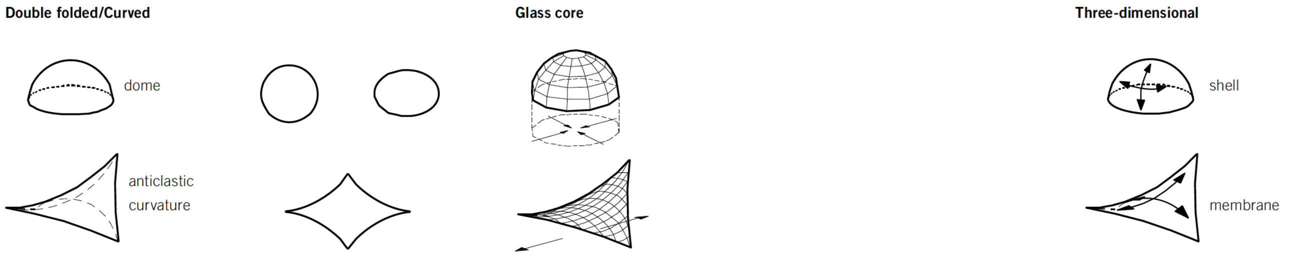

Fig. 44a: Characteristics double curved glass roof (Wurm, 2007)

The glass core is defined as a three-dimensional structure system, meaning that all the loads are transferred in the direction of the meridian and the perimetre (see fig. 44a). Because of a three-dimensional load transfer the area of a dome is only based on axial and/or normal forces, which means that there are almost no bending moments occurring. No bending moments can make the structure very slim as well as with steel (*structural glazing*) as glass (*structural glass*). (Wurm, 2007) Making spans of up to 80 metres possible with steel and up to 25 metres with glass. If the dome has the correct form and the load bearing system is supported correctly, the forces along the meridian will result completely in compression and the forces along the perimetre in tension. This makes it possible to make larger spans of glass cladding between the primary beams, since glass is very strong on compression. In short, even larger spans can be made, especially with steel, but more importantly, spacing between beams can be made bigger. (Veer, Wurm, & Hobbelman, 2003)

Fig. 44b: Structural glazed grid dome (left) & Structural glass plate shell (right) (Wurm, 2007)

5.2.3.1 DESIGN CHALLENGES

Weather protection:

Double curved surfaces can, dependent on the form, pour water down equally over the surface. Meaning live loads from rainwater will be equally divided (see fig. 45). (Wurm, 2007)

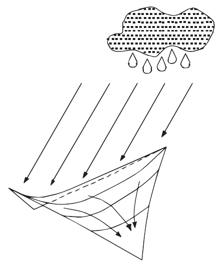

Fig. 45

Solar shading:

In comparison with the single curved roof, sun blinds can also be integrated in the roof structure of the double curved structure. Otherwise, the dome can have a movable sun shading on the outside (see fig. 46). (Wurm, 2007)

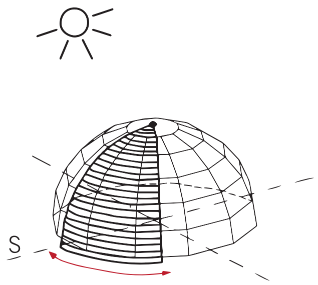

Fig. 46

Ventilation:

Double curved surfaces can enhance the air circulation through the dome, which results in easier manageable natural ventilation (see fig. 47). (Wurm, 2007)

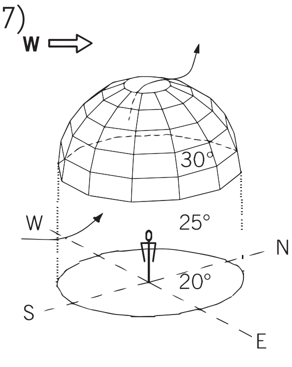

Fig. 47

Acoustic comfort:

Same as single curved surfaces, double curved surface extend the reverberation time and enhances the indoor loudness as well. Acoustic measures can be integrated in the structure, combined with the solar shading (see fig. 48). (Wurm, 2007)

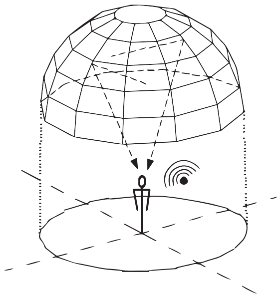

Fig. 48

This chapter compares two different types of glass that are applicable for the building industry. The first is soda-lime-silica, also know as basic glass, a glass type that covers 80% of the glass use in the architectural practice. The other type is alkali-aluminosilicate, which is a new type of glass, mainly used in the electronics industry. However, because of its incredible strength and lightweight a lot of research is conducted to implement alkali-aluminosilicate as a construction and structural material in the architectural practice. (Wurm, 2007) Next to the types of glass 2 different production techniques are discussed: floating (most common, especially for soda-lime-silica) and overflow (special technique, especially for alkali-aluminosilicate) Finally and adjacent to the production techniques, the most common thermal treatments for strengthening glass, namely tempering and chemical strengthening are being discussed.

5.3.1 SODA-LIME-SILICA

Soda-lime-silica covers 85% of all produced glass and is mostly used for windows in the building practice. Soda-lime-silica is used that often, because of its chemical stability and workability. The glass is very easy in maintenance, it can be constantly recycled without decreasing its mechanical strength. (Wikipedia, 2016c)

Mechanical properties:

<u>Density:</u> 2500 KG/m^3
<u>Young's Modulus:</u> 72 GPa
<u>Shear Modulus:</u> 30 GPa
<u>Tensile Strength:</u> 45 MPa
<u>Compressive Strength:</u> 500 MPa
<u>Poisson's Ratio:</u> 0.23
<u>Thermal Conductivity:</u> 1 W/mK (25˚C)
<u>Expansion Coefficient:</u> 90×10^{-7}/˚C

(NSG, 2013)

5.3.2 ALKALI ALUMINOSILICATE

Alkali aluminosilicate contains a high content of alkali ions. These ions increase pressure in the chemical composition of the glass, resulting in an increase of compression strength on the surface of the glass. Because of its strength the glass is much harder and resistant to scratches. Making this glass type high in demand in the smartphone industry. (Wikipedia, 2016b)

Mechanical properties:

<u>Density:</u> 440 KG/m^3
<u>Young's Modulus:</u> 71.7 GPa
<u>Shear Modulus:</u> 29.7 GPa
<u>Tensile Strength:</u> 800 MPa
<u>Compressive Strength:</u> 900 MPa
<u>Poisson's Ratio:</u> 0.21
<u>Thermal Conductivity:</u> 1.6 W/mK (25˚C)
<u>Expansion Coefficient:</u> 84.5×10^{-7}/˚C

(Abrisa, 2014)

5.3.3 FLOATING

Floating glass is a production method that is very commonly used in the glass industry. It works as follows: The materials that are needed to make the glass are mixed together and melted at a temperature of 1600˚C. After the melting, the molten glass runs through a 50-metre bath of molten tin to flatten the glass. After flattening the glass floats and solidifies at approximately 600˚C. After solidification, the glass gets coated cooled, inspected and last but not least cut (see fig. 49). (Simoen, 2016)

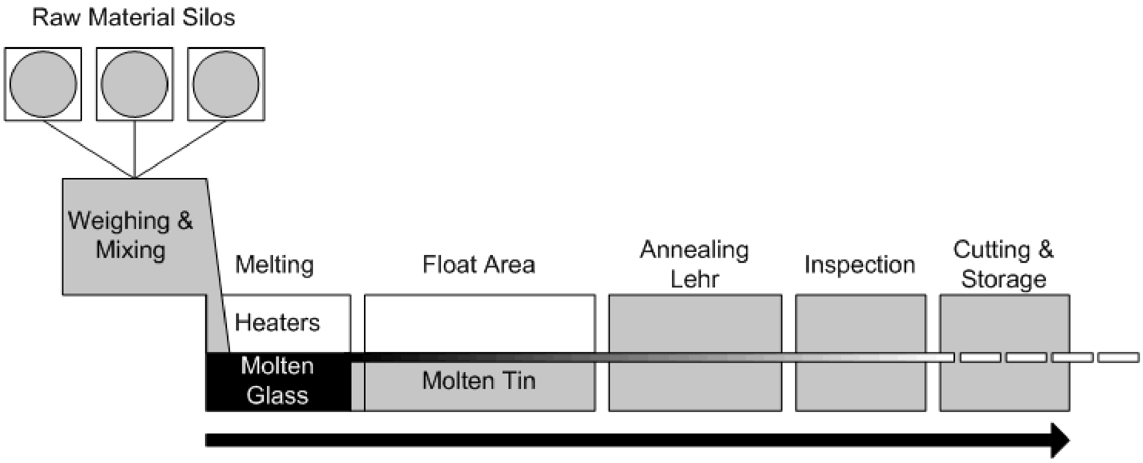

Fig. 49: Float glass process (Tangram Technology, 2010)

5.3.4 OVERFLOW

The overflow fusion draw process is a vertical stretching production process. The raw materials get mixed and melted. The molten glass gets poured into a v-shaped volume which, when completely filled, overflows simulta-neously one both sides and come together at the bottom of the volume to flow down into a glass panel (see fig. 50). With overflowing the glass does not come in contact with solid materials, meaning the molecular structure remains high on tension strength. This progress is based on old glass casting methods and very applicable for producing extremely thin glass panels (0.025-0.1mm). (Schneider, 2015)

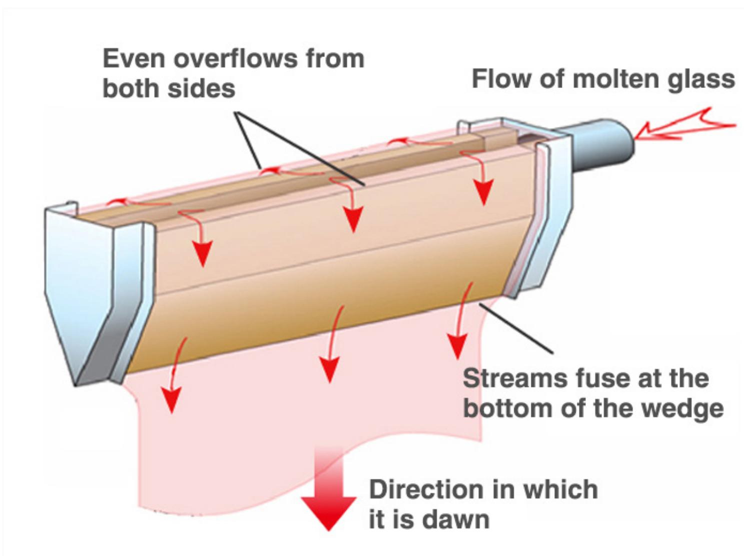

Fig. 50: Overflow glass process (Schneider, 2015)

5.3.5 TEMPERING

Tempered glass can be divided in two types of tempering: fully tempered safety glass and heat strengthened glass. Tempering of glass ensures a fast cooling process on the outer layer and a slow cooling process on the inner layer of a glass panel, resulting in a pre-stressed outer layer of compression and a pre-stressed inner layer of tension (see fig. 51). Such a heat treatment influences the tension and compression strength, however the other mechanical and chemical properties stay unaffected. To make tempering possible, the glass panel has to be at least 4mm thick. (Wurm, 2007)

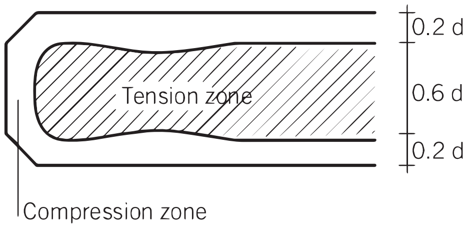

Fig. 51: Compression Tension zones tempering treatment (Wurm, 2007)

Because of the ratio in speed of cooling, fully tempered safety glass is thermally and mechanically stronger than heat strengthened soda-lime-silica. Given another parabolic tension/compression pattern (see fig. 52).

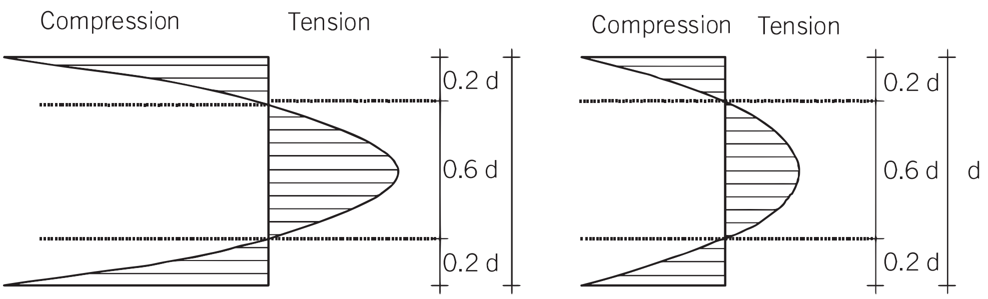

Fig. 52: Compression-tension ratio fully tempered safety glass (left) and heat strengthened glass (right) (Wurm, 2007)

The increased strength of fully tempered safety glass causes a crack pattern of very small glass particles, while heat strengthened give more predictable crack patterns. Both treatments have their advantages: small glass particles mean more fall safety, while large cracks give better structural insight (see fig. 53). (Guardian, 2014)

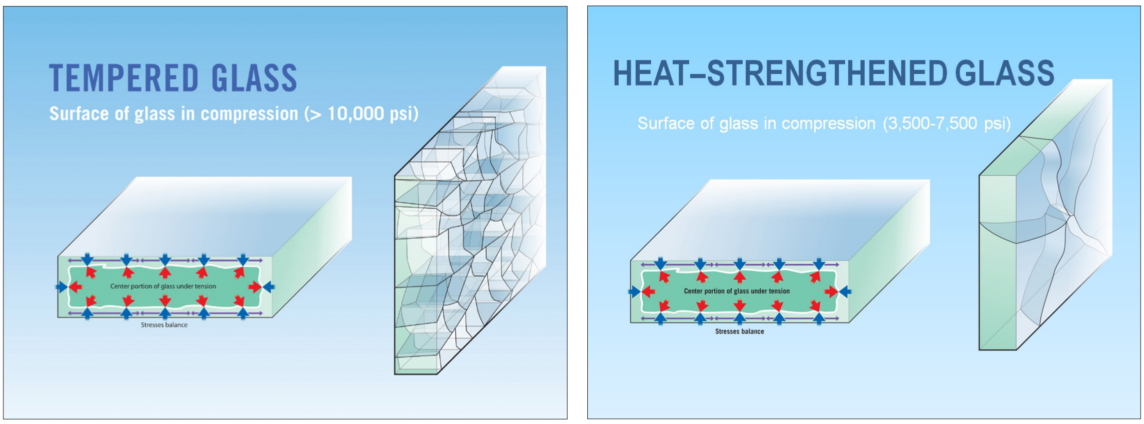

Fig. 53: Crack pattern fully tempered safety glass (left) and heat strengthened glass (right) (Glass Education Center, 2012)

5.3.6 CHEMICAL STRENGTHENING

Alkali-aluminosilicate contains a high content of sodium, meaning it can be pre-stressed chemically by steeping the glass in a hot bath of potassium chloride (see fig. 54). (Overend, Butchart, O'Callaghan, Lambert, & Prassas, 2013)

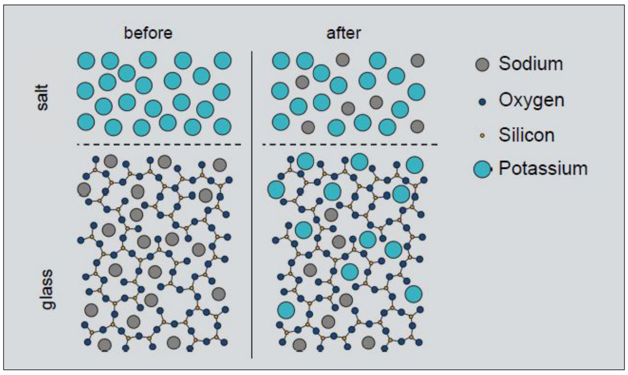

Fig. 54: Process of chemical strengthening (Glass education Center, 2012)

This process will cause through ion exchange densification of the molecular composition, resulting in large compressive stresses on the outer layer of the glass (see fig. 55). (Johnson, 2014)

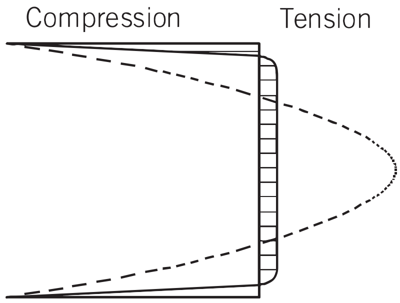

Fig. 55: Compression-tension ratio chemically strengthened glass (Wurm, 2007)

Meaning that overflow Alkali-aluminosilicate gets a very large tensile strength, which makes the glass very bendable. Chemical strengthening only influences the tensile and the compressive strength of the glass and will not influence the stiffness. (Hödemann & Anton, 2016) This chemical process can be applied on a wide range of thicknesses (0.05mm to 20mm) and complex shapes (single, double curved, convex and concave) (see fig. 56). (Wurm, 2007)

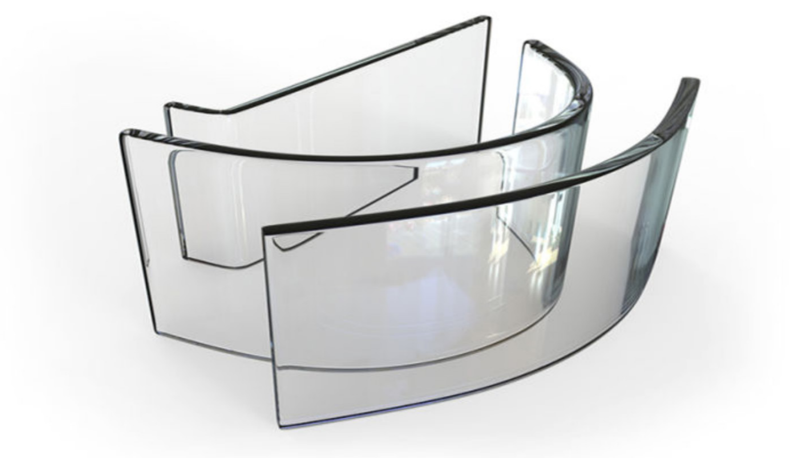

Fig. 56: Chemical strengthening possible with differen shapes (Abrisa, 2014)

From a wide range of glass structures this chapter discusses the most applicable glass structures for the Khalifa International Stadium. Both single curved hybrid lightweight glass structures: The glass barrel-vaulted shell and the hybrid glass arch (see fig. 57). Both applicable as large span secondary structures.

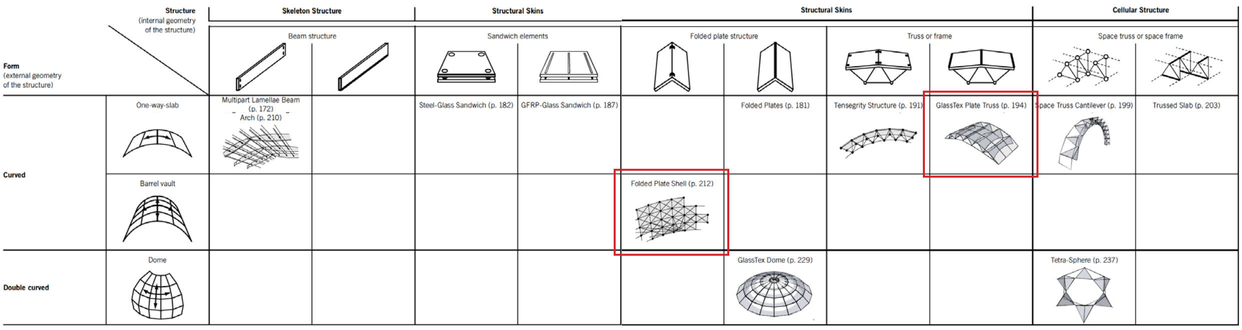

Fig. 57: Types of curved glass structures (Wurm, 2007)

5.4.1 GLASS BARREL-VAULTED SHELL: MAXIMILIANMUSEUM, AUGSBURG

Augsburg's Maximilianmuseum has a historical courtyard that needed to be protected against extreme weather conditions. Next to the weather protection, the museum needed to create more space for exhibitions, without losing the architectural expression of the existing renaissance building. Therefore, in the year 2000, a glass barrel-vaulted shell was designed to protect the courtyard, covering an area of 13.5x37 metres (see fig. 58). (Detail-online, 2001)

Fig. 58: Maximilianmuseum, Augsburg (Detail-online, 2001)

5.4.1.1 STRUCTURAL BEHAVIOUR

The structural behaviour of a barrel-vaulted shell can be divided in two different directions (x- and z-axis) (see fig. 58a). The x-axis is quite similar to the behaviour of a regular profiled beam. Namely, the top edge is mostly in compression, while the bottom edge is in tension (fig. 58b). While the z-axis behaviour is similar to that of an arch (see fig. 58c).

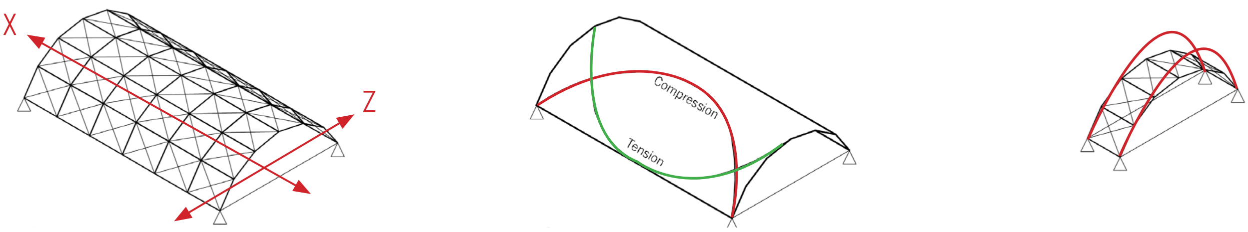

Fig. 59: Structural axes (1), x-axis structural behaviour (2), z-axis structural behaviour (3) (Wurm, 2007) (Andrejevic, 2016)

The barrel-vaulted shell stabilises by diagrid net of prestressed steel cables. The steel cables are connected with cubic shaped nodes to the glass panels. The clamping nodes make sure all the differential forces are transferred through the cables. This way the nodes take care of the mechanical interlock between different connections. Meaning that the glass panels act as structural elements absorbing most of the compression forces (see fig. 60). (Froli & Lani, 2010) (Wurm, 2007)

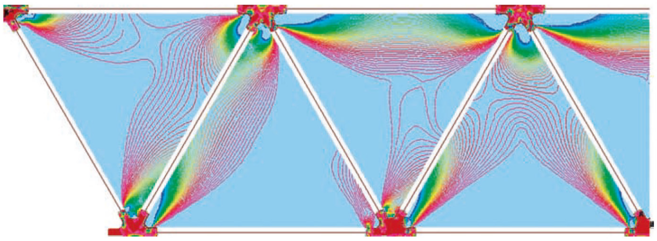

Fig. 60: Compression behaviour through glass panels (Froli & Lani, 2010)

5.4.2 HYBRID GLASS ARCH: PROTOTYPE OF A GLASS ROOF WITH INTEGRATED SOLAR SHADING

A hybrid glass arch called the GlassTex arch is the result of a design for the renovation of an old church. The goal of the design was to get diffuse natural daylight inside the church without the interior overheating from direct sunlight. To accomplish those demands, the roof structure had to be partly transparent and partly translucent. Therefore, the structural form finding resulted in a hybrid glass arch with fabric as sun shading. The prototype represented an arch with a span of 15 metres (see fig. 61). (Wurm, 2007)

Fig. 61: 1:4 Model solar shading intergrated glass structure (Wurm, 2007)

5.4.2.1 STRUCTURAL BEHAVIOUR

The top edge of the GlassTex arch is made out of flat glass plates connected to each other with hinged edge plinths. Meaning the structure is a folded plate arch, acting as a typical arch structure, where the glass elements absorb the compression forces (see fig. 62.1). To prevent inconveniences with live loads, such as wind and snow, the arch has to be stabilised with fabric panels placed in a truss wise disposition. This way the fabric connects to the glass panels and a cable on the bottom of the arch to absorb the tension forces (see fig. 62.2). Resulting in a hinged hybrid glass arch structure where the line of pressure under dead load shape towards the shape of the structure (see fig. 62.3). (Wurm, 2007)

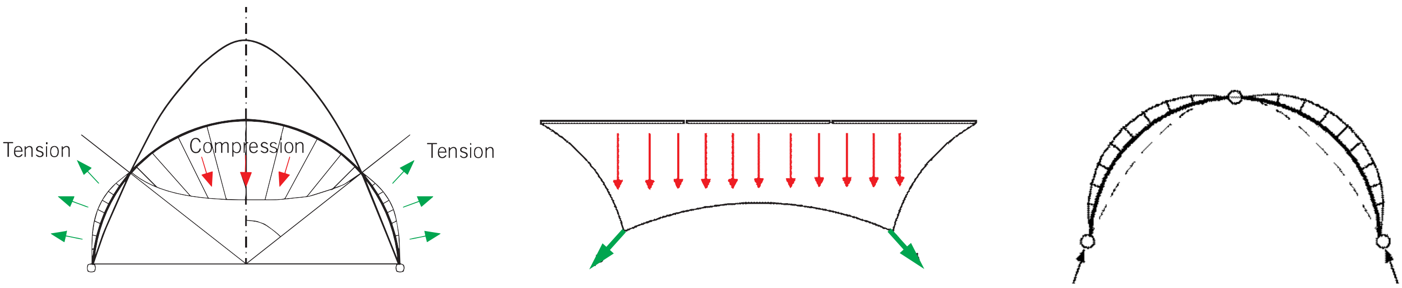

Fig. 62: Compression/tension behaviour arch (1), tension forces cable (2), hinged arch behaviour (3) (Wurm, 2007)

Planar roof structures:

°According to *Wurm*, *2007*, planar structural glazing roofs can reasonably have a span of approximately **20 metres.**

°According to *Wurm*, *2007*, planar structural glass roofs can reasonably have a span of approximately **10 metres.**

Single curved roof structures:

°According to *Wurm*, *2007*, single curved structural glazing roofs can reasonably have a span of approximately **50 metres**.

°According to *Wurm*, *2007*, single curved structural glass roofs can reasonably have a span of approximately **15 metres.**

Double curved roof structures:

°According to *Wurm*, *2007*, single curved structural glazing roofs can reasonably have a span of approximately **80 metres**.

°According to *Wurm*, *2007*, single curved structural glass roofs can reasonably have a span of approximately **25 metres.**

Types of glass:

°According to *NSG*, *2013*, soda-lime-silica has a tensile strength of **45 MPa**

°According to *Abrisa*, *2014*, alkali aluminosilicate has a tensile strength of **800 MPa.**

Thermal treatments of glass:

°According to *Guardian*, *2014*, fully tempering gives glass a surface compressive strength of >**70 MPa.**

°According to *Guardian*, *2014*, heat strengthening gives glass a surface compressive strength of **25-50 MPa.**

°According to *Abrisa*, *2014*, chemical strengthening gives glass a surface compressive strength of **165 MPa.**

6. ROOF DESIGN ANALYSIS

After determining the climate and structural restrictions, the total analysis can be conducted. Before starting with the analysis, a methodology has to be set to make sure that the design will be perfectly tuned between climate and structural demands. The regarding methodology works as shown in the figure on the next page (see fig. 64).
Most of the design and analysis process will take place in Rhinoceros+Grasshopper, with the help of several plugins (see fig. 63). However, to get realistic wind simulations, wind tunnel model tests were conducted to compare them to the computer analyses.
Starting with the climate analysis, 3 form findings from Rhino and Grasshopper will be put through a Computational Fluid Dynamics (CFD) analysis in Autodesk Flowdesign and a realtime wind tunnel model test. These analyses will run in Grasshopper with the help of the earlier named programme, that act as a Grasshopper plugin. The outcome of this plugin analysis is linked to Autodesk Flowdesign, which will generate data into useful values. To test the veracity of the CFD analysis, wind tunnel model tests are conducted to compare the methods. Finally, these values can be measured to the set climate design restrictions.
With a proper wind analysis, the best variant can be determined and used as input for the design of the primary steel structure. With designing a load bearing structure, the form and the structural behaviour needs to be understanded. With the help of Kangaroo and Karamba, which are both plugins for Grasshopper, a parametric optimisation can be made for the design of the primary structure.
After these analyses, the first actual form can be determined, where the next step is a heat and lighting analysis. These analyses will also run in Grasshopper with the help of the GECO. The outcome of GECO is linked to Autodesk Ecotect, which will generate data into useful values. The generated heat and lighting data can give an indication where the roof should be opened or closed, based on a certain heat and lighting input. The result of these inputs will be translated into a so called 'adaptive roof'. The adaptive roof gives a clear base to design the glass structure.
Same as with the primary structure, the heat and lighting analysis gives input for the design of the glass structure, that is going to span between the primary structure. This structure will also be tested on materialisation (CES Edupack), form behaviour (Kangaroo) and FEM (Finite Element Method) (Karamba) analysis. With the FEM analysis it is possible to calculate through the whole structure, giving a clear insight of the total structural behaviour of the roof. After a positive FEM analysis outcome, the final structural properties can be determined and translated into a design.
In the end, the final concept has to be the perfect balance between climate and structure and the right output to elaborate on the technical design.

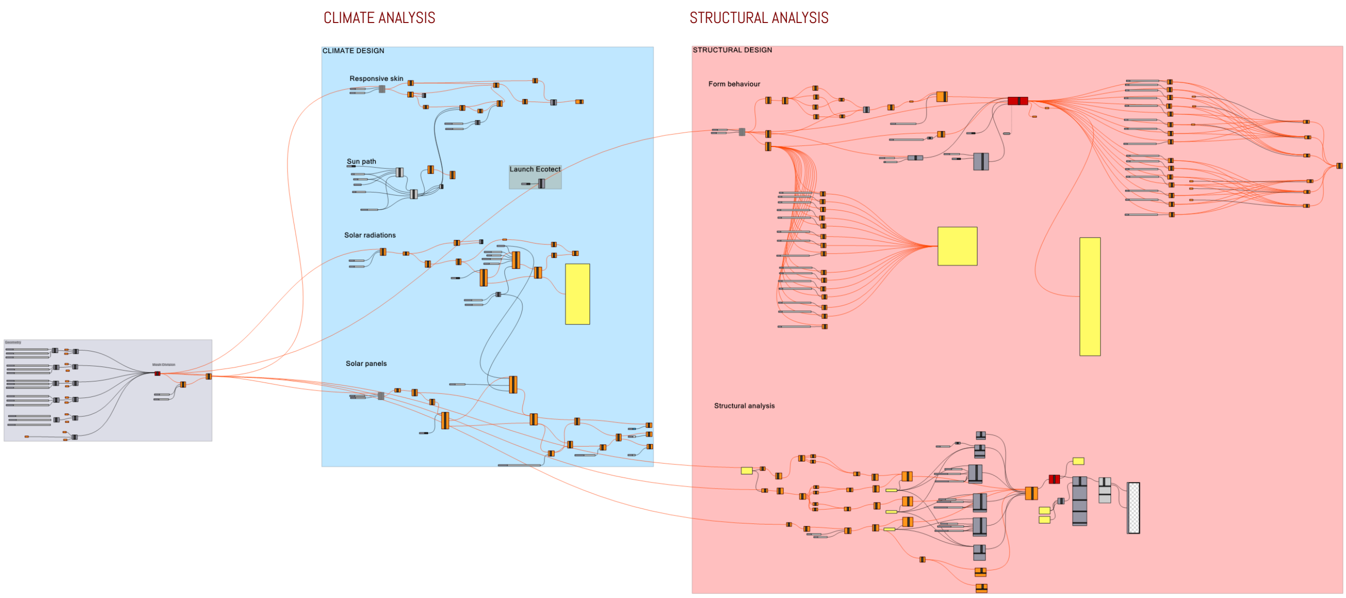

Fig. 63: Complete Grasshopper script including climate and structural analysis (Andrejevic, 2016)

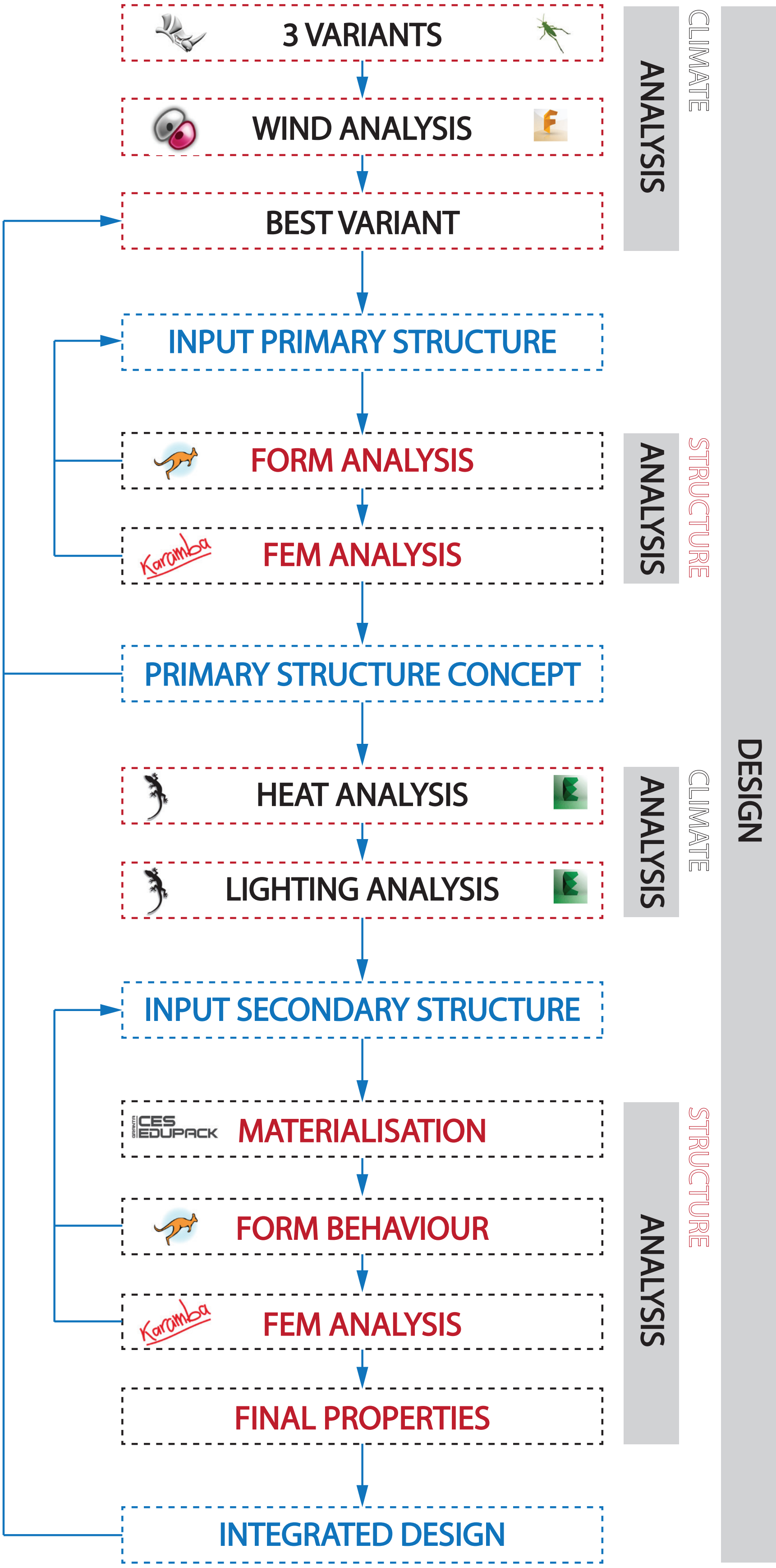

Fig. 64: Design analysis methodology (Andrejevic, 2016)

6.2.1 GRASSHOPPER AS A PARAMETRIC ANALYSIS AND DESIGN TOOL

6.2.1.1 AUTODESK FLOW DESIGN

With Autodesk Flow Design it is possible to conduct a CFD (Computational Fluid Dynamics) analysis, giving the right insight in the geometry behaviour in relation to the wind. With the output of this CFD analysis a comparison to the wind tunnel testing can be made, to get a most realistic outcome of the best variant (see fig. 65).

6.2.1.2 GECO WITH AUTODESK ECOTECT

Using GECO as a plugin for Grasshopper, makes it possible to conduct different climate analyses in Autodesk Ecotect with keeping the design variable. Meaning that the input of Autodesk Ecotect stays linked to Grasshopper's parametricism. With Ecotect it is possible to analyse and calculate different types of solar radiations (in terms of heat and lighting), acoustical properties and the weather situation of any place in the world. For the roof analysis, only heat and lighting analyses will be conducted. Where the output of the analysis results will be used to calculate the most optimal responsive skin (an optimisation of where to place translucent and where to place transparent panels) and the possible placement of PV panels (see fig. 65).

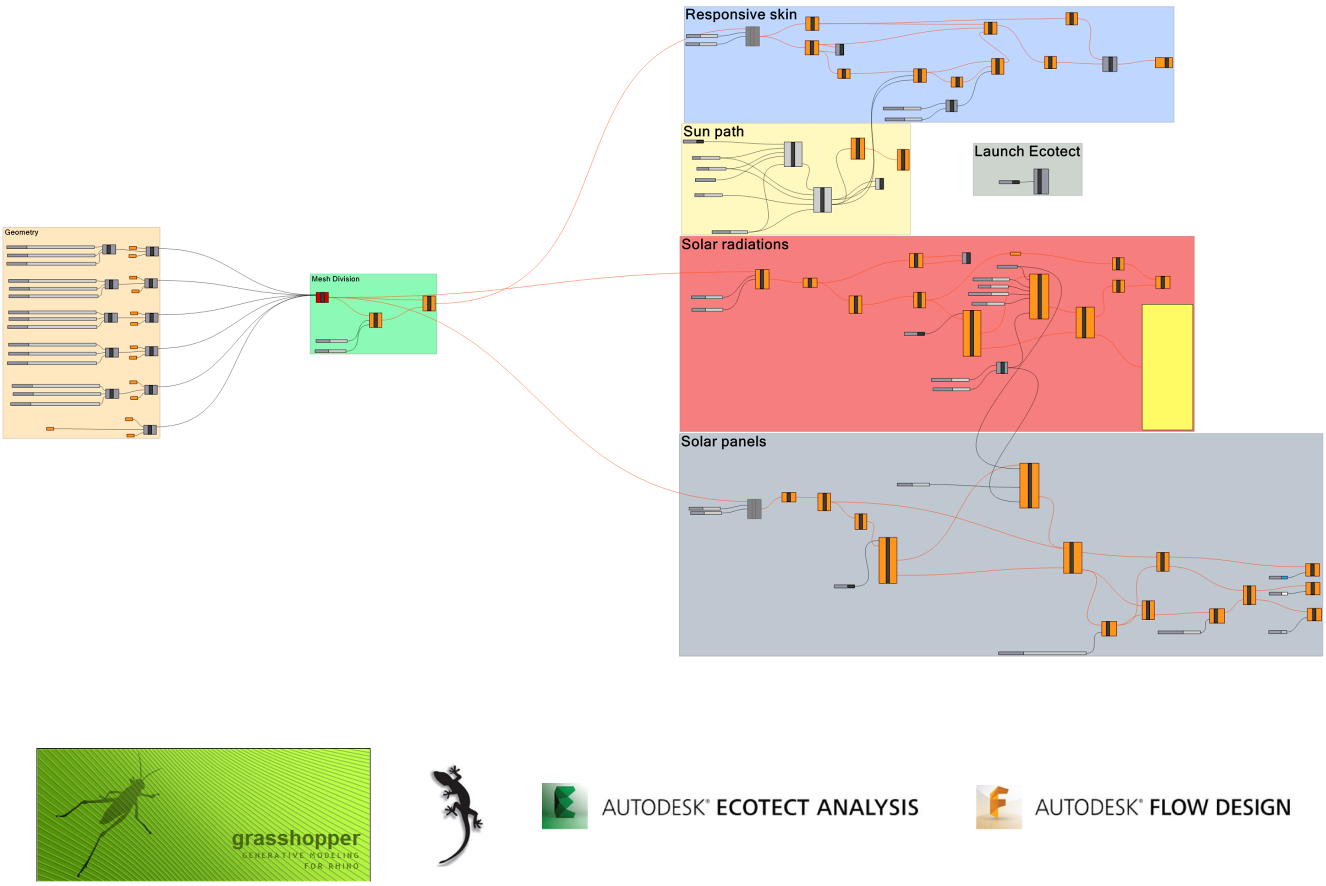

Fig. 65: Climate design analysis script with plugin programmes Autodesk Ecotect and Flow Design (Andrejevic, 2016)

6.3.1 GRASSHOPPER AS A PARAMETRIC ANALYSIS AND DESIGN TOOL

6.3.1.1 KANGAROO

Kangaroo is a Grasshopper plugin that can be used to optimise shapes in terms of the natural behaviour of its own weight. With the help of Kangaroo, the form of the primary and the secondary structure can be analysed before designing the structure and running a FEM analysis. With the form analysis the geometry gets optimised in terms of stiffness and elasticity. This output gives a clear insight in the probable behaviour of the to be designed structure (see fig. 66).

6.3.1.2 KARAMBA

With Karamba it is possible to conduct a full FEM analysis. Giving insight in deformations, axial stresses, utilisations, moments, shearforces, normal forces etc. With this output it possible to optimise the cross sections of the structural elements. Since all the structural properties given are parametric, it is easy to change the input yourself or optimise it with the evolutionary solver command called Galapagos. Design and analysis are this way integrated and making Karamba the ideal tool to design and analyse structures in early stages of the design and engineering process (see fig. 66).

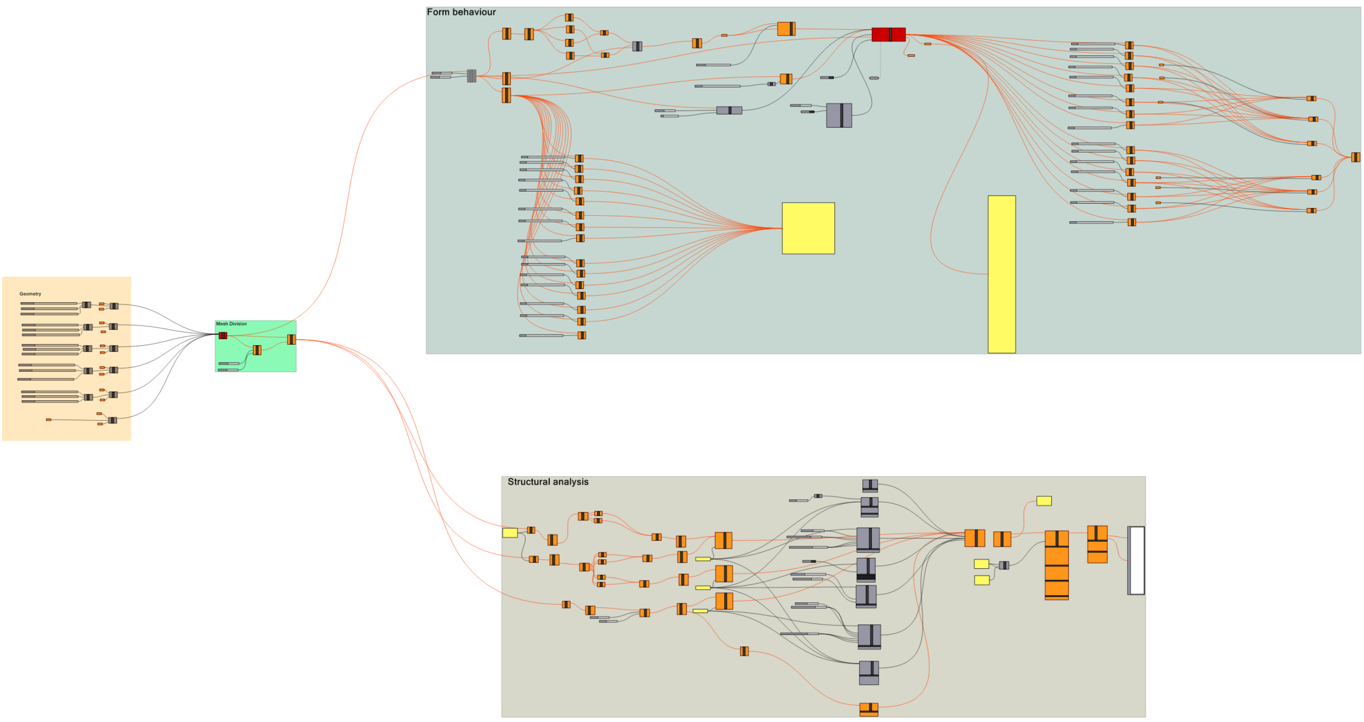

Fig. 66: Structural design analysis script with plugin programmes Kangaroo and Karamba (Andrejevic, 2016)

6.4.1 VARIANTS

For the wind design analysis three variants were made in Rhinoceros+Grasshopper to see which one would be most aerodynamic. Meaning which geometry would give the most linear wind-over-surface acceleration and get the most underpressure on the roof, which would eventually result in natural aspiration.

Variant 1 can be characterised by the form of a dome, symmetrical in the x- and y-axis (see fig. 67).

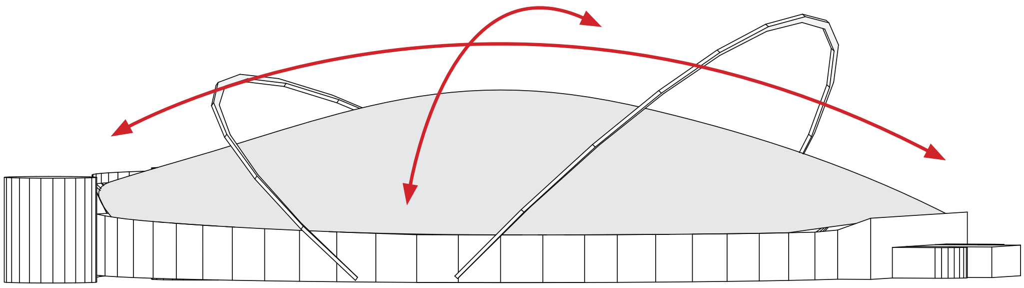

Fig. 67: Variant 1 (Andrejevic, 2016)

Variant 2 can be characterised as two joined domes, only symmetrical in the y-axis (see fig. 68).

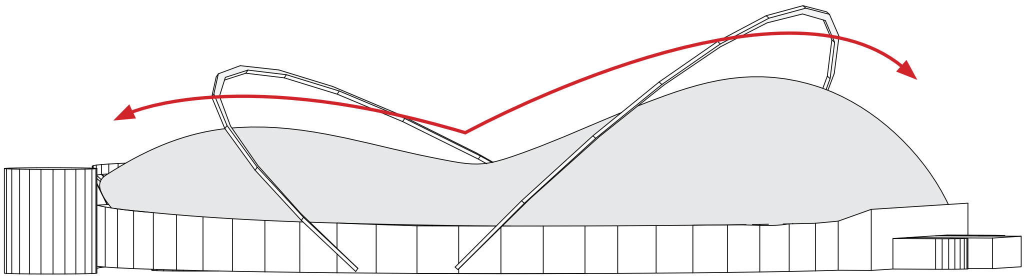

Fig. 68: Variant 2 (Andrejevic, 2016)

Variant 3 can be characterised as a gradually emerging dome, only symmetrical in the y-axis (see fig. 69).

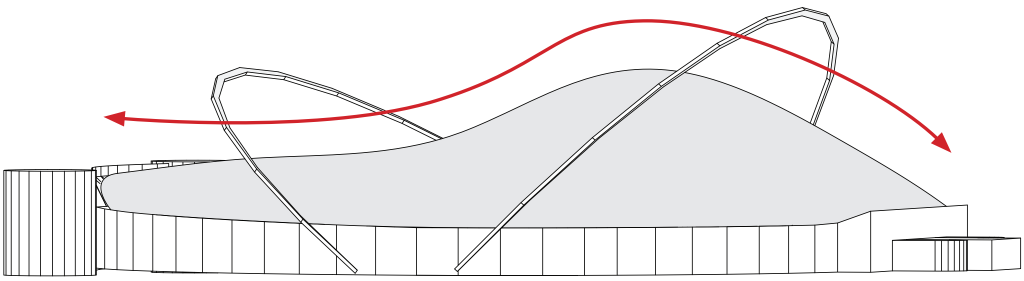

Fig. 69: Variant 3 (Andrejevic, 2016)

6.4.2 COMPUTATIONAL FLUID DYNAMICS ANALYSIS

Using Flow Design to conduct a CFD analysis, gives one clear insight in the aerodynamics and wind adaptability of geometries. Below the three variants shown, tested on acceleration and pressure of air movement. Variant 1 (see fig. 70a) shows a gentle acceleration and a nice divided underpressure near the surface. Variant 2 (see fig. 70b) shows a high acceleration and underpressure at both the humps, while the area in between is in a lee. Variant 3 (see fig. 70c) shows high acceleration and underpressure on top of the hump, while the lower part shows a slight acceleration with mainly overpressure.

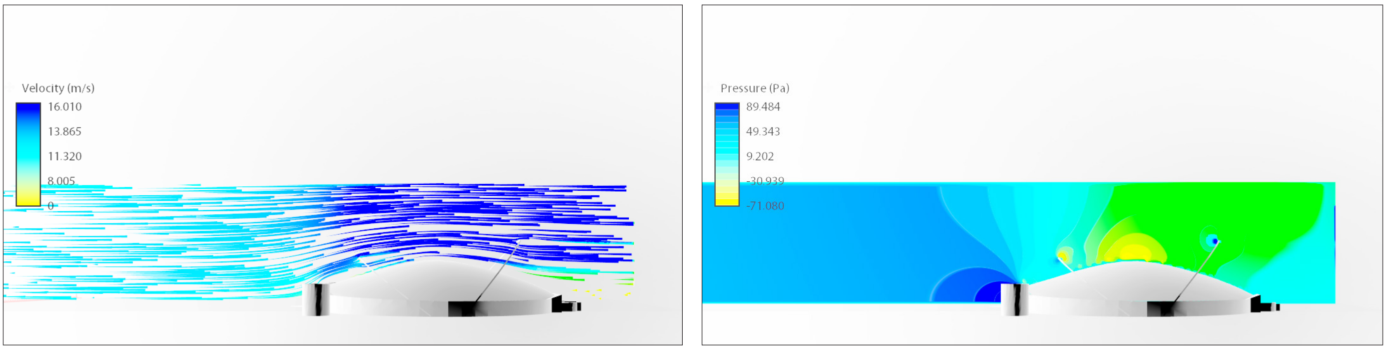

Fig. 70a: CFD Flow Design Variant 1, Air velocity (left) and Pressure (right) (Andrejevic, 2016)

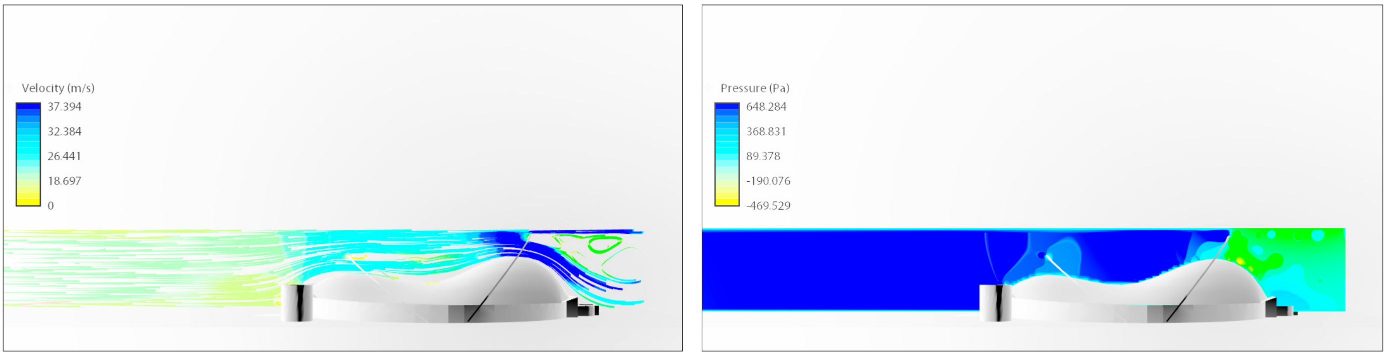

Fig. 70b: CFD Flow Design Variant 2, Air velocity (left) and Pressure (right) (Andrejevic, 2016)

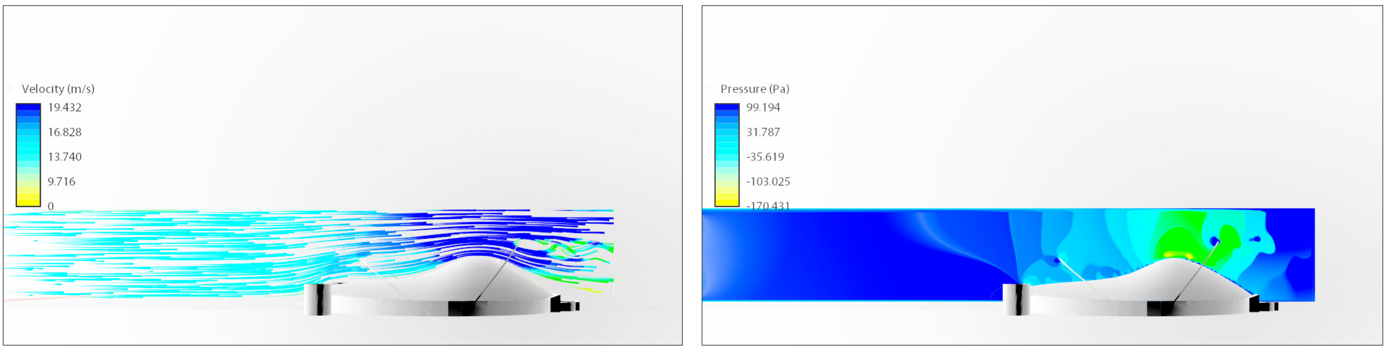

Fig. 70c: CFD Flow Design Variant 3, Air velocity (left) and Pressure (right) (Andrejevic, 2016)

6.4.3 WIND TUNNEL TESTING

6.4.3.1 SETUP

The wind tunnel setup is as follows (see fig. 71a):

°Arduino speed control (a microcontroller kit for building digital devices and interactive objects that can sense and control physical devices) to set wind speed in m/s with accessory wind force (Wikipedia, 2016d)
°Propellers generating wind
°Air velocity meter measuring the air movement
°Geometry filled with sand that gets tested

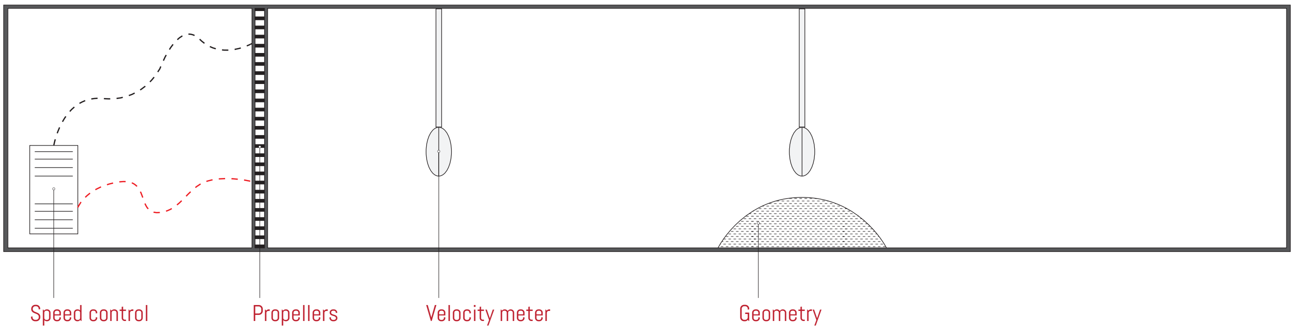

Fig. 71a: Wind tunnel setup (Andrejevic, 2016)

The Arduino speed control sets the propellers to a certain speed, this speed is measured right in front of the propellers with the air velocity meter to check if the Arduino is properly adjusted. If so, the acceleration above the geometries can be measured veraciously (see fig. 71b).

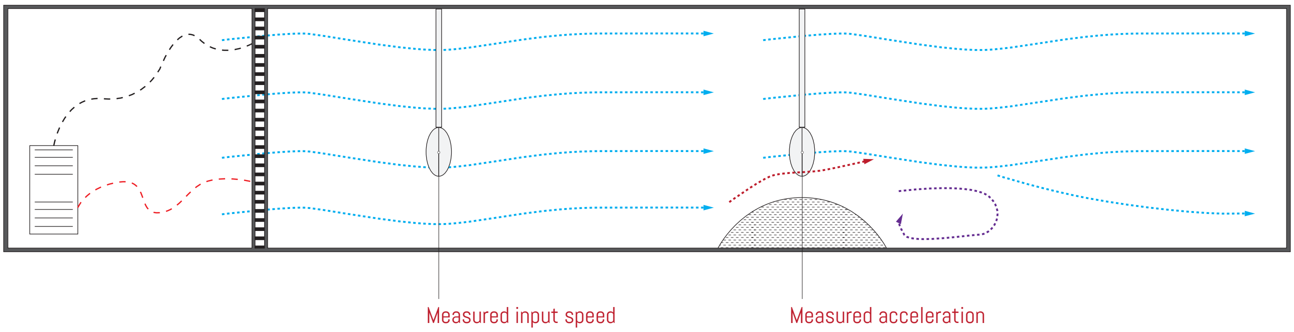

Fig. 71b: Wind tunnel measurement (Andrejevic, 2016)

Sand-geometry behaviour:

Next to the measured accelerations above the geometries, another, more accurate, method can be used to determin whether acceleration takes place on the surface of the geometry. If the geometry is aerodynamically shaped well the sand will gradually blow of because of the underpressure happening near the surface. This way the wind adaptability in terms of aspiration can be determined (see fig. 72).

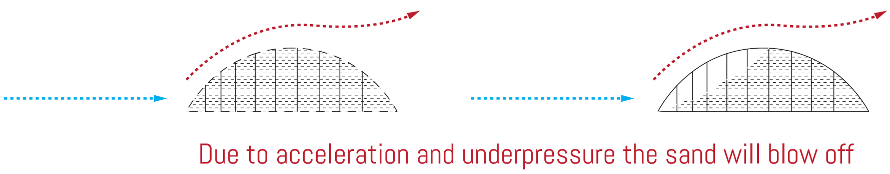

Fig. 72: Sand-geometry behaviour (Andrejevic, 2016)

6.4.3.2 FROM COMPUTATIONAL VARIANTS TO TESTING GEOMETRIES

To translate an extracted GrasshopperRhinoceros model to something tangible, Rhinoceros' plugin Bowerbird can be used to make a waffle grid pattern from the geometry. This pattern can be exported as a line drawing to subsequently be used to laser cut the grid in MDF and creat the desired geometry for the sand testing.. The result can be seen in the figure below (see fig. 73)

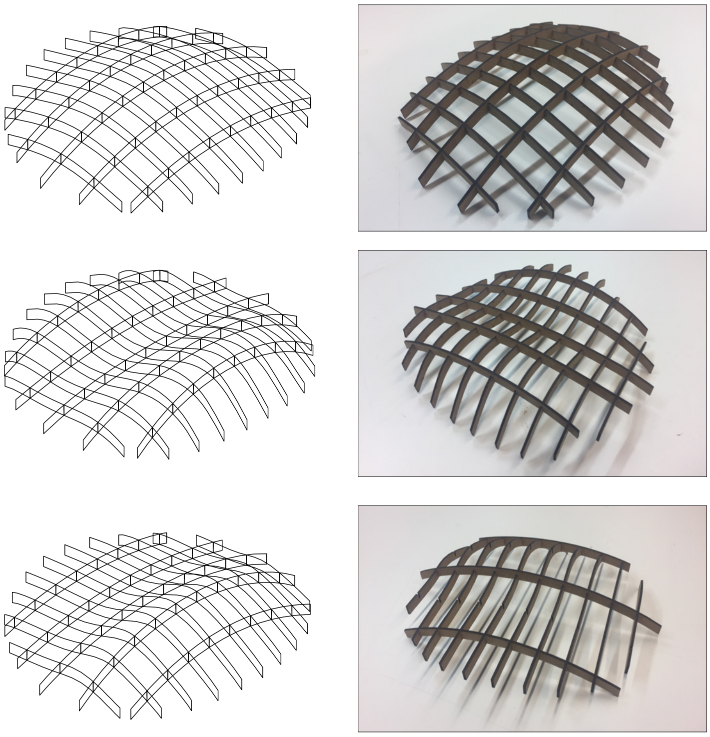

Fig. 73: Waffle grids to make wind tunnel geometries (Andrejevic, 2016)

After assembling the waffle grid, the geometry can be placed in the wind tunnel. The geometry will be filled with sand to get the sand in the right shape before the test runs (see fig. 74).

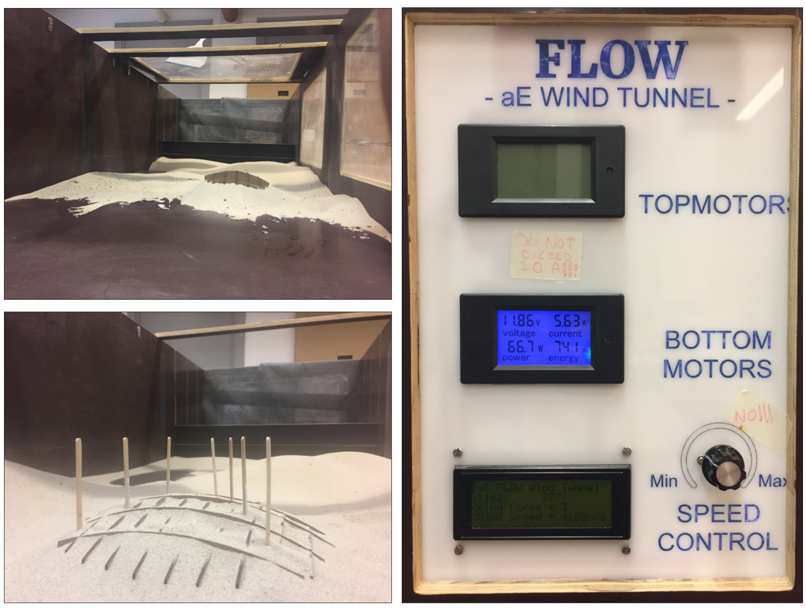

Fig. 74: Waffle grid geometry in wind tunnel setup (Andrejevic, 2016)

6.4.3.3 AIR VELOCITY METER

The air velocity meter gives result of the input speed near the propellers and the acceleration right above the highest point of the geometry (see fig. 75). With this information the influence of the geometry on the wind speed can be determined.

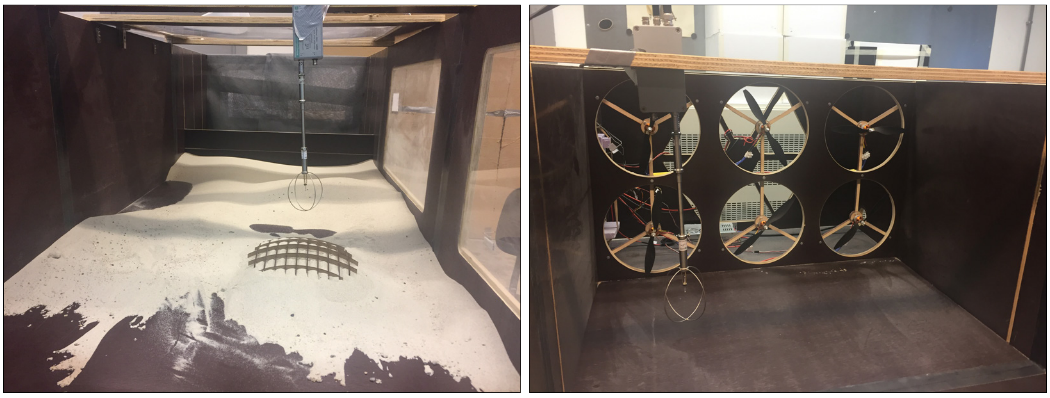

Fig. 75: Positioning the air velocity meter (Andrejevic, 2016)

As shown below the input speed varies between 5.013 and 5.151 m/s with each variant resulting in different accelerations. However the acceleration seems to be linear. With variant 1 gving an acceleration of 7.621 - 7.831 m/s, variant 2; 9.844 - 10.115 m/s and variant 3; 7. 411 - 7.615 m/s (see fig. 76). It can be concluded that variant 2 has the biggest acceleration on its highest point, however this will not say that the acceleration near the surface is sufficient. As shown in the CFD analysis, the first bump of the geometry is causing a blockade, which results in acceleration at a high point but not near the surface. The rest of the surface gets pitched in the lee of the first hump. Concluding that variant 1 give the best acceleration in this test.

	Start speed	Variant 1	Variant 2	Variant 3
Output probe	*U*	*U*	*U*	*U*
V	[m/s]	[m/s]	[m/s]	[m/s]
3,6300	5,013	7,621	9,844	7,411
3,6300	5,030	7,647	9,877	7,436
3,6423	5,104	7,759	10,023	7,546
3,6959	5,110	7,768	10,035	7,555
3,7002	5,112	7,771	10,038	7,558
3,7017	5,101	7,755	10,017	7,541
3,6937	5,124	7,790	10,062	7,575
3,7104	5,133	7,803	10,080	7,589
3,7169	5,141	7,815	10,095	7,600
3,7227	5,144	7,820	10,101	7,605
3,7248	5,143	7,818	10,099	7,603
3,7241	5,139	7,812	10,091	7,597
3,7212	5,142	7,817	10,097	7,602
3,7234	5,145	7,821	10,103	7,606
3,7256	5,149	7,828	10,111	7,612
3,7285	5,151	7,831	10,115	7,615

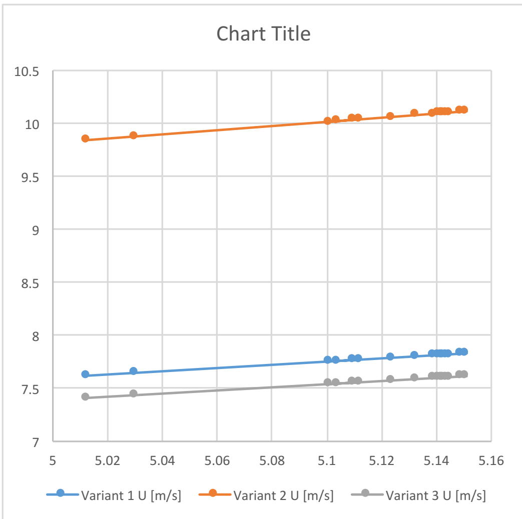

Fig. 76: Output measured air velocities (Andrejevic, 2016)

6.4.3.4 SAND-GEOMETRY BEHAVIOUR

Like mentioned before, sand blowing off means high acceleration and underpressure near the surface. As shown at the following page the three variants behave all differently, however all more or less according to the CFD analysis. Variant 1 (see fig. 77a) has blown off a lot of sand at the first half of the geometry, variant 2 (see fig. 77b) only at the first hump and variant 3 (see fig. 77c) only a bit at the highest part and at the beginning. Concluding that variant 1 gives the most constant acceleration in this test as well.

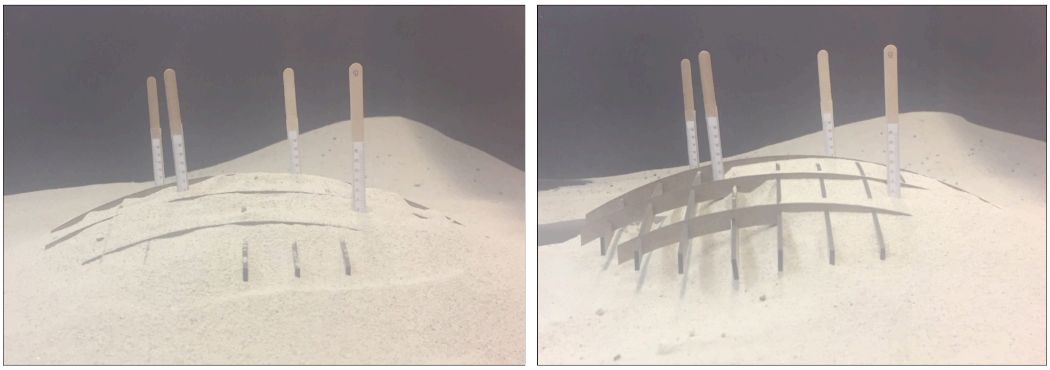

Fig. 77a: Variant 1 sand-geometry behaviour result (Andrejevic, 2016)

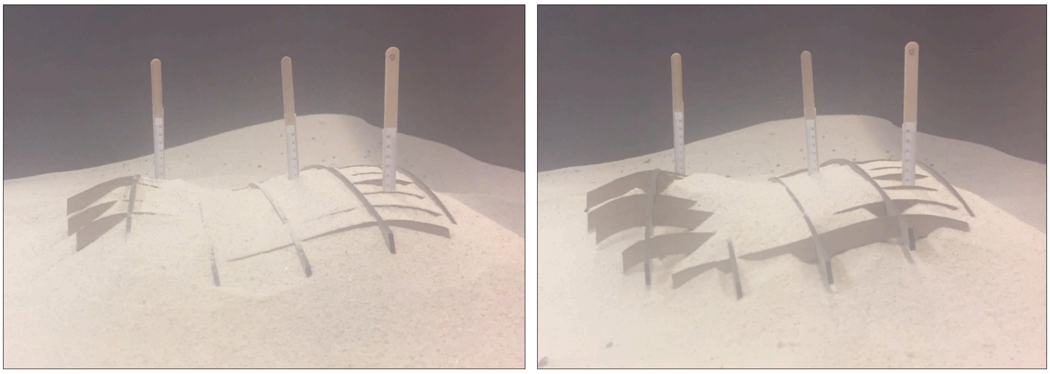

Fig. 77b: Variant 2 sand-geometry behaviour result (Andrejevic, 2016)

Fig. 77c: Variant 3 sand-geometry behaviour result (Andrejevic, 2016)

6.4.4 COMPARING METHODS

The measured differences between the CFD analysis and the wind tunnel test can be seen below. The velocities differ from eachother, because of the size of environments where the speeds were measured (see fig. 78). However, the linearity of the accelerations match significantly, meaning the CFD analysis can be considered significant.

Average speed windtunnel measurements			
Start speed	Variant 1	Variant 2	Variant 3
U	*U*	*U*	*U*
[m/s]	[m/s]	[m/s]	[m/s]
5,118	7,780	10,049	7,566

Average speed flow design			
Start speed	Variant 1	Variant 2	Variant 3
U	*U*	*U*	*U*
[m/s]	[m/s]	[m/s]	[m/s]
5	7,255	8,241	6,195

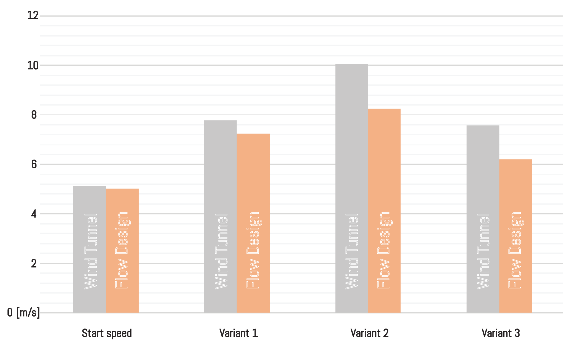

Fig. 78: Methods compared in Microsoft Excel (Andrejevic, 2016)

6.4.5 BEST VARIANT

After CFD analyses, variant 1 shows the best divided acceleration and underpressure near the surface and after the wind tunnel tests, variant 1 blows the most sand off, which confirms the good divided acceleration and underpressure in the CFD analysis. According to its aerodynamics and wind adaptability variant 1 is the best variant (see fig. 79).

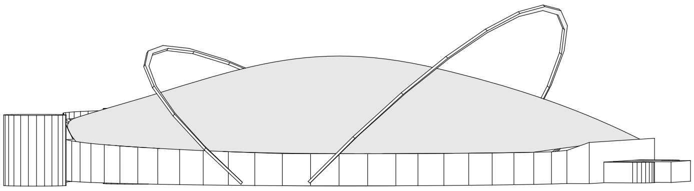

Fig. 79: Beste variant with best aerodynamic geometry (Andrejevic, 2016)

6.4.6 WIND CONCEPT DESIGN

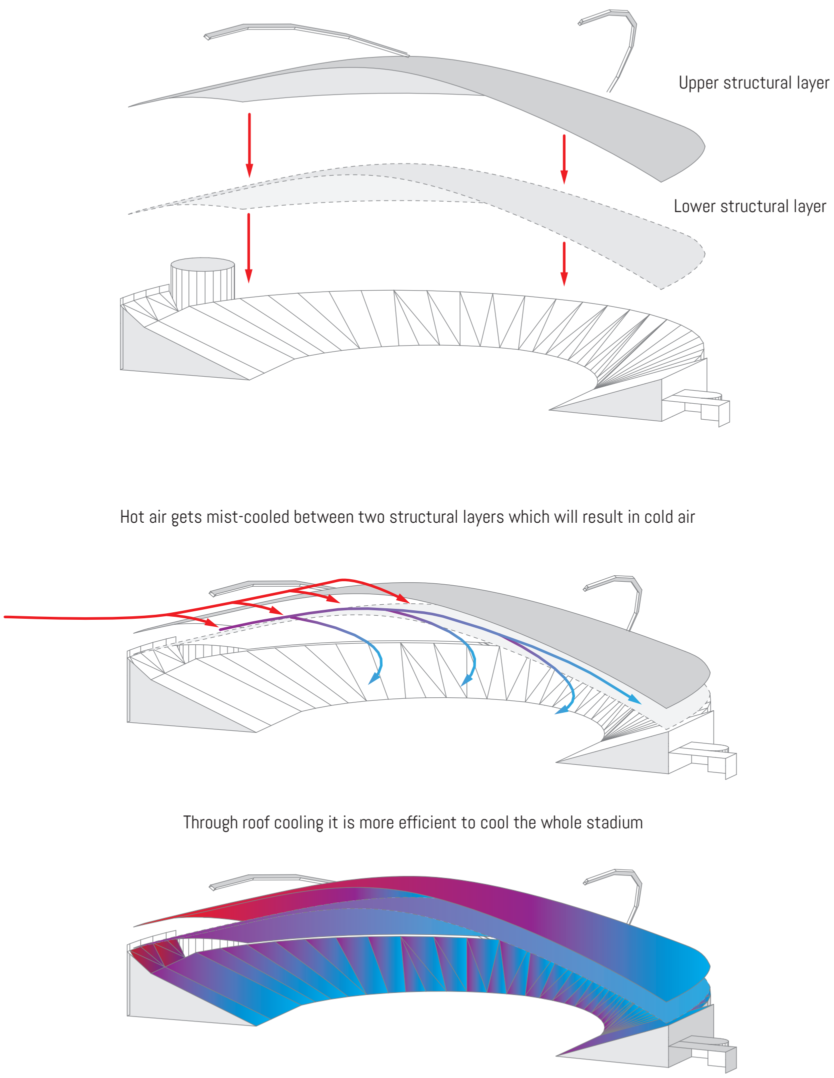

Fig. 80: Wind concept design with characteristics (Andrejevic, 2016)

With the knowledge of the outcome of the wind analyses, a proposal for a structural design for the best variant can be made. In order to design the best variant's shape, the form has to be analysed on its curve behaviour to get insight in where the highest stresses in the primary structure might occur. Because of the large span of the roof a suspension structure is proposed to make a most light possible structure.

6.5.1 KANGAROO FORM BEHAVIOUR

Kangaroo is a tool to conduct Particle Spring System (PSS) calculations, where the goal is to reach an equilibrium state where all the forces are 0. With PSS it is possible to test the form behaviour of a shell. However, to prevent rumpling of the shell, what normally happens with a spring system, the component shell has to be added. This component gives the shell values of a rigid material with bending resistance (steel, wood, glass, etc.), which results in the shell deforming up to its material stiffness (Tedeschi, 2014). With this script it is possible to get insight in the form behaviour of the shell and possible problems in terms of stresses (see fig. 81).

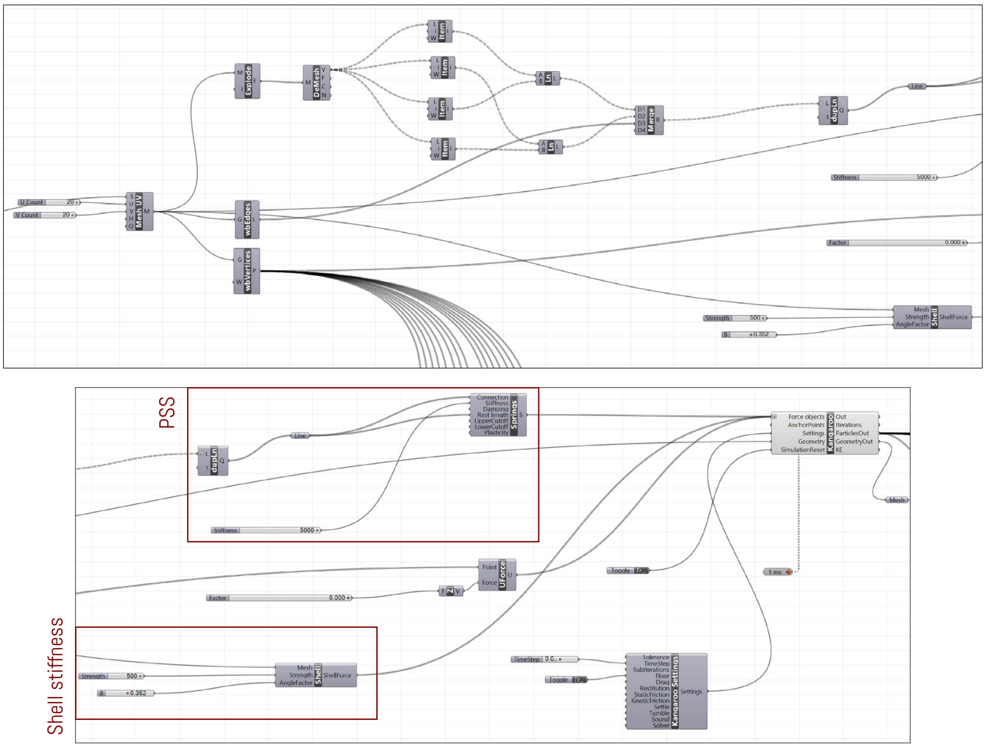

Fig. 81: Setup Kangaroo Script (Andrejevic, 2016)

After running the Kangaroo script on the shape of the best variant, it moves to the position where all the forces equilibrate to 0. Resulting in a bit more flat surface at the edges of the shell. Below shown: the before and after situation (see fig. 82).

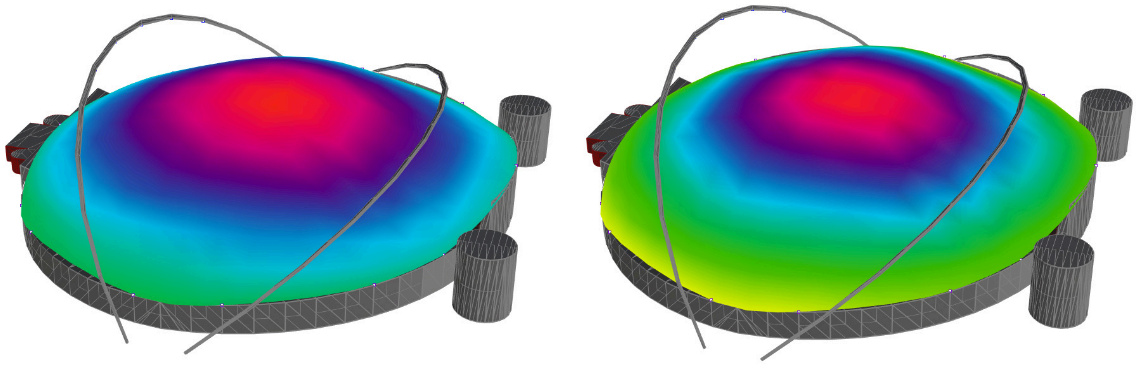

Fig. 82: Outcome Kangaroo form behaviour primary structure (Andrejevic, 2016)

6.5.2 TYPES OF PRIMARY STRUCTURES

This chapter is discussing two types of primary structures possible. The first variant is one where the arches are supported by columns to prevent the arches from moving in its perpendicular direction (see fig. 83.1). The second variant is a more lightweight structure, where only cables are used to balance the arches. Meaning, the cables connected the arches with eachother and to the rigidity ring (see fig. 83.2). By looking at the structural behaviour (in terms of buckling stability and rigidity) of both variants, it can be decided which structure will be most suitable as a primary roof structure for the Khalifa International Stadium.

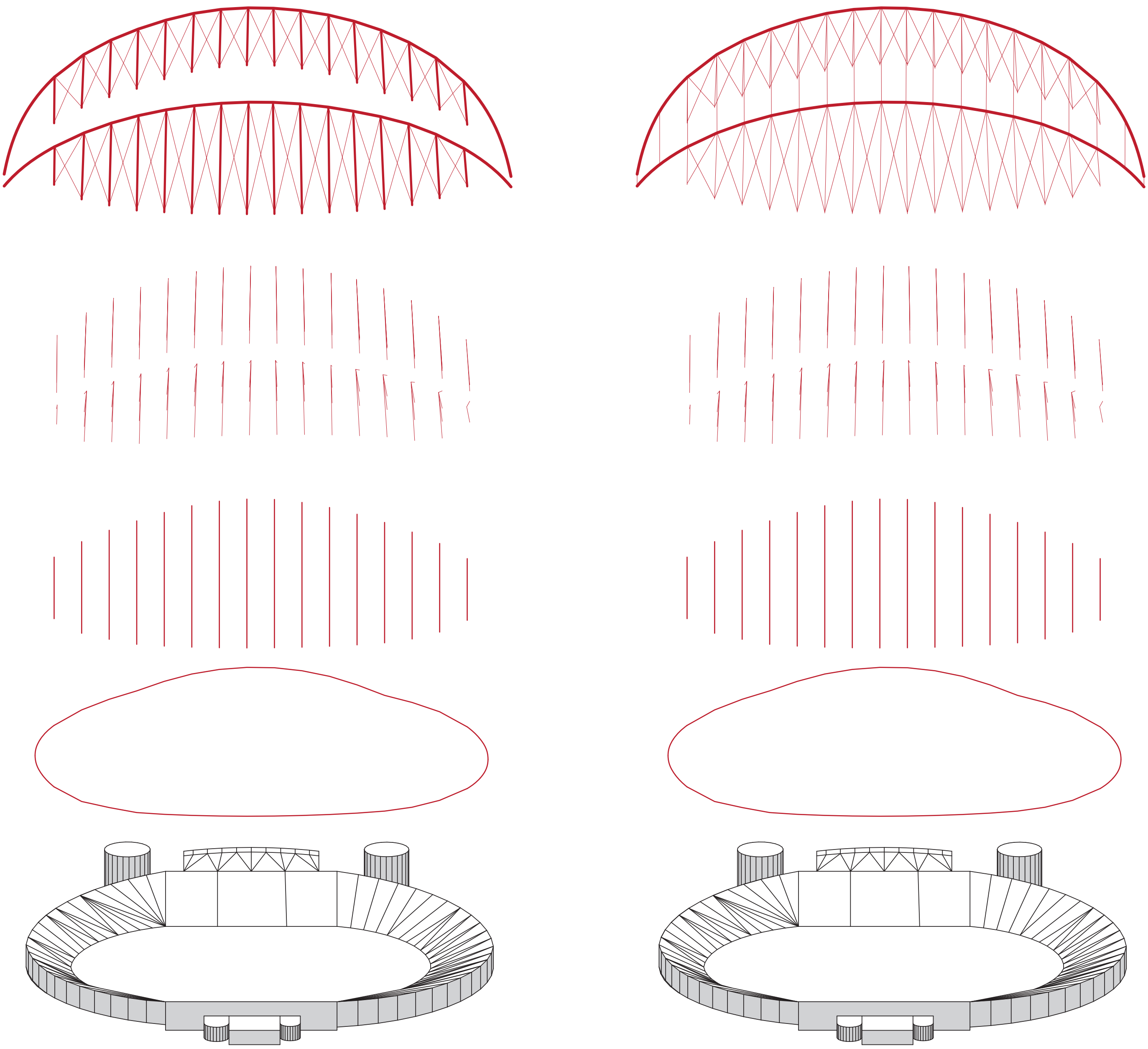

Fig. 83: Build up of with both possible primary structures: columns (left) and cables (right) (Andrejevic, 2016)

6.5.2.1 *WITH COLUMNS*

The first type of structure possible is one with columns support underneath the existing arches (see fig. 84a). With the arches supported it is safer to hang the beams of the primary structure with cables to the arches. With the use of bracing between the columns, the arch structure gets stabilised and shorten the buckling length of the arches and the columns (see fig. 84a). However, the most critical point of this structure is the buckling behaviour of the columns, since they can span up to 50 metres. With the columns hinged on both sides, giving them a buckling span of 50 metres. Therefore, with the use of Euler's buckling equation it is possible to determine the maximum amount of buckling stress possible in a column of 50 metres long. Giving the following outcome:

$$S_{buckling} = \frac{\pi^2 \cdot E \cdot I}{L_b^2 \cdot A} \left[\frac{n}{mm^2} \right]$$

where:

$S_{buckling}$ = buckling stress in N/mm^2
E = Young's modulus in N/mm^2
I = second moment of area in mm^4
L_b = buckling length in mm
A = section area structural profile in mm^2

$$S_{buckling} = \frac{\pi^2 \cdot 210000 \cdot 2.9 \cdot 10^{10}}{50000^2 \cdot 2.83 \cdot 10^5}$$

$$S_{buckling} = 84.96 \ \frac{N}{mm^2} \ (MPa)$$

Maximum buckling stress = 84.96 MPa

Relatively low buckling stress, causing possible problems with unexpected live loads.

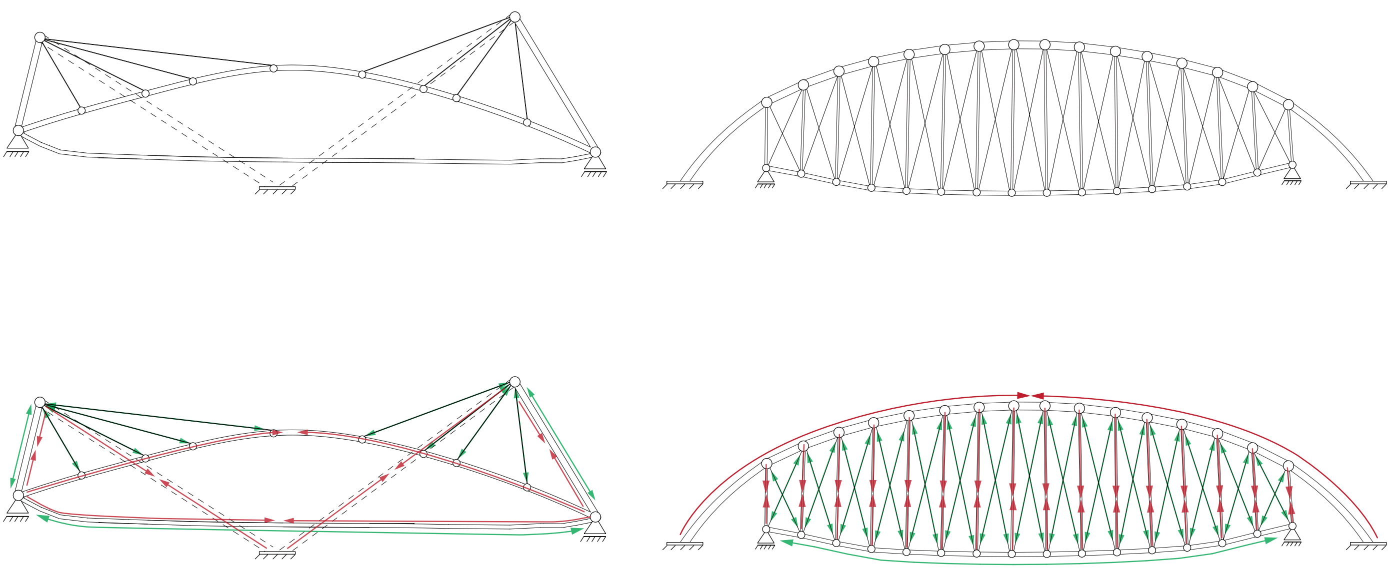

Fig. 84a: Static scheme with tension and compression forces (Andrejevic, 2016)

6.5.2.2 WITH CABLES

The second type of structure possibe is one that completely supports and stabilises the arches with cables (see fig. 84b). By spanning cables between the two arches, they prevent eachother from falling down and thus keep eachother in place. In case of an occurring live load on the roof beams, the arches are tend to move towards on another as a result of a downwards force. To prevent this, the arches have to get connected to the edges of the roof structure with cables (see fig. 84a). With bracing between the cables will shorten the buckling length of the arches, resulting in less impact of buckling on the arch structures. In the case of just using cables, high buckling stress that would occur on the columns, can be neglected and therefore, there is no need to calculate buckling stresses.

$$\cancel{S_{buckling} = \frac{\pi^2 \cdot E \cdot I}{L_b^2 \cdot A} \left[\frac{n}{mm^2} \right]}$$

A primary structure where no columns are used makes the whole much lighter and more efficient to build. Climate wise it gives more space to catch wind and light.
The primary structure executed with cables will be lighter and more sufficient to eleborate upon.

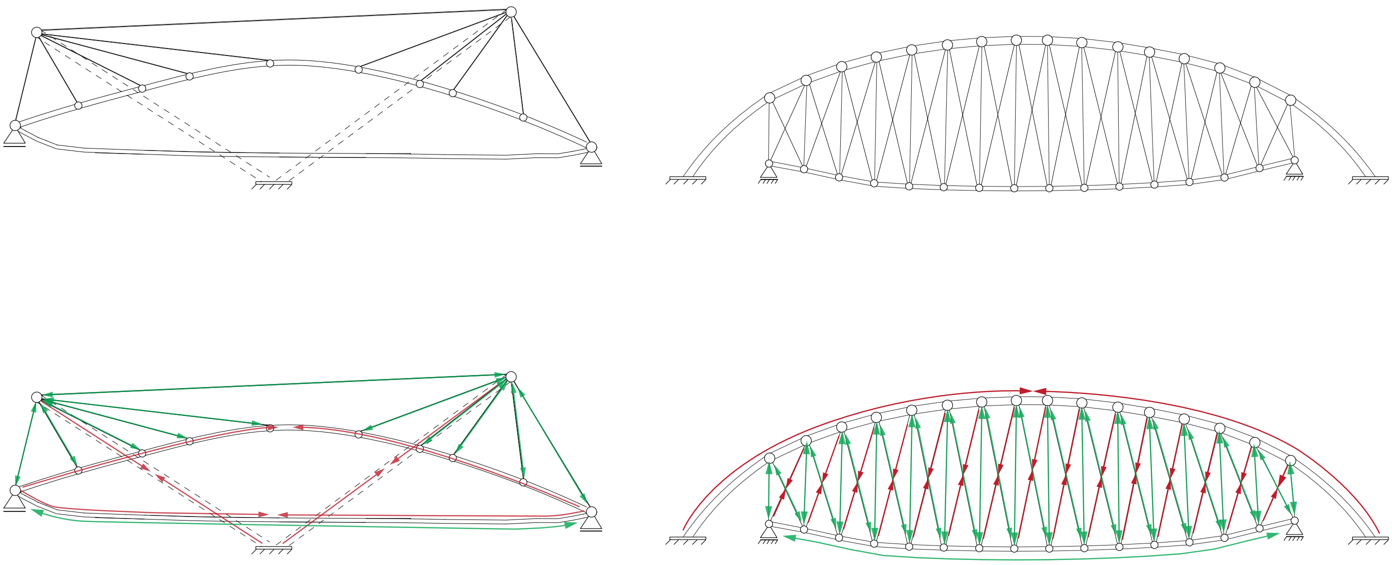

Fig. 84b: Static scheme with tension and compression forces (Andrejevic, 2016)

6.5.3 STRUCTURAL PROPERTIES

The arches are existing, where only cables and beams are added to the arches to create a rigid roof structure.

Arches

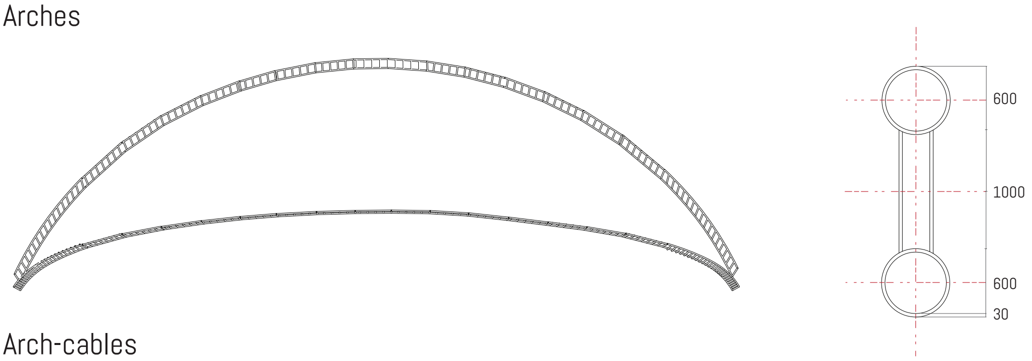

$I_y = 6.9 \times 10^{10}\ mm^4$
$Z_y = 2.4 \times 10^8\ mm^3$
$R_y = 480.7\ mm$
$A = 2.1 \times 10^6\ mm^2$

Arch-cables

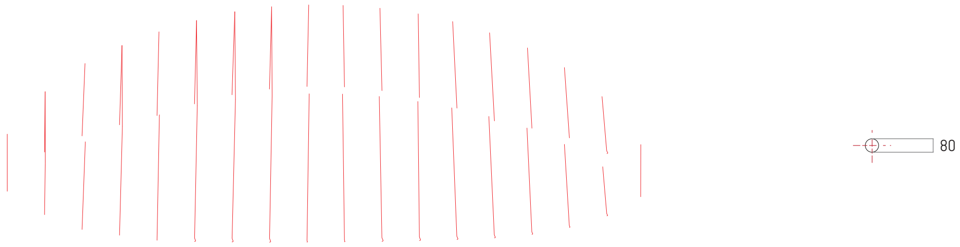

$I_{xy} = 2.0 \times 10^7\ mm^4$
$Z_{xy} = 1.9 \times 10^5\ mm^3$
$R_{xy} = 30\ mm$
$A = 1.4 \times 10^4\ mm^2$

Cables

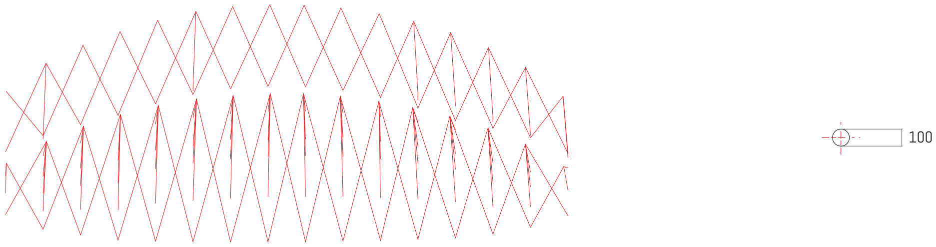

$I_{xy} = 2.5 \times 10^7\ mm^4$
$Z_{xy} = 3.3 \times 10^5\ mm^3$
$R_{xy} = 37.5\ mm$
$A = 1.8 \times 10^4\ mm^2$

Beams

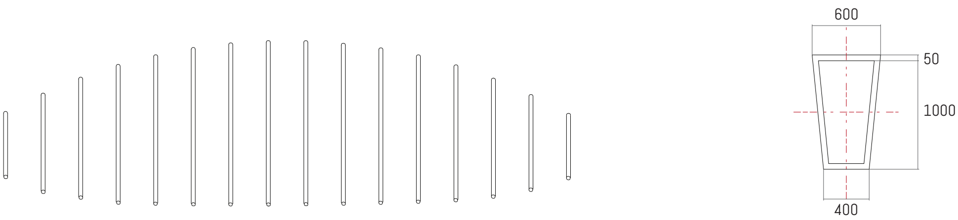

$I_y = 2.35 \times 10^{10}\ mm^4$
$Z_y = 4.2 \times 10^7\ mm^3$
$R_y = 31.8\ mm$
$A = 1.5 \times 10^5\ mm^2$

Edge

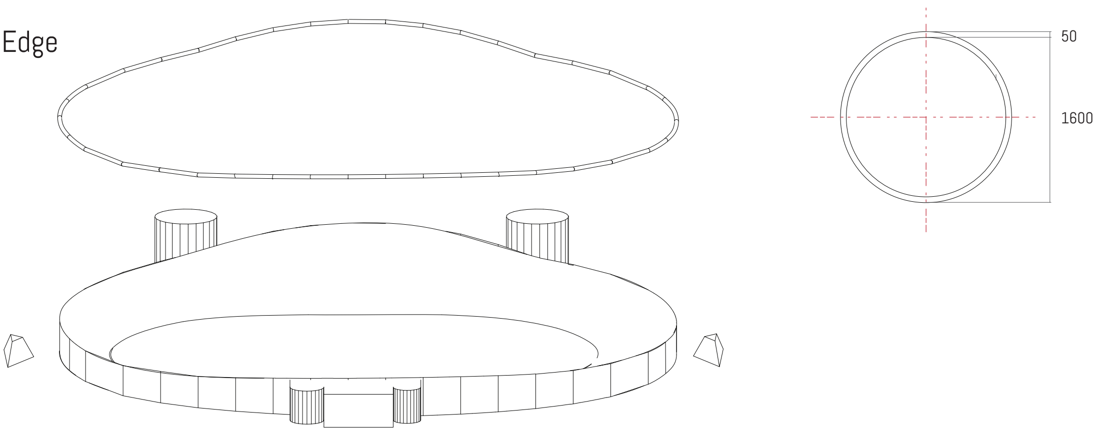

$I_{xy} = 5.8 \times 10^{10}\ mm^4$
$Z_{xy} = 11.6 \times 10^7\ mm^3$
$R_{xy} = 640.4\ mm$
$A = 5.6 \times 10^5\ mm^2$

Fig. 85: Structural properties primary structure (Andrejevic, 2016)

6.5.4 FINITE ELEMENT METHOD ANALYSIS

6.5.4.1 SETUP KARAMBA SCRIPT

Like mentioned before, Karamba can be used to conduct a full FEM analysis. To conduct such an analysis, the input has to be a line drawing made in Rhinoceros and/or Grasshopper. This line drawing has to get exploded before it gets analysed, because the connection nodes will not connect correctly otherwise. With this exploded line drawing the needed structural input can be done in Karamba. Shown below, the five different structural elements, occurring loads, material type and supports determined. All the input is variable and parametric, except for the gravity. To give cables the right behaviour, the element has to get modified to give the command that the cable cannot give any bending resistance (see fig. 86a).

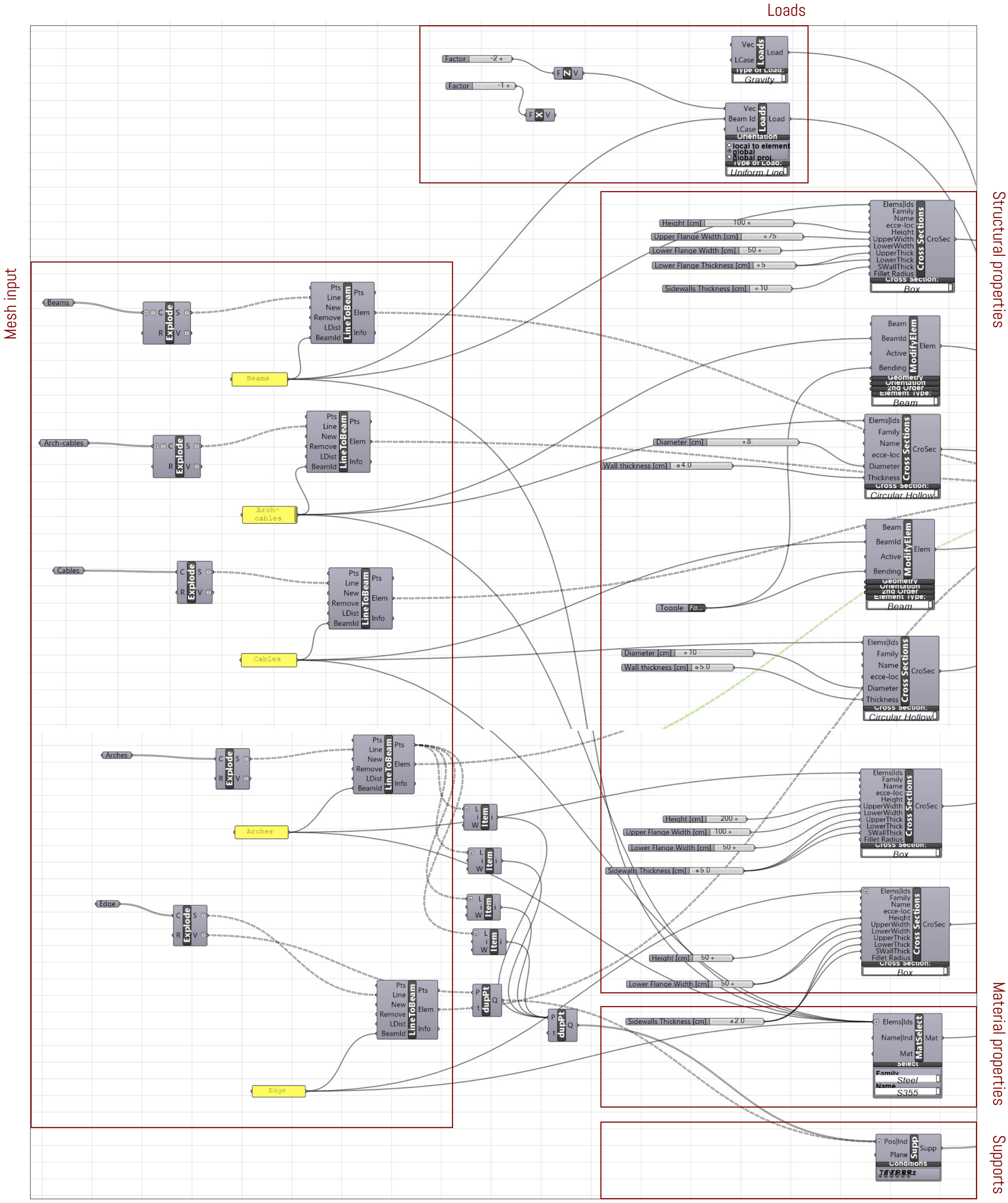

Fig. 86a: Karamba script primary structure (Andrejevic, 2016)

All the described input comes together in the *Assemble* component, from where it gets connected to the *AnalyzeTHI* component. This component gives the maximum displacement as outcome, which can subsequently be translated to the *Modelview* component where the whole build up of the FEM model can be seen. To get a clear overview of different kinds of results, the component *Beamview* has to be attached, to get bending moment, shear force, normal force, utilisation and axial stress results. Below and on the next page shown what the results are of the most optimised primary structure (see fig. 86b).

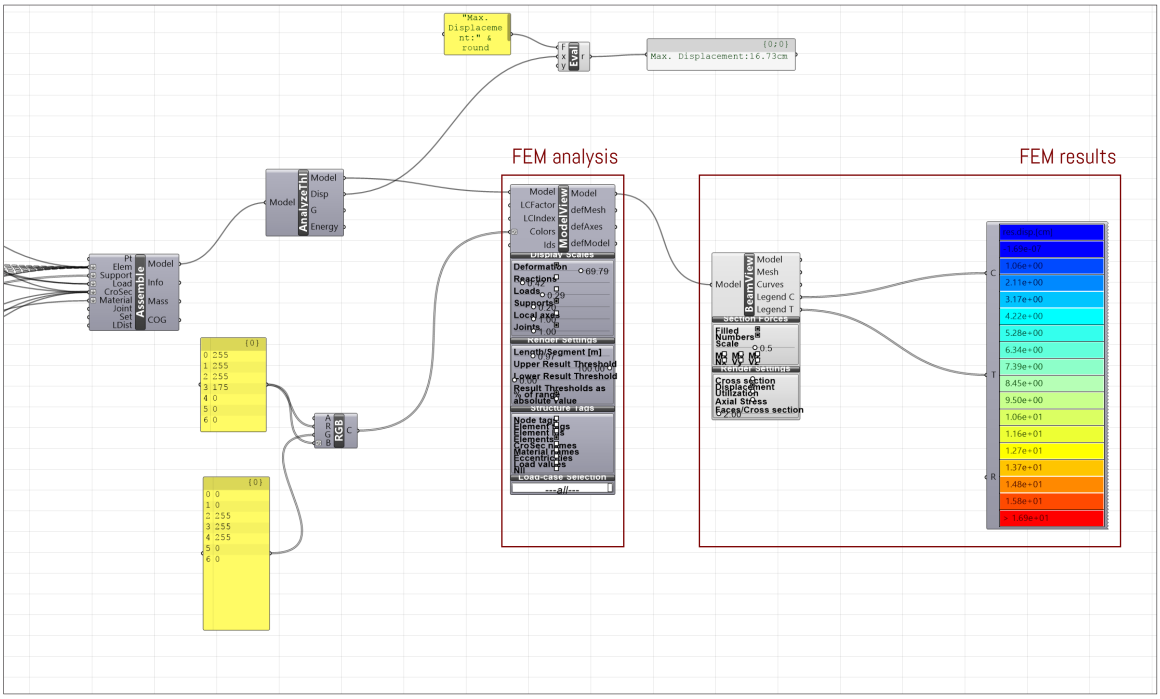

Fig. 86b: Karamba script primary structure (Andrejevic, 2016)

6.5.4.2 CONSIDERED LOADS

The first load considered is the deadload of 1.1 kN/m². Based on an amount of 2,995,200 KG structural steel and 246000 KG glass structures divided over a surface of ca. 30000m², the dead load is determined as 1.1 kN/m². According to NEN/Eurocode standards the live load for a stadium roof in areas like Qatar (no snow loads) is determined as 2.0 kN/m² (see fig. 87). (1994-1-2+C1, 2011)

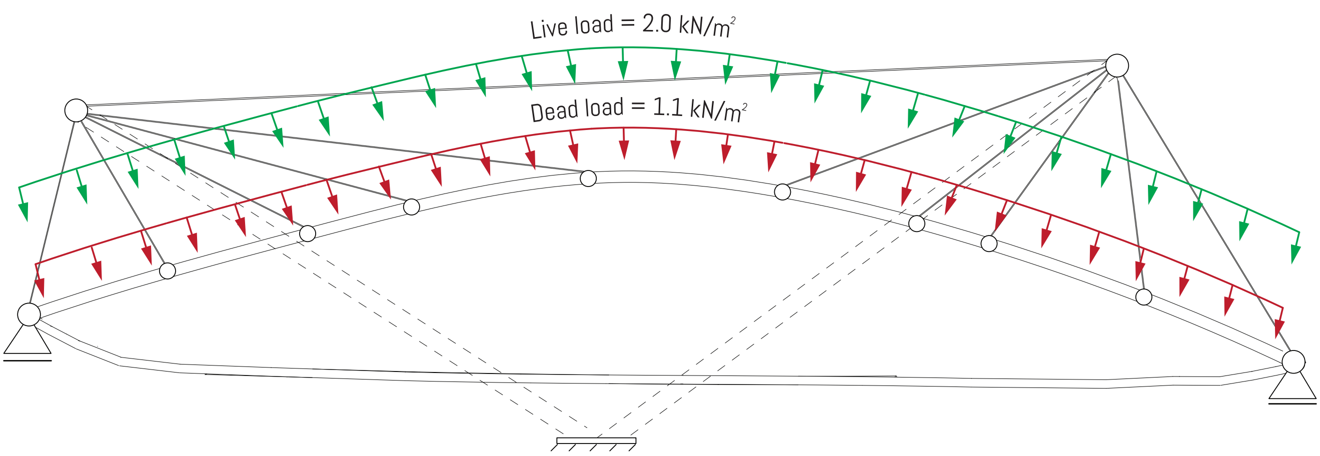

Fig. 87: Determined loads primary structure (Andrejevic, 2016)

BUCKLING BEHAVIOUR ARCHES & BEAMS

The existing arches span over 200 metres, meaning that when extra loads are added to this span, high buckling stresses may occur. The maximum buckling length can be determined from cable knot to cable knot, which is maximum 25 metres. The most natural buckling form behaviour is shown below, with smaller buckling occuring in the arch that is stabilised with bracing between the cables. Which makes the bracing useful as buckling shorteners (see fig. 88).

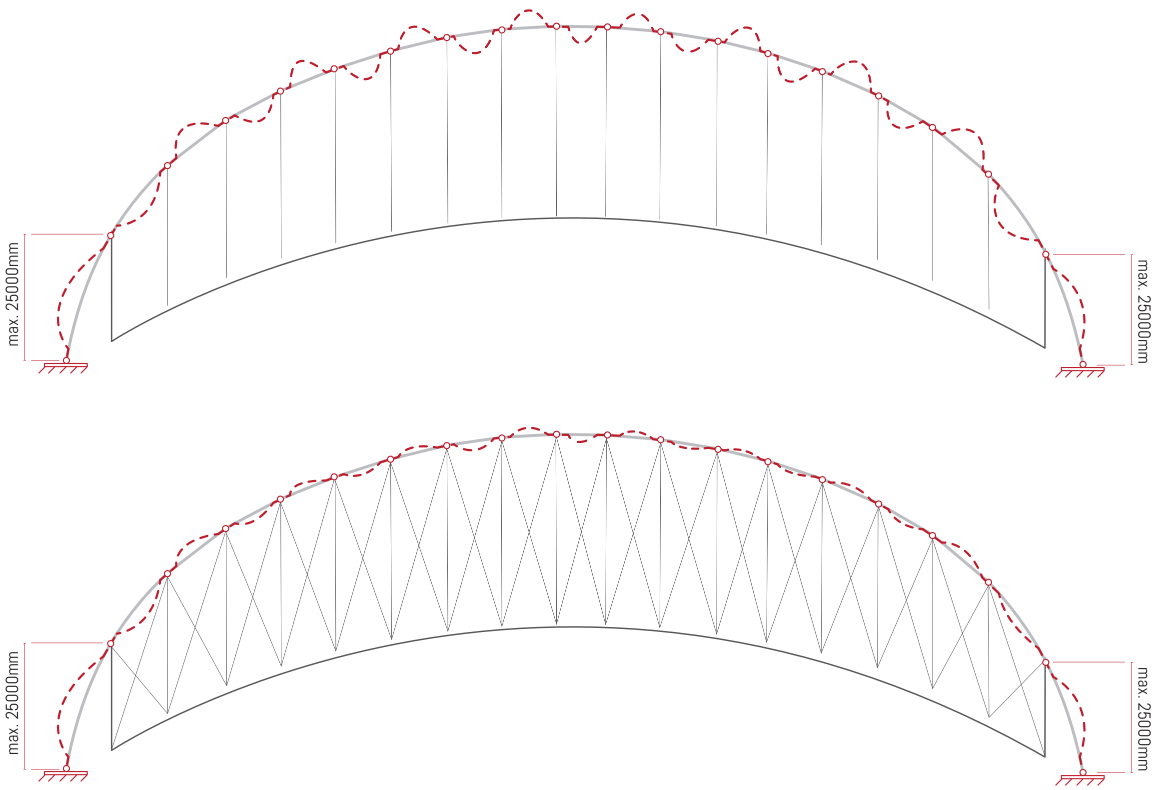

Fig. 88: Influence of bracing on buckling behaviour arches primary structure (Andrejevic, 2016)

To check if these high stresses are an issue, the deformation and the axial stresses have to be determined. Beginning with the high arch, the maximum deformation is ca. 3 cm and the maximum axial stress is ca. 6.9 kN/cm^2 (69 MPa) in compression and 0 in tension (see fig. 89a).

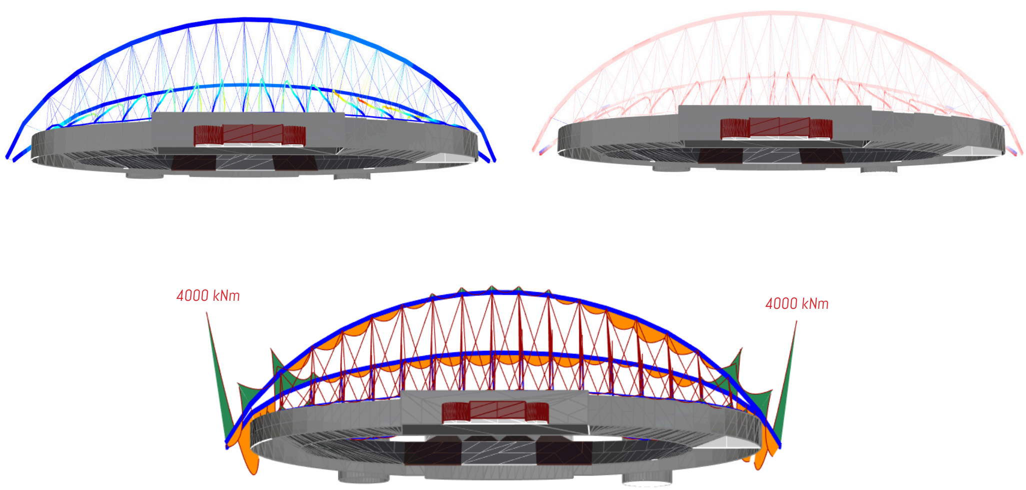

Fig. 89a: FEM results high arch (Andrejevic, 2016)

Secondly in the low arch the maximum deformation is ca. 6.5 cm and the maximum axial stress is 11 kN/cm^2 (110 MPa) in compression and ca. 9.8 kN/cm^2 (98 MPa) in tension (see fig. 89b).

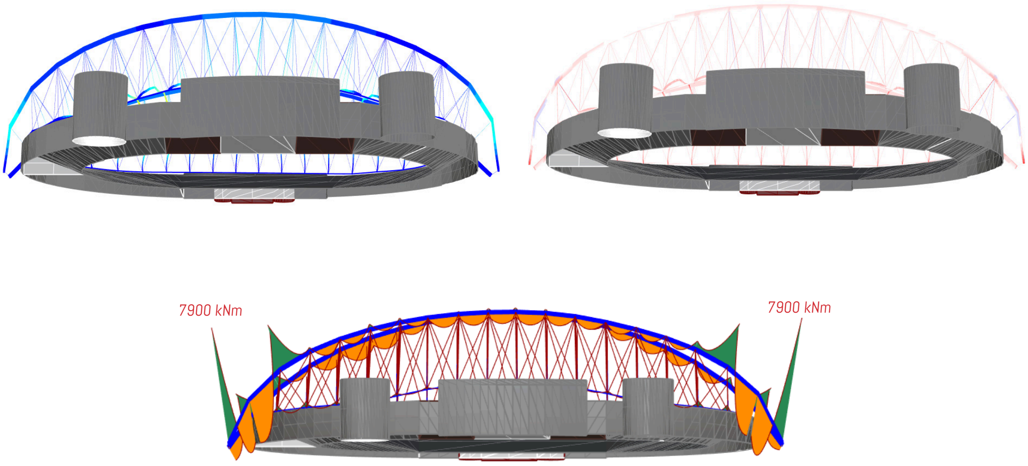

Fig. 89b: FEM results low arch (Andrejevic, 2016)

The low arch absorbs higher forces as a result of higher moments near the concrete clamps where the arches are attached to.

To determine whether the occuring axial stresses will not exceed the maximum buckling stress, Euler's buckling equation will be used:

$$S_{buckling} = \frac{\pi^2 \cdot E \cdot I}{{}_{0.5}L_b^2 \cdot A} \left[\frac{n}{mm^2} \right]$$

Where:

$S_{buckling}$ = buckling stress in N/mm^2
E = Young's modulus in N/mm^2
I = second moment of area in mm^4
${}_{0.5}L_b$ = 0.5 x buckling length in mm, because of fixed position
A = section area structural profile in mm^2

$$S_{buckling} = \frac{\pi^2 \cdot 210000 \cdot 8.9 \cdot 10^{10}}{0.5 \cdot 25000^2 \cdot 2.1 \cdot 10^6}$$

$$S_{buckling} = 436 \frac{N}{mm^2}$$

Maximum buckling stress = 436 MPa

For structural steel S355, the following safety factors has to be taken into account: dead load with an adverse effect gives a factor of 1.2 and live loads a factor of 1.5. (1994-1-2+C1, 2011)

With a Unity Check it will be determined whether the axial stress exceeds the maximum possible bucking stress. Giving the following results, with first checking the high arch only:

$$U.C. = \frac{\sigma_m \cdot 1.2 \cdot 1.5}{S_{buckling}}$$

where:
σ_m = 69 MPa compression stress
Safety factors = 1.2 and 1.5
$S_{buckling}$ = 436 MPa

$$U.C. = \frac{69 \cdot 1.2 \cdot 1.5}{436} = 0.29 < 1$$

Secondly, the low arch:

where:
σ_m = 110 MPa compression stress
Safety factors = 1.2 and 1.5
$S_{buckling}$ = 436 MPa

$$U.C. = \frac{110 \cdot 1.2 \cdot 1.5}{436} = 0.45 < 1$$

Both arches give positive results, meaning they are buckling resistant.

The beams of the primary structure span a maximum length of 180 metres. The beam gets supported at 8 places: 2 fixed supports at the rigidity ring and 6 hinge supports to the suspension cables. Resulting in a maximum beam part length of ca. 25 metres, meaning a 25 metre buckling length. Below is shown what its most natural buckling behaviour would be (see fig. 90). Same as with the arches, the bracing causes less buckling which can be an advantage in terms of distortion.

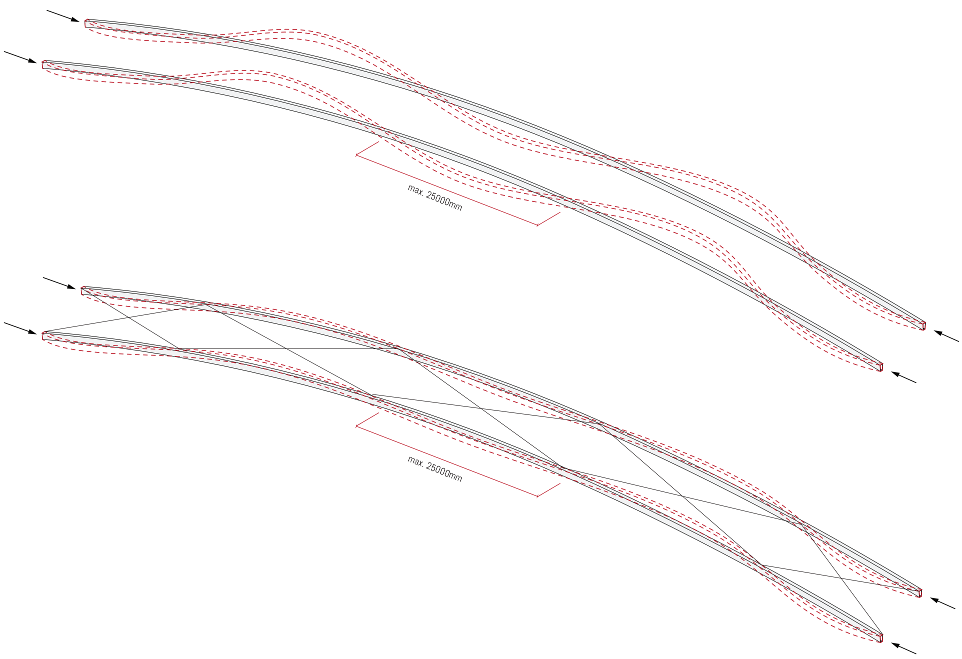

Fig. 90: Buckling behaviour beams with and without bracing primary structure (Andrejevic, 2016)

To know whether the beams are buckling resistant, an analysis is made to get a clear view of the behaviour of the beams. As shown below, the beams without bracing, tend to deform sidewards, with a maximum deformation of 17.7cm over a length of approximately 160 metres. While the beams with bracing have very little distortion with a maximum deformation of 9.3cm over a length of 180 metres. The bracing does not influence the axial stresses, where the highest axial stress occuring is 10.7 kN/m² (107 MPa) in compression.

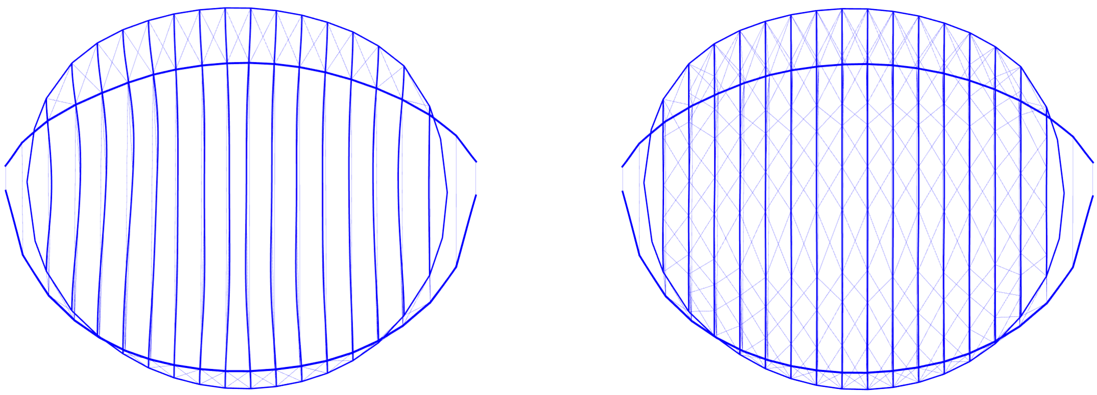

Fig. 91: Difference in distortion of beams with and without bracing (Andrejevic, 2016)

To determine whether the occuring axial stresses will not exceed the maximum buckling stress, Euler's buckling equation will be used:

$$S_{buckling} = \frac{\pi^2 \cdot E \cdot I}{L_b^2 \cdot A} \left[\frac{n}{mm^2}\right]$$

Where:

$S_{buckling}$ = buckling stress in N/mm²
E = Young's modulus in N/mm²
I = second moment of area in mm⁴
L_b = buckling length in mm
A = section area structural profile in mm²

$$S_{buckling} = \frac{\pi^2 \cdot 210000 \cdot 2.35 \cdot 10^{10}}{25000^2 \cdot 1.5 \cdot 10^5}$$

$$S_{buckling} = 519.5 \frac{N}{mm^2}$$

Maximum buckling stress = 519.5 MPa

With a Unity Check it will be determined whether the axial stress exceeds the maximum possible bucking stress. Giving the following results:

$$U.C. = \frac{\sigma_m \cdot 1.2 \cdot 1.5}{S_{buckling}}$$

where:

σ_m = 107 MPa compression stress
Safety factors = 1.2 and 1.5 (1994-1-2+C1, 2011)
$S_{buckling}$ = 519.5 MPa

$$U.C. = \frac{107 \cdot 1.2 \cdot 1.5}{519.5} = 0.37 < 1$$

6.5.4.4 FINAL RESULTS FEM ANALYSIS

The maximum deformation is 9.3cm on a beam of approximately 180m. Because of the bracing, the placing of the beams is stable, meaning that the secondary structure will not completely stabilise the primary structure. Resulting a secondary structure with less chance of possible buckling. (see fig. 90).

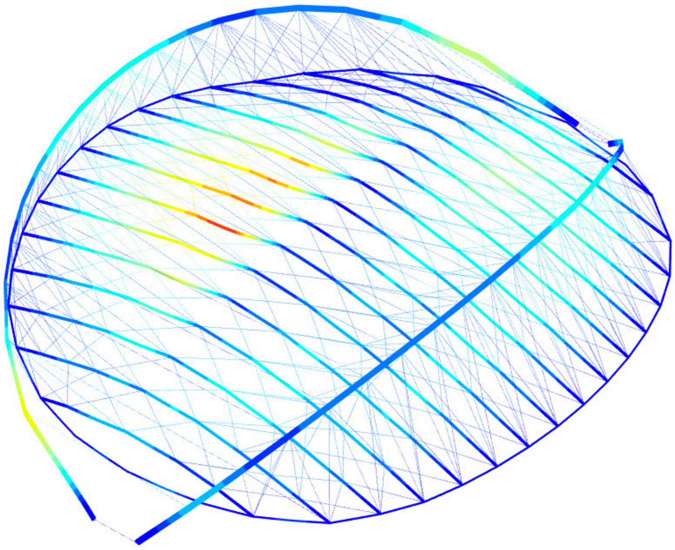

Fig. 92a: Outcome deformations primary structure (Andrejevic, 2016)

The axial stresses are mostly negative in the upper parts and positive in the lower parts of the structural elements. This means that the upper parts are stressed on compression and the lower parts on tension. Except for the cables, which all undergo positive axial stresses. Meaning they are only stressed on tension. The maximum measured axial stress is 10.1 kN/cm^2 (ca. 101 MPa) (see fig. 91).

$$U.C. = \frac{\sigma_m \cdot 1.2 \cdot 1.5}{f_{m;d}}$$

where:
σ_m = 101 N/mm^2 maximum axial stress
Safety factors = 1.2 and 1.5
$f_{m;d}$ = 355 N/mm^2 high strength structural steel

$$U.C. = \frac{101 \cdot 1.2 \cdot 1.5}{355} = 0.51 < 1$$

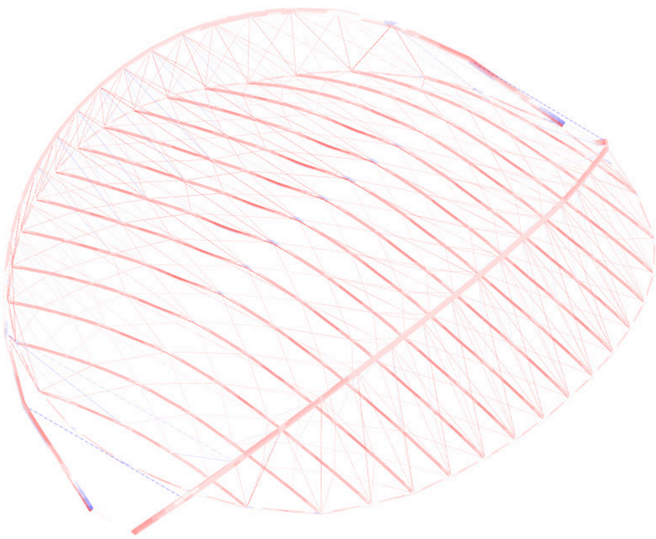

Fig. 92b: Outcome deformations primary structure (Andrejevic, 2016)

The maximum moments can be found at the feet of the arches, where they are around 7900 kNm (see fig. 92c).

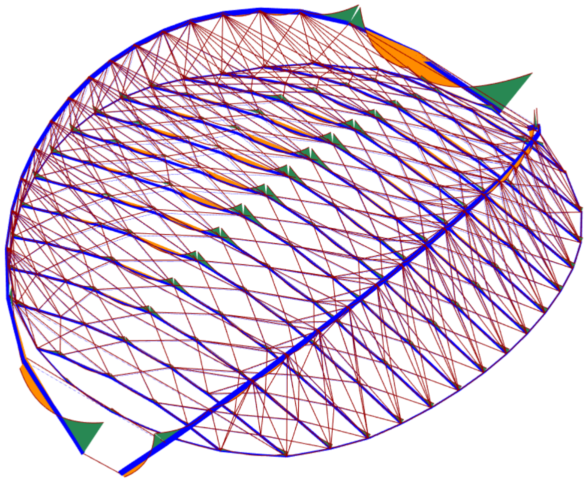

Fig. 92c: Outcome maximum moments primary structure (Andrejevic, 2016)

Like the moments, the highest shear force can be found at the feet of the arches, around 360 kN (see fig. 92d).

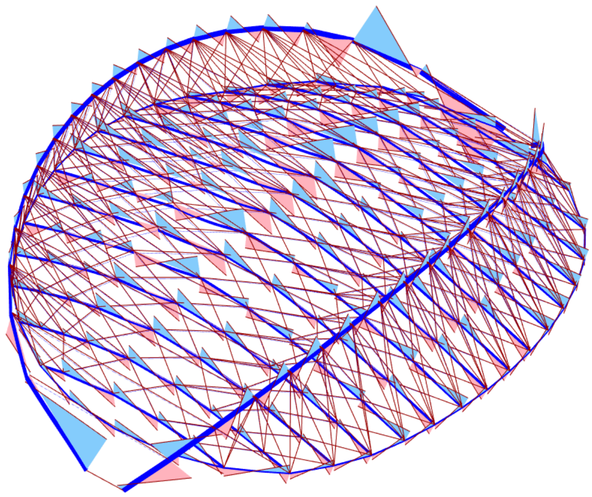

Fig. 92d: Outcome shear forces primary structure (Andrejevic, 2016)

The highest normal forces occur in the beam with the largest span with a resulting force of -3100 kN (see fig. 92e).

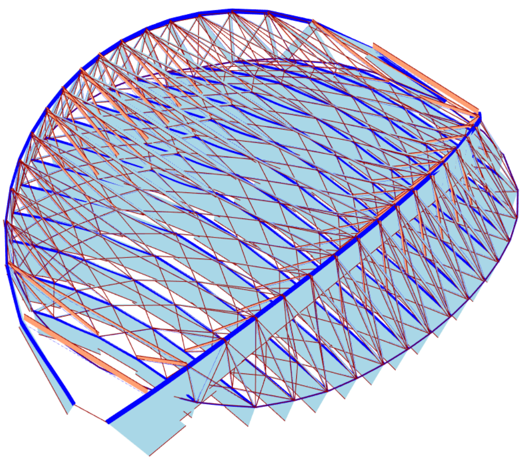

Fig. 92e: Outcome normal forces primary structure (Andrejevic, 2016)

6.5.5 PRIMARY STRUCTURE CONCEPT DESIGN

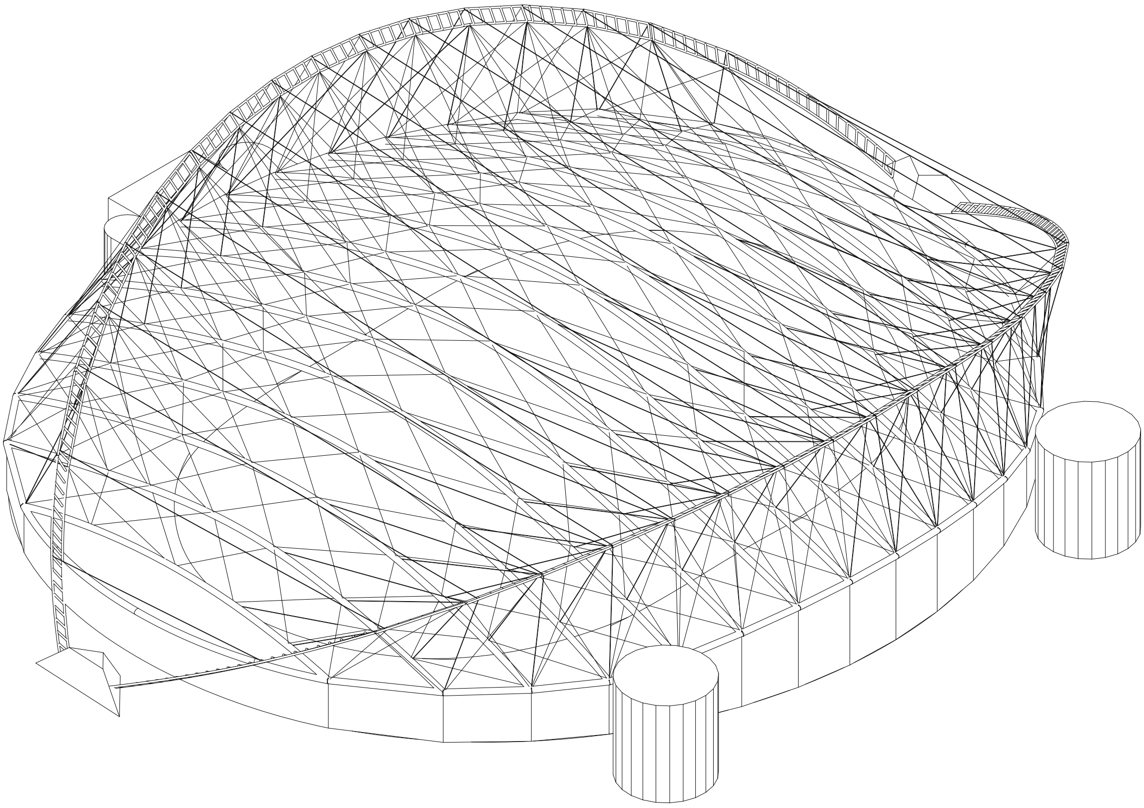

Fig. 93: Design Primary Structure (Andrejevic, 2016)

6.6.1 SUN POSITION

Before conducting the heat and lighting analysis, the right position of the sun has to be determined with input from the location, date and time (see fig. 94). This data input is derived from the programme Autodesk Ecotect, which is fully connected to the Grasshopper script through GECO (plugin) to conduct further analysis. The set location is Doha, Qatar and the set date and time are the 21st of June at 12.00 in the afternoon. The reason why this date and time were set, is the fact that June 21st regards the hottest possible day of the year. Meaning that the analysis will run in the most extreme situation. As can be seen below (see fig. 95), the sun's angle relative to the ground is 87˚ in that time of year. Meaning that the sun is positioned almost directly above the stadium roof surface, which may give interesting analysis results.

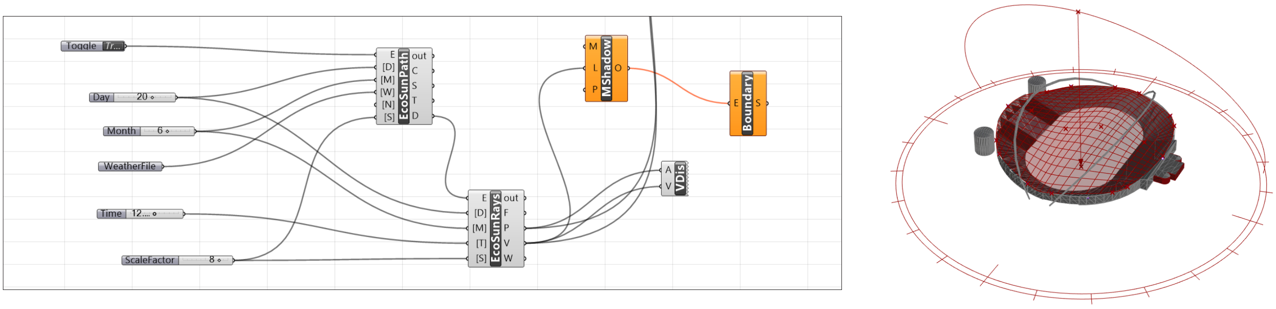

Fig. 94: Sun input in Grasshopper derived from Autodesk Ecotect (Andrejevic, 2016)

6.6.2 HEAT ANALYSIS

The script that supports the heat analysis translates the used geometry as data input to Autodesk Ecotect, to subsequently calculate a certain needed amount of radiation coming from the sun. In the case of a heat analysis, the relevant calculation that has to run is the daily average absorbed radiation. With this data a heating calculation can be conducted. With information about the amount of heating of the sun, the amount of needed cooling can be determined.

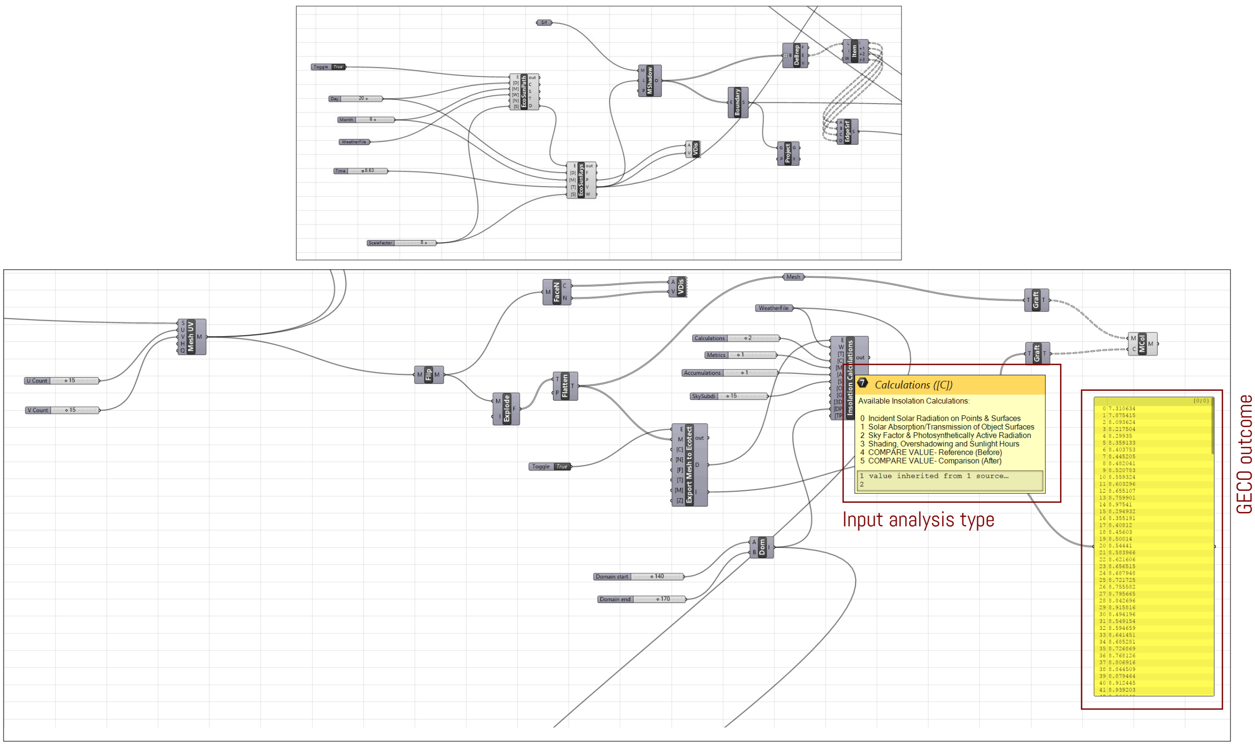

Fig. 95: Scipt heat and lighting analysis (Andrejevic, 2016)

Below is the amount of daily absorbed radiation at the roof surface shown, with an amount varying from 5200 to 6400 Wh/m^2 (920 - 1040 Wh/m^2 peak radiation) (see fig. 96a). This amount of radiation is determined on a surface that is ca. 15% absorbent (solid material). (Abrisa, 2014)

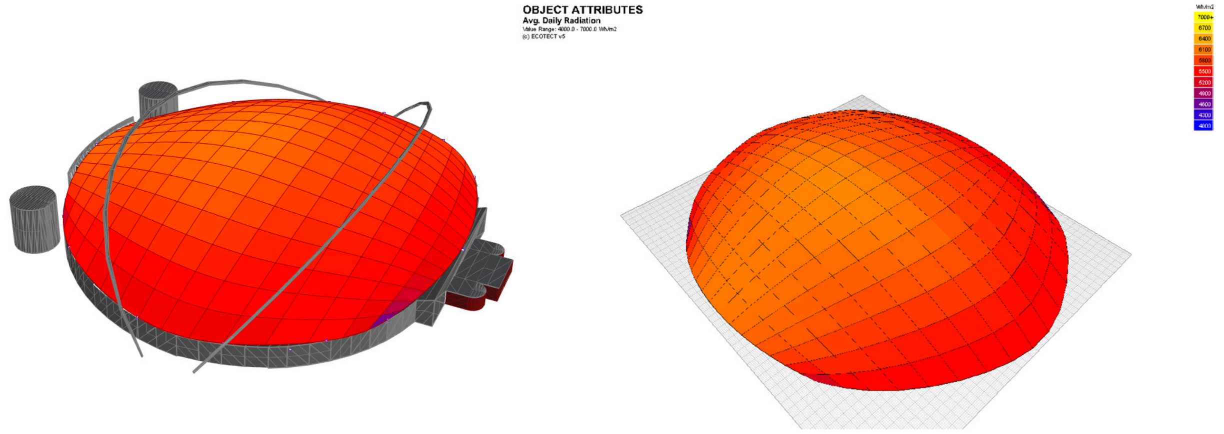

Fig. 96a: Heat analysis roof surface (Andrejevic, 2016)

The absorption amount of the roof surface creates an amount of daily absorbed radiation on the pitch of 6200 Wh/m^2. Showing a slight higher amount of absorbation, because of the absorption value of the grass (see fig. 96b).

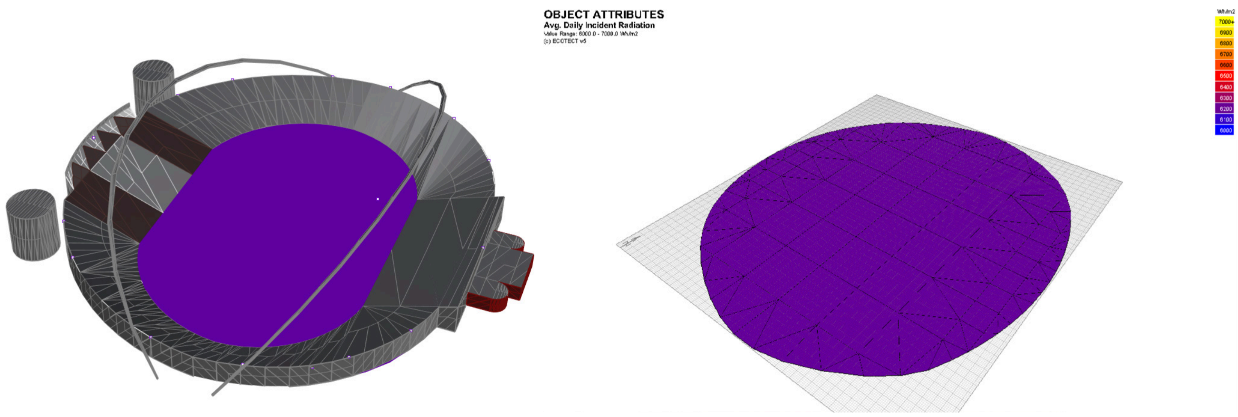

Fig. 96b: Heat analysis pitch surface (Andrejevic, 2016)

6.6.3 LIGHTING ANALYSIS

To start with the lighting analysis, information of the amount of sun hours has to be collected to get insight in the amount of hours the roof surface is exposed to direct sunlight. The eastern part gets about 10 hours of direct sunlight and the western part 11 hours (see fig. 98).

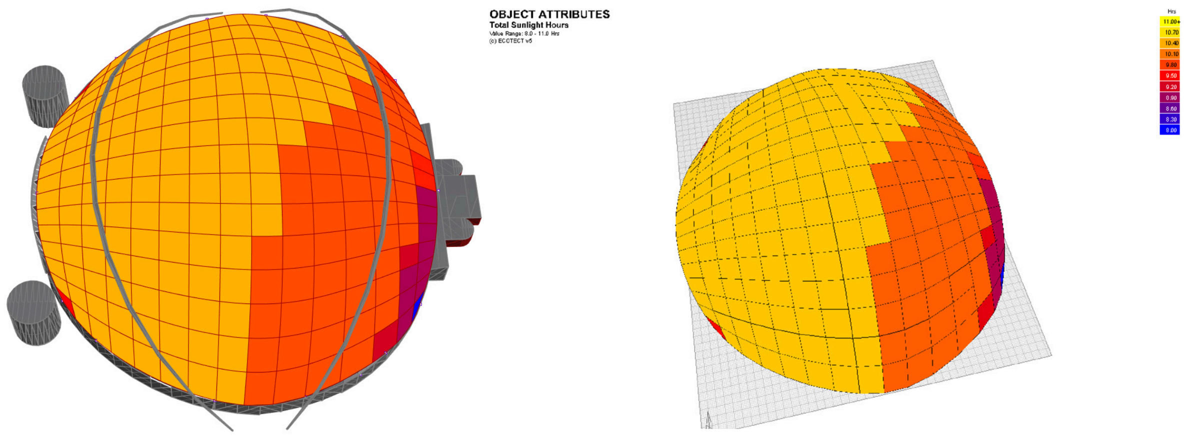

Fig. 97: Amount of hours direct sunlight roof surface (Andrejevic, 2016)

Different from the heat analysis, the lighting analysis shows the amount of Photosyntatically Active Radiation (PAR) absorbed by the surface. Which is used to calculate the needed amount of light to grow the grass. Again the surface is considered to be 15% absorbent. Below shown: the amount of absorbed PAR on the roof surface, varying from 8.5 Wh/m² to 9.7 Wh/m² (see fig. 98a).

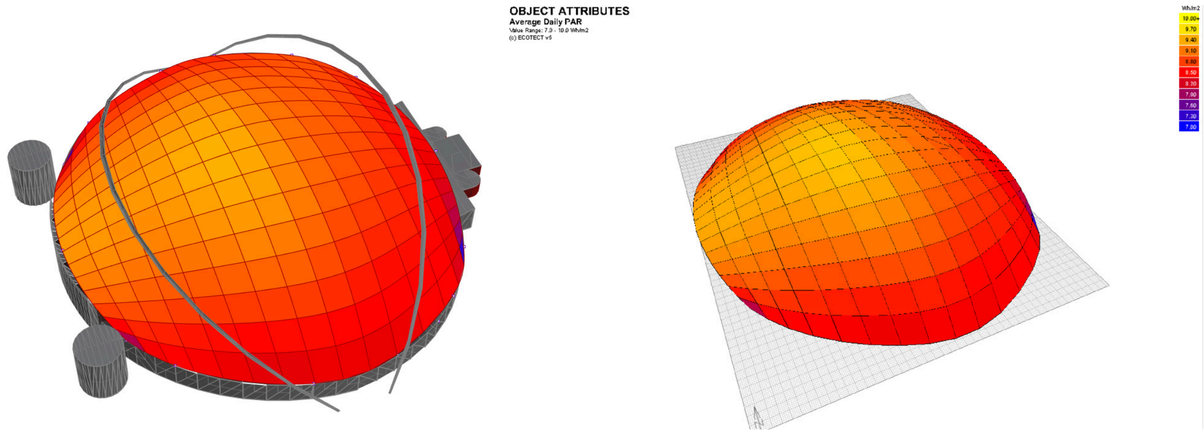

Fig. 98a: PAR analysis roof surface (Andrejevic, 2016)

The amount of PAR that reaches the pitch is and gets absorbed is around 7.6 Wh/m². This value is much lower because the roof absorbing too much direct sunlight, resulting in the grass suffering from this low amount of PAR (see fig. 98b).

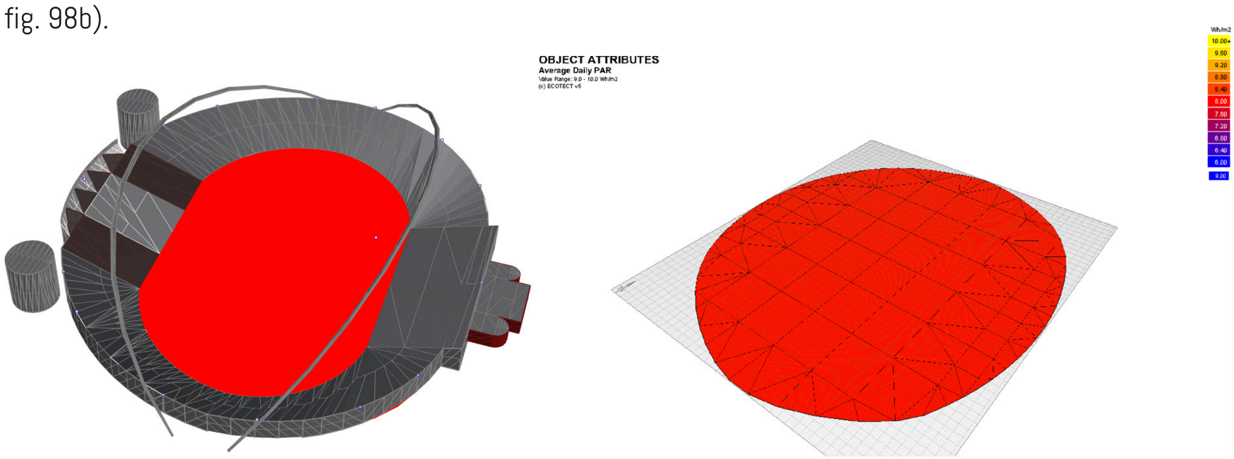

Fig. 98b: PAR analysis pitch surface (Andrejevic, 2016)

6.6.4 RESPONSIVE SKIN

With the responsive skin algorithm it is possible to give a radiation input limit of the pitch, based on the amount of needed heat and/or PAR. With this data input, the algorithm calculates the amount of openings needed to reach that certain amount of heat and/or PAR. These openings stand for direct light passers and ventilation grilles. Below is the algorithm of the response skin shown (see fig. 99a).

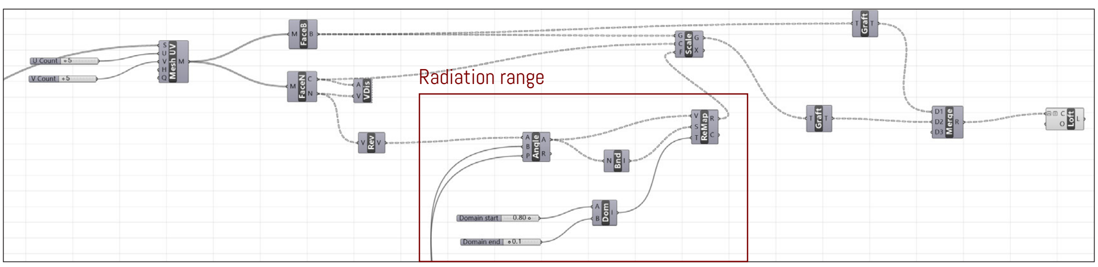

Fig. 99a: Responsive skin script (Andrejevic, 2016)

The figure below shows how the responsive skin algorithm is combined with absorbed heat and PAR as input. The responsive skin gets input from the sun script and from the radiation calculation script. The limit heat of PAR input comes from the radiation script, where the limit is variable (see fig. 99b).

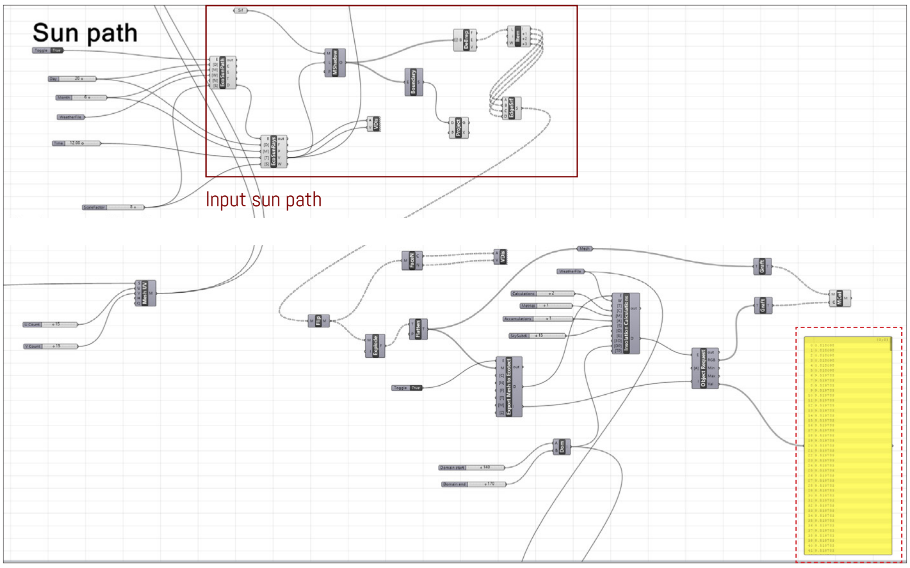

Fig. 99b: Heat and/or PAR input limit script (Andrejevic, 2016)

With a maximum amount of daily absorbed radiation set to ca. 5600 Wh/m^2 (960 Wh/m^2 peak radiation) the responsive skin script comes with the following outcome (see fig. 100a). Almost no openings for direct sunlight.

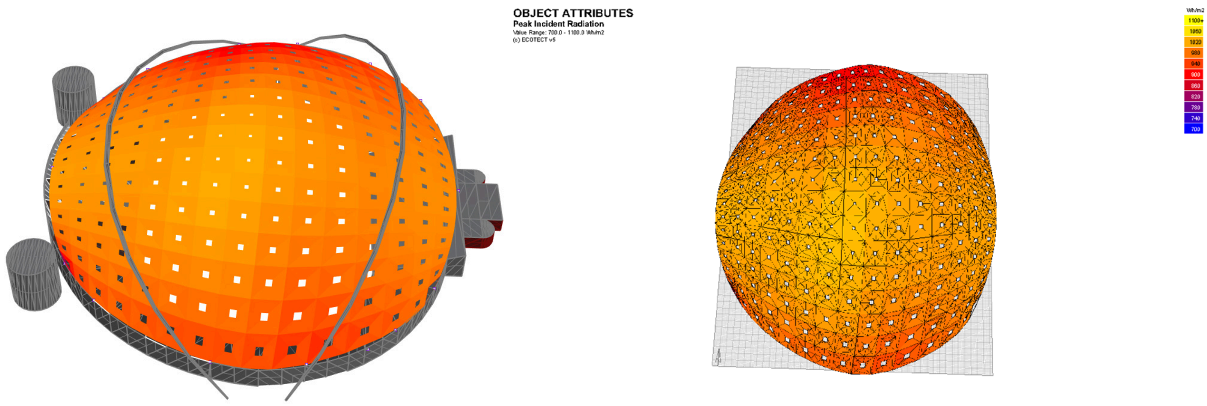

Fig. 100a: Responsive skin outcome based on heat limit (Andrejevic, 2016)

With a maximum amount of absorbed PAR set to ca. 9.0 Wh/m^2 the responsive skin script comes with the following outcome (see fig. 100b). A lot of openings for direct sunlight.

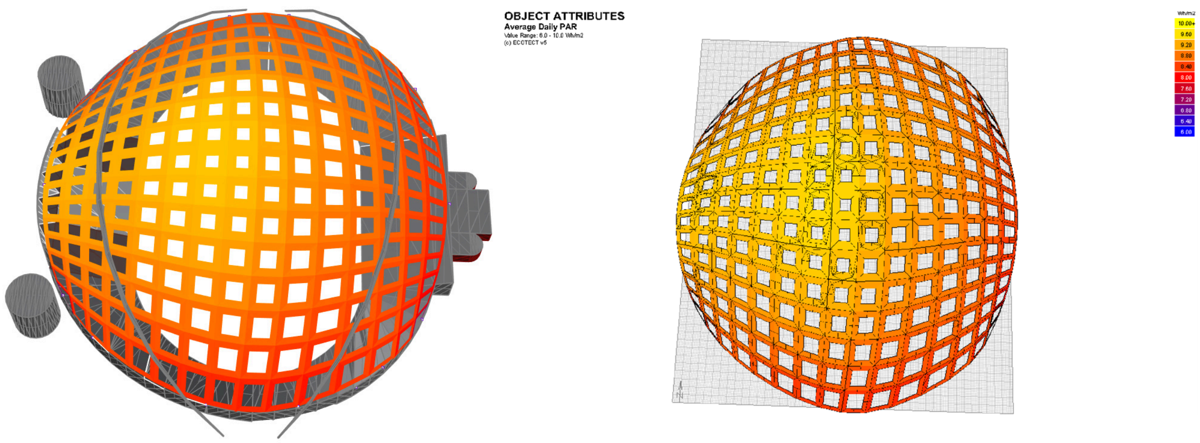

Fig. 100b: Responsive skin outcome based on PAR limit (Andrejevic, 2016)

With the limit amounts of heat and PAR absorption combined, the responive skin script comes with the following outcome (see fig. 101a). The combined outcome gives a clear view of what needs to be achieved in terms of heat reduction and light absorption. The middle part is as closed as possible to keep the heat out, while the sides are open to get enough diffuse light in the stadium.

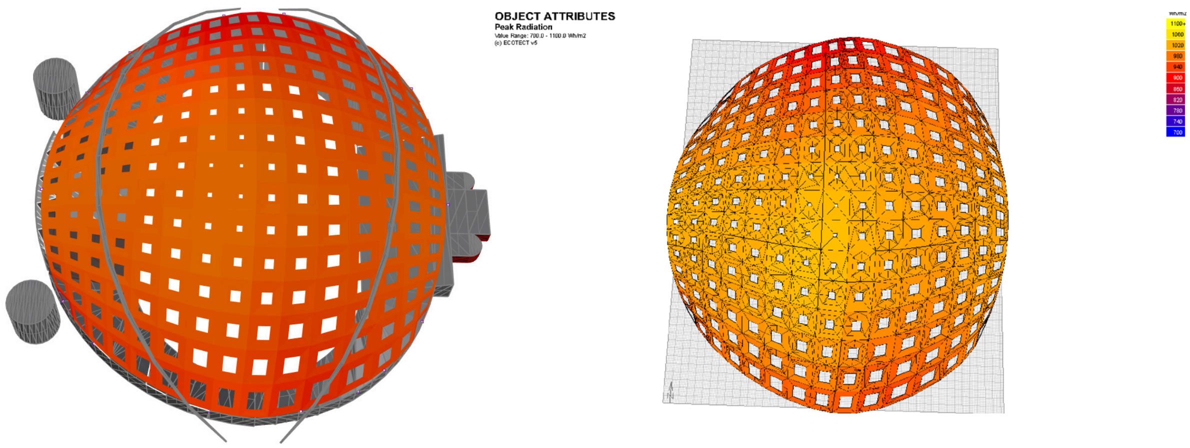

Fig. 101a: Responsive skin outcome based on combined limits (Andrejevic, 2016)

The responive skin outcome gives a reduced amount of daily absorbed radiation, namely ca. 5400 Wh/m^2 (940 Wh/m^2 peak radiation). Which is 800 Wh/m^2 lower than the amount without the responsive skin (see fig. 101b).

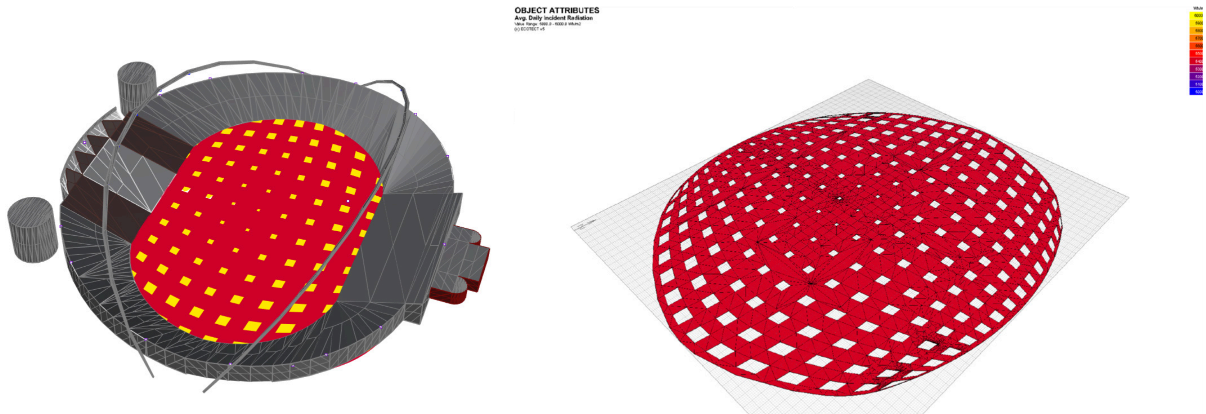

Fig. 101b: Heat analysis responsive skin pitch surface (Andrejevic, 2016)

With the amount of ca. 9.0 Wh/m^2 PAR, the responsive skin gives a small decrease of 0.7 Wh/m^2. This means that even with blocking direct sun light, the amount of needed PAR can be reached with diffuse light (see fig. 101c).

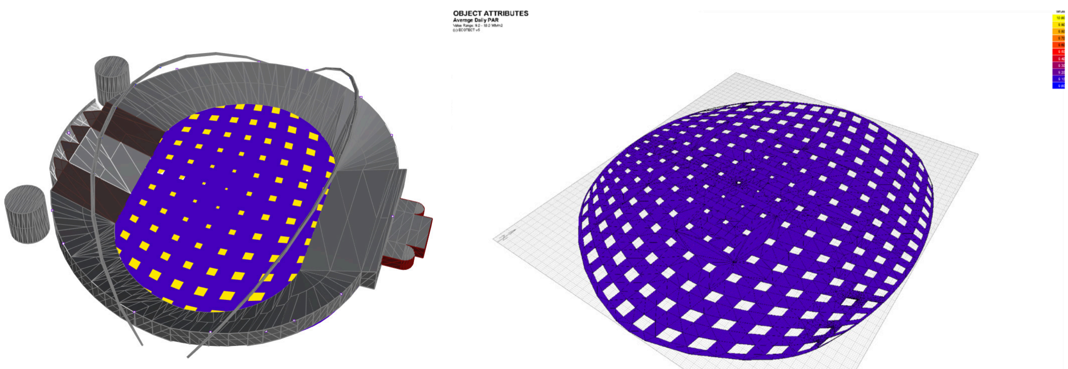

Fig. 101c: PAR analysis responsive skin pitch surface (Andrejevic, 2016)

6.6.5 HEAT AND LIGHTING CONCEPT DESIGN

6200 Wh/m² on a surface with 26% reflectance (Alkali Aluminosilicate) can give a daily heating of 26.77 ˚C. This heating is reduced at the pitch because of the stadium height (see fig. 102). The heating at the pitch is around 16.59 ˚C. (Abrisa, 2014) (Clemenzi, 2011)

26.77 ˚C → 16.59 ˚C

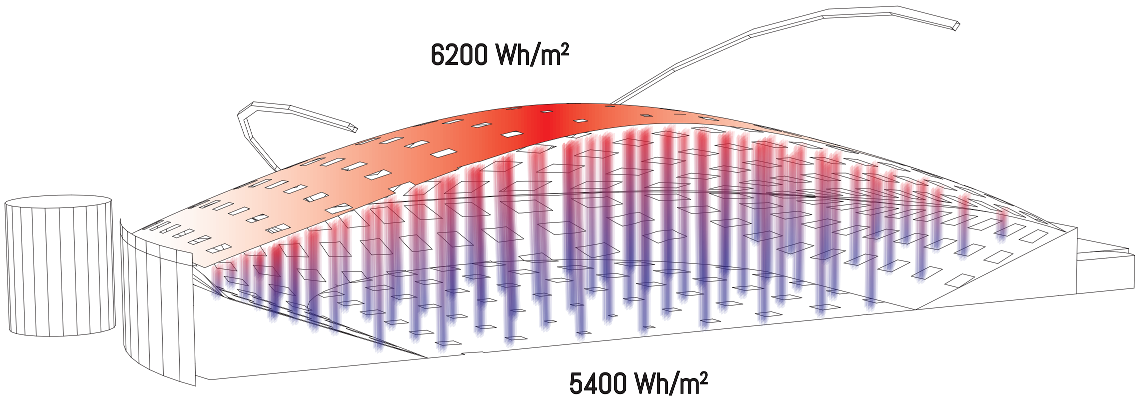

Fig. 102: Heat concept design (Andrejevic, 2016)

In chapter *4.2 Lighting Quality in Stadia* was stated that the average daily PAR value exposed to the pitch should be 3 MJ/m² (11 hours of light), which equals 53 W/m². With the analysis occurs around 9.0 Wh/m² on the field, which equals 99 W/m² daily (see fig. 103).

99 W/m² > 53 W/m²

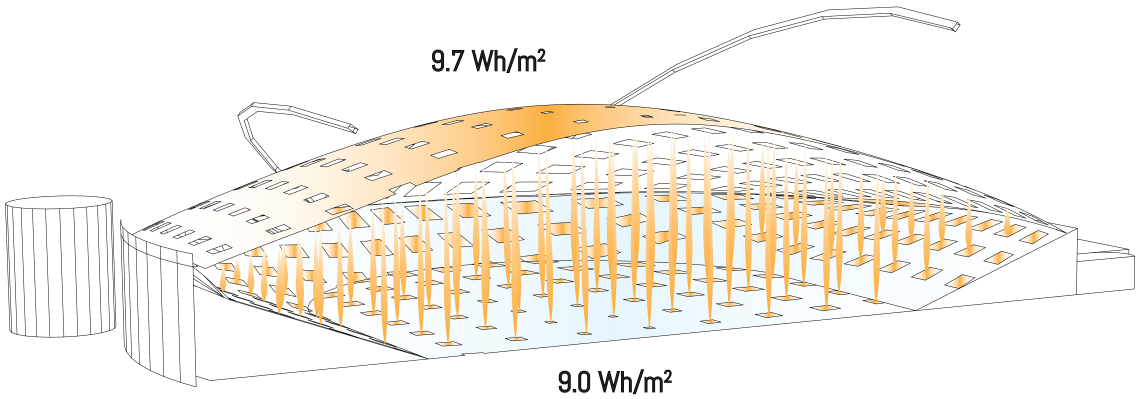

Fig. 103: Lighting concept design (Andrejevic, 2016)

In hot summer conditions it is needed to cool the roof and air condition the whole stadium to lower the heating values.

In order to conduct a full structural analysis on the secondary structure, the concept proposal has to fulfill the restrictions coming out of the heat and lighting analysis. To make a span of 15 metres, a hybrid glass arch is proposed, based on earlier literature research on glass spans (see fig. 104). (Wurm, 2007)

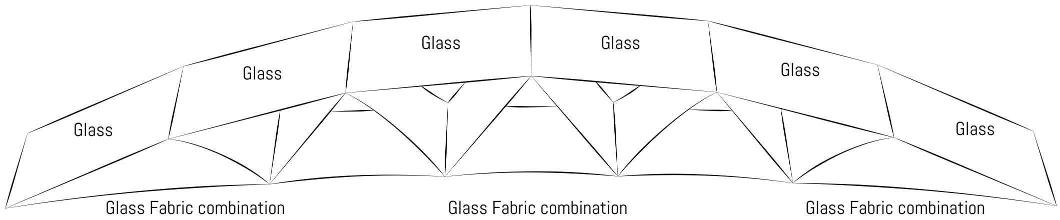

Fig. 104: Arch concept proposal (Andrejevic, 2016)

The upper part of the arch has to be completely constructed out of glass (to get maximum transparency), while the web has to be a clever combination of glass and a certain translucent fabric. The fabric is used to keep direct sunlight from overheating the stadium, while the glass has to let the right amount of diffuse light through.
To find out what the best hybrid glass arch will be, the form will be tested with Kangaroo, following a FEM (Finite Element Method analysis on three possible variants using Karamaba. (see fig. 105).

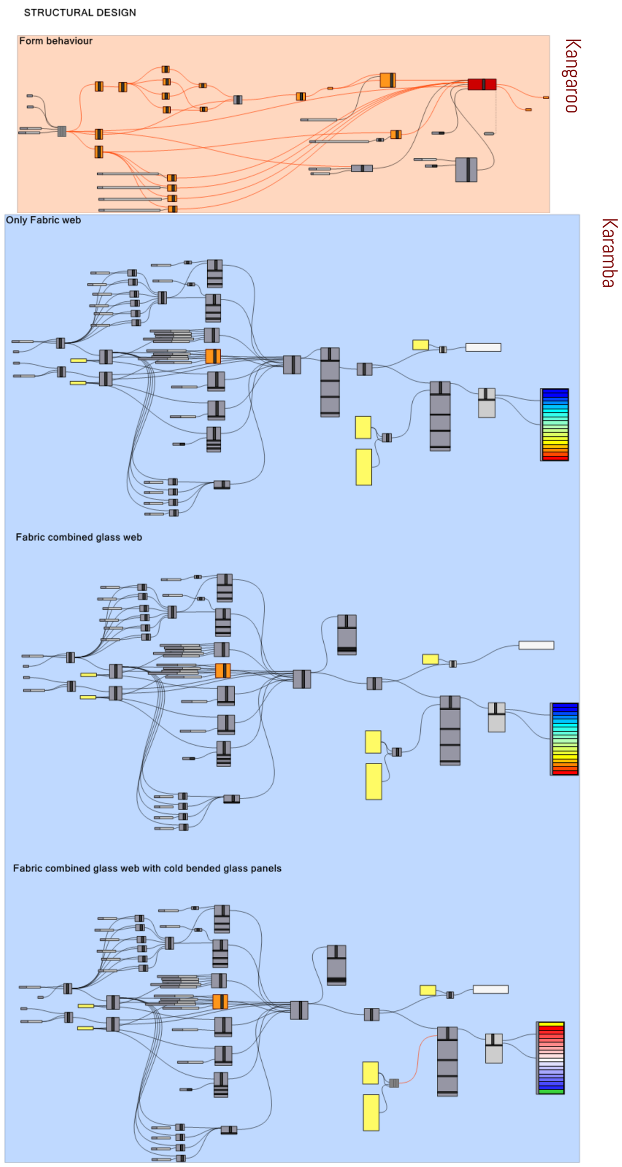

Fig. 105: Secondary structure analysis script (Andrejevic, 2016)

6.7.1 KANGAROO FORM BEHAVIOUR

As explained with the Kangaroo analysis for the primary structure, the plugin is a tool to conduct Particle Spring System (PSS) calculations, where the goal is to reach an equilibrium state where all the forces are 0. The same as done with the primary structure the secondary structure is considered to be a shell that gives bending resistance. To see how the proposed concept arch behaves, the following algorithm was used (see fig. 106).

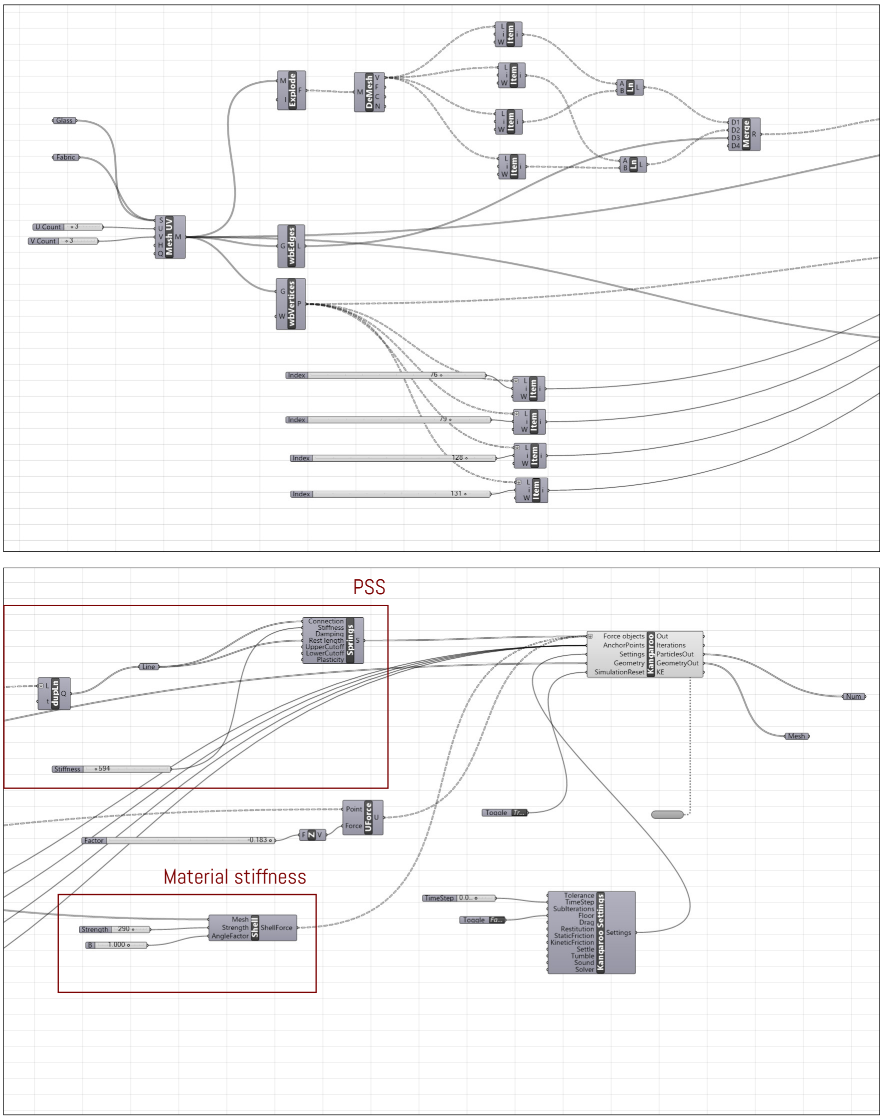

Fig. 106: Setup Kangaroo script secondary structure (Andrejevic, 2016)

From its own shape the arch moves downwards, where it cracks at the web edges (where the red arrows are). Meaning that at that particular hinge, the right reinforcement has to be taken into account (see fig. 107).

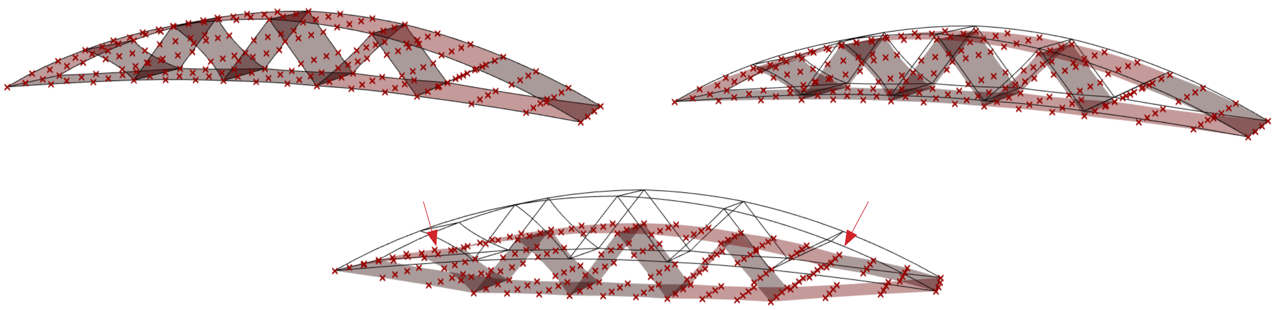

Fig. 107: Outcome Kangaroo form analysis (Andrejevic, 2016)

6.7.2 VARIANTS

To get the most optimal hybrid glass arch, three variants are proposed with different settings and properties. The first variant has the upper part completely made out of planar glass plates, while the web is completely constructed from fabric. The second variant has the upper part made out of planar glass plates as well, however the web is, with looking at the tension/compression behaviour, hybridly constructed with glass and fabric. The third and last variant is in terms of material constructed in the same way as the second variant, only the upper glass panels are slight cold bended. With the small part of the script shown below, it was possible to see the stability behaviour and the deformations of the variants (see fig. 108). Calculating with a dead load of 0.5 kN/m^2 and a liveload of 2 kN/m^2. (1994-1-2+C1, 2011)

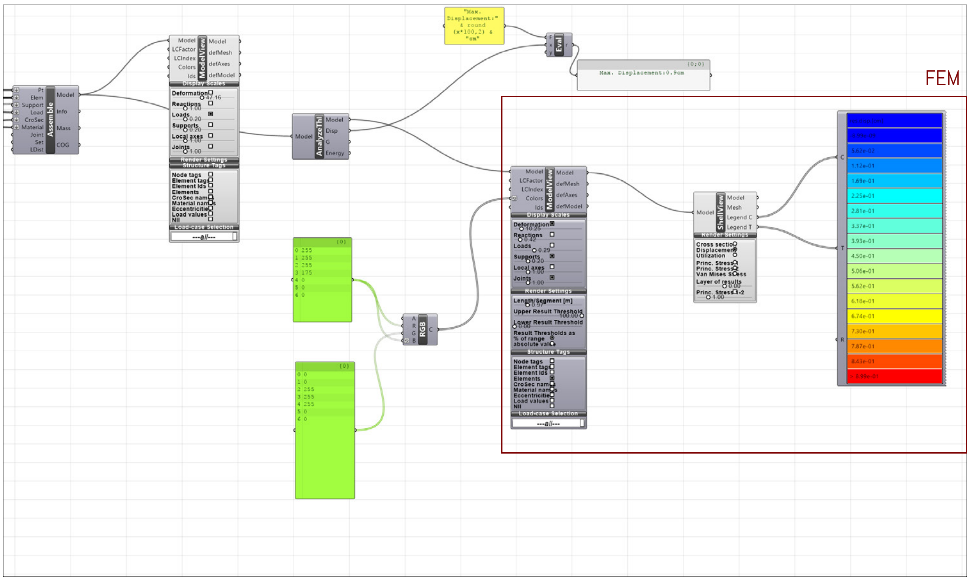

Fig. 108: Short setup Karamba script secondary structure for testing variants (Andrejevic, 2016)

6.7.2.1 STABILITY BEHAVIOUR

Variant 1:

The upper glass plates absorb compression forces, while the web is completely made out of fabric to absorb tension forces. As shown below with the stability and deformation analysis, the compression and tension forces do not equilibrate, resulting in instability and high deformations (see fig. 109). The maximum deformation shown below is 15cm.

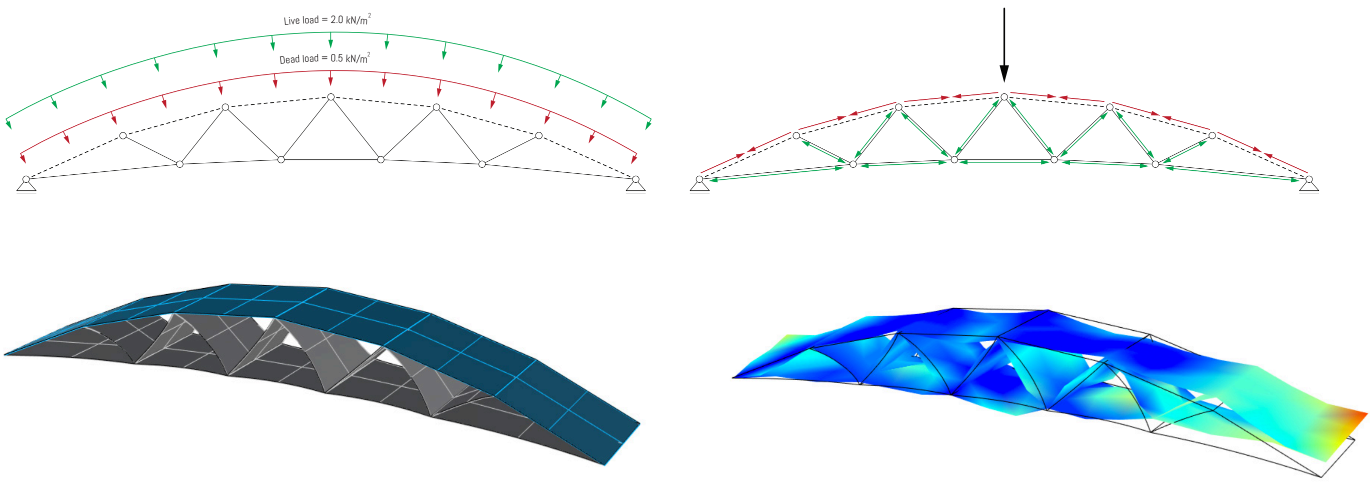

Fig. 109: Variant 1 structural behaviour (Andrejevic, 2016)

Variant 2:

The upper glass plates absorb compression forces and the web is divided in fabric and glass to get the fabric absorb the tension forces and the glass the compression forces. With this equal division of forces the arch makes an equilibrium, resulting in stability and lower deformations. However, the deformation is still 1.5cm, giving the plates a relatively large deformation that can result in high principal stresses (see fig. 110).

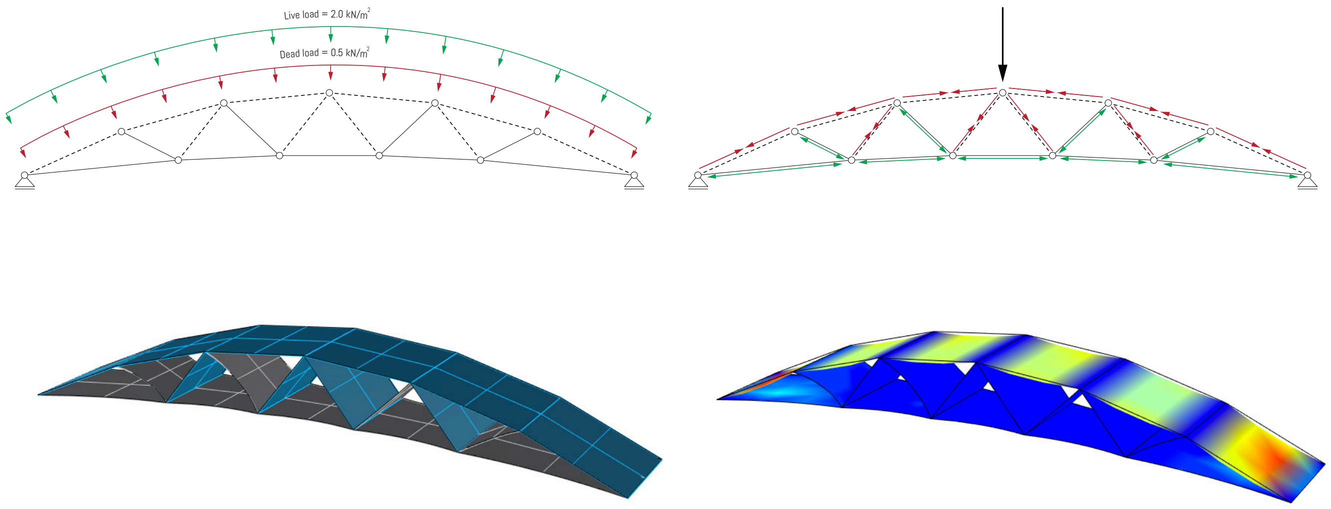

Fig. 110: Variant 2 structural behaviour (Andrejevic, 2016)

Variant 3:

The material division of the arch is the same as with variant 2, but the upper glass plates are cold bended 1cm up right in their normal directions. Resulting in even more stability and very low deformations. The maximum deformation is around 0. 4cm. Different from variant 2, this arch deforms as a whole structure instead of individual plates (see fig. 111).

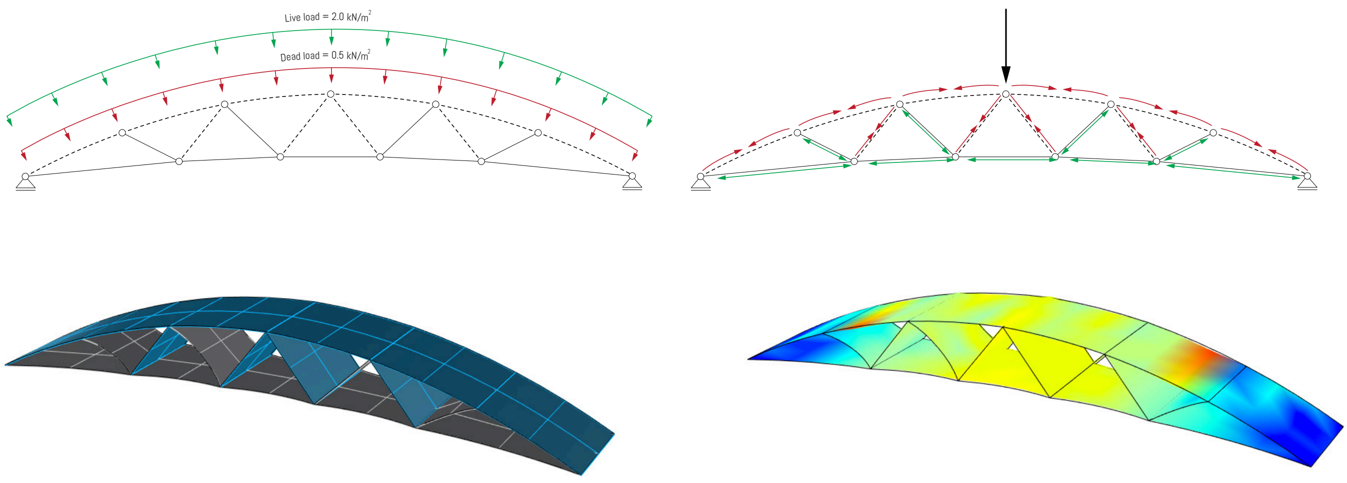

Fig. 111: Variant 3 structural behaviour (Andrejevic, 2016)

Finally resulting in the fact that variant 3 is the variant giving the best results and will be further analysed with a FEM using Karamba.

6.7.3 STRUCTURAL PROPERTIES

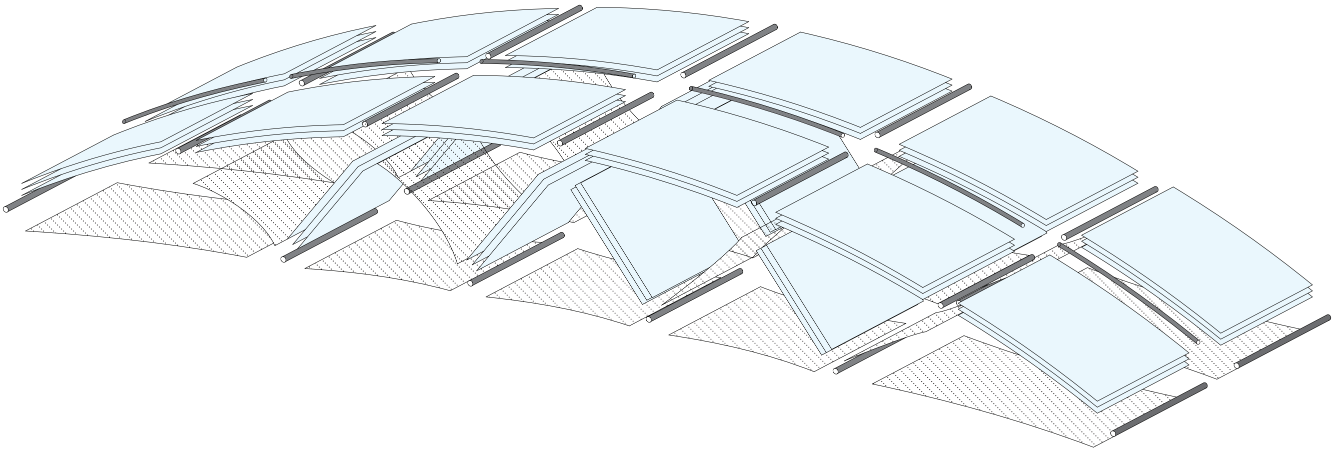

HEMP REINFORCED PTFE

Density: 2300 KG/m^3
Young's Modulus: 1.65 GPa
Shear Modulus: 590 MPa
Tensile Strength: 43 MPa
Compressive Strength: 16 MPa
Poisson's Ratio: 0.5
Expansion Coefficient: 1.8 x 10^{-7}/°C

ALKALI ALUMINOSILICATE

Density: 440 KG/m^3
Young's Modulus: 71.7 GPa
Shear Modulus: 29.7 GPa
Tensile Strength: 300 MPa
Compressive Strength: 900 MPa
Poisson's Ratio: 0.21
Expansion Coefficient: 84.5 x 10^{-7}/°C

(Abrisa, 2014)

Use of cables to reinforce
the woven PTFE at the edges

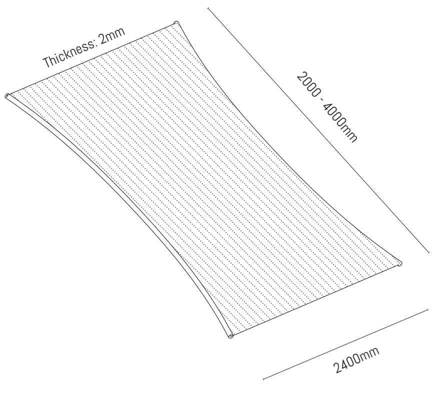

I_{xy} = 13.3 x 10^2 to 26.7 x 10^2 mm^4
Z_{xy} = 13.3 x 10^2 to 26.7 x 10^2 mm^3
R_{xy} = 0.578 mm
A = 40 x 10^2 to 80 x 10^2 mm^2

Alkali aluminosilicate panels laminated with Sentryglas interlayers

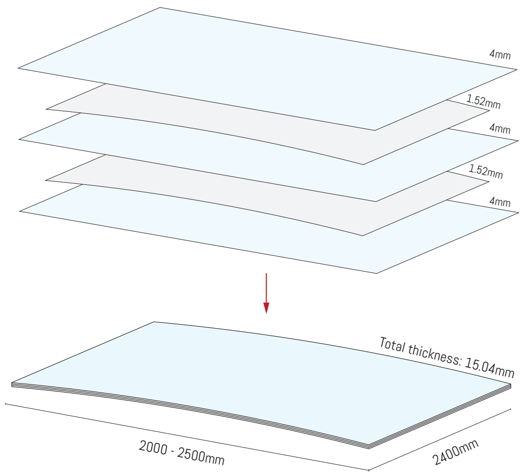

I_{xy} = 56.7 x 10^4 to 70.8 x 10^4 mm^4
Z_{xy} = 75.5 x 10^3 to 94.3 x 10^3 mm^3
R_{xy} = 4.35 mm
A = 30.1 x 10^3 to 37.6 x 10^3 mm^2

Fig. 112: Structural properties secondary structure (Andrejevic, 2016)

6.7.3.1 HEMP REIONFORCED PTFE

The fabric that absorbs the tension stress is PolyTetraFluorEthylene, commonly known as PTFE. To make PTFE applicable for construction, hemp is used to reinforce the polymer. As a second safety measure, cables are stringed to absorb the high tension forces at the edges of the cloth (see fig. 113). Such a build up can ensure a tensile strength of almost 50 MPa.

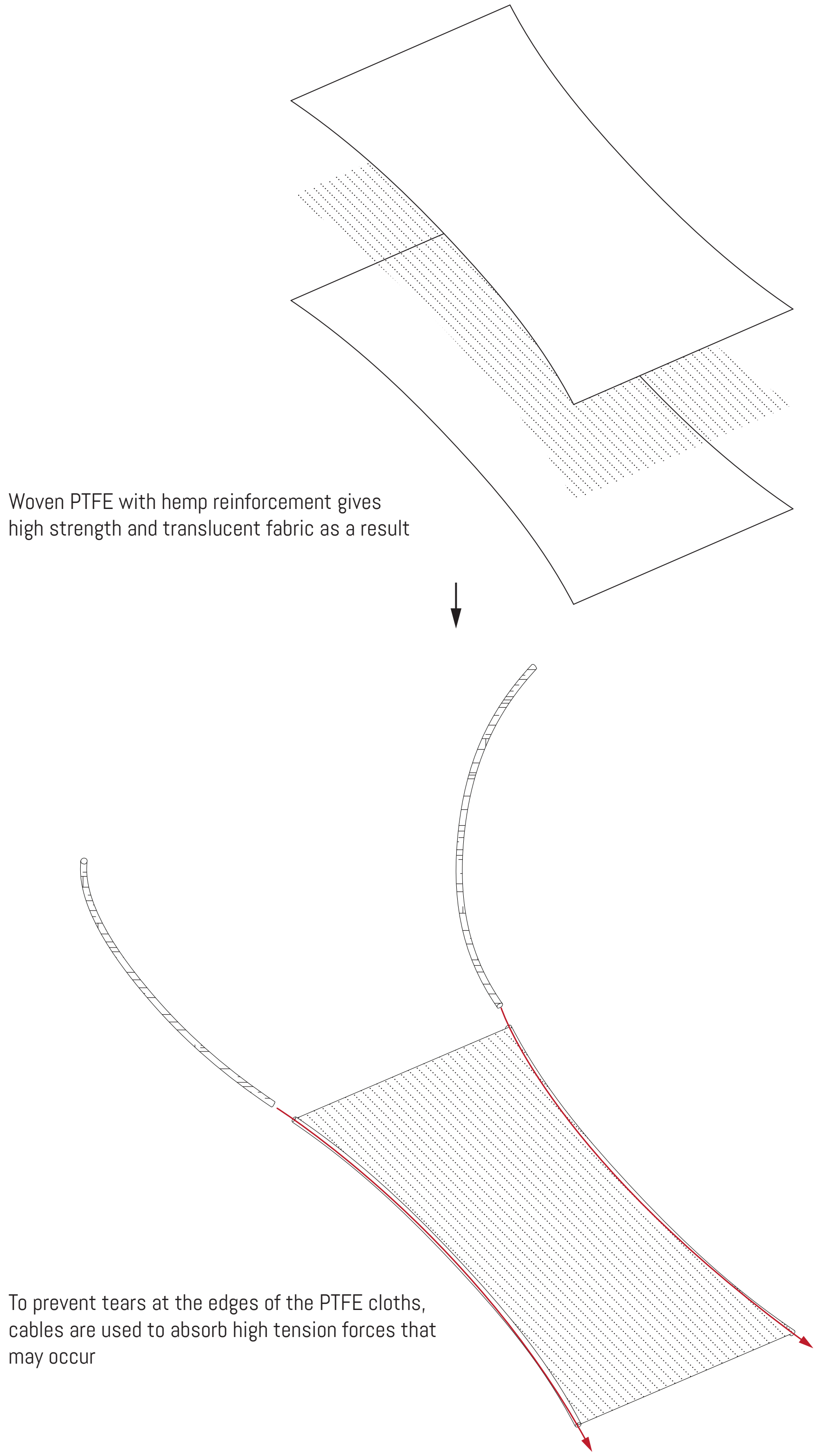

Fig. 113: Build up PTFE fabric part (Andrejevic, 2016)

6.7.3.2 ALKALI ALUMINOSILICATE

To give glass, when used as a structural material, a certain level of safety, the glass has to be laminated with the help of polymer foils. Therefore, cold bending of glass panels in a safe way happens as follows: flat thin glass plates are glued to pre bended hard polymer foils (SentryGlas). This way the panels are cold bended with a small number of distortion. To further prevent distortion, the panels are clamped in metal strips when forming the arch. The sentryglas interlayers will be resistant to the extreme Qatar climate, since they keep working structurally up to 82 ˚C (see fig. 114). (Dupont, 2016)

Planar glass surfaces laminated to pre-bended SentryGlas foils

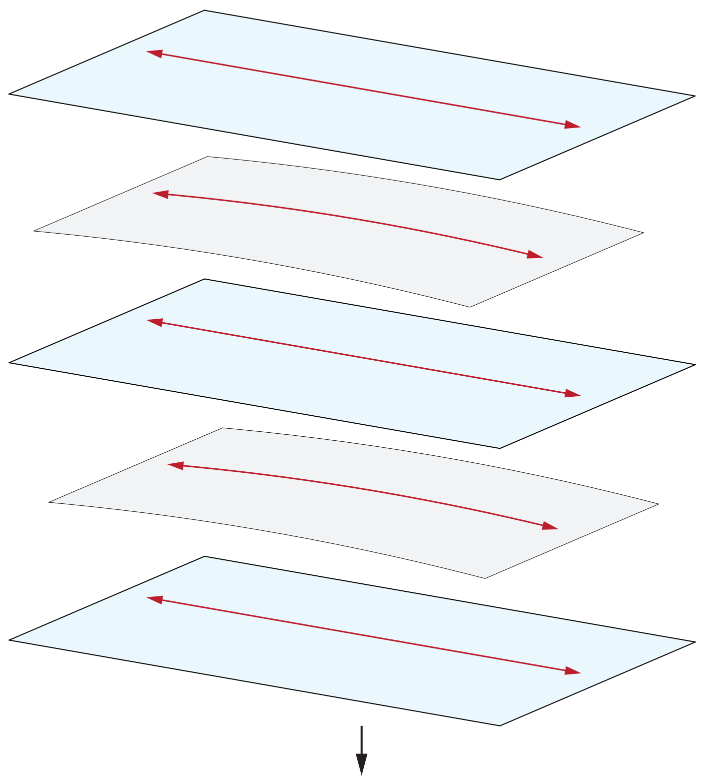

Resulting in a cold bended panel with small distortion

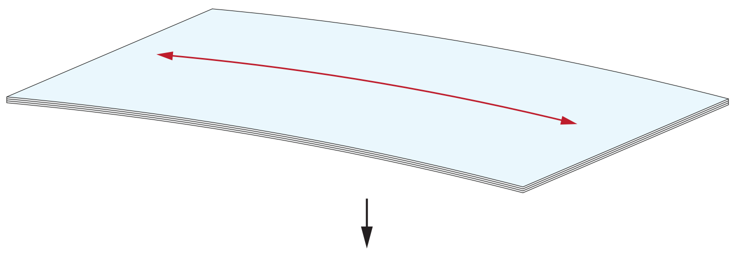

The pre-bended SentryGlas safety interlayers create a single curved plate, however to prevent increasing distortion the curvature the glass plate gets clamped in metal strips on its short and long side

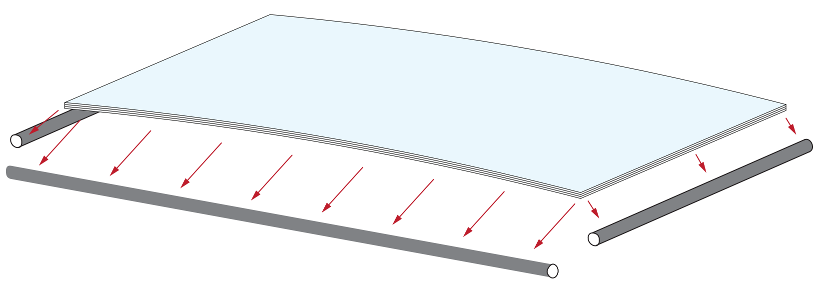

Fig. 114: Build up Alkali Aluminosilicate glass panel (Andrejevic, 2016)

6.7.4 FINITE ELEMENT METHOD ANALYSIS

6.7.4.1 SETUP KARAMBA SCRIPT

The script of the secondary structure maintains the same basics as the script of the primary structure. However, the secondary structure algorithm takes plates and shells as an input, instead of giving vector lines a structural property. Compared to the primary structural analysis, where only an equally divided live load was taken into consideration, the secondary structure also considers movable local live loads over the surface and wind pull loads. This is needed to get clear insight in possible instabilities caused by unexpected asymmetrical loads. Below shown: the glass and fabric as input, translated to material and structural properties. These properties come together with the supports and loads to translate the input into an analytical model (see fig. 115).

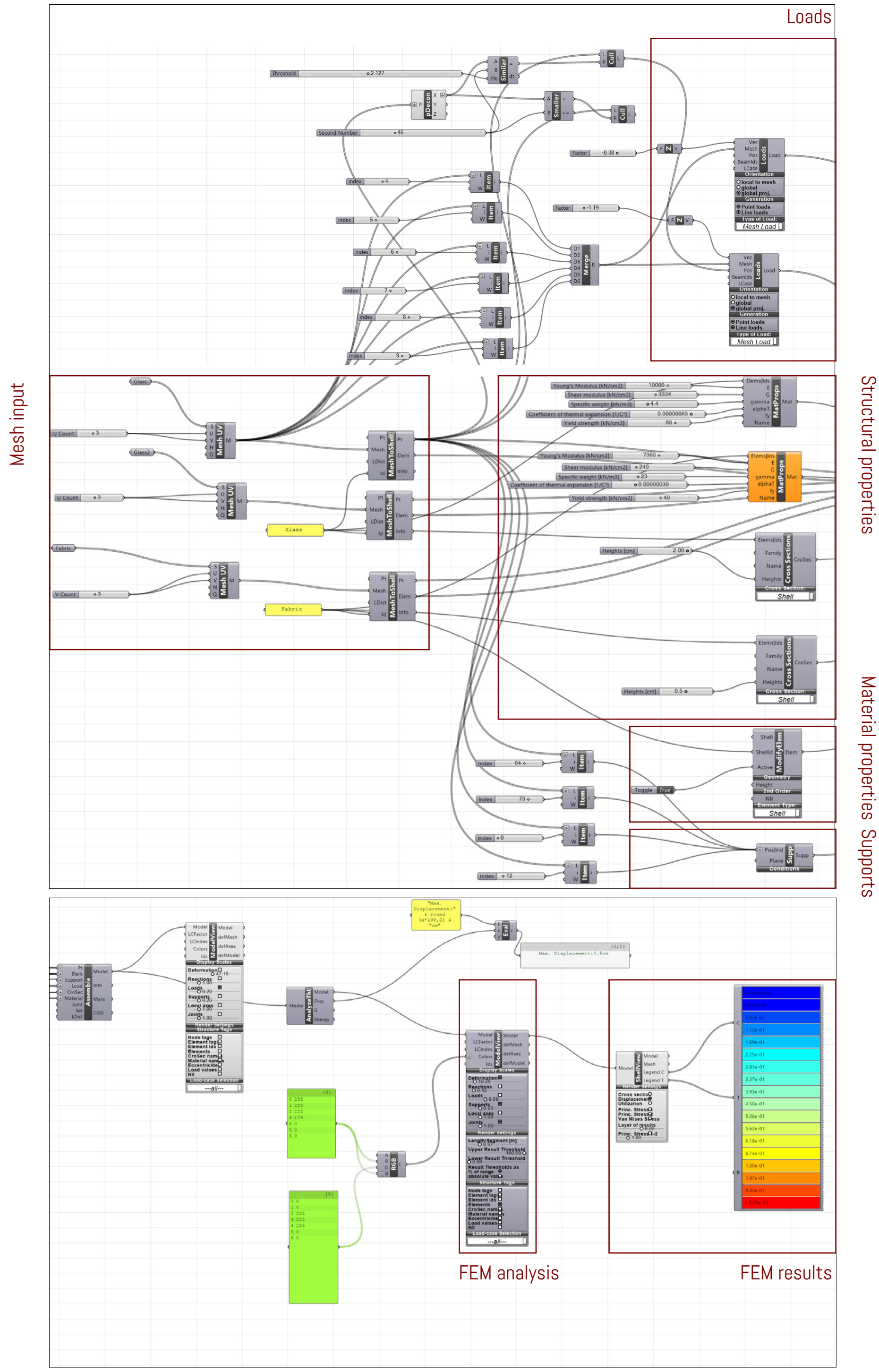

Fig. 115: Karamaba script secondary structure (Andrejevic, 2016)

6.7.4.2 GLASS SAFETY FACTORS

To know which tensile strength is decisive to calculate the strength and possible buckling of glass with, certain safety factors have to be applied. The latest safety standard on structural glass, according to NEN, is as follows:

$$f_{mt;u;d} = \frac{k_e \cdot k_a \cdot k_{mod} \cdot k_{sp} \cdot f_{g;k}}{\gamma_{m;A}} + \frac{k_e \cdot k_z \cdot \left(f_{b;k} - k_{sp} \cdot f_{g;k}\right)}{\gamma_{m;V}}$$

Where:

$f_{mt;u;d}$ = bending tensile strength pre-tensioned float glass in N/mm²
k_e = 1, factor edge quality of float glass
k_a = 0.881, factor surface effect of float glass
k_{mod} = 1.29, modification factor depending on load duration
k_{sp} = 1, factor surface structure
$f_{g;k}$ = 45 MPa, characteristic value bending tensile strength float glass
$\gamma_{m;A}$ = 1.6, material factor where wind gives highest live load
k_z = 1, factor glass zone
$f_{b;k}$ = 120 MPa, characteristic value bending tensile strength pre-tensioned float glass
$\gamma_{m;V}$ = 1.2, material factor of pre-tension

$$f_{mt;u;d} = \frac{1 \cdot 0.881 \cdot 1.29 \cdot 1 \cdot 8.94}{1.6} + \frac{1 \cdot 1 \cdot \left(120 - 1 \cdot 45\right)}{1.2} = 94.46 \ \frac{N}{mm^2} \ (MPa)$$

Bending tensile strength with considered safety factors is 94.5 MPa

6.7.4.3 DEAD & SIDE LOADS WITH TENSION & COMPRESSION BEHAVIOUR

With an equally divided deadload of 0.5 kN/m² and a side load of 0.5 kN/m² (possibly caused by local distortion of the beams of the primary structure) the tension and compression pattern behaves as expected (see fig. 116). Resulting in an arch that is suitable to be the stabiliser of the whole roof structure.

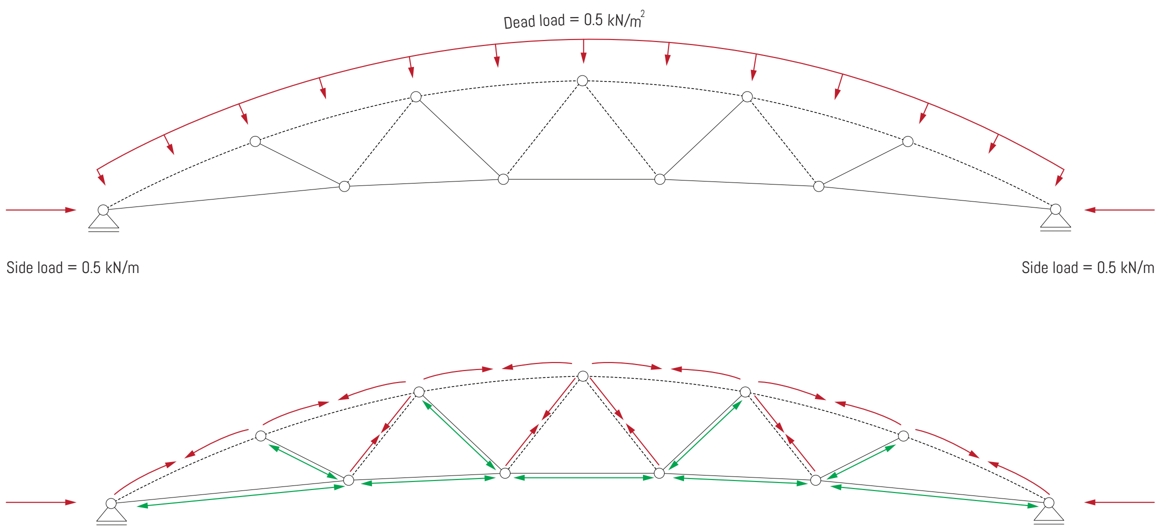

Fig. 116: Determined divided loads secondary structure (Andrejevic, 2016)

Below is the deformation shown, giving a maximum deformation of 8mm in the middle, where all compression come together (see fig. 117a).

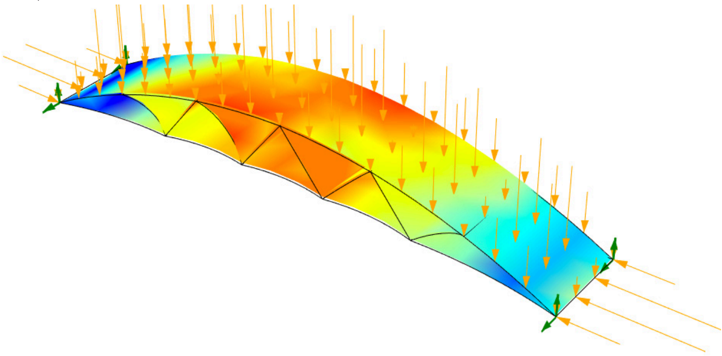

Fig. 117a: Deformation outcome secondary structure (Andrejevic, 2016)

With mostly compression forces (red) flowing through the glass panels and tension forces (blue) through the PTFE cloths, the tension and compression pattern is well divided (see fig. 117b).

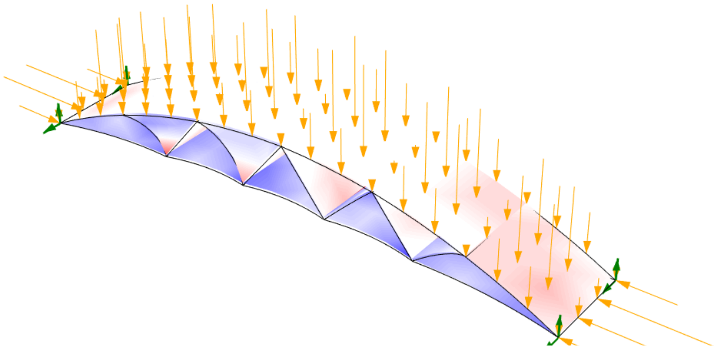

Fig. 117b: Tension/compression outcome secondary structure (Andrejevic, 2016)

Below shown the principal stresses in the alkali aluminosilicate glass plates and PTFE cloths. Giving a maximum compression stress of 0.0081 kN/cm^2 (0.081 MPa) and a maximum tensile stress of 0.088 kN/cm^2 (0.88 MPa). Comparing the occurring compression and tensile forces to the materials' yield strengths, gives the following results (see 117c):

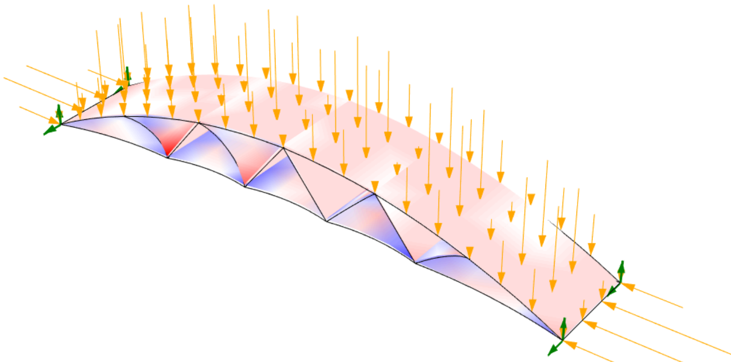

Fig. 117c: Principal stresses outcome secondary structure (Andrejevic, 2016)

$$U.C. = \frac{\sigma_m}{f_{m;d}} \leq 1$$

Where:

σ_m = 0.88 MPa compression stress
$f_{m;d}$ = 94.5 MPa bending tensilestrength NEN standard float glass safety regulations

σ_m = 0.088 MPa tensile stress
$f_{m;d}$ = 43 MPa tensile strength hemp reinforced PTFE

$$U.C. = \frac{0.88}{94.5} = 0.0093 < 1 \qquad U.C. = \frac{0.88}{43} = 0.021 < 1$$

6.7.4.4 LOCAL LIVE LOADS WITH BUCKLING BEHAVIOUR

To test whether the glass hybrid arch is stable in different unexpected situations, the structure was analysed under 5 different local live loads (see fig. 118). This analysis gives a clear sense of the mutual behaviour between the glass panels and the PTFE cloths.

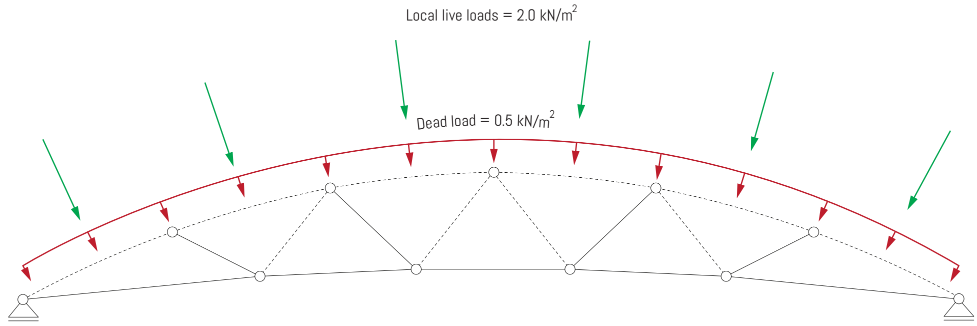

Fig. 118: Determined local loads secondary structure (Andrejevic, 2016)

Below shown: the maximum deformations occurring at all analysed local live loads. The highest deformations take place at the sides of the arch, giving a maximum of 1.98cm. Lower deformations occure in the middle, approximately 1.5cm (see fig. 119).

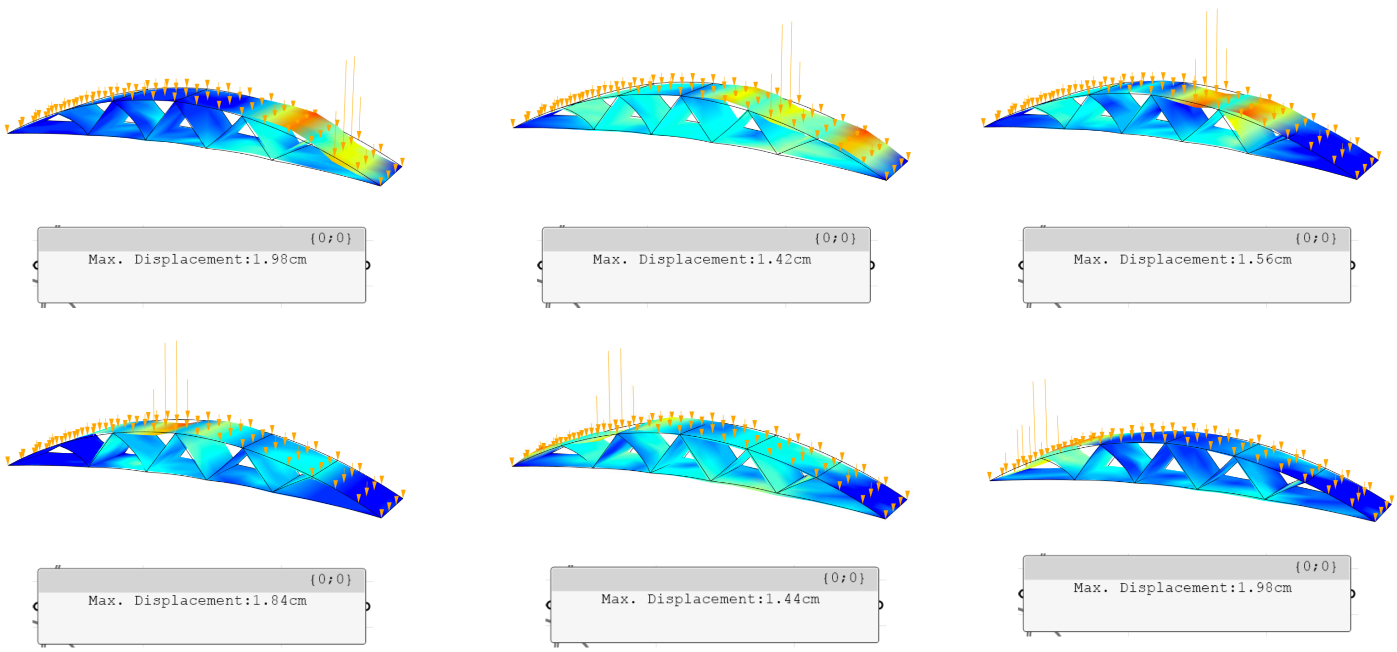

Fig. 119: Deformations outcome local loads secondary structure (Andrejevic, 2016)

To understand what, in terms of deformation, the influence of a local live load is, a single panel has to be analysed on its buckling behaviour. Especially a cold bended glass panel, which is due to its single curved form, sensitive to buckling. On the next page is shown what its buckling behaviour would look like (see fig. 120). At the sides, the panel is clamped, which results in a parabolic shaped buckling movement.

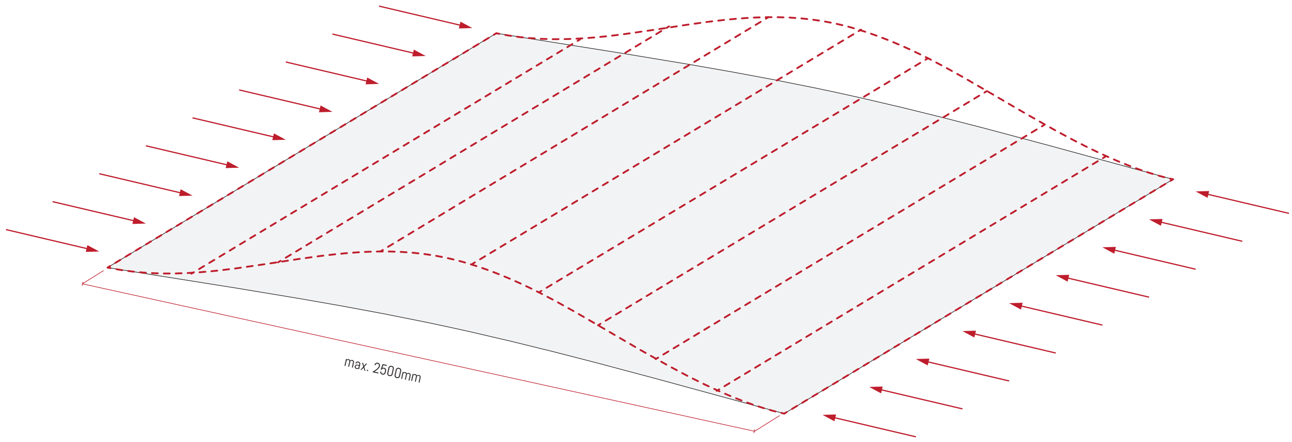

Fig. 120: Buckling behaviour glass panel secondary structure (Andrejevic, 2016)

To test whether this buckling movement is harmful for the stucture and the material, the arch will be analysed on its highest principal compression stresses and measured to the maximum possible buckling stress.

The highest principal compression stress is occurring in the bended panel shown below: 0. 47 kN/cm^2. The highest principal tension stress happens in the cloth attached to the bended panel: 0.15 kN/cm^2 (see fig. 121). Testing the occurring compression stress to buckling gives the following result.

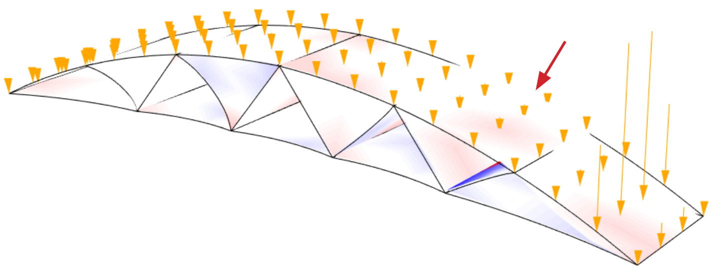

Fig. 121: Principal stresses outcome local loads secondary structure (Andrejevic, 2016)

$$S_{buckling} = \frac{\pi^2 \cdot E \cdot I}{{}_{0.5}L_b^2 \cdot A} \left[\frac{n}{mm^2} \right]$$

Where:

$S_{buckling}$ = buckling stress in N/mm^2
E = Young's modulus in N/mm^2
I = second moment of area in mm^4
${}_{0.5}L_b$ = 0.5 x buckling length in mm, because of fixed position
A = section area structural profile in mm^2

$$S_{buckling} = \frac{\pi^2 \cdot 71700 \cdot 70.8 \cdot 10^4}{1250^2 \cdot 37600} = 8.94 \frac{N}{mm^2} (MPa)$$

Maximum buckling with safety factor included according to new glass NEN standards is as follows:

$$S_{buckling;u;d} = \frac{1 \cdot 0.881 \cdot 1.29 \cdot 1 \cdot 8.94}{1.6} = 6.35 \frac{N}{mm^2} \; (MPa)$$

Giving a maximum buckling stress of 6.35 MPa.

With a Unity Check it will be determined whether the axial stress exceeds the maximum possible bucking stress. Giving the following results:

$$U.C. = \frac{\sigma_m}{S_{buckling}} \leq 1$$

where:

σ_m = 4.7 MPa compression stress
$S_{buckling}$ with safety factors = 6.35 MPa

$$U.C. = \frac{4.7}{6.35} = 0.74 < 1$$

6.7.4.5 WIND LOADS WITH STABILITY BEHAVIOUR

The last structural analysis conducted is the influence of a high wind force. Analysed as one half of the arch under wind press (compression) loads and the other half under wind pull (tension) loads of 1 kN/m^2 (wind force 7). The maximum deformation is 0.7cm (see fig. 122) and the maximum principal stress occuring is ca. 0.35 kN/cm^2 (3.5 MPa).

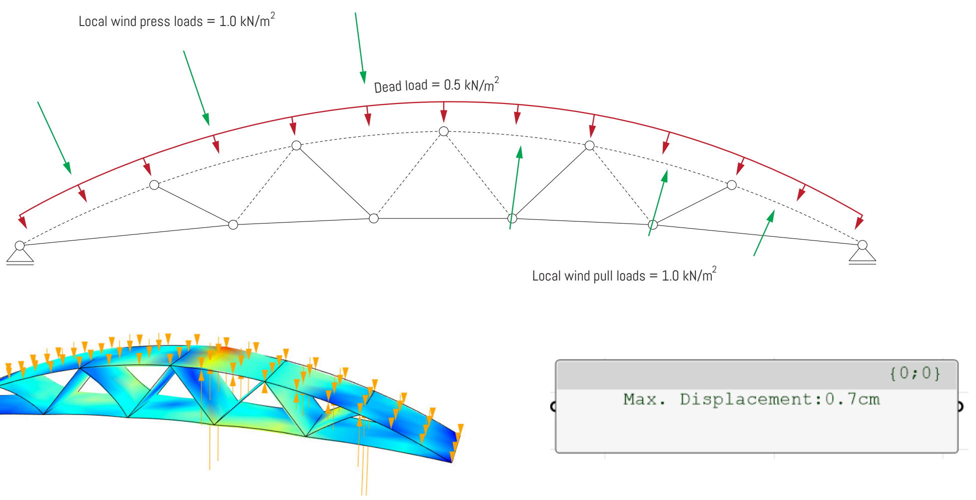

Fig. 122: Wind force incluence on secondary structure (Andrejevic, 2016)

$$U.C. = \frac{\sigma_m}{S_{buckling}} \leq 1$$

where:
σ_m = 3.5 MPa compression stress
$S_{buckling}$ with safety factors = 6.35 MPa

$$U.C. = \frac{3.5}{6.35} = 0.55 < 1$$

6.7.5 SECONDARY STRUCTURE CONCEPT DESIGN

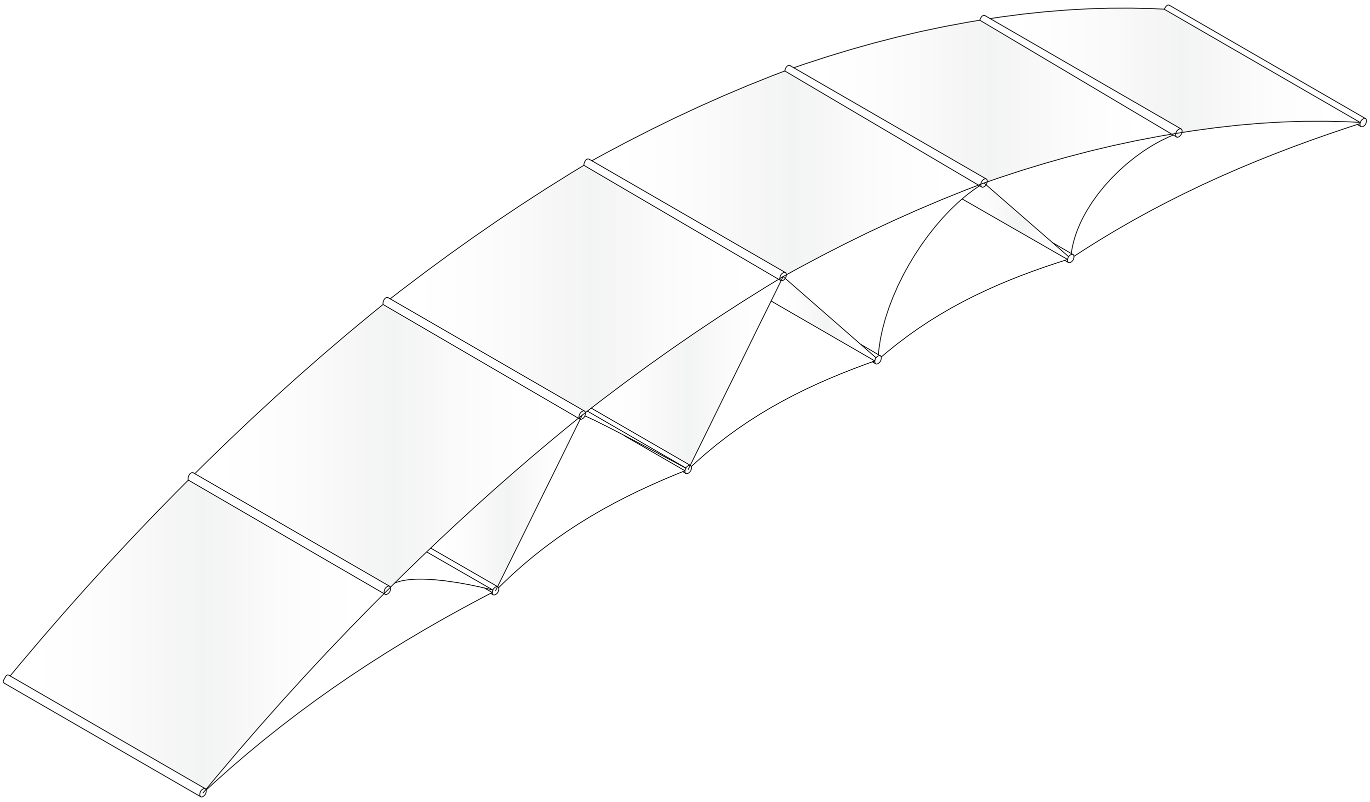

Fig. 123: Desing Secondary Structure (Andrejevic, 2016)

7. FINAL DESIGN

7.1.1 SUNLIGHT FILTERING

Direct sunlight gets diffused by two layers of PTFE fabric, while natural diffuse light gets slightly filtered by one layer of PTFE fabric. This way the right amount of PAR can be reached (see fig. 124).

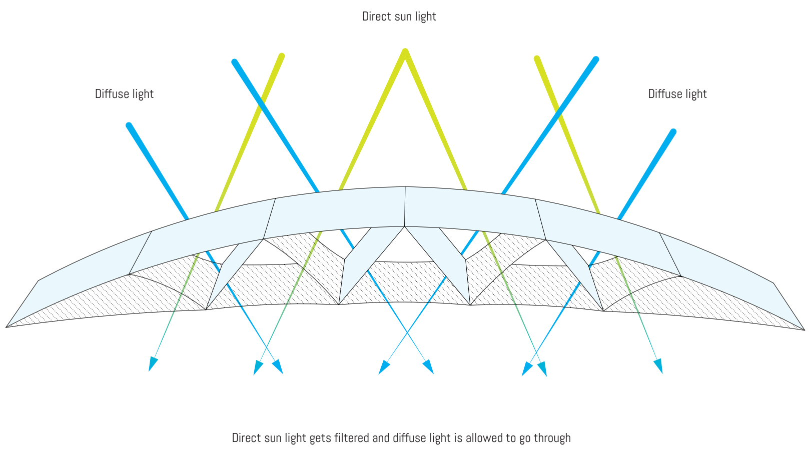

Fig. 124: Sunlight filtering principle (Andrejevic, 2016)

Below can be seen that with the composition of the designed arch, the direct sun light (heat) gets filtered everywhere in the middle of the barrel vaults and the diffuse light goes through. Resulting in of a PAR level of 9.5 Wh/m2 on the field, which is more than enough to give the grass the healthy amount of light they need (see fig. 125).

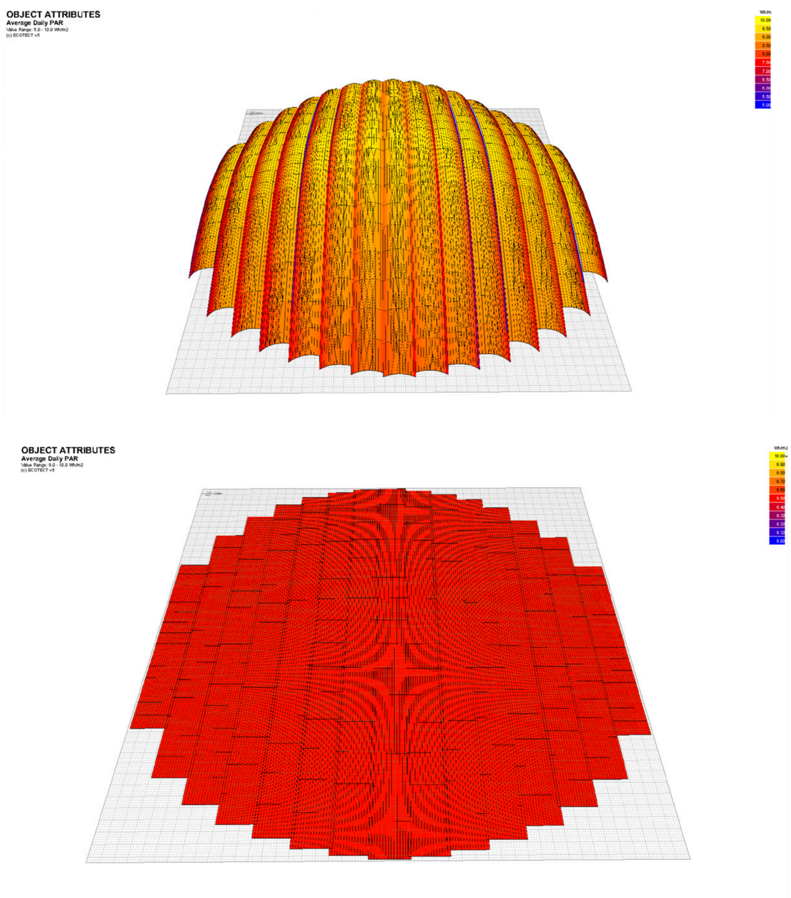

Fig. 125: Final PAR analysis on final design (Andrejevic, 2016)

7.1.2 COOLING SCHEME

The cooling of the stadium happens with an ultrasonic mist cooling principle in the roof and distribution ventilation coming from the stands.

In a winter situation where the average temperature outside is between 20 and 22 °C during the day and between 10 and 12 °C during the night, only roof cooling or heating is needed to achieve the required average temperature on the field and at the stands during the day (see fig. 126a). The amount of cooling needed in winter is as follows:

$$Q_{roof} = U \cdot A \cdot (T_o - T_i)\ [W]$$

Where:

Q_{roof} = cooling load
U = heat transfer coeffecient of roof in W/m^2 K
A = area of roof in m^2
T_o = outdoor temperature in °C
T_i = indoor temperature in °C

$$Q_{roof} = 50 \cdot 22000 \cdot (26 - 22)$$

$$Q_{roof} = 4400\ kW$$

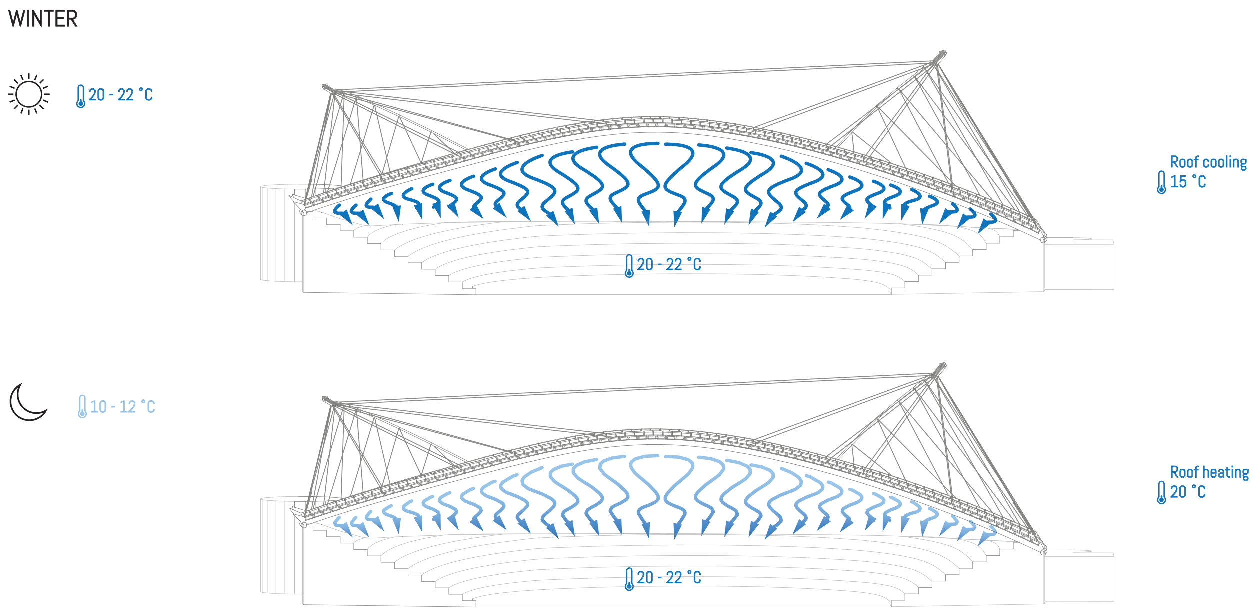

Fig. 126a: Cooling scheme winter situation (Andrejevic, 2016)

In summer situation, where the average temperature is between 36 and 38 °C during the day and between 25 and 27 °C during the night, only roof cooling will is enough to cool the stadium during the night. However, to get the desired indoor temperature during the day, there is, next to the roof cooling, air conditioned distribution ventilation to get the required indoor temperature (see fig. 126b). The amount of cooling in summer is shown on the next page:

$$Q_{roof} = 50 \cdot 22000 \cdot (38 - 22)$$

$$Q_{roof} = 17600\ kW$$

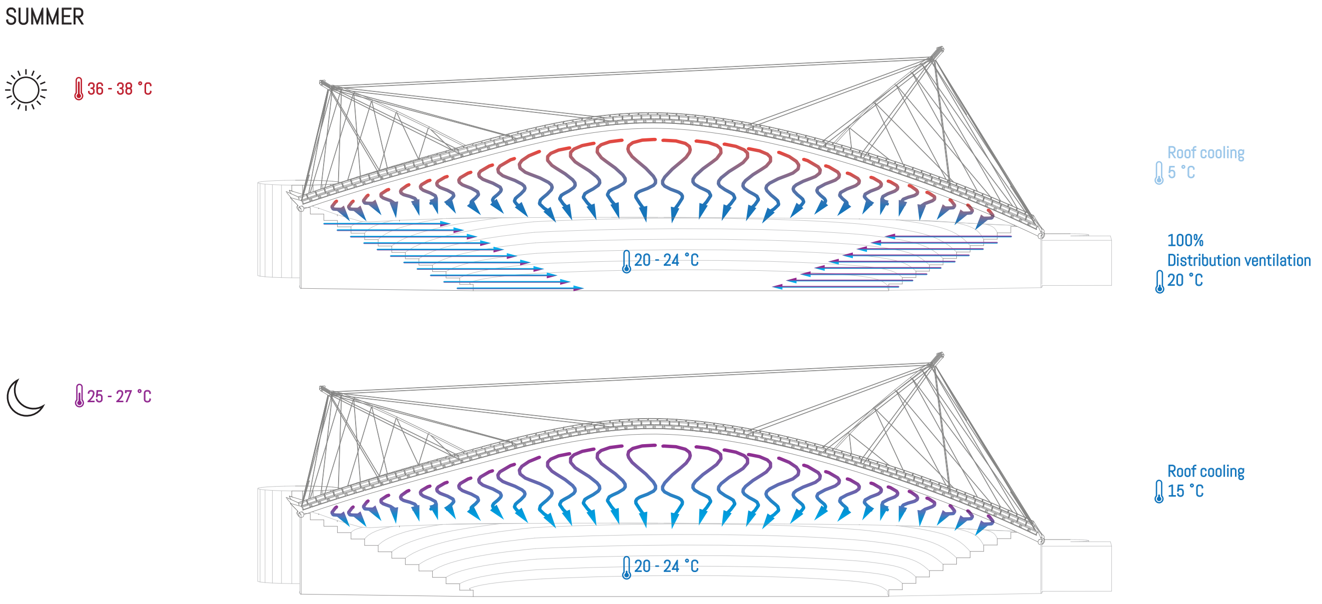

Fig. 126b: Cooling scheme summer situation (Andrejevic, 2016)

As for in the spring/autumn siuation, the night temperature is between 20 and 22 ˚C and the day temperature between 28 and 30 ˚C. Meaning, during the night only roof cooling is needed during the night, but during the day, next to roof cooling, 40% of the distribution ventilation amount is needed to cool the bowl (see fig. 126c). The amount of cooling is as follows:

$$Q_{roof} = 50 \cdot 22000 \cdot (30 - 22)$$

$$Q_{roof} = 8800\ kW$$

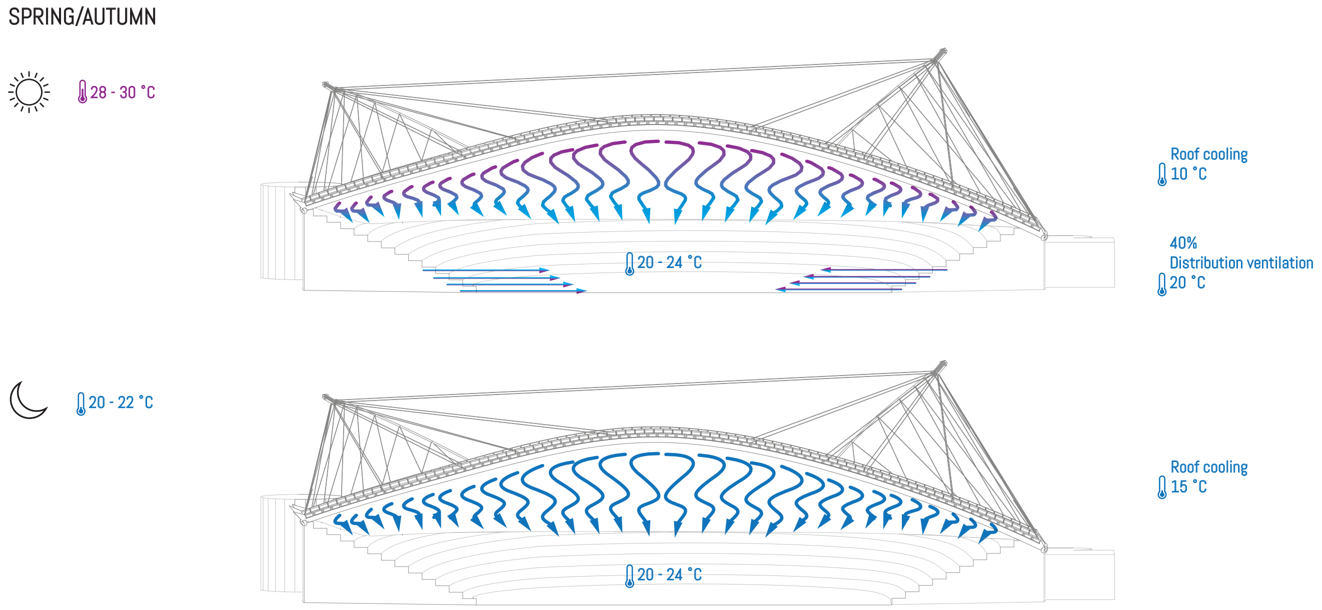

Fig. 126c: Cooling scheme summer situation (Andrejevic, 2016)

7.1.3 VENTILATION SCHEME

The get air into the stadium, the west side of the roof has air inlets to catch wind and accelerate the air through its aerodynamical form to subsequently blow it as cold air into the stadium. To get a certian velocity of air circulation, the air is mechanically extracted at the east side of the stadium (see fig. 127).
As earlier mentioned in chapter *4.1 Aerothermal Quality*, the desired draught rate of a stadium is 25%. According to the draught rate equation the most optimal air velocity to blow air in the stadium is as follows:

$$DR = (34 - t_a) \cdot (v_a - 0.05)^{0.62} \cdot (3.14 + 0.37 \cdot T_u \cdot v_a) \; [\%]$$

Where:

v_a = local air velocity in m/s
T_u = turbulence intensity (σ / v_a) in %
t_a = local indoor air temperature in °C

$$0.25 = (34\text{-}24) \cdot (V_a - 0.05)^{0.62} \cdot (3.14 + 0.37 \cdot 0.5 \cdot V_a)$$

$$V_a = 0.37 \; \frac{m}{s}$$

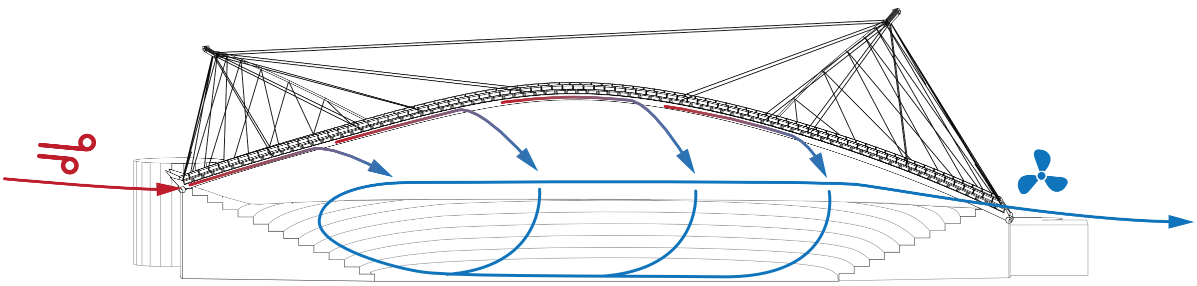

Fig. 127: Air circulation and ventilation scheme (Andrejevic, 2016)

Below is shown that the aerodynamic geometry of the roof in combination with the inlets creates a constant natural air circulation of around 6 m/s. Meaning the shape and composition of the roof work as expected (see fig. 128).

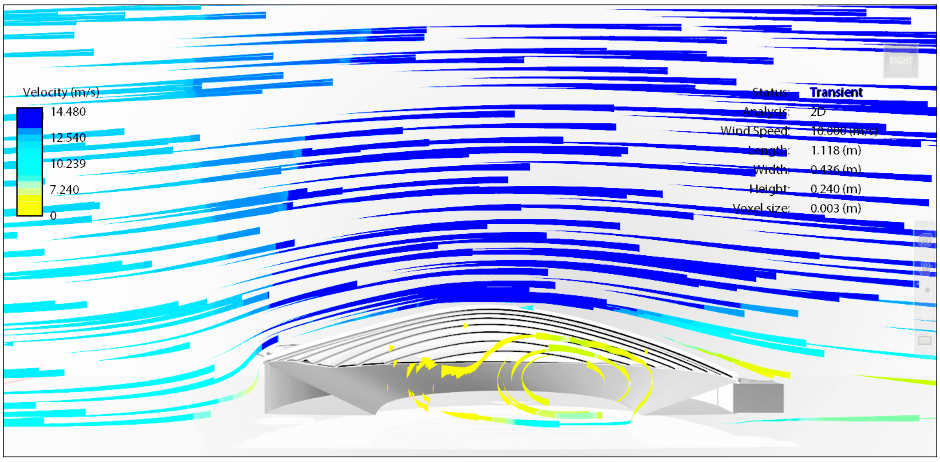

Fig. 128: Final wind analysis on final design (Andrejevic, 2016)

7.1.4 ROOF COOLING

Air that gets via the wind can have a temperature of around 40 °C in summer, to cool this air down to around 20 °C, water vapor of 5 °C gets used. This principle is called ultrasonic mist cooling (see fig. 129).

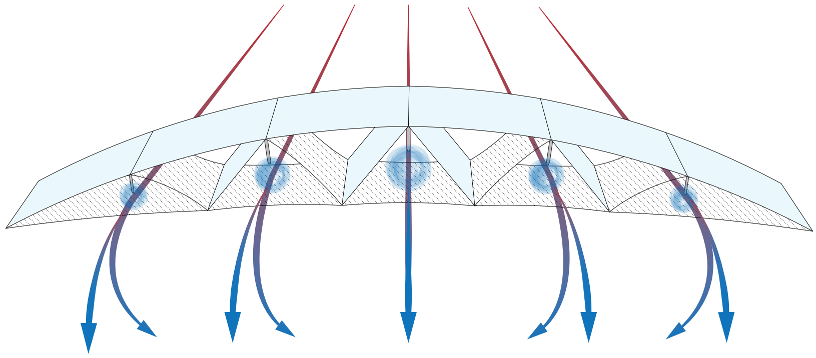

Fig. 129: Mist cooling principle (Andrejevic, 2016)

7.1.5 DISTRIBUTION VENTILATION

The stand acts as a large grille that equally divides the blown air from the air conditioning units (see fig. 130). With this princile the air flow in the stadium gets increased in summer, resulting in a higher level of comfort and better grass conditions.

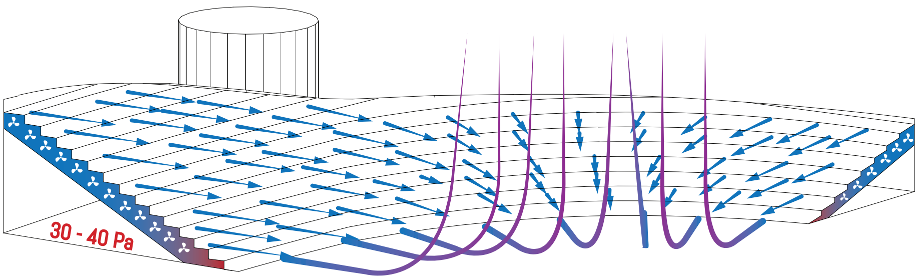

Fig. 130: Distribution ventilation principle (Andrejevic, 2016)

Determining the amount of air inlet needed for proper ventilation in the stadium can be done with the following equation: (TROX, 2015)

$$V_{KR} = \frac{Q_{KR} \cdot C}{0.335 \cdot \Delta t_{AZ}} \left[\frac{m^3}{h}\right]$$

where:
Q_{KR} = cooling load = Q_{roof}
C = temperature gradient of residence area
$\Delta\ T_{AZ}$ = ground temperature difference in residence area

$$C = \frac{t_{1.1} - t_{0.1}}{t_{Abl} - t_{Zul}} = \frac{\Delta t_{AZ}}{\Delta t_R}$$

$$C = \frac{24 - 21}{26 - 18} = 0.375$$

$$V_{KR} = \frac{1.76 \cdot 10^6 \cdot 0.375}{0.335 \cdot 3} = 5.6 \cdot 10^6 \ \frac{m^3}{h}$$

V_{KR} = 5.6 10^6 m^3/h is the ventilation amount needed based on temperature differences in the stadium.

To determine how much of the ventilation air has to be cooled, the equation below can be used. (TROX, 2015) In combination with a chilled roof, ω_L gives an indication of how much of the ventilation needs to be cooled.

$$\omega_L = \frac{V_{min}}{V_{KR}}$$

where:
V_{min} = minimum amount of ventilation based on amount of people present
V_{KR} = 5.6 10^6 m^3/h

$V_{min} = \eta \cdot V_{per}$

$V_{min} = 45000 \cdot 50 = 2.25 \cdot 10^6 \ \frac{m^3}{h}$

$$\omega_L = \frac{2.25 \cdot 10^6}{5.6 \cdot 10^6} = 0.4$$

40% of 5.6 10^6 m^3/h ventilation has to be cooled from the stands.

For the use of distribution ventilation from the stands, a common way of air inlet is a grill system called 'staircase swirl diffusers'. These kind of diffusers can give a supply speed of ca. 32 l/s (115 m^3/h) in hot climates, with a required distance of 600 to 1000mm between one another (see fig. 131). (Puttemans, 2006)

Fig. 131: Staircase swirl diffuser (Andrejevic, 2016)

The amount of needed staircase swirl diffusers can be calculated as follows:

$$V_{KR} = \frac{5.6 \cdot 10^6}{113} = ca.\ 49000$$

In total an amount of 49000 diffusers are needed to supply the stadium of the needed ventilation and cooling. Giving an amount of 1 diffuser per seat.

7.2.1 BUILD UP COMPLETE STRUCTURE

The whole structure exists out of the following:
˚Two existing arches (fig. 136a)
˚Primary structure with stability cables, suspension cables, steel beams and rigidity ring (see fig. 136b).
˚Secondary structure with thin glass and PTFE fabric (see fig. 136c).

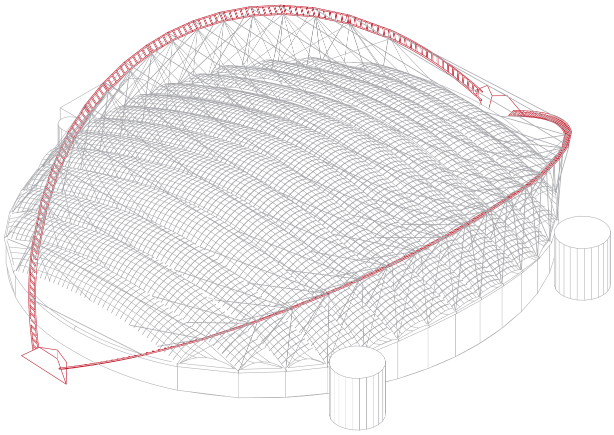

Fig. 132a: Existing arches (Andrejevic, 2016)

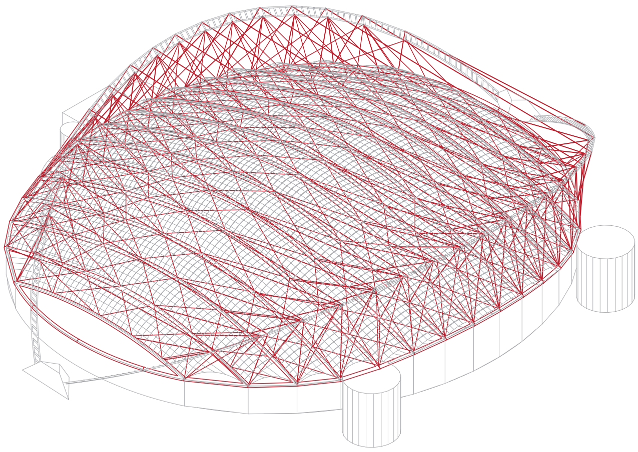

Fig. 132b: Primary structure (Andrejevic, 2016)

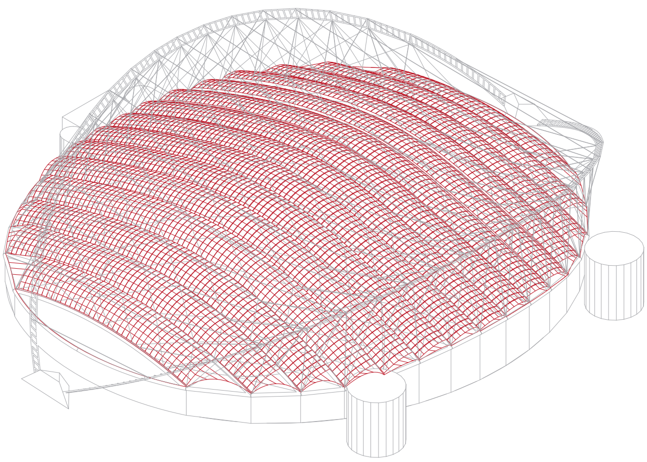

Fig. 132c: Secondary Structure (Andrejevic, 2016)

7.2.2 PRIMARY STEEL STRUCTURE

The primary structure is completely made out of steel, with use of only arches, beams and cables. No columns are used, which means the structure is carried out as light as possible. Below is shown how the primary structure stabilises (see fig. 133).

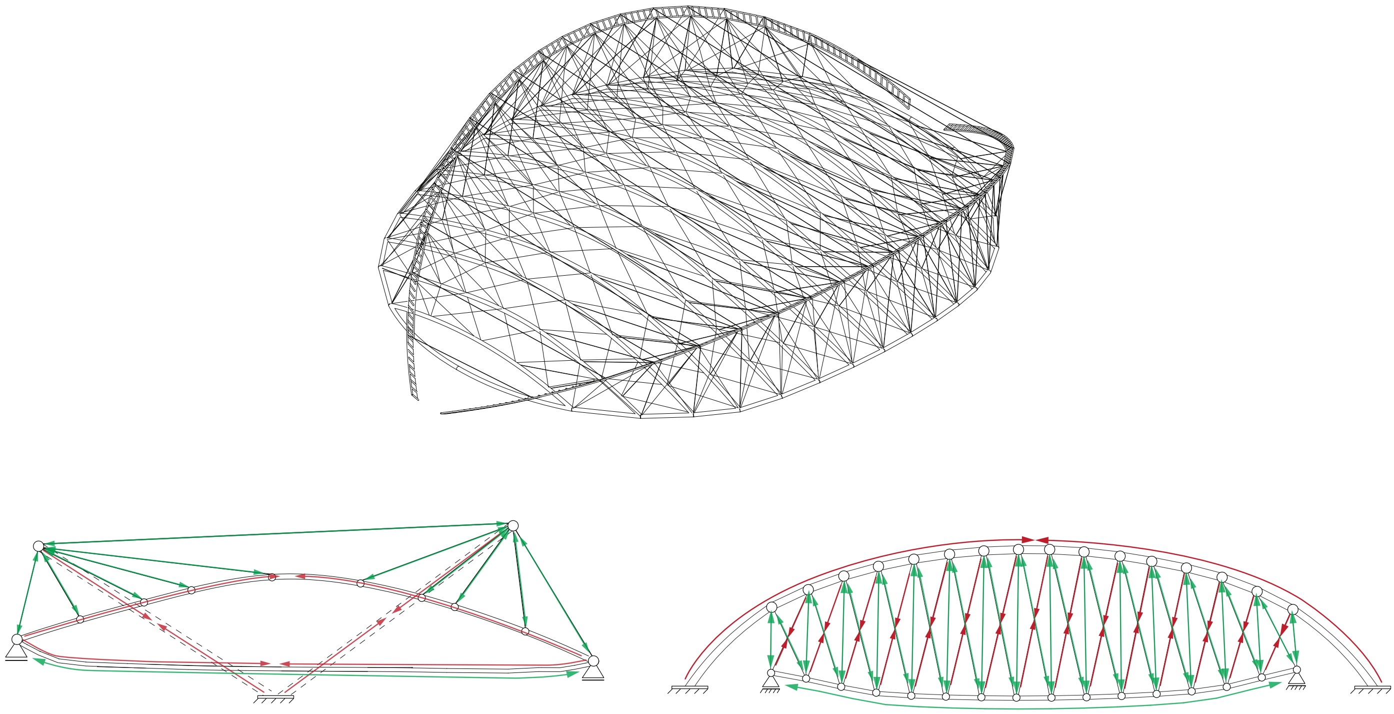

Fig. 133: Design Primary Structure with static stability schemes (Andrejevic, 2016)

7.2.3 SECONDARY GLASS STRUCTURE

The secondary structure is a hybrid glass arch structure, meaning that only glass and fabric are used to make a stable structure. Using the glass to absorb compression forces and fabric to absorb tension forces. Below is shown how the secondary stucture stabilises (see fig. 134).

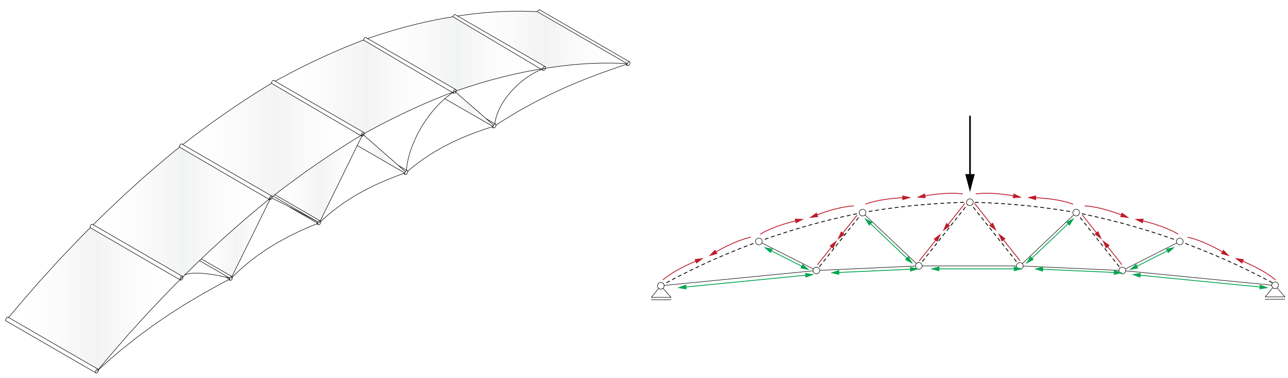

Fig. 134: Design Secondary structure with static stability scheme (Andrejevic, 2016)

7.2.4 COMPLETE ROOF STRUCTURE

The hybrid glass arches span between the primary structure beams, which helps the primary structure stabilising, next to the bracing, even more and makes the roof a complete structure. With a wind force coming from the, a possible divided load can occur in the middle of the roof. Resulting in the glass arches absorbing mostly compression forces, which causes upper compression and lower tension in the beams, which remit the forces to the stability and the stadium. The wind pressure also makes the suspension and the outer arch cables pull, where to to stabilise the structure, half of the cables absorb tension and half of the cables become zero-forces (see fig. 135).

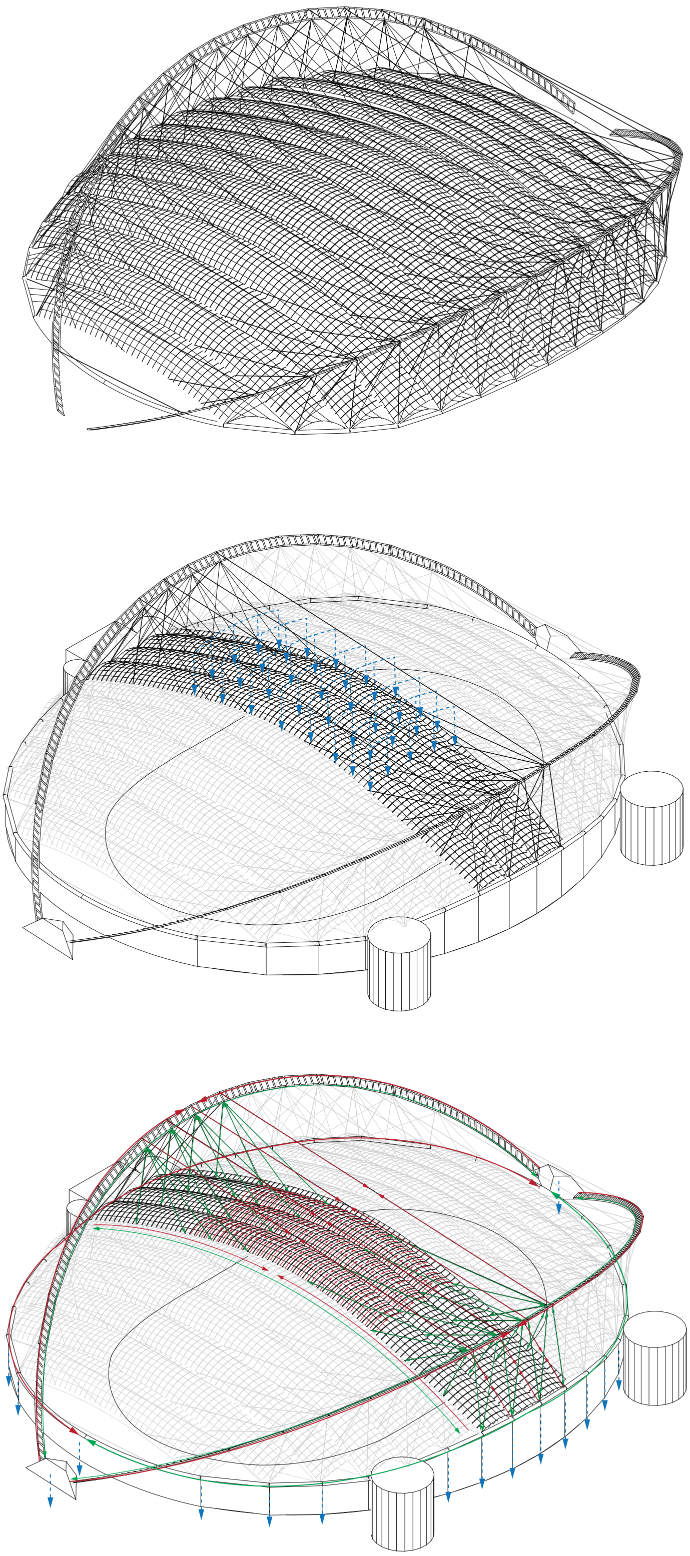

Fig. 135: Design complete structure with complete stability scheme (Andrejevic, 2016)

7.2.5 BUILDING SEQUENCE

7.2.5.1 PRIMARY STEEL STRUCTURE

Below shown; the steps of the building sequence of the primary structure (see fig. 136).

1. Rigidity ring gets attached to existing structure of the stadium.
2. New cables get attached to the arches to stabilise existing arches.
3. Suspension cables get attached to the arches for suspension of the beams.
4. Beams get spanned and stabilised with bracing to finish primary structure.

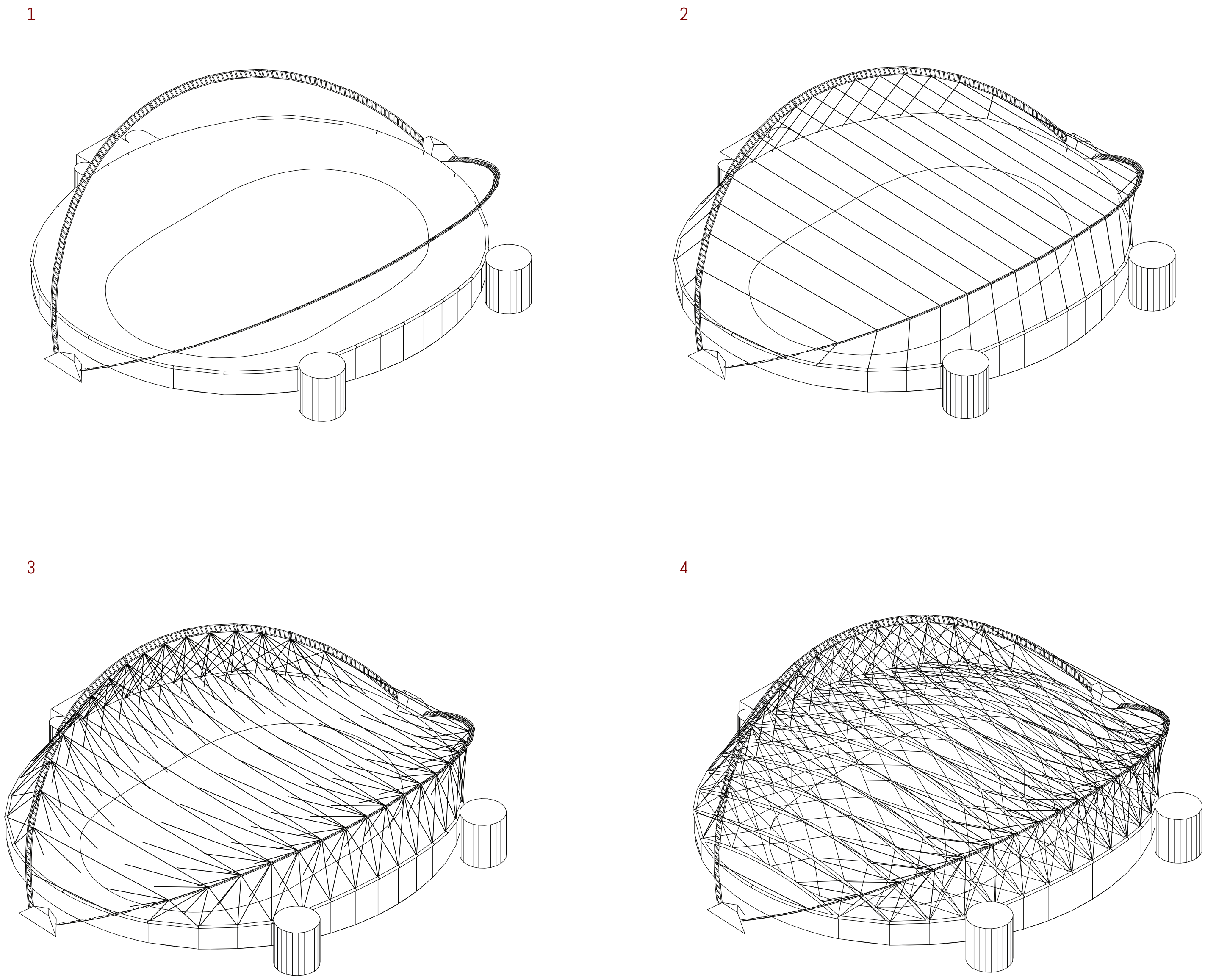

Fig. 136: Buidling sequence primary structure (Andrejevic, 2016)

7.2.5.2 SECONDARY GLASS STRUCTURE

Below shown; the steps of the building sequence of the secondary structure (see fig. 137).

1. At both sides, two PTFE clots get attached to one glass panel. Creating a triangle, which is rigid. Resting on scaffolding to get the arch in the correct position.
2. One glass panel and one PTFE cloth get attached to the both sides. Creating the next triangle. Resting on an extended part of the scaffolding to keep the correct positions.
3. Two PTFE cloths at both sides are added to continue the triangle pattern. Resting on the final scaffolding structure.
4. Two glass panels are attached at both sides and complete the upper part of the arch.
5. The last PTFE cloth gets attached in the middel to equilibrate the structure.
6. Finally, the scaffolding can be removed.

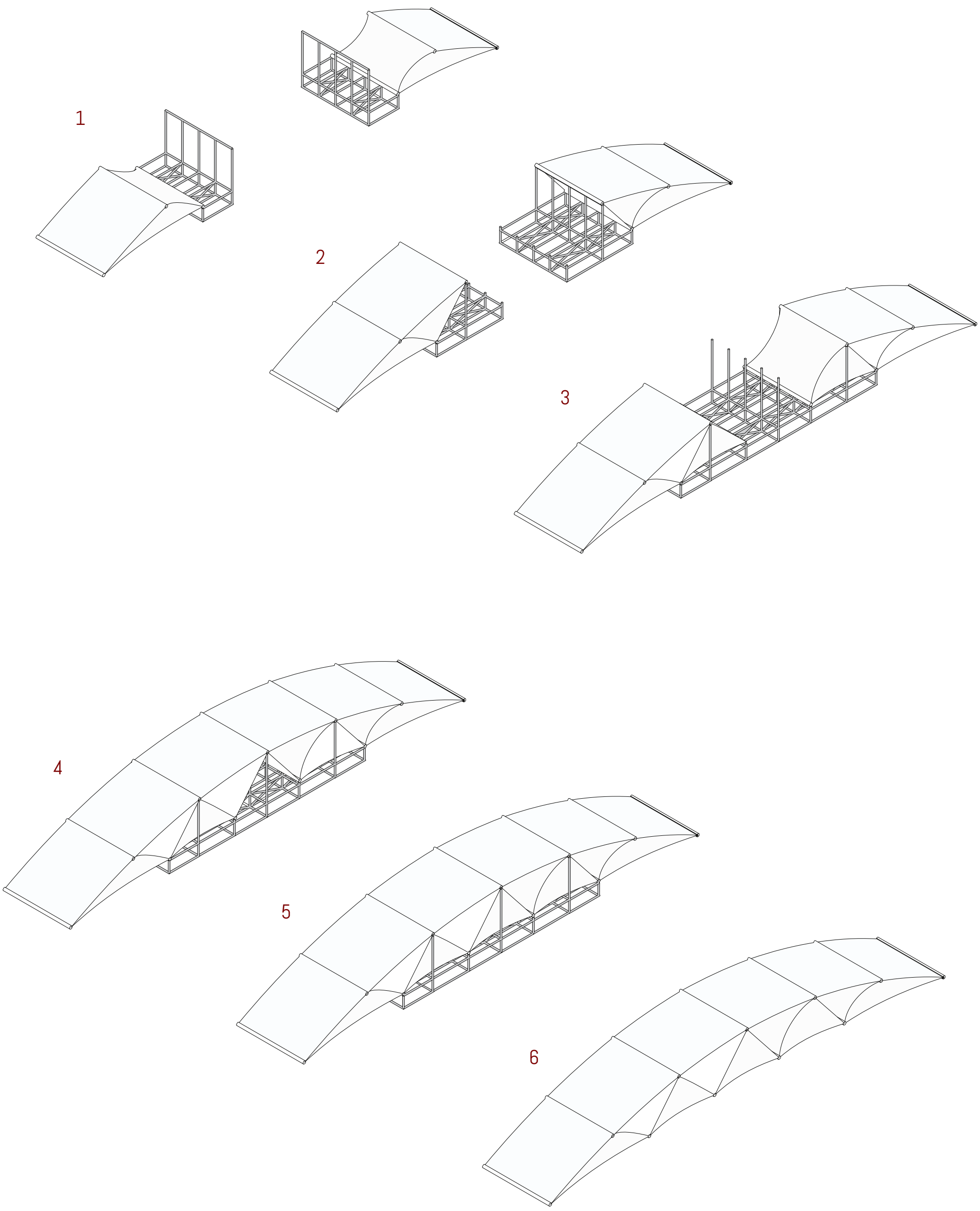

Fig. 137: Buidling sequence secondary structure (Andrejevic, 2016)

7.2.5.3 COMPLETE STRUCTURE

Below shown; the steps of the building sequence of the secondary structure (see fig. 138).

1. Arches are delivered pre fabricated and attached to structure, starting at one of the sides of the roof.
2-3. Up to the middle of the roof the secondary structure get placed on the beams of the primary structure.
4. The same happens from the other half of the roof and the roof structure is finished, with an amount of 1003 arches.

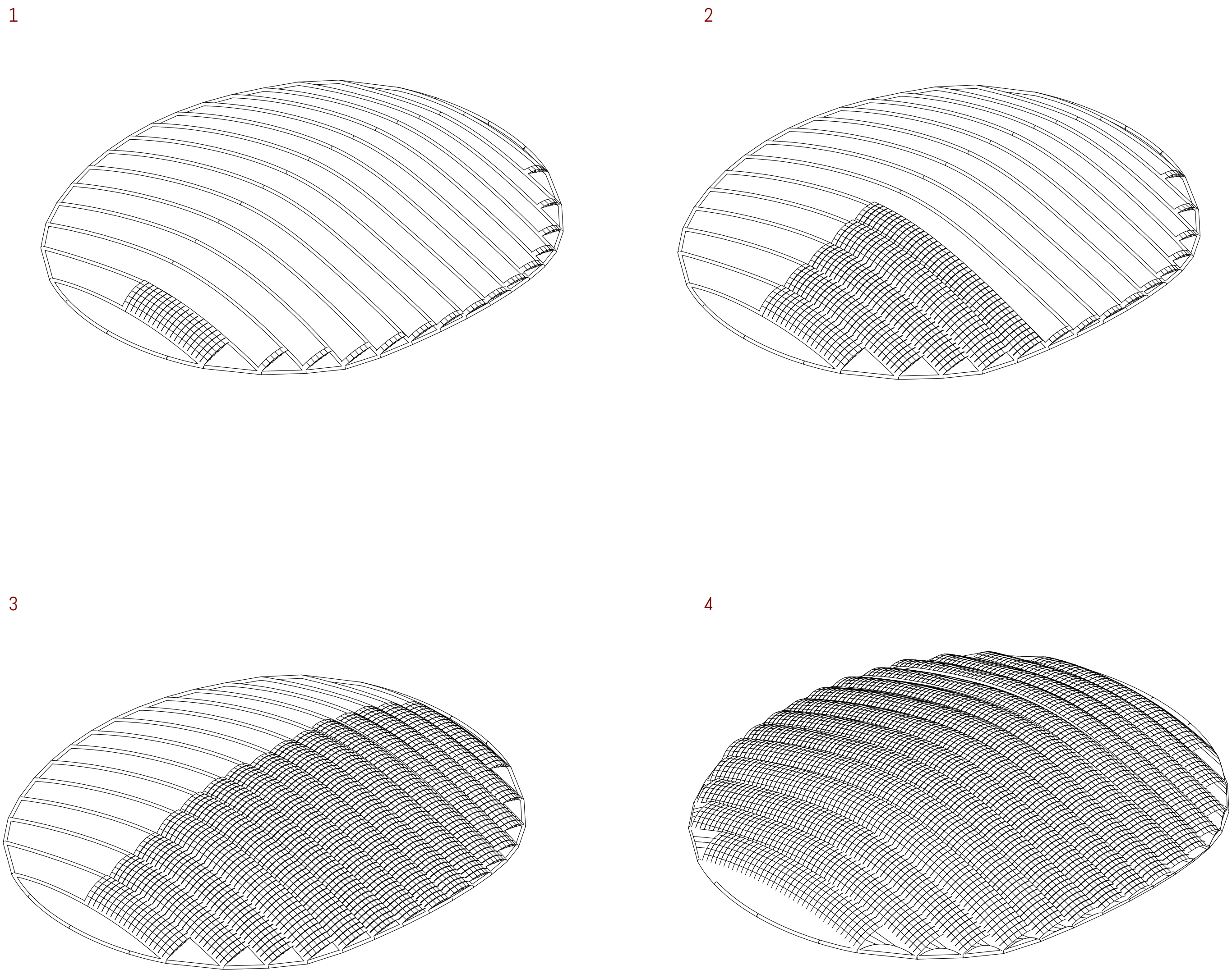

Fig. 138: Buidling sequence complete structure (Andrejevic, 2016)

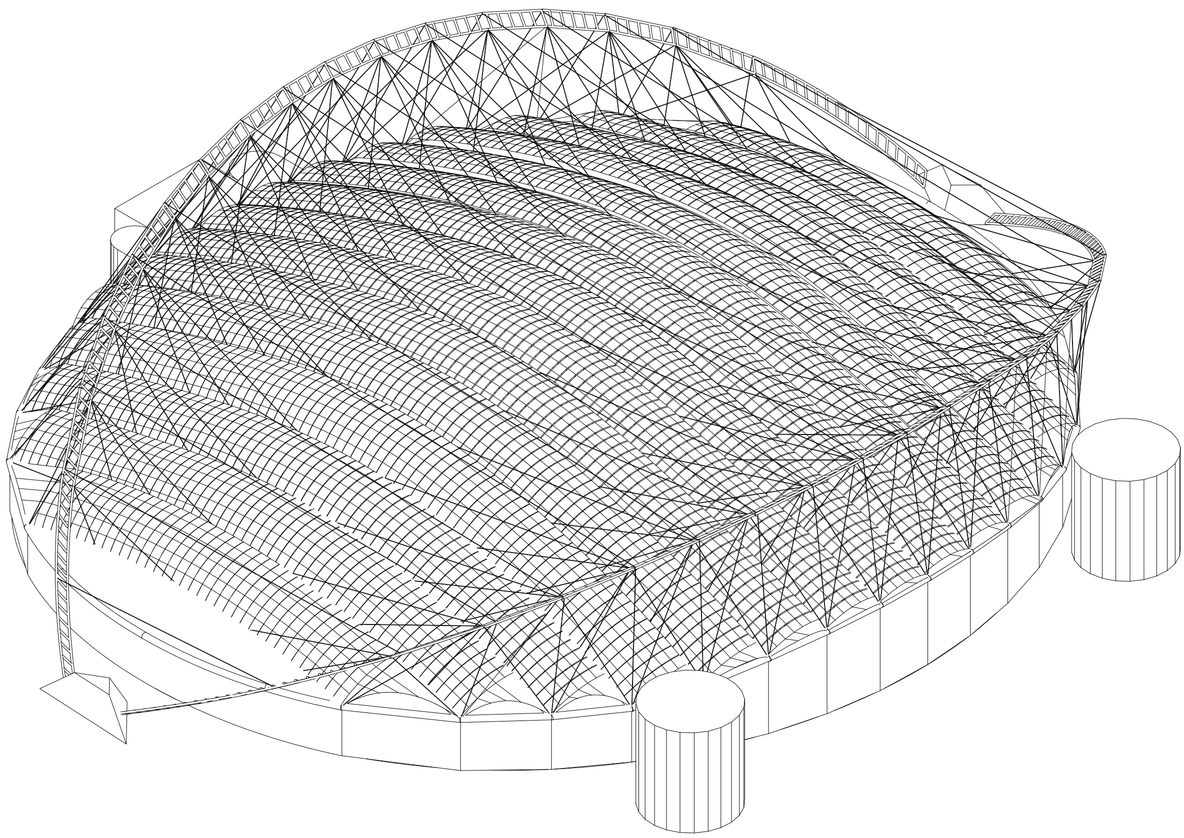

Fig. 139: Final Complete Design (Andrejevic, 2016)

8. ELABORATION

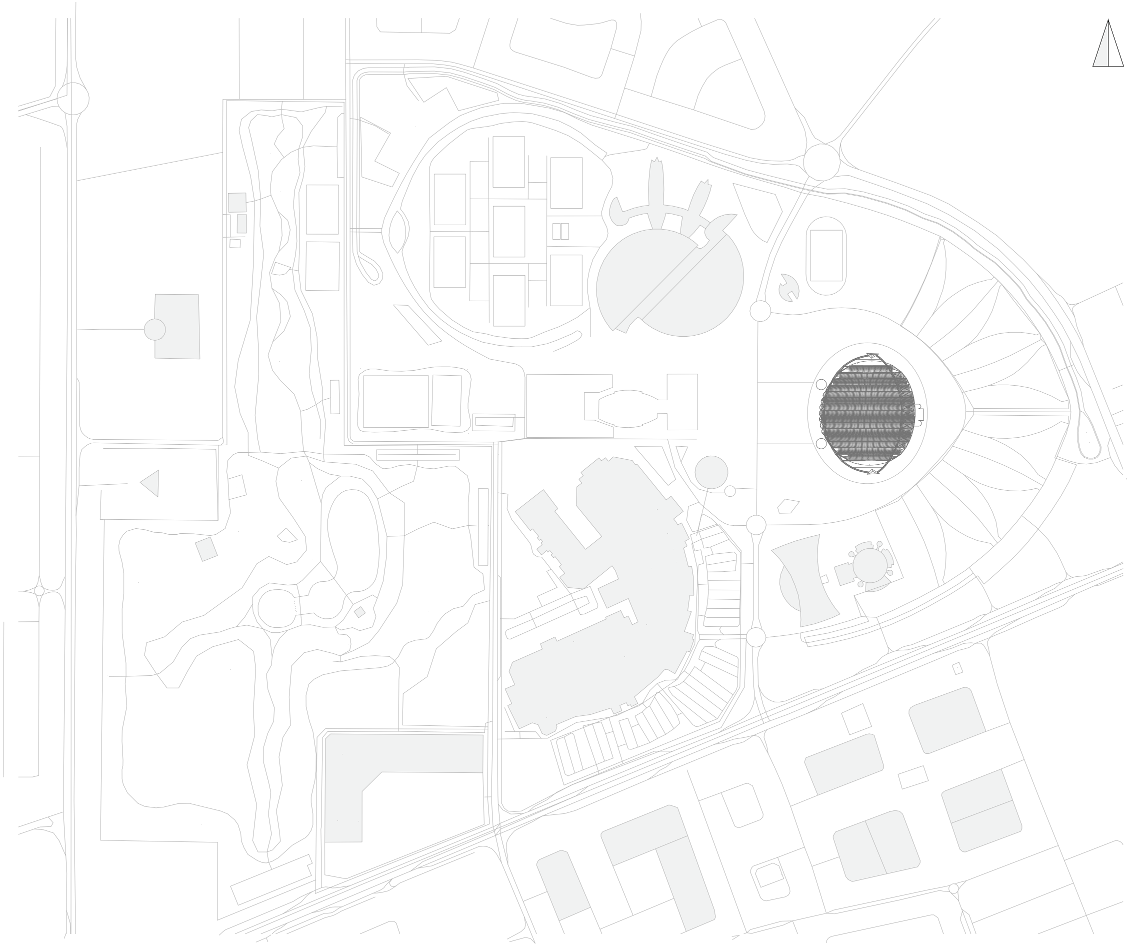

North

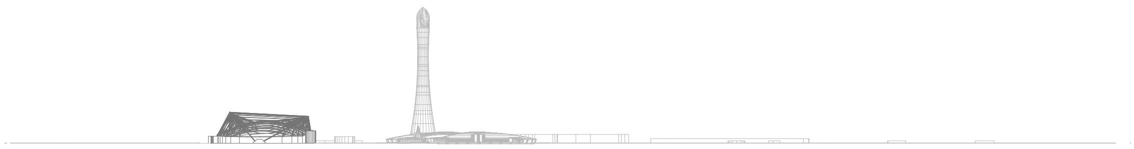

East

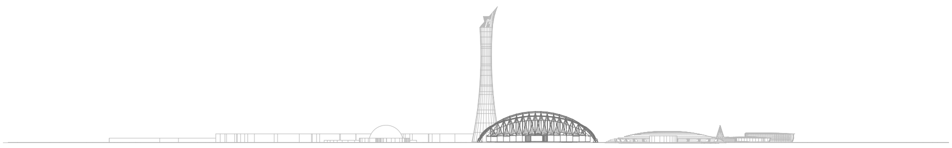

South

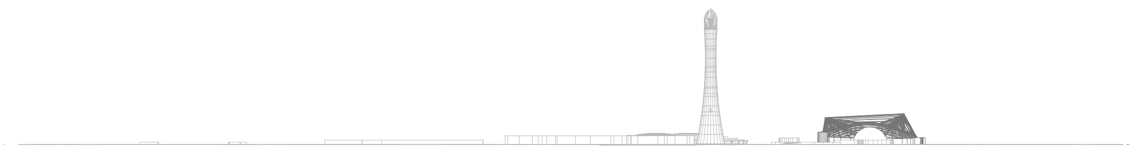

West

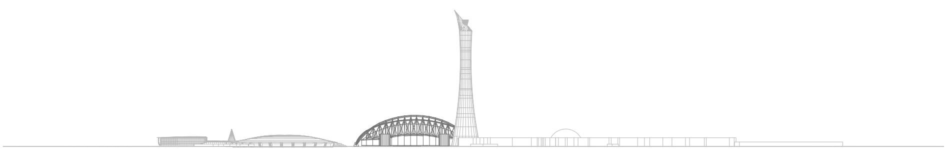

Top

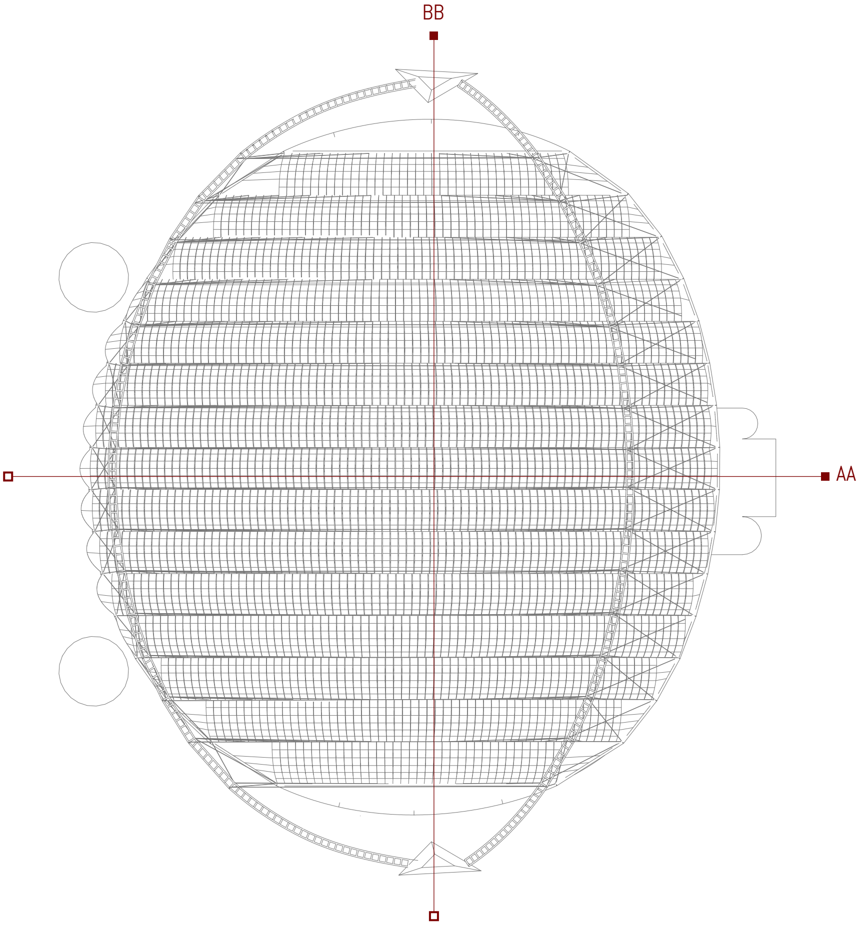

Long side

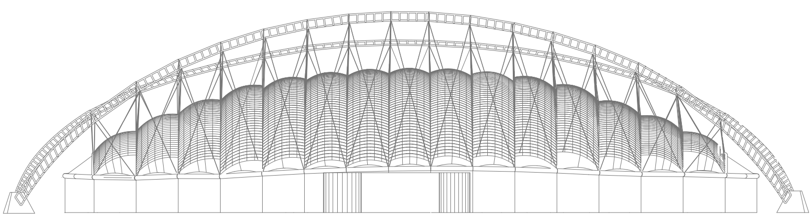

Short side

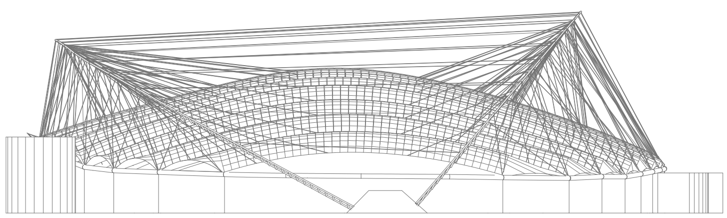

AA

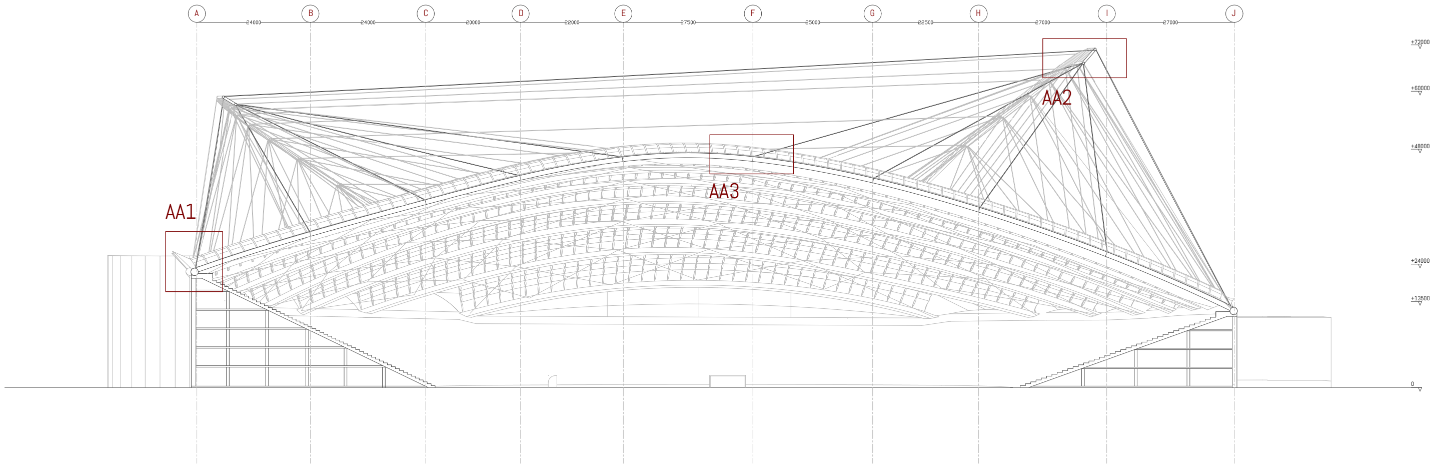

A
B
C
D
E
F
G
H
I
J
AA1
AA2
AA3

BB

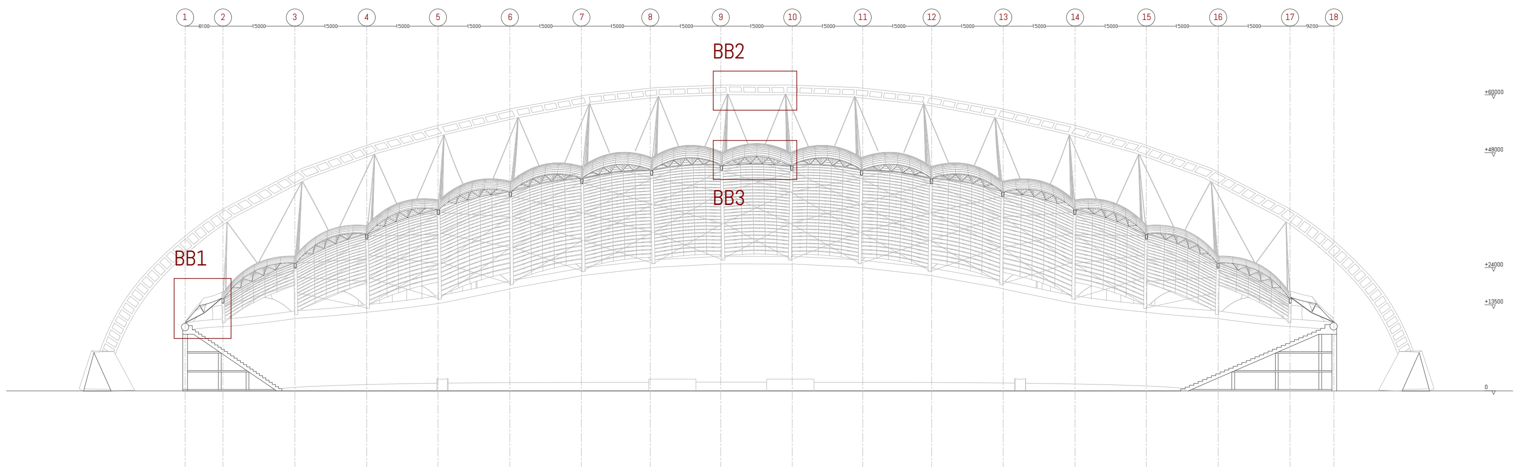

1
2
3
4
5
6
7
8
9
10
11
12
13
14
15
16
17
18
BB1
BB2
BB3

Details AA2+BB2

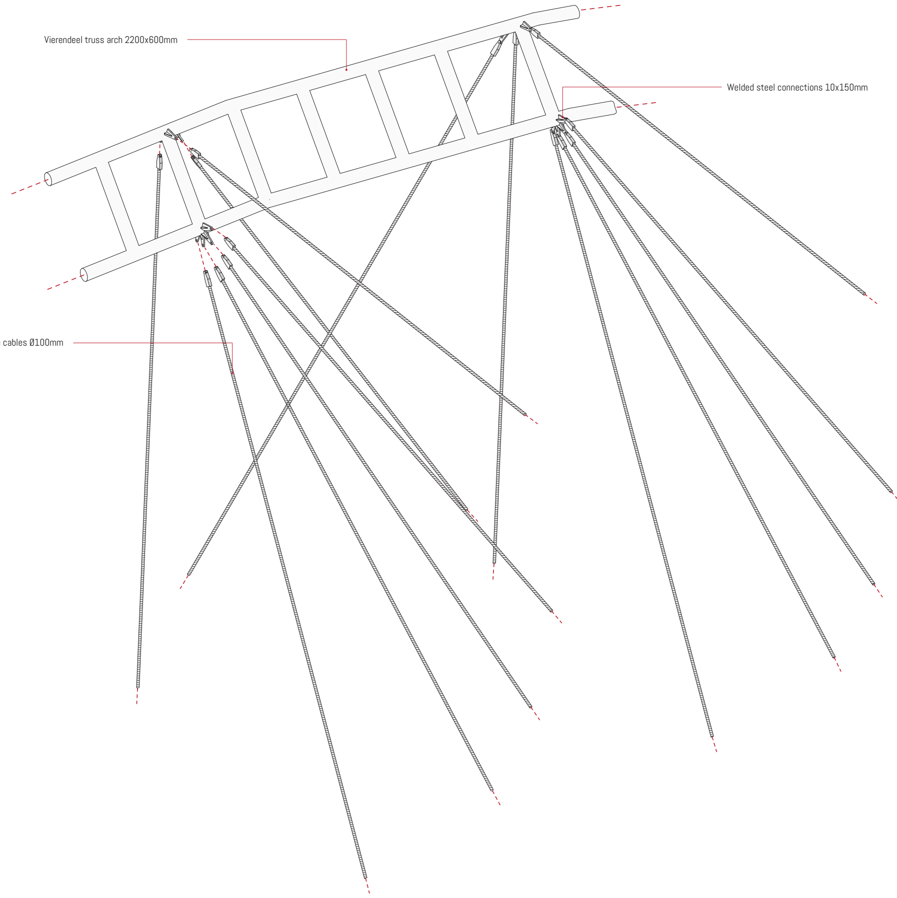

Details AA1+BB1

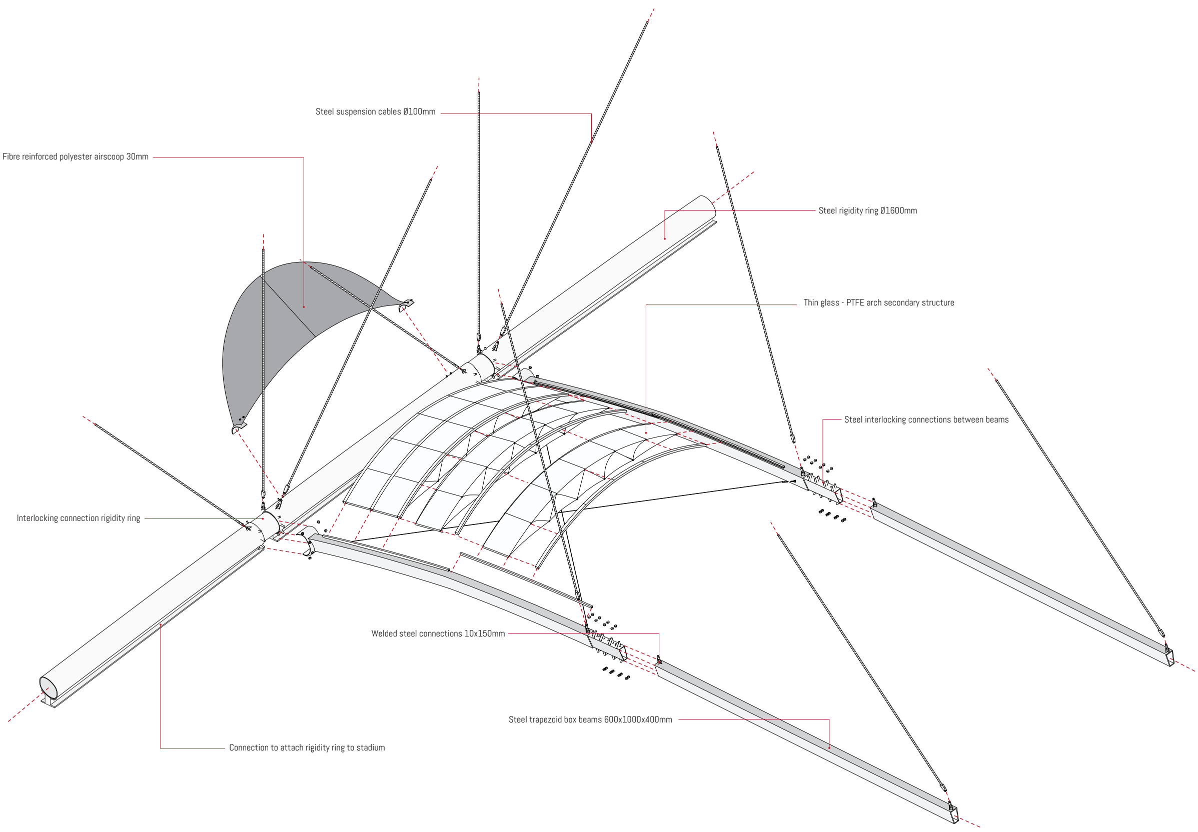

Detail BB3

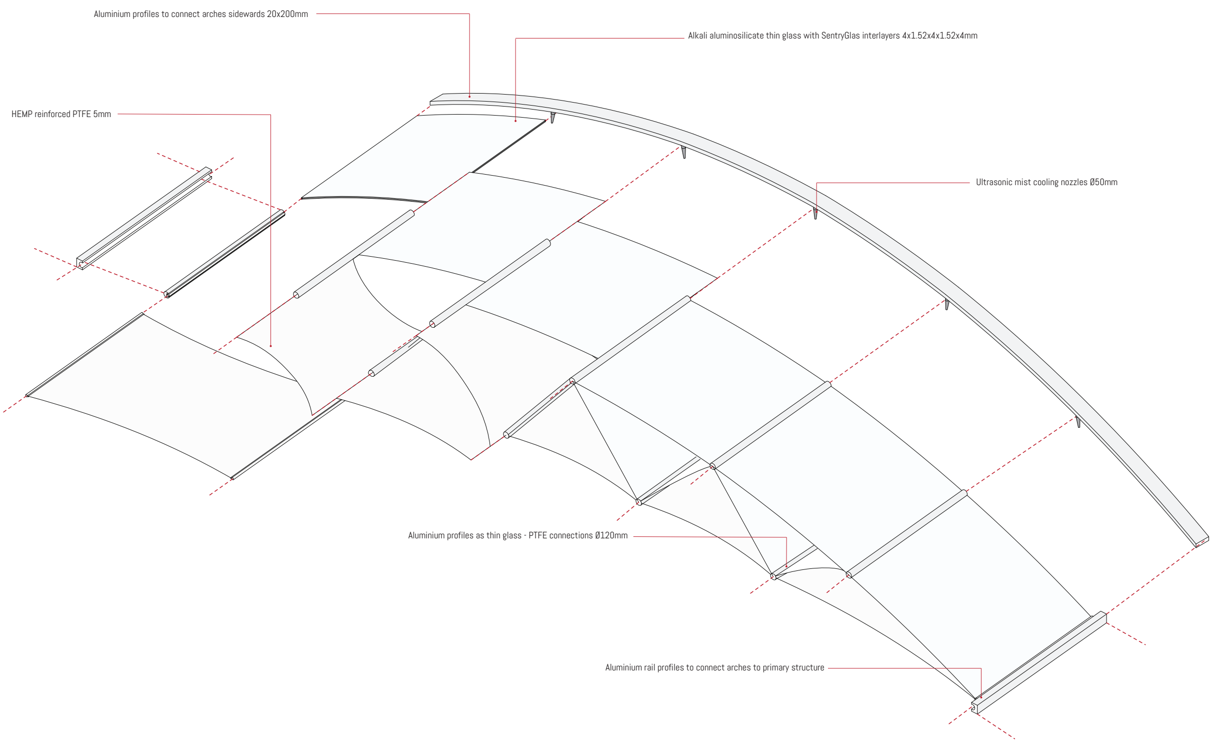

Detail BB1

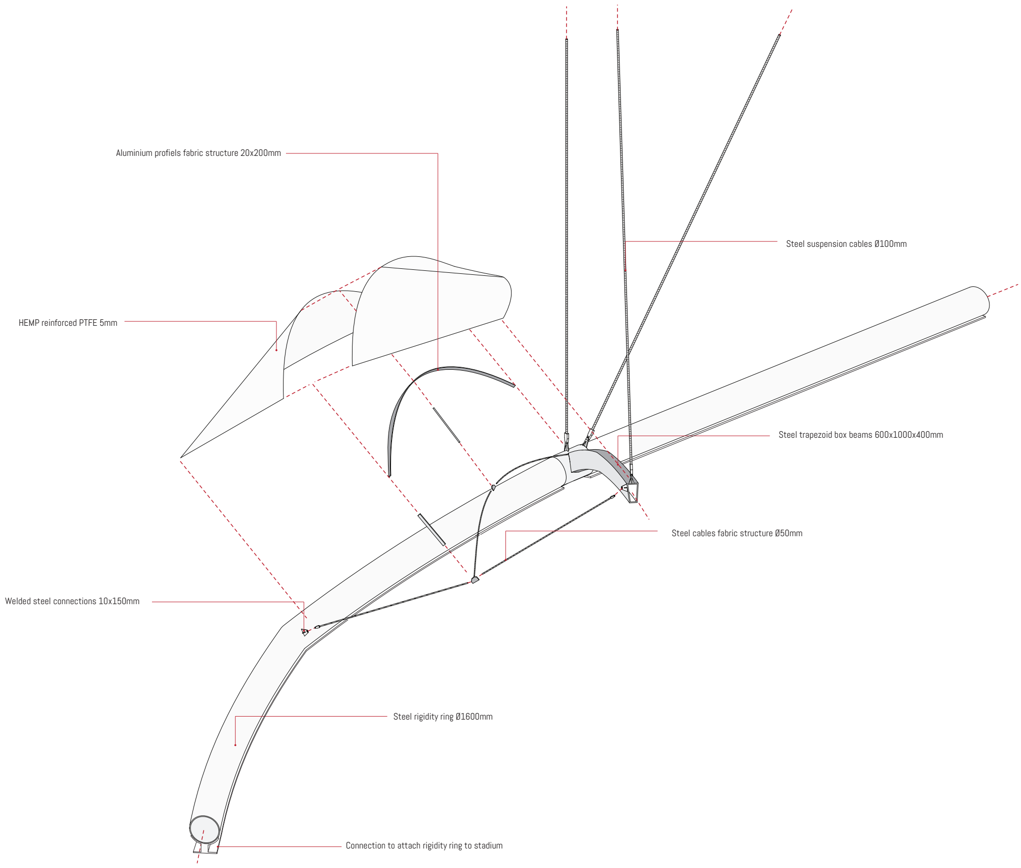

Detail AA

DETAIL AA1 **1:20**

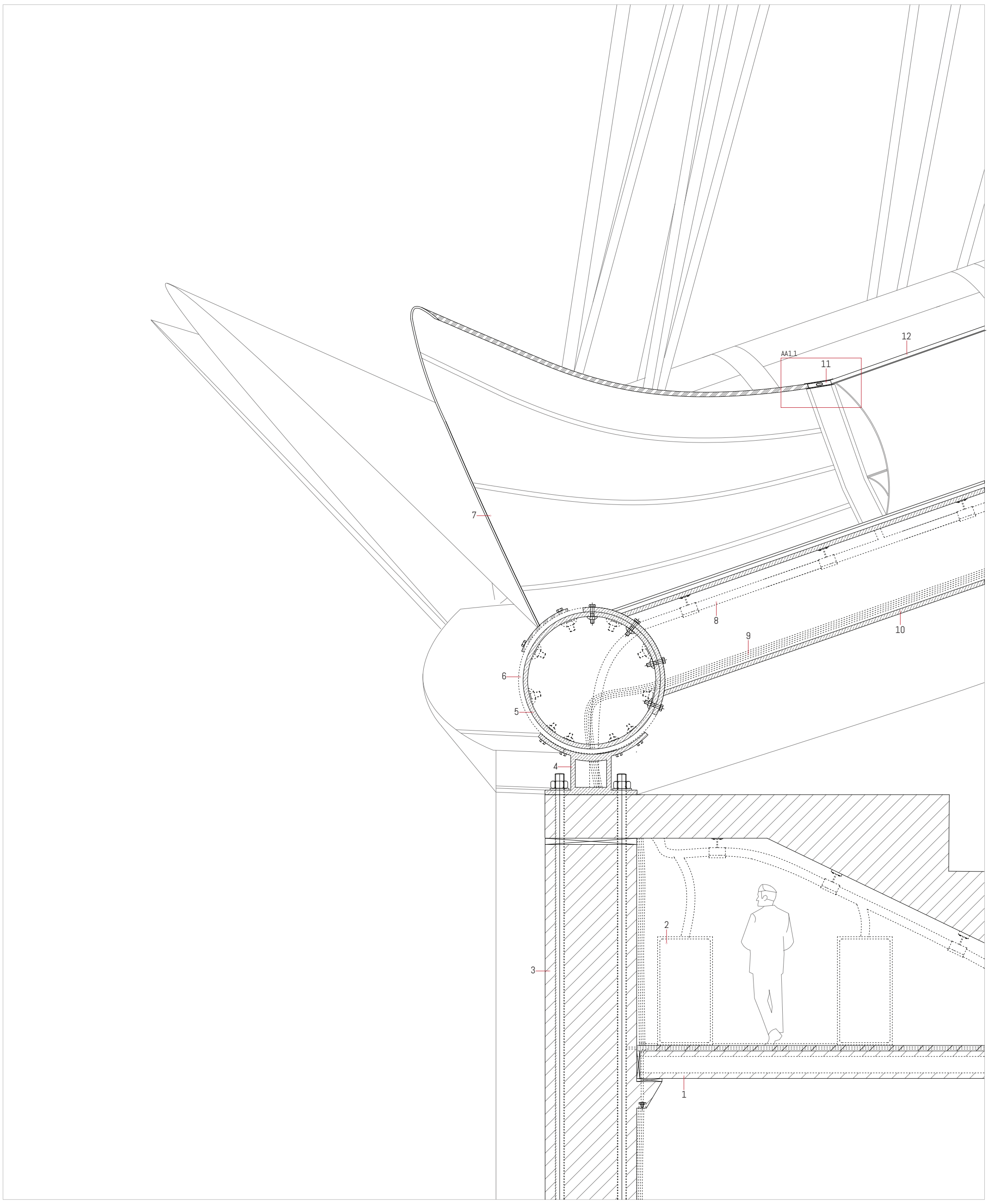

DETAIL AA2 **1:20**

DETAIL AA3 **1:20**

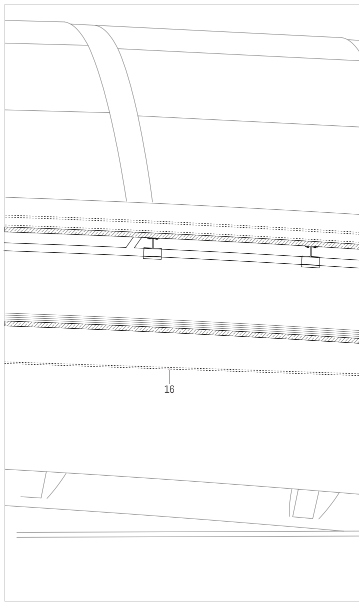

DETAIL AA1.1 **1:5**

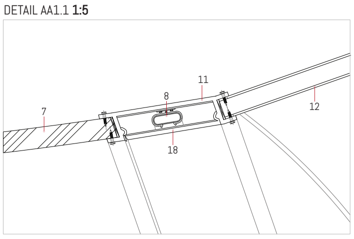

1. Concrete core slab floor 300mm 2. Roof and stadium cooling installations 3. Existing reinforced concrete stadium structure 4. Steel foot connection to concrete 5. Steel interlocking connections between rigidity tube rings 6. Steel rigidity ring, Ø1600mm 7. Fibre reinforced polyester airscoop 30mm thickness 8. Water tubing for ultrasonic mist cooling
17. Steel interlocking connections between beams 18. Operable part aluminium connection for maintenance

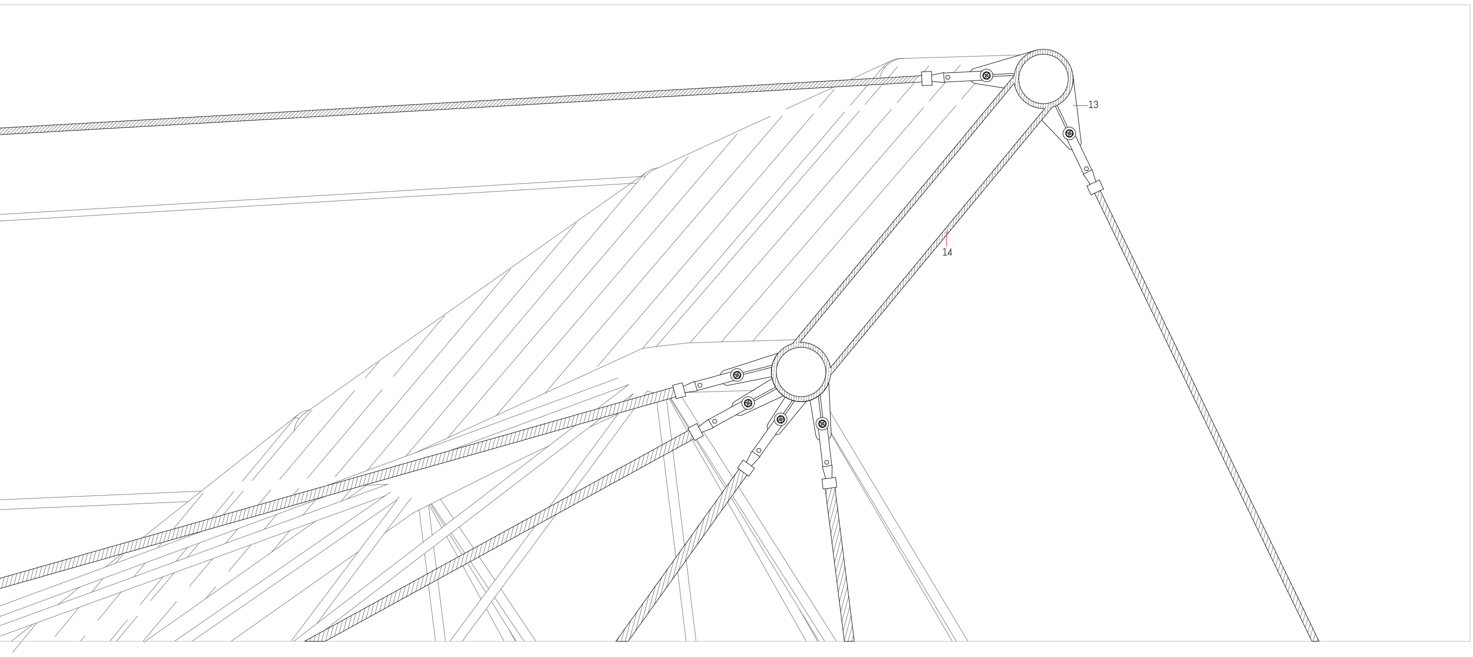

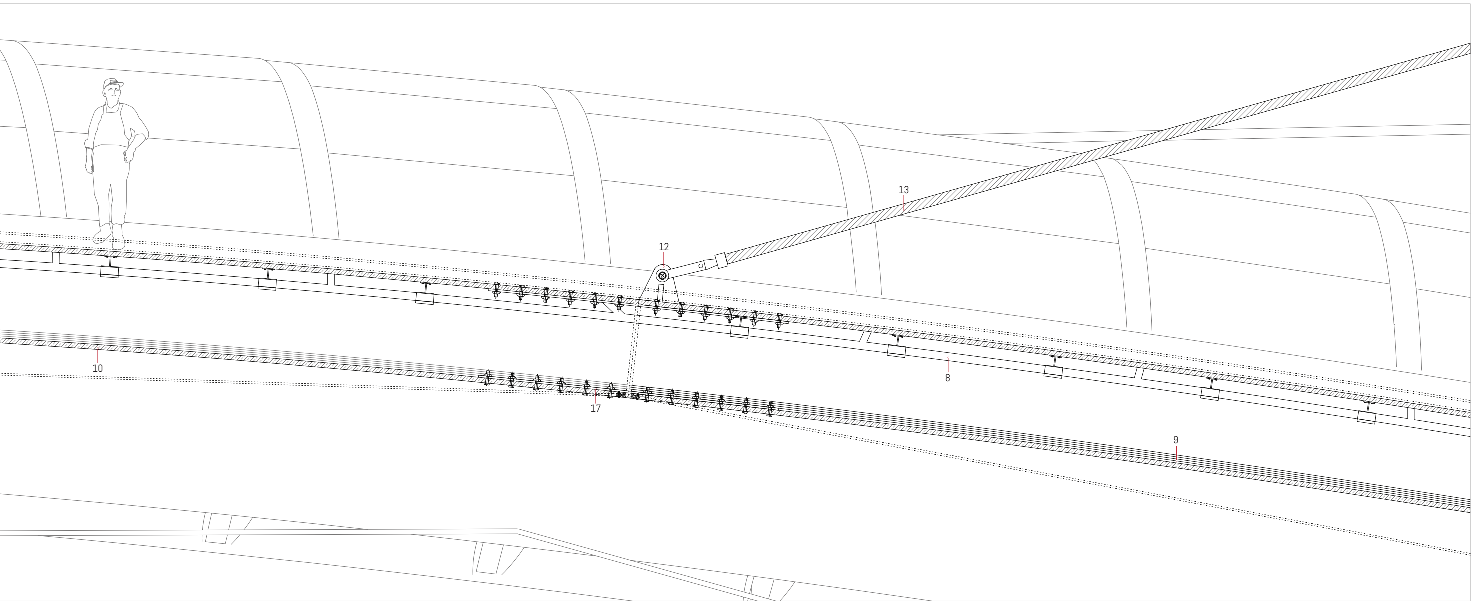

9. Electricity cabling 10. Steel trapezoid box beams 600x1000x400mm 11. Aluminium profiles to connect arches sidewards 20x200mm 12. Aluminium profiles to connect arches sidewards 20x200mm 13. Welded steel connections 10x150mm 14. Vierendeel truss arch 2200x600mm 15. Steel suspension cables Ø100mm 16. Bracing cables Ø20mm

Detail BB

DETAIL BB1 **1:20**

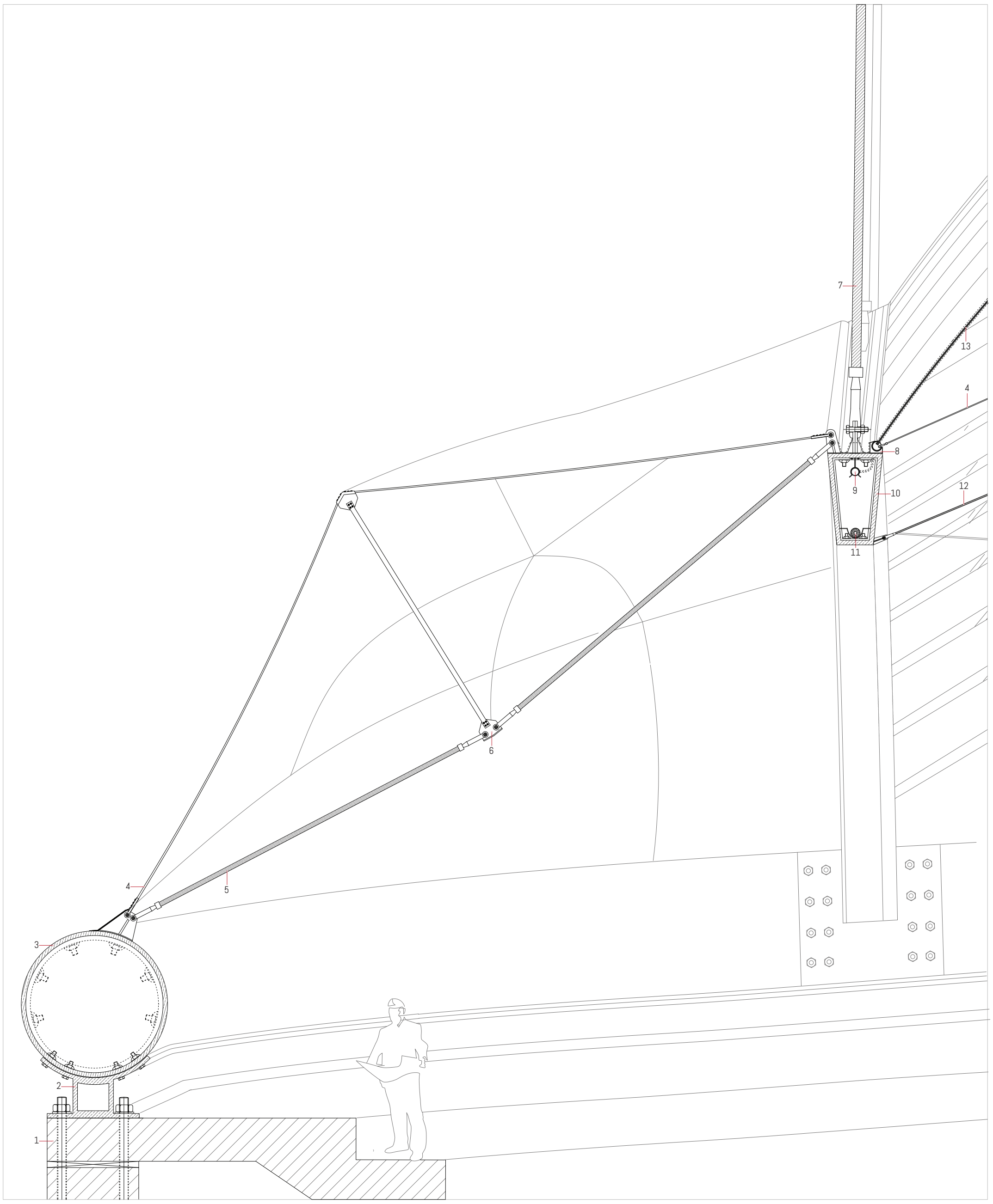

DETAIL BB2 **1:20**

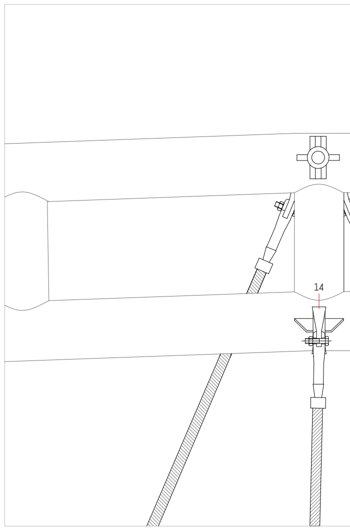

DETAIL BB3 **1:20**

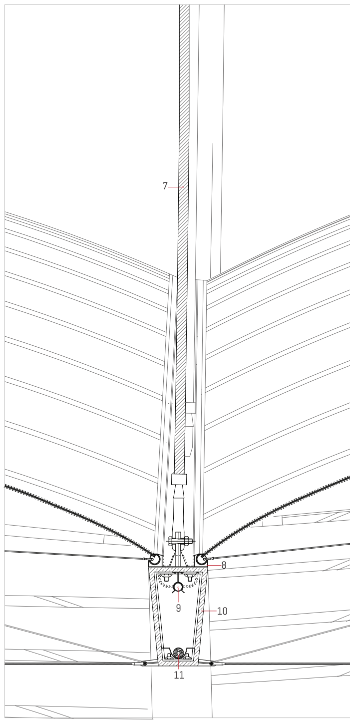

DETAIL BB3.1 **1:5**

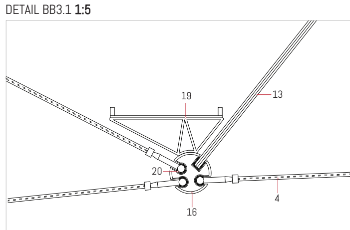

1. Existing reinforced concrete stadium structure 2. Steel foot connection to concrete 3. Steel rigidity ring Ø1600mm 4. Hemp reinforced PTFE 5mm 5. Steel cables fabric structure Ø50mm 6. Aluminium profiles fabric structure 20x200mm 7. Steel suspension cables Ø100mm 8. Aluminium rail profiles to connect arches to primary structure 9. Water tubi

17. Aluminium profiles to connect arches sidewards 20x200mm 18. Ultrasonic mist cooling nozzles Ø50mm 19. Crawling path for maintenance 20. Structural adhesive 21. Blind structural bolds

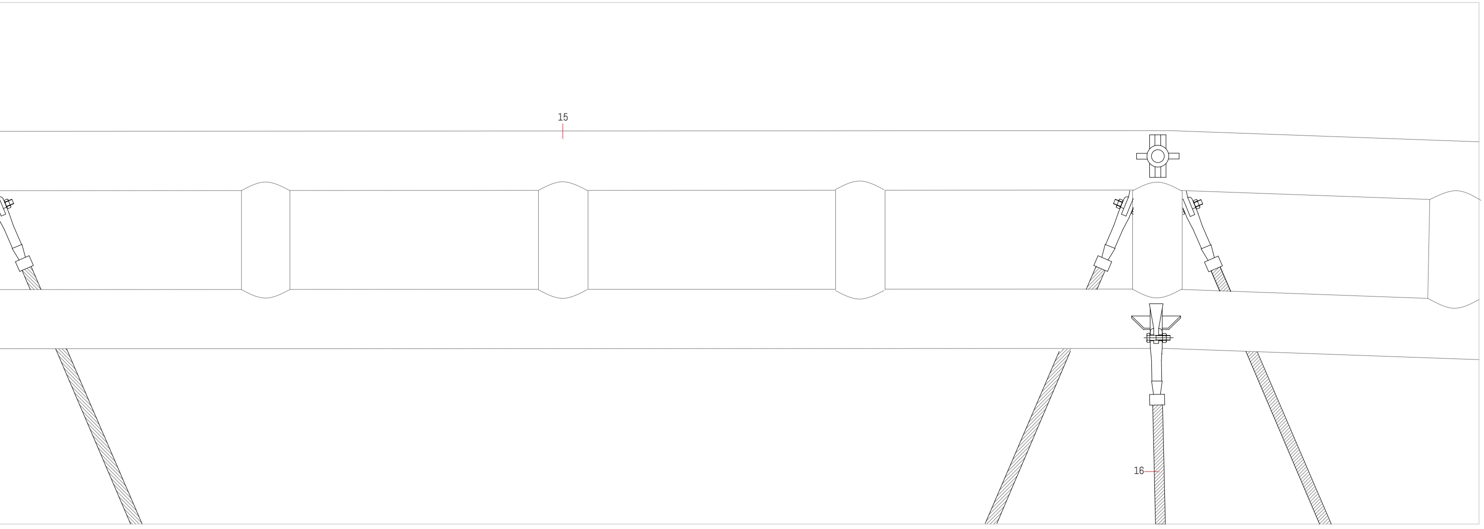

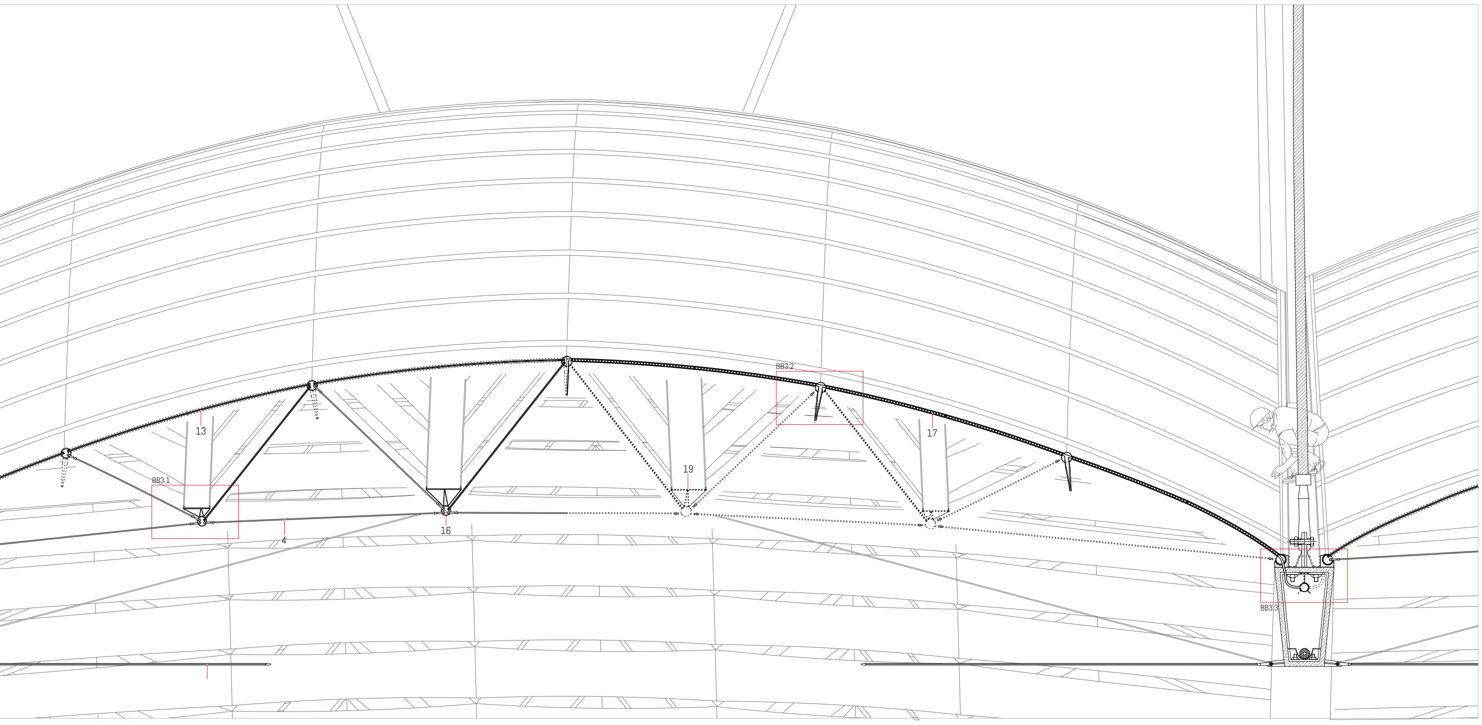

DETAIL BB3.2 **1:5**

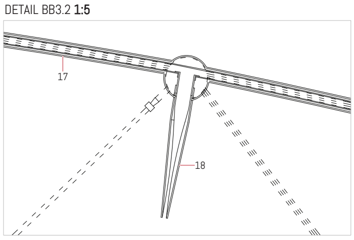

DETAIL BB3.3 **1:5**

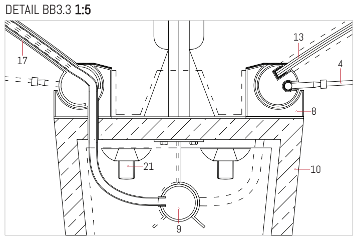

ng for ultrasonic mist cooling 10. Steel trapezoid box beams 600x1000x400mm 11. Electricity cabling 12. Bracing cables Ø20mm 13. Alkali aluminosilicate thin glass with SentryGlas interlayers, 4x1.52x4x1.52x4mm 14. Welded steel connections 10x150mm 15. Vierendeel truss arch 2200x600mm 16. Aluminium profiles as glass-fabric connections Ø120mm

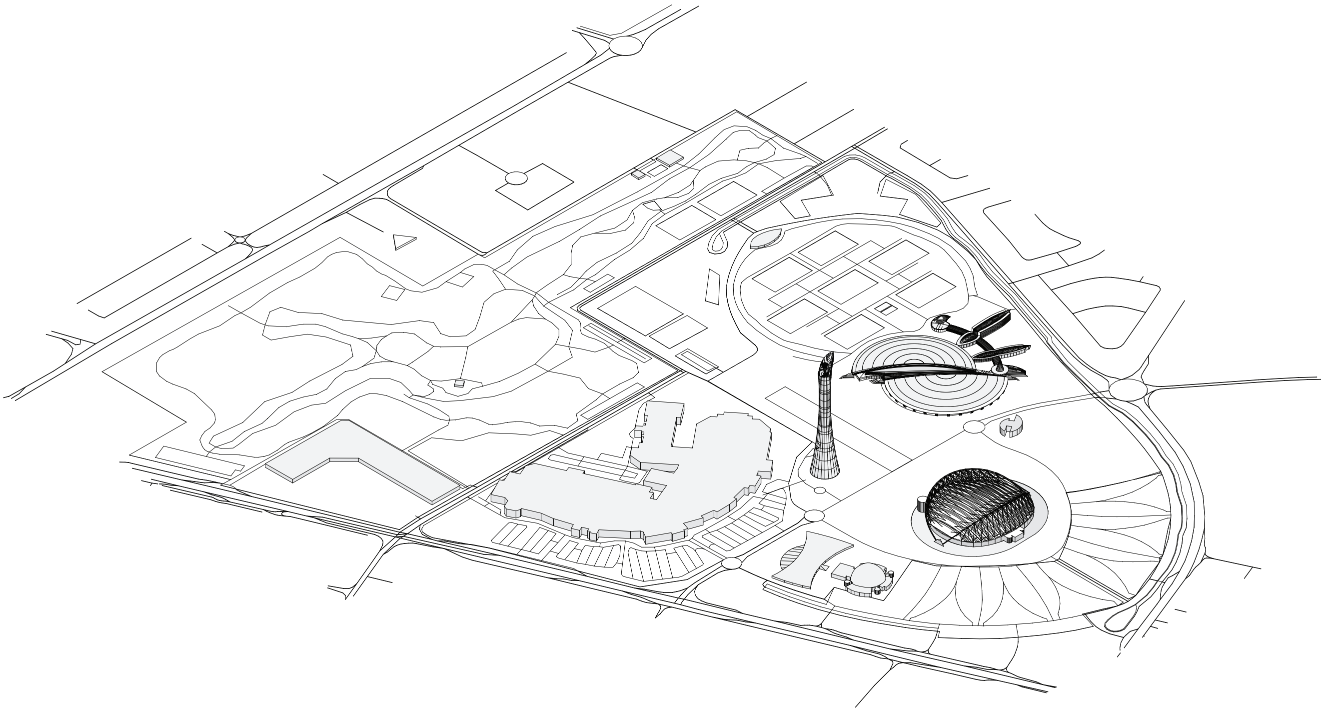

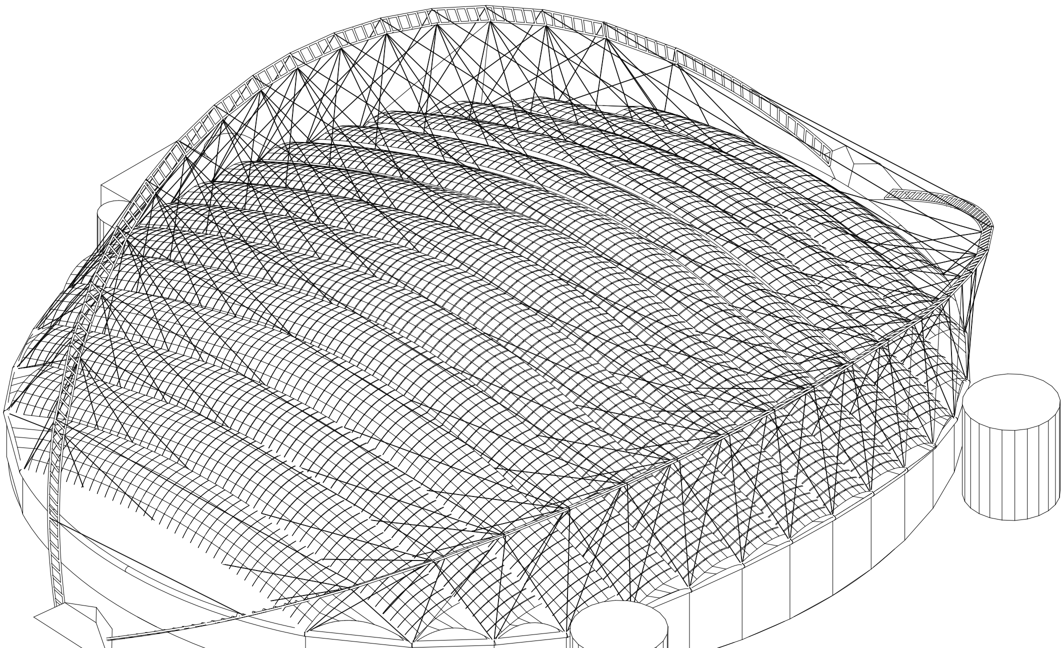

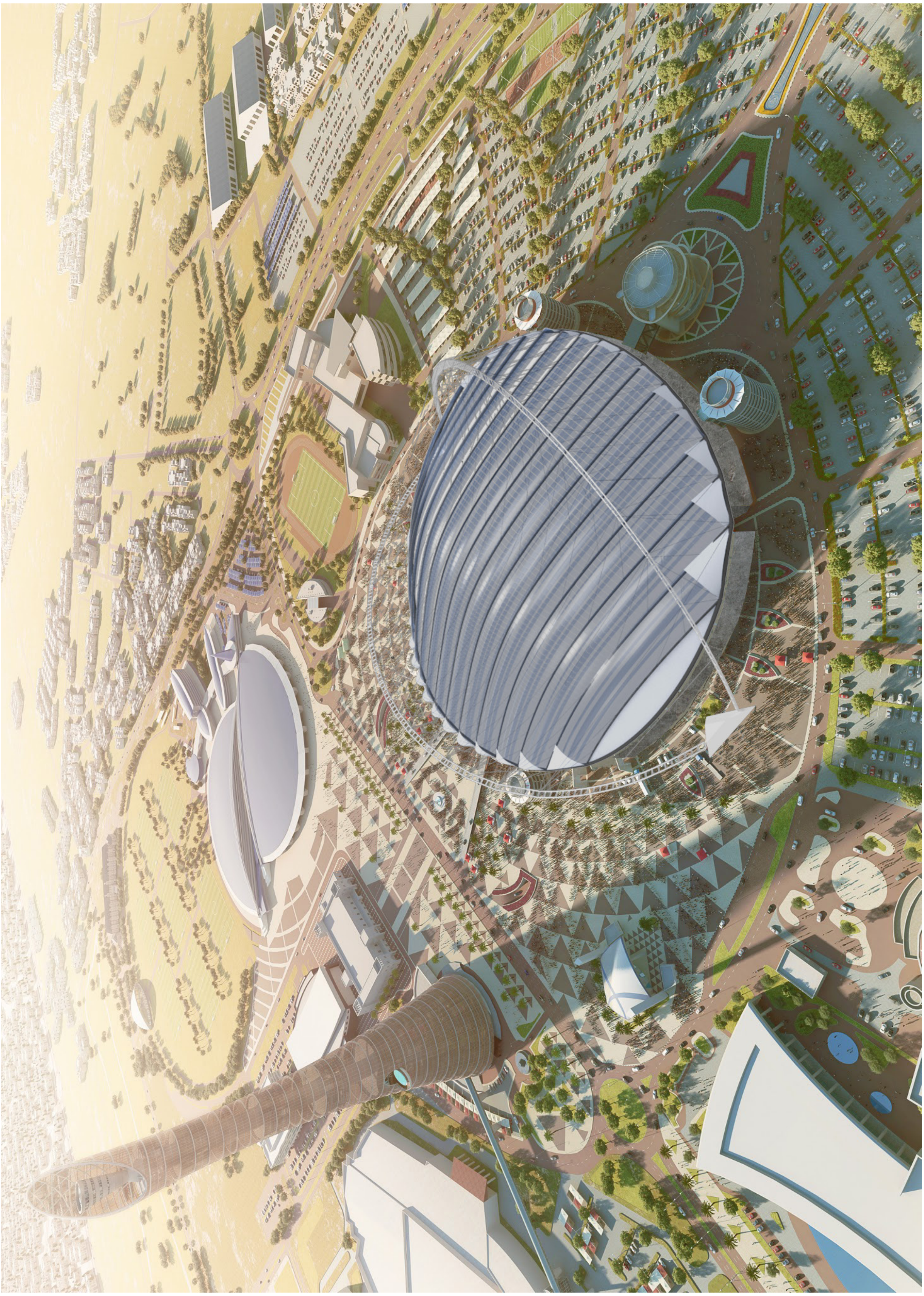

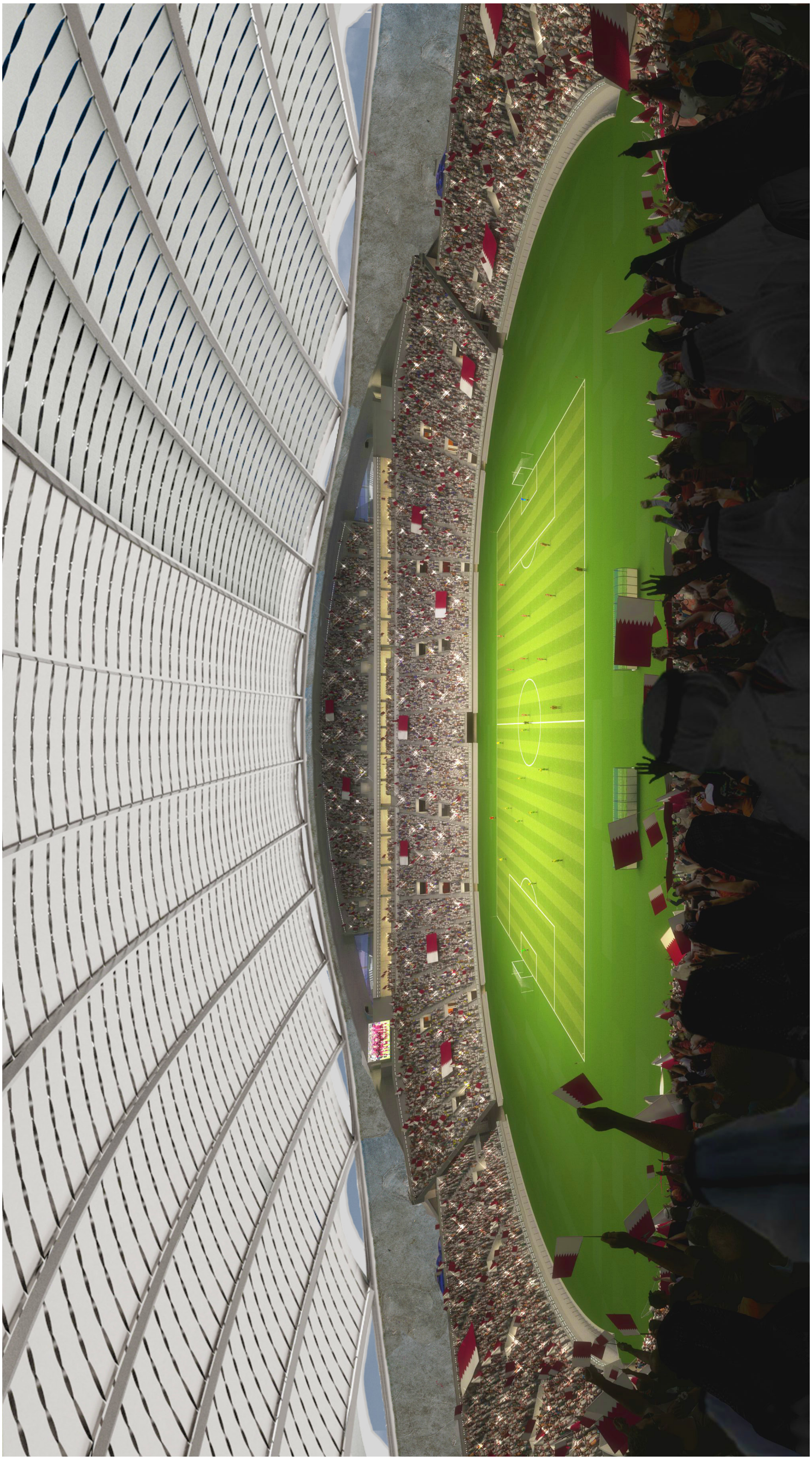

9. CONCLUSIONS

8.1 STADIUM CLIMATE DESIGN: A STRUCTURAL DESIGN STIMULATOR FOR OPTIMAL S-IEQ

The semi-indoor environmental quality of stadia (S-IEQ) is, in modern day, of high value. The following methods and approaches that where conducted during this graduation project give insight in the important things of climate design for stadia. Looking at the three most import aspects of S-IEQ in stadia: wind design in terms of aerothermal quality, heat design in terms of aerothermal quality and lighting design in terms of lighting quality. These aspects demonstrate sustainability, durability and energy-efficiency. The described outcome is based on parametric design and analysis using Rhinoceros+Grasshopper.

Wind design, the engine of aerothermal quality:

In terms of wind design, aerothermal quality arises from air circulation. To power the air circulation naturally, the stadium was analysed in its area. With this analysis, the density of the area, the average velocity and direction of the wind were investigated. Resulting in knowledge about the influence of the wind on the existing situation of the stadium. With this information, CFD (Computational Fluid Dynamics) and wind tunnel tests could be simulated, where subsequently different roof geometries could be tested. Testing three variants, with all completely different freeform geometries, the most optimal geometry could be found. A geometry that gives the highest acceleration and under pressure near the roof surface. Resulting in a roof geometry that enhances the inside air flow and makes natural ventilation possible in a stadium. With this approach, the influence of the wind is a tool to design, rather than being a blockade later in the design process. Designing by wind can be an improvement on stadium design, where sustainability is the key factor.

Heat design, the solution to aerothermal quality:

In terms of heat design, aerothermal quality arises from heat reduction in hot climates. In order to reduce high amounts of heat in hot climates, the stadium geometry that came from the wind analysis, was analysed on the amount of heat absorbed by the surface which then influenced the stadium pitch. The output information coming from the analysis, could be used to generate an adaptive roof result, where openings are added to the surface to keep the heat of the sun out and ventilate the hot air. This information in an early stage of a design process can give very clear insight in the composition of the shading design of the roof's structural design. As with the wind, in this case the heat is a design tool, instead of a problem that might occur in a later stage of the design process. Carefully designing by looking at the amount of heat ensures energy-efficiency to be key factor.

Lighting design, the solution to natural turf:

Lighting design for stadia is driven by the amount light that is needed to grow natural turf. To make natural turf growth happen in S-IEQ areas, the resulting stadium geometry from the wind analysis was analysed on the amount of PAR (Photosynthetically Active Radiation) absorbed by the surface. The surface amount of PAR absorbed influences the amount of PAR reaching the pitch. With this analysed data, an adaptive roof result could be generated. Same as with the heat analysis, a calculation on the amount of openings was made, to get the right amount of PAR on the stadium pitch. The same as for the heat analysis, a lighting analysis in an early design stage can help with the composition with the stadium roof's structural design. Resulting in light as a design tool for natural turf, instead of late phased design problem in terms of grass growth. With good lighting related turf design, the value of durability will be embraced.

8.2 STADIUM STRUCTURAL ROOF DESIGN: AN INNOVATIVE ROOF DRIVEN BY CLIMATE DESIGN

The outcome of a structural design that was fed by the importance of climate design in stadia resulted in an interesting balance between structural feasibility and climate technical demands. Looking, at first, at the primary structure to be made from steel that is based on the most aerodynamic geometry that came from the wind design and analysis. Secondly, the secondary structure to be made from glass and fabric that is based on the needed shading for heat and openings for PAR. The described outcome is based on parametric design and analysis using Rhinoceros+Grasshopper.

Primary steel structure, a wind based aerodynamic design:

Designing a steel structure based on the wind geometry and wind analysis principles was an interesting challenge in terms of wind and structural feasibility. To minimally blockade the wind and the light, the structure had to be a lightweight structure with a span of almost 200 metres. To design such a structure, the two existing arches, that are crossing over the stadium, were used to suspend the steel roof beams and make them as slim as possible. To prevent the arches from deforming, they were attached with cables to one another and to the stadium. This way, only cables where used to span the beams almost 200 metres, resulting in a lightweight structure that causes almost no blockade to the wind and the light. The proposed structure was, throughout the process, analysed and changed constantly to meet to right climate and structural requirements. With the early knowledge about the climate demands, the roof structure design tackled possible later staged design problems. Resulting the steel primary structure to be an efficient structure, supporting the principles of sustainability.

Secondary glass structure, a lighting and heat based shading design:

The design of the secondary structure, using only thin glass and fabric as structural materials, was challenging in terms of lighting and heat, but extremely challenging in terms of the structural feasibility of thin glass and fabric. To stay in lightweight terms, like the primary structure, the secondary structure was made of just thin glass and fabric. The fabric will help shading to keep the heat out, but the glass will help to get the right amount of diffuse light in to let the grass grow. Therefore, the secondary structure was meant to span 15 metres between the primary structure beams. In order to span a length of 15 metres with just glass and fabric, a composition of glass and fabric had to be made, which resulted in an arch. This arch composition had to the meet the structural requirements that all the glass panels absorbed the principal compression forces and the fabric the principal tension forces. And the climate requirements where direct sunlight got filtered from the heat, but diffuse light could go through the glass. The form finding process required structural optimisation and final analyses to make sure, such an arch could be designed. Again, with early knowledge about climate and structural demands, structural errors in later stages can be prevented. The resulted arch was a perfect example of climate meeting structural design, where efficiency is highly valued.

8.3 INFLUENCE OF PARAMETRIC DESIGN ANALYSIS

In the earlier mentioned process of the climate and structural design, Rhinoceros+Grasshopper played the key role in making the outcome of the analysis and the design parametric. The reason why these early stage analyses can influence the design very easily is because of the in- and output flexibility parametricism can cope with. All analysis and design aspects influence one another and can easily adapt and integrate in modern technology, due to algorithmic based parametric design. This new feature of designing, engineering and analysing will make the design process in practice more efficient, faster and less error driven. As a building technologist standing in the middle of design and engineering, this tool is the language between designers and engineers of the future.

8.4 RECOMMENDATIONS FOR FURTHER RESEARCH

°Design of a stadium roof with most optimal S-IEQ for extremely cold climates
°Comprehensive research building geometry aerodynamics to improve natural ventilation
°Comprehensive research most optimal transparent roofs for stadia
°Design of an acoustically optimised stadium roof
°Comprehensive optimisation primary structure of a stadium roof
°Comprehensive research on the use of new structural materials to design lightweight primary structure for stadium roof
°Comprehensive research on making maximum possible span using only thin glass
°Comprehensive structural analysis on buckling behaviour thin glass

10. REFLECTION

The roof design of the Khalifa International Stadium (KIS) is a final product of comprehensive climate research and analyses which are decisive to how the roof structure is researched, analysed and designed. The climate design gained its input from adaptability, meaning that the climate context was determinative to what the design would have to conquer. On the other hand, the structural design gained its input from geometries and properties of the climate design. This makes the climate design a product of design by research/context and the structural design a product of research by design. With this approach called parametric design and engineering, the design could be optimally integrated (see figure below).

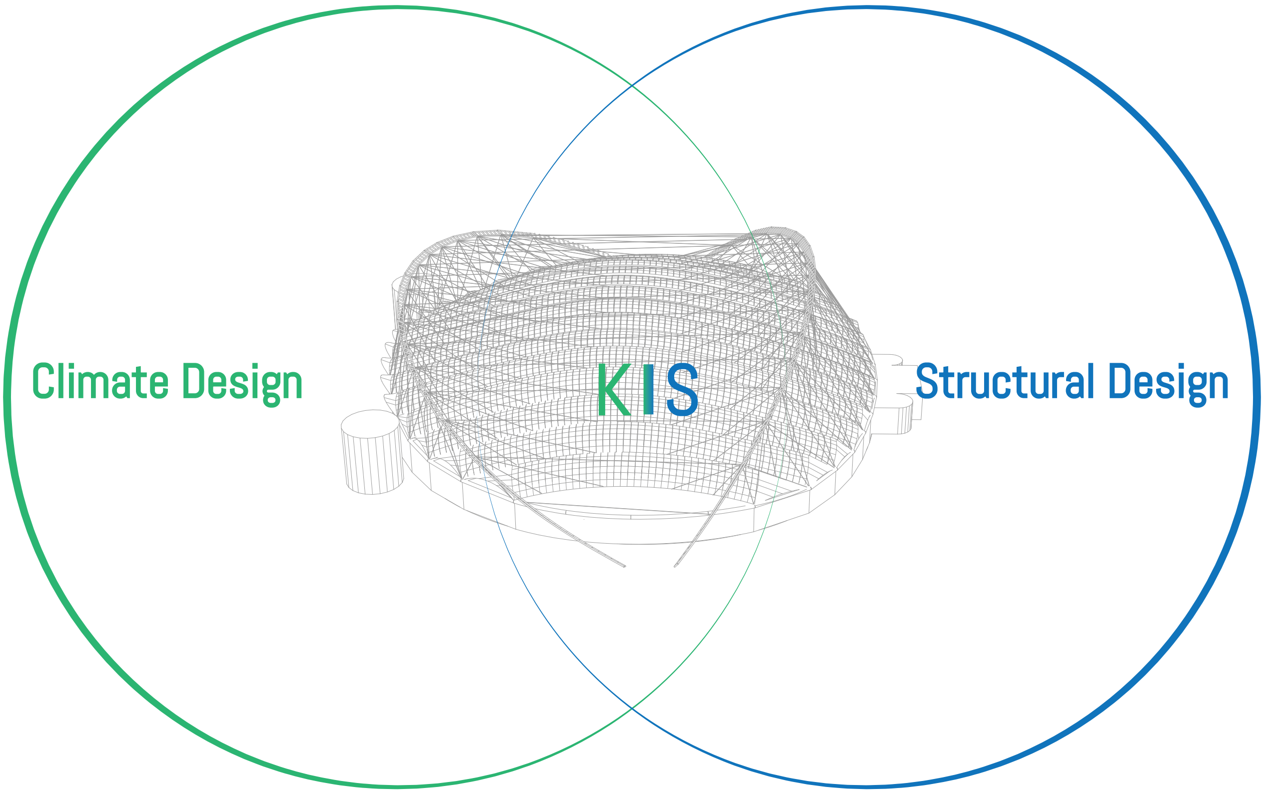

Academically:

Looking at the graduation lab theme of MSc Building Technology: Sustainable Design Graduation, the approach of designing a maximum transparent climate roof in Qatar is a challenge where sustainability and innovation are of great importance. Only with use of new sustainable and energy efficient analysis techniques and building technologies it is possible to design a maximum transparent roof that is cooling at the same time.
The first chosen design and analysis methodology was to first design all the needed climate aspects and afterwards design the whole structure. However, if the climate and the structural design/analysis have constant interaction, the final design would be more integrated. This resulted in a methodology where the influence of the wind decided the final form of the primary steel structure and the influence of lighting and heating decided the final form of the secondary glass structure. Which created a final structural supported climated design and a climate supported structural design. This final methodology fitted, in my opinion, well in the approach of the Sustainable Design Graduation Studio. Which is doing research by design, design by research or combining them to come to a suitable and sustainable solution in the architectural, design, engineering and technology practice.

Socially:

The social context of the design is the most critical point of the graduation project. The 2022 World Championship of Qatar is controversial, because of its extreme climate and poor labour conditions. The reason why Qatar is a good location to implement such a roof design, is to create awareness on what is possible in the fields of sustainability in such extreme climate conditions. Nevertheless, the disabuse of labour is something that cannot be justified, but unfortunately this is not the main focus in the field of building technology.

Practically:

The overall design, analysis and engineering approach resulted in a complex but interesting design on the fields of structure and climate. In the future to make the design more reliable, it would be more sufficient to do next to parametric computer calculations also physical tests in every discipline. The early stage Rhinoceros+Grasshopper analyses gave insight in the multiple design solutions of climate adaptive structural design. However, to test the real feasibility of certain design solutions, the climate situation has to be modelled and tested with actual climate measurement tools and the innovative structural materials tested to a material science level. The reason why physical tests always have to be conducted next to computer driven analyses, is to foresee unpredictable uncertainties. However, due to lack of time and people in relation to knowledge during this graduation project, the only physical test that was conducted: was the wind tunnel test. There were two reasons why the wind was tested physically: the first reason is that the wind is the most important factor of the design and the second reason was to determine the fluctuation of air movement, which you cannot predict with a CFD analysis. Next to the fact that physical tests are needed to determine the verity of the Rhino+Grasshopper analysis, it is very interesting to see what one individual can achieve with the help of parametricism (algorithmic aided parametric design and engineering). Parametricism will make the future of building will be more efficient, smarter, faster and less divided. In the end, designing such a large and complex object is too complicated to be conducted by one person and should be always elaborated by a team. However, this process was very instructive on what is most valueable in terms of stadium design and engineering. Resulting in knowledge and understanding of certain tools, where, as a building technologist, I will be able speak the designer's and the engineer's language.

LITERATURE

Abrisa. (2014). Corning® Gorilla® Glass.

Arens, E., Gonzalez, R., & Berglund, L. (1986). Thermal Comfort under an extended range of environmental conditions. ASHRAE Transaction, 10.

Auliciems, A., & Szokolay, S. V. (1997). Thermal Comfort. Passive and Low Energy Architecture International, 61.

Bluyssen, P. M. (2009). The Indoor Environment Handbook. USA: Earthscan, RIBA.

Bouyer, J., Vinet, J., Delpech, P., & Carré, S. (2007). Thermal comfort assessment in semi-outdoor environments: Application to comfort study in stadia. Elsevier, 13.

Clemenzi, R. (2011). Science Facts - Temperature Conversions. Retrieved from http://mc-computing.com/Science_Facts/Temperature_Conversions.html

Culley, P., & Pascoe, J. (2015). Stadium and Arena Design (Vol. 2). London, UK: ICE Publishing.

Danks, R., Good, J., & Philips, D. (2010). Turf and Plant Health and Sunlight Availability Analysis. Retrieved from London:

Detail-online. (2001). Maximilian Museum in Augsburg. Retrieved from http://www.detail-online.com/article/maximilian-museum-in-augsburg-15670/

Eurocode 4: Design of composite steel and concrete structures, ICS (2011).

FIFA. (2011). Football Stadiums. Retrieved from Zurich, Switzerland:

Frazer, A. H. (2005). Design Considerations for Retractable-roof Stadia. Massachusetts Institute of Technology, 58.

Froli, M., & Lani, L. (2010). Glass Tensegrity Trusses. Structural Engineering International, November 2010.

Gamble, S., Soligo, M., & Hunter, M. (2007). Technotes: Issue no. 12. Retrieved from London:

Guardian. (2014). Heat-treated Glass. Retrieved from USA:

Hödemann, S., Anton, J., & Murata, T. (2016). Gradient scattered light method for non-destructive stress profile determination in chemically strengthened glass. Journal of Materials Science, 2016.

Hooff, T. v., & Blocken, B. (2009). Couple urban wind flow and indoor natural ventilation modelling on a high resolution grid: A case study for the Amsterdam ArenA stadium. Elsevier, 14.

Johnson, C. P. (2014). The use of non-membrane structural glass: A Primer for Architects and Designers. Skidmore, Owings & Merrill, 2014.

Lautenbach, M., Heringa, P., & Vercammen, M. (2007). Acoustics for large scale indoor pop events. ISRA2007, 6.

Legacy, S. C. f. D. (2016). Khalifa International Stadium. Retrieved from http://www.sc.qa/en/stadiums/khalifa-international-stadium

Luxemburg, R. C. J. v., Hak, C. C. J. M., Heijnen, P. H., & Kivits, M. (2009). Stage acoustics: experiments on 7 stages of concert halls in the Netherlands. Internoise 2009, Innovations in practical noise control.

Navvab, M. (1999). Integration of Daylighting and Sport Lighting Systems Design for Turf Growth in an Indoor Football Stadium. LEUKOS, 63-80.

NSG. (2013). Properties of Soda-Lime Silica Float Glass.

Overend, M., Butchart, C., O'Callaghan, J., Lambert, H., & Prassas, M. (2013). Glass reinforced glass. Glass Performance Days 2013, 229-231.

Puttemans, M. (2006). Ontwerp en werking van verdringingsventilatie in historische concertzalen. (MSc Graduation), University of Gent, Gent.

QFA. (2010). 2022 FIFA World Cup Bid Evaluation Report: Qatar. Retrieved from England:

Sartori, I., Napolitano, A., & Voss, K. (2012). Net zero energy buildings: A consistent definition framework. Elsevier, 13.

Schneider, J. (2015). Thin glasses - the future envelope? . The future envelope 2015 obtanium, 2015.

Dupont (2016), SentryGlas®. Retrieved from https://www.dupont.com/products-and-services/construction-materials/safety-glass-interlayers/brands/sentryglas-ionoplast-interlayer.html

Simoen, C. (2016). Thin Glass: A study on the feasibility of thin chemical strengthened Aluminosilicate glass as a new material in the building industry. Retrieved from Delft:

Sofotasiou, P., Hughes, B. R., & Calautit, J. K. (2014). Qatar 2022: Facing the FIFA World Cup climatic and legacy-challenges. Elsevier, 27.

Soligo, M. J., Lankin, J. B., & Irwin, P. A. (1998). Environmental loads and microclimate impacts on sports facilities. Stadia 2000, 13.

Spagnolo, J. (2003). A field study of thermal comfort in outdoor and semi-outdoor environments in subtropical Sydney, Australia. Building and Environment, 38.

Szucs, A. (2004). Stadia in the environment – environment in stadia. Plea2004, 6.

Szucs, A., Moreau, S., & Allard, F. (2005). Spectators' aerothermal comfort assessment method in stadia. Elsevier, 14.

Szucs, A., Moreau, S., & Allard, F. (2008). Aspects of stadium design for warm climates. Elsevier, 9.

Tedeschi, A. (2014). AAD_Algorithms-Aided Design. Italy: Le Penseur.

Tolloczko, J. J. A., & Clarke, J. N. (1999). Stadia, Arenas & Grandstands. Cardiff, Wales: Spon press.

TROX. (2015). Verdringing: Principe en selectie.

Veer, F. A., Wurm, J., & Hobbelman, G. J. (2003). The Design, Construction and Validation of Structural Glass Dome. Glass Processing Days, 2013, 1.

Wikipedia. (2015a). Chase Field. Retrieved from https://en.wikipedia.org/wiki/Chase_Field

Wikipedia. (2015b). Paul Brown Stadium. Retrieved from https://en.wikipedia.org/wiki/Paul_Brown_Stadium

Wikipedia. (2016a). Amsterdam ArenA. Retrieved from https://en.wikipedia.org/wiki/Amsterdam_Arena

Wikipedia. (2016b). Aluminosilicate. Retrieved from https://en.wikipedia.org/wiki/Aluminosilicate

Wikipedia. (2016c). Soda-lime-silica glass. Retrieved from https://en.wikipedia.org/wiki/Soda-lime_glass

Wikipedia. (2016d). Arduino. Retrieved from https://en.wikipedia.org/wiki/Arduino#Hardware

Wurm, J. (2007). Glass Structures. Switzerland: Birkhäuser Verlag AG.

LIST OF SYMBOLS

A = Area in m^2 or mm^2

δ = Standard deviation

DBT = Dry Bulb Temperature

DR = Draught Rate

E = Young's modulus in N/mm^2

$f_{mt;u;d}$ = bending tensile strength

I = Second moment of area in mm^4

K = Structural safety factor symbol

L_b = Buckling length in m

$L_{e;\Omega}$ = Radiant flux of light

PAR = Photosynthetically Active Radiation

Q = Heating/cooling load

R = radius in mm

$S_{buckling}$ = Buckling stress in N/mm^2

σ_m = tension/comopression stress in N/mm^2

t = Temperature

T = Time in s

T_u = Turbulence intensity

U = heat transfer coefficient

U_v = Average wind velocity in m/s

U.C. = Unity Check for safety of structures < 1

v = Velocity in m/s

V = Volume in m^3

V_{kr} = ventilation amount

WCI = Wind Chill Index

WCT = Wind Chill Temperature

Wh/m^2 = Amount of heat/lighting

Ψ = Ratio symbol

Z = First moment of area in mm^3